



HAL
open science

In vitro experimentation and modeling of drug release from polymeric carriers for the development of drug eluting stents

Navideh Abbasnezhad

► **To cite this version:**

Navideh Abbasnezhad. In vitro experimentation and modeling of drug release from polymeric carriers for the development of drug eluting stents. Biomechanics [physics.med-ph]. HESAM Université, 2021. English. NNT : 2021HESAE040 . tel-03681570

HAL Id: tel-03681570

<https://pastel.hal.science/tel-03681570>

Submitted on 30 May 2022

HAL is a multi-disciplinary open access archive for the deposit and dissemination of scientific research documents, whether they are published or not. The documents may come from teaching and research institutions in France or abroad, or from public or private research centers.

L'archive ouverte pluridisciplinaire **HAL**, est destinée au dépôt et à la diffusion de documents scientifiques de niveau recherche, publiés ou non, émanant des établissements d'enseignement et de recherche français ou étrangers, des laboratoires publics ou privés.

ÉCOLE DOCTORALE SCIENCES ET MÉTIERS DE L'INGÉNIEUR
Laboratoires de LIFSE & PIMM - Campus de Paris

THÈSE

présentée par : **Navideh ABBASNEZHAD**

soutenue le : **27 September 2021**

pour obtenir le grade de : **Docteur d'HESAM Université**

préparée à : **École Nationale Supérieure d'Arts et Métiers**

Spécialité : **Biomécanique et ingénierie pour la santé**

In vitro experimentation and modeling of drug release from polymeric carriers for the development of drug-eluting stents

THÈSE dirigée par :
Professeur Farid BAKIR

et co-encadrée par :
Docteur Stéphane CHAMPMARTIN Docteur Mohammadali SHIRINBAYAN

Jury

F. KOSKAS

A. TREMANTE

V. BOUDY

B. MAUREL

A. AHMADI-SENICHAULT

S. CHAMPMARTIN

M. SHIRINBAYAN

F. BAKIR

Professeur, Chirurgien vasculaire, CHU Pitié-Salpêtrière

Professeur, Florida International University

MC. Praticien Hospitalier, Université Paris Descartes

Professeure, Chirurgienne vasculaire, CHU de Nantes

Professeure, Arts et Métiers

MC-HDR, Arts et Métiers

Docteur, Arts et Métiers

Professeur, Arts et Métiers

Rapporteur

Rapporteur

Examineur

Examinatrice

Examinatrice

Examineur

Examineur

Examineur

Acknowledgements

I would like acknowledging all the people who have accompanied me in the recent years during the preparation of my thesis. First and foremost I am extremely grateful to Prof. Farid Bakir, Dr. Mohammadali Shirinbayan and Dr. Stéphane Champmartin, for their continuous supervision, invaluable advices, and their guidance throughout my research work.

I'm highly appreciative to the members of my PhD committee: the professors Blandine Maurel, Azita Ahmadi-Senichault, Fabien Koskas, Andres Tremante and Dr. Vincent Boudy, for their valuable feedbacks and encouragements.

I also wish to thank the professors Abbas Tcharkhtchi, Smaine Kouidri, Sofiane Khelladi and Véronique Favier for their precious guidance.

My gratitude extends equally to the “Foundation Arts et Métiers, réseau santé” for the funding my PhD studies.

I would like thanking my friends and lab-mates, for the cherished time spent together.

My biggest thanks goes to my beloved family for all her support. I dedicate this thesis to my mother, my sister and the memory of my late father.

ACKNOWLEDGEMENTS

Résumé

Le système cardiovasculaire est sujet à des maladies graves telles que l'athérosclérose, principale cause de décès au cours des dernières décennies. Les techniques thérapeutiques continuent de s'améliorer aujourd'hui : angioplastie par ballonnet, stent nu, stent à élution médicamenteuse, stent biorésorbable. La thrombose de stent est l'une des complications graves de l'angioplastie. Le maintien d'une dose adéquate d'anticoagulants et d'agents antiplaquettaires pendant le traitement peut minimiser le risque de thrombose. L'optimisation des paramètres suivants peut améliorer la cinétique de libération du médicament au cours de cette thérapie : concentration initiale, solubilité et taille des particules du médicament, propriétés de la matrice polymère et méthodes d'enrobage. Dans cette thèse, nous avons développé un appareil bio-pertinent dans lequel nous pouvons considérer l'impact des choix de conception, et celui des propriétés des deux milieux mimés sur la libération du médicament. Ces deux milieux sont la circulation sanguine systolique-diastolique et la paroi artérielle. De plus, nous avons analysé et quantifié l'effet du schéma d'écoulement, du revêtement polymère et du type de médicament sur les tests de libération in vitro. Nous avons également développé des modélisations robustes permettant de caractériser le comportement cinétique des porteurs de médicaments. Ces modèles ont été validés sur des études de cas prenant en compte les effets de la charge médicamenteuse initiale et le type de flux. Ces développements permettent ainsi de définir des choix de conception pour de nouveaux systèmes d'administration de médicaments en réponse à un profil de libération souhaité.

Mots-clés : Appareil bio-relevant, Stent à élution de médicament, Mécanismes et cinétique de libération, Écoulement sanguin pulsatile, Modélisation, Simulations numérique.

RESUME

Abstract

The cardiovascular system is prone to severe diseases such as atherosclerosis, most important cause of death in the recent decades. Therapeutic techniques continue to improve today: balloon angioplasty, bare stent, drug-eluting stent, bioresorbable stent. Stent thrombosis is one of the severe complications of the angioplasty. Maintaining an adequate dose of anticoagulants and antiplatelet agents during the therapy can minimize the risk of thrombosis. Optimizing the following parameters can improve the kinetics of the drug release during this therapy: initial concentration, solubility and particle size of drug, properties of the polymer matrix and coating methods. In this thesis, we have developed a bio-relevant apparatus in which we can consider the impact of the design choices, and that of the properties of the two mimicked media on the release of the drug. These two media are the systolic-diastolic blood circulation and the arterial wall. Furthermore, we have analyzed and quantified the effect of the flow pattern, polymer coating and type of drug on the in vitro release tests. We have also developed some robust modeling allowing the characterization of the kinetic behavior for the drug carriers. These models were validated on case studies taking into account the effects of the initial drug load and the type of flow. These developments thus make it possible to set design choices for new drug delivery systems in response to a desired release profile.

Keywords: Bio-relevant apparatus, Drug-eluting stents, Drug release mechanisms and kinetic, Pulsatile blood flow, Modeling, Numerical simulations.

ABSTRACT

Table of contents

Acknowledgements	3
Résumé	5
Abstract	7
List of tables	16
List of figures	31
1 Introduction	33
1.1 Motivation	33
1.2 Thesis objectives	37
1.3 Thesis outlines	38
1.4 Thesis main achievements	39
2 Literature review	41
2.1 Drug release mechanisms	42
2.1.1 Physical mechanisms	42
2.1.1.1 Diffusion controlled phenomenon	42
2.1.1.2 Physical degradation/erosion	43
2.1.1.3 Osmosis pressure-based release	44

TABLE OF CONTENTS

2.1.1.4	Swelling based phenomenon	44
2.1.1.5	Dissolution based phenomenon	45
2.1.1.6	Ion exchange phenomenon	47
2.1.2	Chemical mechanisms	47
2.1.2.1	Chemical degradation	47
2.1.3	Drug uptake	47
2.2	Design conception of drug-eluting stents	50
2.2.1	Different geometrical models of drug-eluting stents	50
2.2.2	Polymers in the case of drug-eluting stents	53
2.2.2.1	Bio-durable polymers	53
2.2.2.2	Biodegradable polymers	53
2.2.3	Drugs in the case of drug-eluting stents	56
2.3	Characteristics of the test condition	57
2.3.1	Release compartment	57
2.3.1.1	Artificial lumen	57
2.3.1.2	Artificial tissue	59
2.3.2	Release test methods	61
2.3.2.1	Static condition	62
2.3.2.2	Dynamic condition	62
2.3.3	Apparatus for release testing	64
2.3.4	Analytical tools to determine drug release	67
2.4	Modelisation and simulation	68
2.4.1	Semi-empirical models	68
2.4.2	Mechanistic model of drug release profile	78
2.4.3	Simulation of drug release profile	81

TABLE OF CONTENTS

2.4.4	In vitro-in vivo correlations and acceleration method	83
2.5	Summary	87
3	Materials and methods	89
3.1	Materials	90
3.2	Samples preparation	91
3.3	Bio-Relevant Apparatus (BRA)	93
3.3.1	Specification and description of the BRA	93
3.3.2	Generation pulsed circulation	96
3.3.3	Mimicking arterial system	99
3.4	In vitro drug release procedure and associated measurement	102
3.4.1	Protocol of the UV-Vis method	102
3.4.2	Protocol of the gravimetry method	104
3.5	Characterization methods	106
3.5.1	Microscopic observations	106
3.5.2	Differential Scanning Calorimetry (DSC)	106
3.5.3	Thermo Gravimetric Analysis (TGA)	106
3.5.4	Dynamic Mechanical Thermal Analysis (DMTA)	107
3.5.5	Fourier-Transform InfraRed spectroscopy (FTIR)	107
3.5.6	Drug solubility	107
3.5.7	Tensile testing	107
3.5.8	Permeability measurement of the hydrogel	107
3.5.9	Fluorescence spectroscopy	108
4	Experimental results - In vitro drug release	109
4.1	Primary characterization of materials	110
4.1.1	Polyurethane	110

TABLE OF CONTENTS

4.1.2	PLGA	112
4.1.3	Hydrogel	116
4.2	Drug release in artificial lumen	119
4.2.1	Factors influencing the in vitro drug release	119
4.2.1.1	Effect of solvent evaporation	120
4.2.1.2	Effect of polymer thickness	121
4.2.1.3	Effect of the initial percentage of the loaded drug	123
4.2.1.4	Effect of flow rate	132
4.2.2	Investigation of drug release mechanisms	138
4.2.3	Evaluation of the mechanical, physical and chemical properties of the polymeric drug carriers during release	147
4.2.3.1	PU loaded with diclofenac epolamine	148
4.2.3.2	PLGA loaded with diclofenac sodium	154
4.3	Drug release in artificial lumen and tissue	165
4.3.1	Presence of artificial tissue in drug release system	165
4.3.2	Steady and non-steady flow rates	167
4.3.3	Presence of the metal layer on the polymer layer	171
4.3.4	Distribution pattern of luminescence particles in the gel	173
5	Modeling and simulation - (in-silico modeling of drug release)	177
5.1	Kinetic and accelerating model	177
5.2	Mechanism-based model	191
5.2.1	Application of the mechanism-based model for PU-DE	192
5.2.2	Application of the mechanism-based model for PLGA-DS	205
5.3	Numerical simulation	212
6	Conclusions and perspectives	223

TABLE OF CONTENTS

6.1	Conclusions	224
6.2	Perspectives	226
	Bibliographie	229
	Appendix	260
	A List of the publications	261
	B Résumé de thèse	265
B.1	Introduction	265
B.2	Etat de l'art	270
B.2.1	Mécanismes de libération de médicament	270
B.2.2	Conception de stents à élution médicamenteuse	271
B.2.2.1	Différents modèles géométriques de stents à élution médicamenteuse	271
B.2.2.2	Polymères dans le cas des stents à élution médicamenteuse	272
B.2.2.3	Médicaments dans le cas des stents à élution médicamenteuse	274
B.2.3	Caractéristiques de la condition d'essai	275
B.2.3.1	Lumière artificielle	275
B.2.3.2	Tissu artificiel	276
B.2.4	Méthodes d'essai de relargage	277
B.2.4.1	État statique	277
B.2.4.2	État dynamique	278
B.2.5	Appareils pour les essais de libération de médicament	279
B.2.6	Modélisation et simulation	282
B.2.6.1	Modèles semi-empiriques	282
B.2.6.2	Simulation du profil de libération du médicament	283
B.3	Résultats expérimentaux	285

TABLE OF CONTENTS

B.3.1	Libération de médicaments dans la lumière artificielle	285
B.3.1.1	Effet du pourcentage initial du médicament chargé	285
B.3.1.2	Effet du débit	291
B.3.2	Évaluation des propriétés mécaniques, physiques et chimiques des supports polymères de médicaments pendant la libération	294
B.3.2.1	PU chargé de diclofénac épolamine	294
B.3.2.2	PLGA chargé de diclofénac sodique	299
B.3.3	Libération de médicaments dans la lumière et le tissu artificiel	306
B.3.3.1	Débits constants et non constants (pulsatile)	306
B.3.3.2	Présence de la couche métallique sur la couche polymère	312
B.3.3.3	Distribution des particules de luminescence dans le gel	315
B.4	Modélisation et simulation	317
B.4.1	Modèle cinétique	317
B.4.2	Modèle basé sur les mécanismes	323
B.4.3	Simulation numérique	334
B.5	Conclusion	341

List of tables

2.1	A comparison of the amount of drug release in different types of stents and polymer coatings [26]	52
2.2	Comparing the results of carbidopa and levodopa release with different models [177] .	70
2.3	Release behavior for different mg of tablet components: Glycerylbehenate/ Hydroxypropylmethyl cellulose 1) 50/50 2) 25/75 3) 75/25 4) 100/0 5) 0/100 [182]	73
2.4	R ² values for the release kinetics of in vitro drug release from Moxifloxacin-loaded PLGA nanoparticles. MNx means 1 drug: x polymer [191]	75
2.5	Comparison of the value of “m” with shape of the matrix and related mechanisms [195]	76
2.6	Analysis of dynamic swelling data for xanthanechitosan capsules using Higuchi, Korsmeyer-Peppas, and Peppas-Sahlin [194]	76
4.1	Values related to the Higuchi model by fitting the experimental results	141
4.2	Regression constants for different mathematical models for PU-10%DE, 20%DE, 30%DE-Q0	144
4.3	Values related to the Peppas model by fitting the experimental results	147
4.4	The values related to the free volume fraction parameters for the samples of PLGA-Pure, PLGA-5% and PLGA-10% DS	156
5.1	Values related to the percentage of the contribution of the mechanisms associated in the drug release and affecting release kinetic (t_c = characteristic time).	197
5.2	Values related to the unknown parameters	208

LIST OF TABLES

5.3	Values related to the unknown parameters with neglecting one mechanism for each case	209
5.4	Values related to the unknown parameters for PLGA-10%DS-Q7.5 from the BSDE model obtained by the correlation of the values of the parameters and direct application of the BDSE model	211
5.5	Predicted diffusion coefficient (m^2/s) at different conditions	213
B.1	Valeurs liées aux paramètres inconnus	330
B.2	Valeurs liées aux paramètres inconnus en négligeant un mécanisme pour chaque cas . .	331
B.3	Coefficient de diffusion calculé (m^2/s) à différentes conditions	335

List of figures

1.1	Schematic of the material choice in the various stents [2–10]	34
1.2	Coronary restenosis after coronary angioplasty with the balloon [24]	35
1.3	In-stents coronary restenosis after coronary angioplasty with the bare metal stents [24]	36
1.4	Late thrombosis after drug-eluting stents, adopted and modified from [24]	36
2.1	Schematic representation release mechanisms: (a) diffusion through water-filled pores, (b) diffusion through the polymer, and (c) erosion [43]	43
2.2	Osmosis-controlled release from (a) osmotic pump or (b) monolithic system [55]	45
2.3	Two-stage of swelling [58]	46
2.4	Schematic representation of the dissolution process for polymer molecules, blue lines represent polymer chains and yellow dots represent solvent molecules. (a) polymer mo- lecules in solid state just after being added to a solvent; (b) a swollen polymeric gel; (c) solvated polymer molecules dispersed into a solution [61]	46
2.5	The geometrical configuration of the DDS. This consists of some durable structure (shaded grey) coated with a thin layer of polymer of thickness l_0 containing the drug (red). The polymer layer is in contact with the biological tissue of thickness l_1 (orange). The drug is transported from the polymer coating via dissolution and diffusion to the tissue where it is subject to diffusion and advection in its free phase and may bind to drug binding sites. Diagram is not to scale [70].	48
2.6	Transmural equilibrium distribution of labeled dextran (\blacklozenge), paclitaxel (\square), and rapa- mycin (\blacklozenge) in 0.040-mm-thick bovine internal carotid tissue segments [72].	49

LIST OF FIGURES

2.7	Drug-eluting stent strut cross-sections, (a) is a DES strut with a drug loaded polymer matrix and stent strut (b) has a transport regulating topcoat [97]	54
2.8	Model proposed by Li et al. [96] for coating the stent with the polymer layers	54
2.9	(a) NEVO open-cell design. Multiple laser-cut reservoirs hold a blend of PLGA and sirolimus in mechanically stable stent struts. Sigmoidal bridge elements connect the circumferential strut rings. (b) Drawing shoes a detailed view of the filled reservoirs. (c) Scanning electron micrograph of a reservoir [106]	56
2.10	Schematic overview of the in vitro test setup (A) and photograph of the vFTC equipped with a 2 wt% agarose gel (B); 1) vFTC, 2) media container, 3) PBS of pH 7.4, 4) paddle stirred at 50 rpm, 5) peristaltic pump, 6) heated water bath, a) glass beads, b) stainless steel disc, c) hydrogel [140]	66
2.11	(a) Incubation setup carried out in 100 ml glass flasks. Flow-through cells were equipped with an agarose hydrogel based on deionised water (vFTC (deionised water)) or run without a second compartment (FTC). (b) triamterene from stent coatings into media over time with vessel-simulating flow-through cell, flow-through cell (USP 4), or paddle apparatus (USP 2); flow rate 35 ml/min, paddle speed 50 rpm [35, 159]	66
2.12	Separation mechanism by HPLC [168]	67
2.13	Higuchi kinetics model of Levodopa and Carbidopa [177]	71
2.14	Zero-order plot of F8 composed of: 20 mg Eletriptan Hydrobromide, 50mg Chitosan, 25 mg Sodium alginate, 52 mg Lactose, 2 mg Magnesium Stearate, 1 mg Talc; with the total weight of 150 mg as a tablet [180]	72
2.15	Concentration versus time profile for the drug solution in the dialysis bag placed in the flask for a different shaking speeds for 0.03 g drug in 10 ml buffer ($C_0=32$ mg/l for 0, 50, 100 rpm and $C_0=31$ mg/l for 150 rpm) [181]	73
2.16	Mass evolution inside the polymer matrix during dissolution time. Drug and polymer mass evolution are depicted in green and water mass evolution is depicted in blue, and the red color shows the percentage of the drug released [188]	74

LIST OF FIGURES

2.17	Release of Amoxicillin from whole tablet surface plotted according to Hopfenberg equation: (●) predicted values calculated according to Hopfenberg equation; (○) observed data; (+) predicted and observed (when the two points overlap), Tablet composition; 15% Methocel K4M+5% PEG 4000 [197]	77
2.18	Schematic of a drug-eluting stent and its different layers and the contact mediums . . .	79
2.19	(a) Experimental and theoretical(BR model) R6G release profile from PEGylated nanoparticles at different temperatures, (b) experimental and theoretical (BRD model) drug release profile from PLGA nanoparticles at different temperatures [208]	80
2.20	Model simulation matches experimental data of sirolimus release from PLGA coating [162]	81
2.21	Normalized drug concentration distribution (a) in the premier study with considering constant drug concentration, at the second study with varying concentration (b) at steady-state flow rate and (c) pulsed flow pattern [80]	82
2.22	(a) velocity field [m/s] in concentric (left) and eccentric (right) stenosis models, (b) Normalized drug concentration distribution into the arterial wall in concentric (left) and eccentric (right) stenosis models after one month [221]	84
2.23	Illustration of convolution and deconvolution in IVIVC development [224]	85
2.24	(a) In vitro and (b) in vivo, release profiles of paclitaxel and sirolimus from PLGA/ACP coated stents [154]	86
2.25	Comparison of the in vitro and in vivo profiles with time-scaling factor [127]	86
2.26	In vitro release profiles of Risperdal Consta 25 mg long acting injection (risperidone microspheres) in 0.05 M PBS pH 7.4 at 37°C (time scaled) and 45°C (n = 3). Insert shows linear correlation between real time (37°C) and accelerated (45°C) fraction released [231]	87
3.1	Chemical formula of (a) PU and (b) PLGA	91
3.2	Chemical formula of (a) epolamine and (b) diclofenac sodium	91
3.3	Fabrication process of PU samples loaded with DE	92
3.4	Pressure waveforms at different heart rates [233]	94

LIST OF FIGURES

3.5	Flow rate waveforms for different pulse rates [233]	95
3.6	Schematic of the bio-relevant apparatus	95
3.7	Geometric parameters and the hydraulic design of (a) the impeller and (b) the volute [235]	97
3.8	Characteristics of the pressure-flow rate for diverse speed of rotation of the impeller [235]	97
3.9	Centrifugal pump for generating the pulsed flow [235]	98
3.10	Loop of the command of pulsed flow and regulator of the number of pulses per minute	98
3.11	Loop for capturing the values of pressure, flow rate and temperature in Labview . . .	100
3.12	LabView program showing the command of the pulse to the pump (on the left) and acquisition of the flow rate and pressure during a pulsed test (on the right)	100
3.13	Schematic of the chambers	101
3.14	Compartment containing the hydrogel and the polymeric samples	103
3.15	(a) Absorption peaks obtained from some of the diclofenac sodium concentration in PBS with UV-Vis, (b) Calibration curve obtained for diclofenac sodium in PBS . . .	103
3.16	Algorithm showing the protocol of the gravimetry method	105
3.17	Procedure to measure the diffusion coefficient of drug in gel	108
4.1	DSC results of polyurethane and DE	111
4.2	DMTA curve of pure PU	111
4.3	Tensile properties of three non-charged PU samples	112
4.4	FTIR spectra of (a) PU and (b) diclofenac epolamine and (c) PU-DE sample	113
4.5	SEM images of (a) non-loaded PU from the side of the sample (b) diclofenac epolamine and (c) PU sample loaded with 10%DE	114
4.6	DSC of PLGA-pure and diclofenac sodium	114
4.7	DMTA results of pure PLGA	115
4.8	Tensile test curve of pure PLGA	116
4.9	FTIR results of (a) pure PLGA and (b) diclofenac sodium (c) PLGA-DS film	117

LIST OF FIGURES

4.10	DSC of (a) PLGA-pure, (b) diclofenac sodium powder and (c) diclofenac sodium in the PLGA-10%DS film after sample preparation	118
4.11	Concentration profiles of DS in hydrogel at different distances of diffusion after different time intervals at static state	119
4.12	Mass loss of the polymeric samples of PLGA-10%DS during the drying in the TGA versus the time of drying	120
4.13	Optical images of the PLGA films after drying of 300 minutes at the temperatures of (a) 23°C and (b) 40°C	121
4.14	Drug release results of the PLGA-10%DS prepared at different drying temperatures of 23°C, 40°C, 45°C and 50°C, and released at the temperature of 37°C in PBS at the flow rate of 7.5 ml/s	122
4.15	Cumulative drug release curves from PU-10%DE at the flow rate of 7.5 ml/s for two different thickness of samples, 2 and 0.3 mm, in accordance to the release time	122
4.16	(a) Water absorption and (b) Drug release percentage for PU with different percentage of DE in flow-less state	124
4.17	(a) Water absorption and (b) Drug release for different percentage of drug at steady flow with flow rate of Q=7.5 ml/s	125
4.18	SEM micrographs: (a) DE (b) PU-10%DE (300 μm) (c) PU-10%DE (1 mm) (d) PU-20%DE (1 mm) and (e) PU-30%DE (1 mm) from the thickness side of the samples after one hour of the test at the flow rate of 7.5 ml/s	126
4.19	Cumulative drug release curves from PU-10%DE at the flow rate of 7.5 ml/s for two different percentages of 10% and 20% DE versus to the release time	128
4.20	Micrographs of the (a) PU-10%DE and (b) PU-20%DE at Q7.5 after drug release of 96h from the side and (c) PU-10%wt and (d) PU-20%wt from the surface side	128
4.21	Comparison of the gravimetry method with UV-Vis method for PU-10%DE-Q7.5	129
4.22	Cumulative drug release from PLGA films with 5% and 10% DS at Q=0 ml/s	131
4.23	Water absorption percentages for PLGA-Pure, 5% and 10% DS at the static state	132

LIST OF FIGURES

4.24	Optical microscopic observations of the samples (a) PLGA-5%DS after 12 hours, (b) PLGA-5%DS after 48 hours, (c) PLGA-10%DS after 12 hours, (d) PLGA-10%DS after 48 hours, (e) PLGA-10%DS after 12 hours from the edge of the sample, of drug release test in the static state	133
4.25	(a) Water absorption and (b) drug release for PU with 10% of DE at different flow rates	134
4.26	Cumulative drug release curves from PU-10% DS at the flow rate of 0 and 7.5 ml/s	135
4.27	Gradient of concentration at t and $t+\varepsilon$ for the static and continuous flow rate	135
4.28	Cumulative drug release from PLGA films with 10% DS at the flow rates of 0, 6.5, 7.5 and 15 ml/s	137
4.29	SEM micrographs of PLGA-10%DS after 48 hours of drug release at (a), and (c) the flow rate of 0, (b), and (d) flow rate of 7.5 ml/s, but at different magnifications	138
4.30	Water absorption percentages for PLGA pure, 5% and 10% at flow rates of (a) 0 and (b) 7.5 ml/s	139
4.31	Algorithm for defining the mechanisms contributed during the release from a drug loaded carrier	140
4.32	Step analyzing by Higuchi model for the experimental tests of drug release with different drug loads (10, 20, and 30%) at the (a) static condition, (b) continuous state with the flow rate of 7.5 ml/s and (c) continuous state with the flow rate 23.5 ml/s	142
4.33	Regression results of (a) PU-10, 20, 30%DE-Q0 and (b) PU-10, 20, 30%DE-Q7.5 in two steps with Korsmeyer- Peppas model	143
4.34	Contribution of diffusion versus the time of release at (a) different flow rates for the PU-10%DE (b) different initial drug percentages at the flow rate of 7.5 ml/s	144
4.35	DMTA curve of PU loaded 10% mass of DE at various times and flow-less state	149
4.36	(a) Multi frequency DMTA tests: glass transition temperature evolution of PU-10%DE sample and (b) linear regression of WLF equation for PU-Pure, PU-10%DE, PU-20%DE	150
4.37	Stress-strain curves of PU samples with (a) 0 and (b) 10%DE, at the flow rate of zero and (c) 0, (d) 10%DE and (e) 20%DE at the flow of 7.5 ml/s, at different time intervals	151

LIST OF FIGURES

4.38	Material characteristics of the PU samples with different percentages of DE after release test in the static and continuous state	153
4.39	Glass transition temperature of the PLGA-Pure, PLGA-5%DS and PLGA-10%DS after different time intervals of incubation tests	155
4.40	Multi frequency DMTA tests: glass transition temperature evolution of pure PLGA and (b) linear regression of WLF equation on the results obtained from DMTA tests for the PLGA samples	156
4.41	FTIR spectroscopy after (a) static and (b) continuous drug release for PLGA pure after certain time of incubation	157
4.42	Micrographs of the PLGA samples in PBS at zero flow rate after (a) 0, (b) 1, (c) 12, (d) 24, (e) 48 hours	158
4.43	Stress-strain curves of the tensile test for the samples of PLGA (a) pure, (b) 5%, and (c) 10%DS after incubation in the static state	159
4.44	Stress-strain curves of the PLGA (a) pure and (b) 10% DS after release test at the flow rate of 7.5 ml/s	160
4.45	Material characteristics of PLGA samples with different percentages of DS after drug release test in the static and continuous state	161
4.46	Tensile test of the PLGA with 10% of DS after 1 and 24 hours of drug release test at static state	162
4.48	SEM micrographs of the PLGA-10%DS after drug release of 48h in the static state after tensile test with the magnification of (left) 1 mm and (right) $200 \mu\text{m}$	163
4.47	SEM micrograph of the PLGA-10%DS before release test	163
4.49	Schematic of the variation of the polymer properties during and after drug release	164
4.50	Cumulative drug release curves in media and hydrogel from (a) PU-10%DE (b) PLGA-10%DS at at the flow rate of 7.5 ml/s in accordance to the release time,	166
4.51	Polymer film contacted (right) from one side with a gel and the other side with the lumen flow, (left) from one side with impermeable surface and the other side with the lumen flow	167

LIST OF FIGURES

4.52	Schematic of the hydration of the polymeric samples in the contact with or without the hydrogel and the fluid circulating in the system	167
4.53	Flow rates related to the three patterns of the flow performed in this study (corresponding to the flow in the carotid artery)	168
4.54	Drug release from the PLGA films with 10% DS at different flow rates in (a) PBS, (b) gel	169
4.55	SEM micrographs of PLGA-10%DS samples after 48h for (a) pulsed flow and (b) steady flow at 7.5 ml/s	170
4.56	Schematic representing the thickness of boundary layers created at two different flow rate (right figure is for the case with higher flow rate than the left figure)	170
4.57	Probable pathways of the drug to the release medium	171
4.58	Drug release results from PLGA-10% DS to the (a) PBS medium, (b) hydrogel, at the pulsed flow with and without presence of metal layer	173
4.59	Hydration of the polymeric samples in contact with fluid and hydrogel with and without the presence of metal layer	173
4.60	Representing the mechanisms contributed to the drug release at the (a) initial and (b) late time of hydration of the polymeric samples	174
4.61	Schematic of the position of the polymer + metal layer on the hydrogel and the two slices chosen for the analysis	174
4.62	Qualitative distribution of phosphorescence in the hydrogel (slice 1 shown in figure 4.61)	175
4.63	Qualitative distribution of phosphorescence in the hydrogel (from the slice 2 shown in figure 4.61)	175
5.1	Common release profiles and steps during the release	179
5.2	Release profile of a certain drug in a certain polymeric matrix	180
5.3	One step fitting of data results with different mathematical models	181
5.4	(a) Step defining for the release profile of the figure 5.2 by the aid of the Higuchi model (b) Reconstruction the data points by using Higuchi fit	181

LIST OF FIGURES

5.5 (a) Step defining by the aide of Douglas-Peucker algorithm and the constants needs for defining the model (b) reconstruction the data points by using model 182

5.6 Cumulative release of DE from PU matrix in (a) $Q = 0\text{ ml/s}$ (b) $Q = 7.5\text{ ml/s}$ and (c) $Q = 23.5\text{ ml/s}$ 183

5.7 Experimental results obtained from PU-10%DE at (a) $Q = 0\text{ ml/s}$, (b) $Q = 7.5\text{ ml/s}$, (c) $Q = 23.5\text{ ml/s}$, and traced in the form of $\text{Log}(M_t/M_{95\%})$ versus to the $\text{Log}(t/t_{95\%})$ 184

5.8 Correlation between the values of $n_i = n_1$ and reduced Reynolds number 185

5.9 (a) Correlation between the values of the maximum time of the release in accordance to the drug concentration (fitting equation: $y = -A \times \text{Ln}(C\%) + B$) (b) Values of coefficients obtained from figure 5.9 (a) versus to the \overline{Re} number 186

5.10 Experimental data obtained with (a) PU-10 and 20% DE at the flow rate of 6.5 ml/s , R^2 are respectively 0.99 and 0.98 (b) PU-15%DE at the flow rate of 7.5 ml/s , $R^2 = 0.98$; at $T=37^\circ\text{C}$ 187

5.11 Results for predicting the release behavior of different percentage of DE in the matrix of the PU at the flow rate of 7.5 ml/s 187

5.12 Impact of the initial drug loading of PLGA: relative dexamethasone release kinetics [266] 188

5.13 Experimental results obtained from dexamethasone release from PLGA (a) 2.5 %, (b) 5%, (c) 10% of drug, traced in the form of $\text{Log} M_t/M_i$ versus to the $\text{Log} t/t_i$ 189

5.14 Correlation between the values of (a) n_1 , (b) n_2 , (c) $M_{max(i=1)}$, (d) $M_{max(i=2)}$, (e) $t_{max(i=1)}$, (f) $t_{max(i=2)}$, versus to the concentrations of 2.5%, 5% and 10% of dexamethasone 190

5.15 Data experimental of the study [266] and the predicted curves of the model 191

5.16 Comparing the data release of [267] with the model 192

5.17 Flowchart of the proposed method 193

5.18 Schematic of the phenomena occurring during the release. Yellow prism is the polymer matrix, white spheres are the drug particles on the surface contact in fluid medium, golden spheres are inside the polymeric matrix and the arrows show the direction of the flow from inside out or inverse to the matrix 193

LIST OF FIGURES

5.19	Comparing the calculated values with the equation 16 and the experimental data of diclofenac release from the PU matrix, (a) for three different drug concentrations; 10, 20, and 30% at the flow rate of 7.5 <i>ml/s</i> (b) and for the PU with 20% of drug at the flow rates of 0, 7.5, and 23.5 <i>ml/s</i>	197
5.20	Contribution of each mechanism during the drug release from PU films with the three different percentages of the drug at the flow rate of 7.5 <i>ml/s</i>	199
5.21	The variation of the release parameters (▲ diffusion coefficient, ■ kinetic of burst, ● osmotic pressure) for the drug release from PU films with the three different percentages of the drug (10, 20, and 30%) at the flow rate of 7.5 <i>ml/s</i>	200
5.22	Comparison of the values of free volume fraction and osmotic pressure at the flow rate of 7.5 <i>ml/s</i> for the samples with three different drug concentrations (● PU-30%DE, □ PU-20%DE, ▲ PU-10%DE)	200
5.23	Contribution of each mechanism during the drug release from PU-20%DE of the drug at the different flow rates of 0, 7.5 and 23.5 <i>ml/s</i>	201
5.24	The variation of the release variables (▲ diffusion coefficient, ■ kinetic of burst, ● osmotic pressure) for the drug release from PU films with the 20 percentage of the drug at the different flow rates of 0, 7.5 and 23.5 <i>ml/s</i>	202
5.25	Comparison of the values of permeability and osmotic pressure for samples of PU-20%DE at three different flow rates of 0, 7.5 and 23.5 <i>ml/s</i>	202
5.26	Correlation between (a) diffusion coefficient, (b) burst constant, (c) osmotic pressure versus the concentration	203
5.27	Correlation between (a) diffusion coefficient, (b) burst constant, (c) osmotic pressure versus to the flow rate	203
5.28	Comparison of the predicted release profile obtained by the model and the experimental data for the case (a) PU-15%DE-Q7.5 <i>ml/s</i> , (b) PU-20%DE-Q6.5 <i>ml/s</i>	204
5.29	Experimental drug release from the PLGA matrix with 10%DS at the flow rates of 0, 6.5 and 15 <i>ml/s</i>	204
5.30	Comparing the optical observation of the PLGA-10%DS-Q6.5 after (a) 1h and (b) 24h	206

LIST OF FIGURES

5.31	Experimental drug release from the PLGA matrix with 10% of drug at the flow rates of 0, 6.5 and 15 <i>ml/s</i> with the adjustment models (considering burst, diffusion, swelling and erosion mechanisms)	207
5.32	Experimental drug release from the PLGA-10%DS-Q0, Q6.5, Q15 with the model adjusted with different mechanisms	209
5.33	Exponential fit of the contribution of each mechanisms in drug release vs flow rate	210
5.34	Comparison between the results of the BSDE model obtained by the correlation of the values of the parameters and direct application of the BDSE model for PLGA-10%DS-Q7.5 with the experimental results	211
5.35	Geometrical model of the numerical domain with polymer film	213
5.36	Mesh independence study with different mesh sizes at $t = 0.1 d$	214
5.37	Mesh distribution at (a) inlet of flow channel and (b) around polymer film	214
5.38	Flow topology around polymer film at different flow rate (a) 6.5 <i>ml/s</i> , (b) 7.5 <i>ml/s</i> and (c) 23.5 <i>ml/s</i>	216
5.39	Drug distribution in the mid-plane of the polymer film parallelly to the flow direction at different flow rates (initial drug dosage of 10% and $t = 1 d$)	217
5.40	Drug distribution on the lateral sides of the polymer film at different time for the flow rate of 7.5 <i>ml/s</i> and initial drug dosage of 10%	217
5.41	Drug release from polymer at different flow rate with drug dosage of 10%	219
5.42	Drug release from polymer at different flow rate with drug dosage of 20%	220
5.43	Drug release from polymer at different flow rate with drug dosage of 30%	220
5.44	Drug release from polymer at different flow rate with drug dosage of 15%	221
5.45	Characteristic time versus initial drug concentration at different flow rates	221
B.1	Coronary restenosis after coronary angioplasty with the balloon [24]	267
B.2	Resténose coronaire intra-stents après angioplastie coronaire avec les stents métalliques nus [24]	268

LIST OF FIGURES

B.3	Thrombose tardive après stents à élution médicamenteuse, adoptée et modifiée à partir de [24]	268
B.4	Les sections transversales de l'entretroise de stent à élution médicamenteuse, (a) est une entretroise DES avec une matrice polymère chargée de médicament et l'entretroise de stent (b) a un moyen de transport couche de finition régulatrice [97]	273
B.5	Aperçu schématique de la configuration de test in vitro (A) et photographie du vFTC équipé d'un gel d'agarose à 2 (B); 1) vFTC, 2) conteneur de média, 3) PBS de pH 7,4, 4) palette agité à 50 tr/min, 5) pompe péristaltique, 6) bain-marie chauffé, a) billes de verre, b) disque en acier inoxydable, c) hydrogel [140]	282
B.6	(a) Installation d'incubation réalisée dans des flacons en verre de 100 ml. Les cellules à flux continu ont été équipées d'un hydrogel d'agarose à base d'eau déminéralisée (vFTC (eau désionisée)) ou ont fonctionné sans deuxième compartiment (FTC). (b) triamtérène des revêtements de stents dans les médias au fil du temps avec un écoulement simulant le vaisseau cellule, cellule à écoulement continu (USP 4) ou appareil à palettes (USP 2); débit 35 ml/min, vitesse de pagaie 50 tr/min [35, 159]	283
B.7	Distribution de concentration de médicament normalisée (a) dans la première étude en considérant une concentration de médicament constante, dans la deuxième étude avec une concentration variable (b) à un débit à l'état d'équilibre et (c) un schéma de flux pulsé [80]	285
B.8	(a) Absorption d'eau et (b) pourcentage de libération de médicament pour le PU avec un pourcentage différent de DE à l'état sans écoulement	288
B.9	(a) Absorption d'eau et (b) Libération de médicament pour différents pourcentages de médicament à débit constant avec un débit de $Q=7.5\text{ ml/s}$	289
B.10	Micrographies SEM : (a) DE (b) PU-10%DE (300 μm) (c) PU-10%DE (1 mm) (d) PU-20%DE (1 mm) et (e) PU-30%DE (1 mm) du côté épaisseur des échantillons après une heure de test au débit de 7,5 ml/s	290
B.11	Libération cumulative de médicament à partir de films PLGA avec 10% DS aux débits de 0, 6,5, 7,5 et 15 ml/s	293

LIST OF FIGURES

B.12 Micrographies SEM de PLGA-10%DS après 48 heures de libération du médicament en (a) et (c) le débit de 0, (b) et (d) un débit de 7,5 <i>ml/s</i> , mais à différents grossissements	294
B.13 Courbes contrainte-déformation des échantillons PU avec (a) 0 et (b) 10%DE, au débit de zéro et (c) 0, (d) 10%DE et (e) 20%DE au débit de 7,5 <i>ml/s</i> , à différents intervalles de temps	296
B.14 Caractéristiques matérielles des échantillons PU avec différents pourcentages de DE après test de libération à l'état statique et continu	298
B.15 Micrographies des échantillons PLGA en PBS à débit nul après (a) 0, (b) 1, (c) 12, (d) 24, (e) 48 heures	301
B.16 Spectroscopie FTIR après (a) libération statique et (b) continue du médicament pour le PLGA pur après un certain temps d'incubation	302
B.17 Courbes contrainte-déformation de l'essai de traction pour les échantillons de PLGA (a) pur, (b) 5%, et (c) 10%DS après incubation à l'état statique	302
B.18 Courbes contrainte-déformation du PLGA (a) pur et (b) 10% DS après test de libération au débit de 7,5 <i>ml/s</i>	303
B.19 Caractéristiques matérielles des échantillons PLGA avec différents pourcentages de DS après test de libération du médicament à l'état statique et continu	304
B.20 Micrographies SEM du PLGA-10%DS après libération du médicament de 48h à l'état statique après essai de traction avec un grossissement de (gauche) 1 <i>mm</i> et (droite) 200 μm	306
B.21 Débits liés aux trois modèles de flux réalisés dans cette étude (correspondant au flux dans l'artère carotide)	308
B.23 Libération de médicaments à partir des films PLGA avec 10% DS à différents débits dans (a) PBS, (b) gel	309
B.24 Micrographies SEM d'échantillons PLGA-10%DS après 48h pour (a) un débit pulsé et (b) un débit constant à 7,5 <i>ml/s</i>	310
B.25 Schéma représentant l'épaisseur des couches limites créées à deux débits différents (la figure de droite est pour le cas avec un débit plus élevé que la figure de gauche)	311

LIST OF FIGURES

B.26 La libération du médicament résulte du PLGA-10% DS vers (a) le milieu PBS, (b) l'hydrogel, au débit pulsé avec et sans présence de couche métallique 314

B.27 Hydratation des échantillons polymériques en contact avec fluide et hydrogel avec et sans présence de couche métallique 314

B.28 Représenter les mécanismes qui ont contribué à la libération du médicament au moment (a) initial et (b) tardif de l'hydratation des échantillons polymères 315

B.29 Schéma de la position de la couche polymère + métal sur l'hydrogel et les deux tranches choisies pour l'analyse 316

B.30 Distribution qualitative de la phosphorescence dans l'hydrogel (tranche 1 représentée sur la figure B.29) 316

B.31 Répartition qualitative de la phosphorescence dans l'hydrogel (à partir de la tranche 2 représentée sur la figure B.29) 317

B.32 Cumulative release of DE from PU matrix in (a) $Q = 0 \text{ ml/s}$ (b) $Q = 7.5 \text{ ml/s}$ and (c) $Q = 23.5 \text{ ml/s}$ 320

B.33 Résultats expérimentaux obtenus à partir de PU-10%DE en (a) $Q = 0 \text{ ml/s}$, (b) $Q = 7,5 \text{ ml/s}$, (c) $Q = 23,5 \text{ ml/s}$, et tracé sous la forme du journal ($M_t/M_{95\%}$) par rapport au journal ($t/t_{95\%}$) 321

B.34 Corrélation entre les valeurs de $n_i = n_1$ et réduite Le numéro de Reynold 322

B.35 (a) Corrélation entre les valeurs du temps maximum de libération en fonction de la concentration du médicament (équation d'ajustement : $y = -A \times \text{Ln}(C\%)+B$) (b) Valeurs des coefficients obtenues à partir de la figure reff4.9 (a) par rapport au nombre \overline{Re} 324

B.36 Les données expérimentales obtenues avec (a) PU-10 et 20% DE au débit de 6.5 ml/s , R^2 sont respectivement de 0.99 et 0.98 (b) PU-15%DE au débit taux de $7,5 \text{ ml/s}$, $R^2 = 0,98$; à $T=37^\circ\text{C}$ 324

B.37 Résultats pour prédire le comportement de libération de différents pourcentages de DE dans la matrice du PU au débit de 7.5 ml/s 325

B.38 Organigramme de la méthode proposée 326

LIST OF FIGURES

B.39 Libération expérimentale de médicament à partir de la matrice PLGA avec 10% de médicament aux débits de 0, 6,5 et 15 ml/s avec les modèles d'ajustement (compte tenu des mécanismes d'éclatement, de diffusion, de gonflement et d'érosion)	329
B.40 Libération expérimentale de médicament à partir du PLGA-10%DS-Q0, Q6.5, Q15 avec le modèle ajusté avec différents mécanismes	332
B.41 Comparaison entre les résultats du modèle BSDE obtenus par la corrélation des valeurs des paramètres et application directe du modèle BDSE pour PLGA-10%DS-Q7.5 avec les résultats expérimentaux	333
B.42 Modèle géométrique du domaine numérique avec film polymère	335
B.43 Répartition des mailles à (a) l'entrée du canal d'écoulement et (b) autour du film polymère	336
B.44 Topologie d'écoulement autour du film polymère à différents débits (a) 6,5 ml/s , (b) 7,5 ml/s et (c) 23,5 ml/s	338
B.45 Répartition du médicament dans le plan médian du film polymère parallèlement à la direction du flux à différents débits (dose initiale de 10% et $t = 1 d$)	339
B.46 Répartition du médicament sur les faces latérales du film polymère à différents instants pour un débit de 7,5 ml/s et un dosage initial du médicament de 10%	340
B.47 Libération de médicament à partir d'un polymère à différents débits avec un dosage de 10%	342

LIST OF FIGURES

Chapitre 1

Introduction

Content

1.1	Motivation	33
1.2	Thesis objectives	37
1.3	Thesis outlines	38
1.4	Thesis main achievements	39

1.1 Motivation

The cardiovascular system is composed of the heart, network of blood vessels (arteries, veins, and capillaries) and blood. In this complex system, the heart plays the role of a displacement pump that pulses and sets blood into motion in the different vessels with an average flow rate at rest of about 5.4 l/min. The cardiovascular system is prone to severe diseases such as atherosclerosis (hardening of the artery by the formation of lipid plaque inside a blood vessel), which may lead to the partial or complete obstruction (called ischemia) of the blood flow through the circulatory system. Referring to the literature, coronary artery diseases are among the most important causes of death in the recent decades. They will affect about 23.4 million people between now and 2030 [1]. To overcome this problem, scientific advances are in process. They started about 40 years ago and the techniques continue to improve today: balloon angioplasty, bare stent, drug-eluting stent, bioresorbable stent. Figure 1.1 summarises the different stents from the material view [2–10].

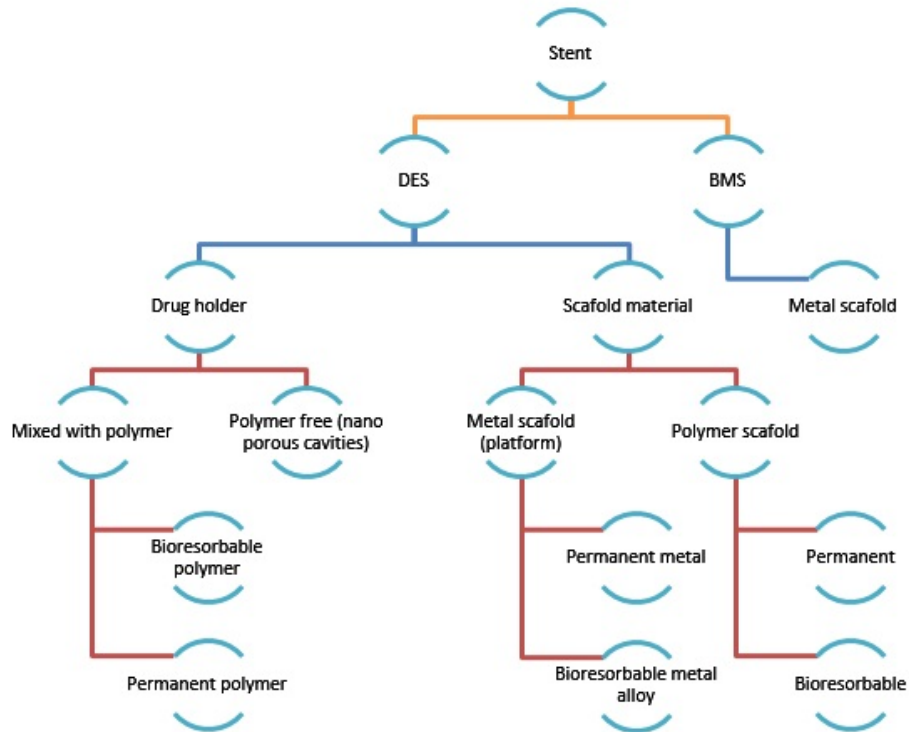


FIGURE 1.1 – Schematic of the material choice in the various stents [2–10]

As we know, a stent act as a foreign object for our immune system and this one may respond to this intrusive object in a variety of ways: macrophages (white blood cells) accumulate around the stent, and nearby smooth muscle cells (SMC) proliferate, disrupting the process of endothelialization; migration and proliferation of vascular SMC from the media to the intima, generating an extra cellular matrix layer in the intima (intimal hyperplasia) followed by a narrowing of the luminal area [11, 12]. It is likely that the phenomenon of thickened intima is due to the leukocytes that adhere to the activated endothelium and disrupt its recovery [1, 13–15]. In some cases, the vessel may fail due to the formation of a blood clot called thrombosis as a response of the endothelium to the mechanical forces and shear stresses (to tear and splinter the atherosclerotic plaque) caused by the stent apposition procedure that can denude the intima layer and cause some bleedings [13, 16]. Whilst the intima layer exists denuded, it is rapidly targeted by an inflammatory response, increasing the death of the cells [11]. Endothelial denudation during the angioplasty is unavoidable, which is the reason neointimal hyperplasia always occurs. However, an intact endothelium is needed to control vascular SMC proliferation and prevent

1.1. MOTIVATION

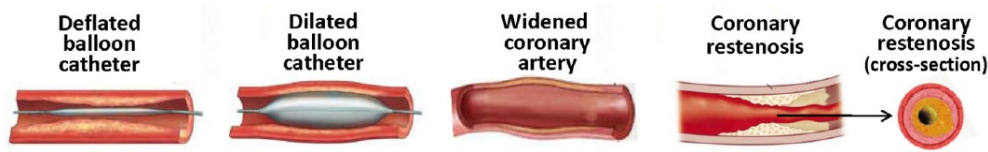


FIGURE 1.2 – Coronary restenosis after coronary angioplasty with the balloon [24]

the thrombus formation [17, 18].

Stent thrombus (ST) is one of the major complications of the angioplasty. It is reported in 2010 that annually about 0.3-0.6 % of stenting with DES is followed by stent thrombosis followed by an increased human mortality by 10-30% [19]. Stent malapposition, late or incomplete re-endothelialization and polymer induced inflammation are the main reasons for the inflammation and late thrombosis [7, 11, 20].

The feasible way to decrease the ST is to prevent the risk of bleeding after stenting using anticoagulants and antiplatelet agents (the healthy endothelium also affords the anti-inflammatory support due to natural anticoagulant protein C [13]). Maintaining the dose of drug during the therapy can minimize the risk of thrombosis [21]. To overcome these problems, the amount of drug, its type and its delivery strategy should be optimized.

The very first angioplasties, based on balloon expansion in the artery, faced the problems of elastic recoil and neointimal hyperplasia and were the reason of 40-60% of restenosis in the years 1977-90 [22, 23]. Figure 1.2 shows the phenomenon of restenosis after angioplasty with only balloon.

It is noteworthy that there are second generations of balloons coated with drugs, commonly paclitaxel, to overcome in-stent restenosis. In this case drug should be transferred rapidly during the contact of the balloon with the vessel wall, which lasts approximately one minute. Some researchers are interested in this technic as this method decreases the risk of bleeding, avoids the risky presence of a foreign object in the body and limits the side effects [25]. However, this method was not completely developed for various reasons, mainly because of the promising results of the stents. The first generation of stents were bare metal stents wherein the incidence of restenosis decreased to 20-30% due to the elimination of elastic recoil between 1991-2003 (figure 1.3) [26–28].

In order to decrease further the cases of restenosis and neointimal hyperplasia, the second generation of stents appeared in 2003 [29]: the drug-eluting stents. These stents were coated by a polymer

1.1. MOTIVATION

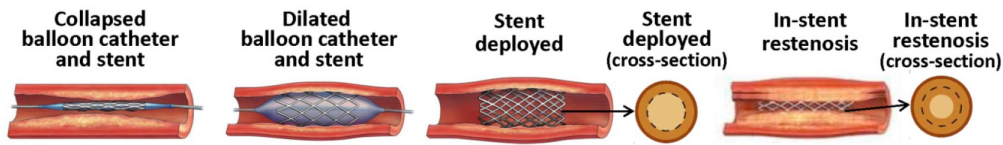


FIGURE 1.3 – In-stents coronary restenosis after coronary angioplasty with the bare metal stents [24]

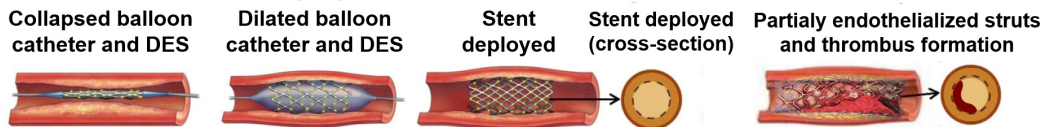


FIGURE 1.4 – Late thrombosis after drug-eluting stents, adopted and modified from [24]

layer containing an active substance used to reduce neointimal hyperplasia. The incidence of restenosis decreased to about 3-20 % (shown in figure 1.4).

The scenario does not end here and DES have not yet supply all the demands in angioplasty. Although the use of DES rather solved the problem of restenosis, the issues of denuded intima and the related inflammation and thrombosis still persist and open a wide range of research about it [13, 18, 30].

These problems could be solved thanks to an optimization of the drug release kinetics (which firmly affects the drug maintenance in the tissue wall and influences the vascular healing and therapy process) and the stent apposition in the vessel [31]. Drug distribution in the arterial wall depends on many parameters such as the type of drug and its initial concentration, drug release rate into the arterial wall, drug solubility, particle size, binders, wetting, properties of the polymer matrix, coating methods, eluting direction, coating thickness, pore sizes in the coating, release conditions (release medium, temperature, pH), Reynolds's number and blood flow kinetics, ... [1, 32–34]. Optimizing these parameters and investigating their effects can improve the kinetics of the drug release during the therapy. Current researches in this regard based on human and animal models confront several limitations. The inability to perform regular in vivo tissue and blood samples decreases the possibility to investigate the drug release and characterize the drug carrier during the release time.

Furthermore, in vivo experiments usually focus on the levels of drugs in the blood instead of the concentration of drugs in the wall of the blood vessel, although this is the aim of the therapy [35].

However, the drug concentration in the tissue can only be calculated following stent removal in animal models. Many studies have shown that reducing the risk of sacrificing the living body as well as reducing the costs of in vivo trials has not been possible without increasing the accuracy of in vitro testing. In addition, using the ex vivo environment has been one of the most effective ways to analyze the physical, chemical, mechanical, and other properties of the tissue in interaction with the implanted biomaterial. Although these methods cannot exactly replicate the conditions that occur inside a living organism, they can, however, mimic the in vivo conditions and lead to reliable testing results by providing controlled environments. Therefore reproducing similar conditions remains an enormous challenge for the researchers. Further, the kinetics of the drug release can be modeled and estimated by mathematical and, or, physical models which can help to predict the release profile under different conditions.

1.2 Thesis objectives

The general aim of this work is to develop an in vitro bio-relevant and a robust modeling allowing the characterization the models of drug carriers. In which the impact of the design choices and the properties of the two mediums mimicking the blood circulation and the arterial wall on the release of the drug is considered. The work focuses on in vitro studies, which are less complex and more reproducible than in vivo conditions and it develops into three objectives:

i. Development of a bio-relevant apparatus in order to optimize some control parameters approaching in vivo conditions as close as possible, such as considering a tissue compartment and generating a systolo-diastolic flow pattern;

ii. Analysis and quantify the effect of some factors like; the flow conditions of artificial blood, drug delivery system components, biodegradable and non-biodegradable polymer coating, or hydrophilic and hydrophobic type of drug on the in vitro release tests, and;

iii. Development and validation of models allowing to simulate and predict the release profile as functions of some factors like, the initial drug loading or flow rate. These models permit in order to make design choices for new systems of drug delivery in function of the desired release profile.

1.3 Thesis outlines

The rest of this thesis comprises five chapters.

Chapter 2 provides a bibliographic review about the state of art of the drug-eluting stents in terms of geometrical shape, coating material, drug release model, parameters influencing the drug release kinetics and the particular numerical studies.

Chapter 3 presents the experimental materials and methods developed during this thesis. In the first section, we explain our choices concerning the materials used to model the polymer-matrix and the selected drugs. The second section presents the bio-relevant apparatus designed to perform the tests. The third section describes the procedure adopted for samples manufacturing. We present in the fourth section the methods implemented for the determination of the release kinetic-profiles. The description of the other physical and mechanical characterization tools, allowing more robust analysis and explanation of the mechanisms involved, is the subject of the fifth section.

Chapter 4 presents the experimental in vitro release tests performed on various conditions to investigate the effect of these factors on the polymer carriers and, in consequence, on the release behavior. The first section discusses about the primary characterization of materials used in this study. The second section presents the effect of the diverse factors influencing the in vitro drug release in the artificial lumen, their mechanisms of the release and also evaluation of the mechanical, physical and chemical properties of the polymeric drug carrier during the release. Ultimately, the last section represents the effect of some parameters like pulsed flow and artificial tissue layer in the release profile.

The improvement of mathematical models simulating the spatio-temporal behavior of drug delivery systems will make it possible to reduce their development time. Therefore, in a chapter V, we have focused on various types of modeling: empirical, mechanistic and also numerical simulation. The first section of this chapter is related to a mathematical model based on the release kinetics. This predictive model considers two parameters: the flow rate and the initial concentration. The second part proposes a mechanistic model based on the physical mechanisms involved in the release from the drug delivery carriers. Ultimately, the third part is devoted to a numerical simulation and a comparison of their results with the experimental results used in the first section for the kinetic model.

Finally, in chapter 6, the outstanding accomplishments achieved in this thesis are presented and summarily possible improvements of the investigated strategies and suggestions for future work are

detailed.

1.4 Thesis main achievements

According to the bibliography, a lot of work has been done in the field of drug delivery. It can be deduced from these studies that, due to the great importance of intrinsic properties of the compounds of drug carriers in the release profile, researchers have recently begin to study and analyze more precisely the stent materials rather than directly examine drug release profile from a final commodity. This approach is very helpful in choosing the design parameters.

Compared to oral drug delivery, for which the advances are highly significant, the improvements in the case of stents are still rather slow.

Among the elements to progress in this area, a bio-relevant device that can simulate real conditions is required; this device can be helpful to properly analyze the behavior of the compounds subject to the variation of miscellaneous parameters.

The lack of these points in studies on drug-eluting stents has led us to design a bio-relevant test bench that can approach to real conditions. This device is able to simulate both the lumen and the tissue of the artery. Moreover, this test bench can reproduce the systolo-diastolic flow patterns encountered in blood flows.

This bibliographical review also points out the lack of information concerning the evolution of the main mechanical properties of the polymer. For this reason, two different types of polymers have been investigated mechanically before and during drug release in addition to the main physico-chemical properties.

Besides, mathematical models, which can predict drug release behavior by considering physical and chemical mechanisms associated to the used compounds, can be effective in this regard. To do so, a model to predict the release profile based on the mechanisms associated with release from the different types of polymers was developed. Moreover, an accelerated two-parameter kinetic model, considering the flow rate and the initial drug load, was elaborated.

Finally, many models and simulations are available among the literature but validations based on bio-relevant in vitro tests are missing. In this study, we present also a comparison between a numerical simulation, a mathematical model and experimental results.

1.4. THESIS MAIN ACHIEVEMENTS

Chapitre 2

Literature review

Content

2.1	Drug release mechanisms	42
2.1.1	Physical mechanisms	42
2.1.2	Chemical mechanisms	47
2.1.3	Drug uptake	47
2.2	Design conception of drug-eluting stents	50
2.2.1	Different geometrical models of drug-eluting stents	50
2.2.2	Polymers in the case of drug-eluting stents	53
2.2.3	Drugs in the case of drug-eluting stents	56
2.3	Characteristics of the test condition	57
2.3.1	Release compartment	57
2.3.2	Release test methods	61
2.3.3	Apparatus for release testing	64
2.3.4	Analytical tools to determine drug release	67
2.4	Modelisation and simulation	68
2.4.1	Semi-empirical models	68
2.4.2	Mechanistic model of drug release profile	78
2.4.3	Simulation of drug release profile	81
2.4.4	In vitro-in vivo correlations and acceleration method	83
2.5	Summary	87

This chapter contains a bibliographic review about the state of art of the drug-eluting stents in terms of geometrical shape, coating material, drug release model, parameters influencing the drug release kinetics and the main numerical and analytical studies.

2.1 Drug release mechanisms

There are different mechanisms that can control the drug release in a drug delivery system: dissolution, diffusion, osmosis, degradation, swelling, erosion are among these mechanisms. Their presence depend on the ensemble of the delivery system and may act simultaneously or at different steps of a delivery process. It is common for a system or device to present more than one of them, but the classification of the mechanisms of release is generally based on the main mechanism. Besides the properties of the polymer coating, active substance delivery, kinetics and related mechanisms depends on the type of the active substance and environmental conditions. Some of the key parameters are for example the physical and chemical properties of the active substance, such as molecular weight, water solubility, particle size, viscosity of the solvent, ... [18, 36–38]. Some of these parameters are used in mathematical models in order to help us to predict the release behavior from the drug carriers. Mathematical models have always been one of the most effective ways to improve the design and development of different carriers for the drug delivery system (lower costs as well as less laboratory tests). In addition, they have always been important to determine the mechanisms of drug release and release kinetics from various systems, such as osmotic systems, degradable, or non-degradable systems.

2.1.1 Physical mechanisms

2.1.1.1 Diffusion controlled phenomenon

Diffusion-controlled release mechanism is the common mechanism that exists in the polymeric drug delivery systems. For a non-biodegradable polymer matrix, drug release is due to the concentration gradient by either diffusion (classical Fickian diffusion) or matrix swelling (enhanced diffusion). For biodegradable polymer matrix, release is normally controlled by the hydrolytic cleavage of polymer chains that leads to matrix erosion, even though diffusion may be still dominant when the erosion is slow. In the case of the polymeric matrix wherein the active substance is uniformly dispersed in the matrix, active substance molecules which are nearer to the surface have less distance to migrate and

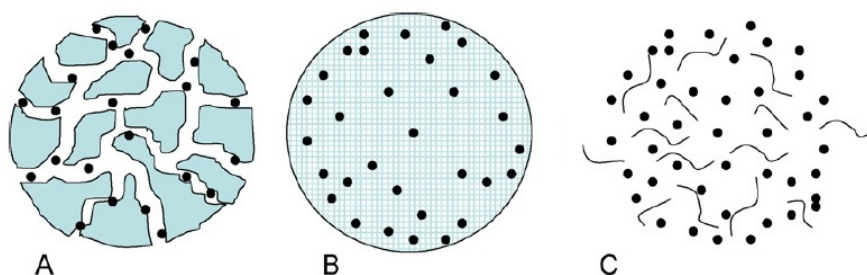


FIGURE 2.1 – Schematic representation release mechanisms: (a) diffusion through water-filled pores, (b) diffusion through the polymer, and (c) erosion [43]

release faster compared to the molecules which are far from the surface. In addition, diffusion in the polymeric matrix happens via two possibilities [39]:

Diffusion through water-filled pores:

It is very dependent on the structure of the polymer, therefore it is dependent on the fabrication process. The pores must be open pores, connected to the surface of the system and large enough so that the solute can go out through them. Diffusion through water-filled pores (figure 4.11 (a)) is the actual type of the release mechanism. Otherwise, the diffusion happens in the polymer, which is the other type of the diffusion, or it would be transported by the osmotic pressure in the case of hydrophilic substance, which will be discussed later.

Diffusion through the polymer:

In this type of mechanism, the rate of release is highly dependent on the physical state of the polymer. Below the glass transition temperature, when the polymer is in glassy state, the release rate is slower than when the polymer is in rubbery state. Moreover, crystalline region of the polymer has a greater potential for sorption and faster kinetics for sorption than amorphous region [40]. Figure 4.11 (b) represents the schematic of this mechanisms. In their study, Raval et al. [41] have stated that this mechanism takes place for both durable and bio-degradable polymeric holders but especially it is the controlling mechanism of release for the durable polymeric holders [42].

2.1.1.2 Physical degradation/erosion

Physical degradation, such as hydrolysis or erosion, are the kind of degradations that can play a role in all polymers. Hydrolytically degradable polymers have the ability to release the carried drug during

2.1. DRUG RELEASE MECHANISMS

the hydrolysis along with the breakage of their bonds [44]. As mentioned above another mechanism is the swelling of the polymers which accompanies the hydrolysis mechanisms. Different parameters affect the degradation of the polymers such as temperature, pH of the medium, molecular weight, geometry, morphology, glass transition temperature and preparation methods of the polymer films [34, 45–47]. Figure 4.11 (c) shows the schematic of this mechanism.

2.1.1.3 Osmosis pressure-based release

This kind of release occurs when the active substance molecules pass through a porous semipermeable membrane. The system of the osmotic pump reservoir consists in an inner core containing the drug and a substance with osmotic activity, coated with a semipermeable membrane. When osmosis occurs, the core volume expands, which pushes the drug solution out through the delivery ports [48]. Apart from the reservoir system, this mechanism can also happen for the polymeric films or micro-particles. In their study, Horkay et al. [49] show the coupling between the osmotic pressure and the swelling phenomenon (see section 2.1.1.4)

Actually due to the hydrophilicity of the polymer network, osmotic pump is occurring and its significance is increased when a hydrophilic solute is deposited in the matrix, as in the case of swelling-controlled release systems [50]. In a study on the swelling of PLGA nano-particles by Gasmi et al. [51], they have stated that when the encapsulated particles are large molecules (therefore unable to diffuse through the polymer), the osmotic pressure is substituted by the swelling. Moreover it was described in [43], that PLGA absorbs a large amount of water because its polymeric structure with mobile chains can easily swell; consequently the significant increase of water content results in an increase in osmotic pressure which can be compensated probably by swelling and polymer chains rearrangement. This mechanism is not based on diffusion and the polymer degradation must be negligible. [52–54]. Figure 2.2 shows a schematic of this mechanism. Figure 2.2 (a) shows the osmotic pump in the reservoir system and figure 2.2 (b) is for the matrix shaped drug delivery systems.

2.1.1.4 Swelling based phenomenon

The polymer swelling is due to the huge quantities of water absorbed by the drug carrier system. The mobility of the macromolecules increases as soon as water diffuses into the polymer; this effect is called polymer chain relaxation. The swelling, depending on the type of the polymer, can produce

2.1. DRUG RELEASE MECHANISMS

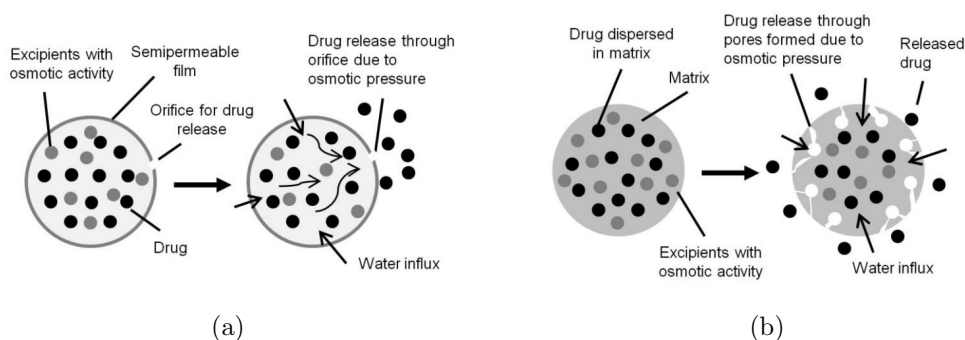


FIGURE 2.2 – Osmosis-controlled release from (a) osmotic pump or (b) monolithic system [55]

two opposite drug release behaviors: it was revealed that the diffusion of the drug in the water-swollen polymer was increased compared to the non-swollen polymer due to the creation of the free volume fraction. However, some studies indicated that the swelling of the non-degradable polymers decreases the release rate because it increases the pathway of the drug in the matrix to reach the release medium [56, 57].

In a study by Ritums [58] one can note that swelling is inseparable from the diffusion. This phenomenon is explained in figure 2.3: initially the films are dry but as soon as they are immersed, the water molecules start to diffuse into the film and therefore the swelling begins. The dry (non-swollen) core of the film imposes a compressive stress on the outer wet (swollen) side inhibiting the inward water diffusion. As long as the core is still dry, the film swells into the external direction (stage I). When water reaches the center of the film, the swelling of the sample can happen in all the directions (stage II), thereafter the diffusion rate increases up to the saturation point.

2.1.1.5 Dissolution based phenomenon

This mechanism of release deeply depends on the type of polymer and can occur in the reservoir form and matrix form drug holders. For hydrosoluble polymers, they degrade rapidly and cannot retain the drug sufficiently long. For polymers which are not dissoluble, they degrade slowly over the time by hydrolysis and can fulfill the delivery function for months. In the literature, it is noted that these mechanisms are observed in the bio-degradable polymers [59, 60]. Figure 2.4 shows an example of the mechanism of the dissolution of a polymer in a solvent. Moreover the mechanism of dissolution does not just relate to the polymer but also to other components in the drug delivery systems such as tablets, capsules, etc.

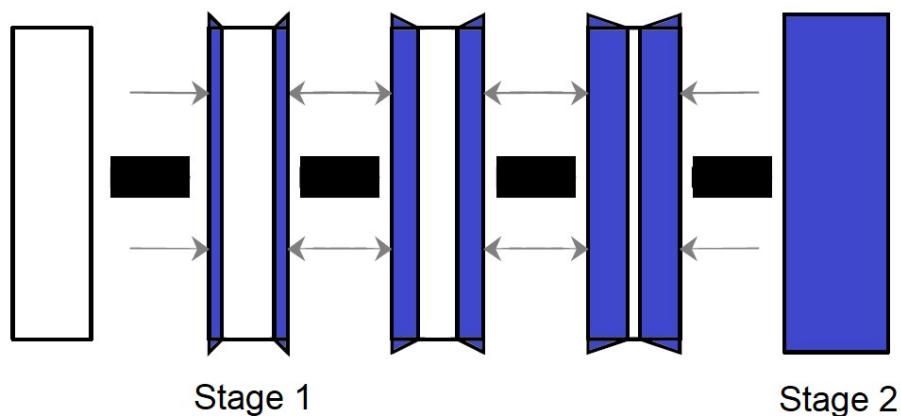


FIGURE 2.3 – Two-stage of swelling [58]

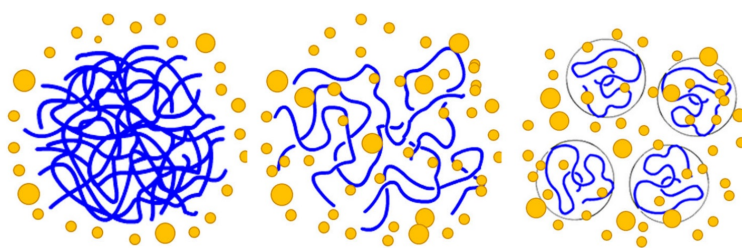


FIGURE 2.4 – Schematic representation of the dissolution process for polymer molecules, blue lines represent polymer chains and yellow dots represent solvent molecules. (a) polymer molecules in solid state just after being added to a solvent; (b) a swollen polymeric gel; (c) solvated polymer molecules dispersed into a solution [61]

2.1.1.6 Ion exchange phenomenon

This mechanism takes place when the polymers are insoluble and have acidic or basic group in their chemical functional groups. In this case, the active substances are bonded to the matrix by electrostatic interactions. The mechanism of release depends on the negative or positive charges of the active substance and of the insoluble polymer. Ions having the same charge as the active substance molecules, substitute with them and give the chance of drug molecules to release. This method is normally used for the oral solid dosage form and it is not recommended for the drugs with short half-life. This mechanism is important for taste masking, improving drug stability, improving physical characteristics of the drug carrier and also for the dissolution of poorly soluble drugs [62–64]. This method is mainly used in the transdermal drug delivery, nasal, oral and ophthalmic drug delivery [65].

2.1.2 Chemical mechanisms

2.1.2.1 Chemical degradation

Most often degradation occurs because of oxidation or enzymatic degradation. Chemical degradation is a kind of release in which the active substance is covalently conjugated to the hydrophilic polymers. This kind of release is referred to as chemical mechanism and is based on enzymatic degradation in the polymer. For this type of release, the kinetics is controlled by the enzyme concentration and by the physico-chemical properties of the medium such as pH. This chemical mechanism does not allow a large variety of parameters in order to control the release [66]. First this phenomenon needs chemical modification of the drug molecules (called prodrug) before its delivery [67]. The degradation by oxidation generally occurs at low temperatures so that thermal degradation is negligible. Consequently, it is typically a very slow reaction and the studies suggest that polymers should not oxidize significantly at normal temperatures [68].

2.1.3 Drug uptake

After the drug release from the polymeric carrier by the different associated physical and/or chemical mechanisms, the released drug is subject to diffusion, advection and binding in the biological tissue [69]. Binding to specific receptors occurs due to the combination of the drug with the components of the biological tissue. Non-specific binding can also happen by trapping the drug in the extracellu-

2.1. DRUG RELEASE MECHANISMS

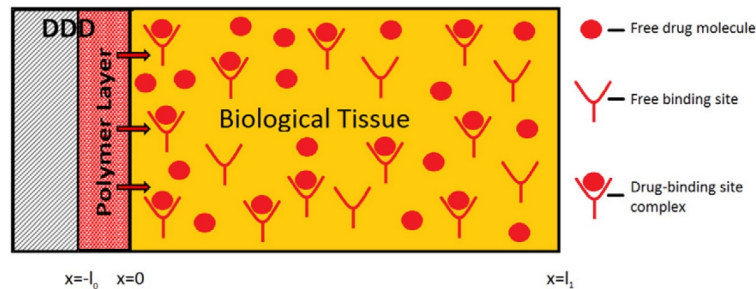


FIGURE 2.5 – The geometrical configuration of the DDS. This consists of some durable structure (shaded grey) coated with a thin layer of polymer of thickness l_0 containing the drug (red). The polymer layer is in contact with the biological tissue of thickness l_1 (orange). The drug is transported from the polymer coating via dissolution and diffusion to the tissue where it is subject to diffusion and advection in its free phase and may bind to drug binding sites. Diagram is not to scale [70].

lar medium. These are certainly the most difficult and challenging mechanisms to model and control in a drug delivery system releasing its drug in a living tissue. Indeed the arterial wall is a porous heterogeneous tissue, consisting in the intima (the layer in contact with the lumen), the media and the adventitia. The properties of each layer is different, therefore each layer has its different diffusion coefficient, porosities and binding properties. Typically, diffusion and drug binding occur in the tissue, sometimes made of a multilayered structure, whilst in some cases there is convection because of a pressure gradient across the tissue.

Drugs must bind to intracellular or extracellular proteins to have a biological effect. This binding can take two forms: nonspecific interactions, such as those influenced by charge or water affinity, and specific binding to the individual drug. Figure 2.5 displays these two phenomena. The rate at which the drug penetrates in the tissue depends highly on its porosity. There exists a balance between the capacity of an artery to absorb a drug and the rate at which the drug is presented in the arterial tissue. It is notable that the number of the free receptors affects the binding results, where the limit is the saturation of all the receptors. However, this is a reversible action: after binding, the drug may unbind and thereafter diffuse outer layer of the tissue [70] and the freed receptors can rebind with the large amount of drug that has been left in the extracellular medium [71].

Moreover, in addition to the properties of the tissue layer for its interaction with the active substance, the biological properties of the used drug are very important and the binding time of the drug will depend on both these properties. In this regard, hydrophilic drugs are few in the hydrophobic

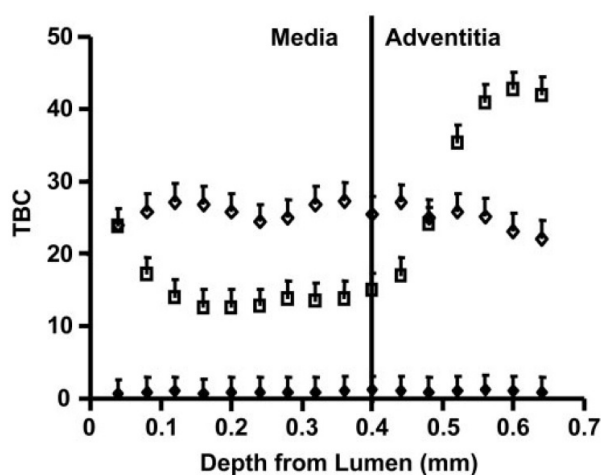


FIGURE 2.6 – Transmural equilibrium distribution of labeled dextran (\blacklozenge), paclitaxel (\square), and rapamycin (\blacktriangle) in 0.040-mm-thick bovine internal carotid tissue segments [72].

arterial wall but numerous in the lumen. For hydrophobic compounds, the layers of the artery act in a reverse manner. For example, the movement of paclitaxel and rapamycin (hydrophobic drugs) is likely impeded by the more water-rich regions of the blood vessel wall and enhanced by lipid pools or even the protein-studded elastin lamina. The multilayered structure of the arterial wall also influences the binding process in addition to the hydrophobic or hydrophilic properties of the drug. Indeed, transmural drug distribution profiles are markedly different for the two compounds and each one has different binding receptors. Moreover, the distribution of tissue-binding proteins or receptors are not uniform in space or time. As an example: the receptors for rapamycin, distribute evenly through the media and adventitia, whereas those for paclitaxel, distributes heterogeneously in the sub-intimal space. Heparin is so soluble and diffusible that it simply cannot stay in the artery for more than a few minutes after release and has no effect on intimal hyperplasia when eluted from a stent.

Figure 2.6 shows the examples of the different drug distribution at the different layers of artery [72]. It is notable that the scenario is even more complicated when the healthy and injured tissues does not have the same characteristics. For example Hwang et al. [73] have studied the influence of the presence of the blood clots in the vicinity of the stent struts. Depending to the type of the clots, the transport of the active substance can be retarded because it moves slowly through the clots with higher red cell content. In contrast, when the clots have higher diffusivity, drug is delivered more quickly to the artery. In addition, another issue is that the thrombosis (blood clots) are unpredictable

and irregular and can have different effects on the kinetics of the drug transport [73].

2.2 Design conception of drug-eluting stents

2.2.1 Different geometrical models of drug-eluting stents


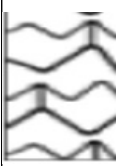
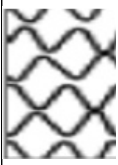
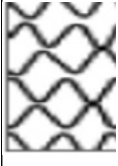


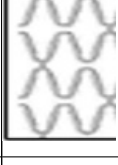
A stent looks like a small expandable cylindrical wire mesh tube that acts as a permanent scaffold to keep blood vessels open when they are subject to atherosclerosis. They are used at different locations in the body but we focus here only on the ones used to heal cardiovascular diseases. Depending on the manufacturer, different geometries exist and are summarized in table 2.1 [26]. As this study reveals, there are various geometrical parameters in the stents and it is very difficult to evaluate how a particular parameter influences the release behavior. To obtain a clear and consistent conclusion, it would be better to limit the variation of these parameters. This is the strategy used in many studies (moreover when the other external parameters are the same, the results can be beneficial for the other kinds of the drug delivery systems (DDS) such as patches, implants, micro-particles, and etc.). For example Joachim Loo et al. [74] have investigated experimentally the drug release of two kinds of hydrophobic and hydrophilic drugs from two types of polymer coatings (PLGA and PLLA films). In this study, the active surface is a $2 \times 2 \text{ cm}^2$ parallel to the flow with a thickness of $55 \mu\text{m}$ fabricated by an irradiated-multi-layer approach. In another paper, Pang et al. [75] study the release of ibuprofen from PLGA films with the dimension of about 33 cm^2 and the thickness in the range of $2\text{-}5 \mu\text{m}$. Another example is the study about the drug-eluting stents by Steele et al. [76] where the paclitaxel releases from the PEG/PLGA films with the dimension of $3 \times 1 \text{ cm}^2$ and the thickness of $15\text{-}20 \mu\text{m}$ are investigated. To understand the effect of the shear stress on the release kinetics of the sirolimus from the PLGA, Zheng et al. [77] have used PLGA films with a 0.11 mm thickness. Considering samples with simplified geometries like films also facilitate the study of the characterization of materials. For example, Vey et al. [78] have investigated the degradation of the PLGA films with different ratios of co-polymers with L/G molar compositions with the thickness of 0.3 mm in Phosphate Buffer Saline (PBS) solution. O'Brien et al. [79] study the effect of the pulsed flow on the fluorescein-sodium distribution from the polyurethane films coating a single stent strut with the dimensions of $0.24 \times 0.35 \times 1.5 \text{ mm}^3$. Their study is particularly valuable to investigate the coupling between hemodynamics and drug release from a stent strut. In some other studies [79–82] the whole stent is modelled as a single rectangular strut

2.2. DESIGN CONCEPTION OF DRUG-ELUTING STENTS

to investigate the drug distribution.

2.2. DESIGN CONCEPTION OF DRUG-ELUTING STENTS

TABLE 2.1 – A comparison of the amount of drug release in different types of stents and polymer coatings [26]

	Cypher	Taxus Express	Endeavor	Resolute	Xience-V	Promus Element	BioMatrix
Manufacturer	Cordis	Boston Scientific	Medtronic	Medtronic	Abbott Vascular	Boston Scientific	Biosensors
Platform	Bx-Velocity	Express	Driver	Driver	Vision	Omega	Gazelle
Design							
Material	SS	SS	MP35N CoCr	MP35N CoCr	L605 CoCr	PtCr	SS
Thickness of struts μm	140	132	91	91	81	81	112
Polymer	PEVA, PMBA	SIBS	PC	BioLinx	PBMA, PVDF- HFP	PBMA, PVDF- HFP	PLA
Polymer thickness μm	12.6	16	4.1	4.1	7.6	6	10
Drug	Sirolimus	Paclitaxel	Zotarolimus	Zotarolimus	Everolimus	Everolimus	Biolimus
Drug conc. $\mu g/cm^2$	140	100	100	100	100	100	156
Drug release in 4 weeks	80%	<10%	100%	70%	80%	80%	45%
Late lumen loss (mm)	0.1719	0.3920	0.6137	0.2738	0.1639	0.1570	0.1342

2.2.2 Polymers in the case of drug-eluting stents

2.2.2.1 Bio-durable polymers

The polymers used to coat the stents are numerous: poly(ethylene-co-vinyl acetate) (PEVA) coating for better biocompatibility [83], poly(butyl methacrylate) (PBMA) for slow sustained drug release [84], durable fluoropolymer [85, 86], silicone, and polyurethane. These polymers may be responsible for vascular inflammation, delayed endothelialization/healing and hyper sensitivity reactions, therefore they are associated with an enhanced risk of stent thrombosis [87].

2.2.2.2 Biodegradable polymers

Some other stents are coated with various biocompatible and biodegradable coatings. Referring to the different researchers, the main polymers used are poly(L)-lactic acid (P(L)LA) [88], PDLLA [89], poly(lactide-co-caprolactone) (PCL) [88], poly(lactide-co-glycolide) (PLGA) [88] polyethylene glycol (PEG), polyglycolide (PGA) [60], PLGA-PEG, PU [90–92], etc. The mentioned polymers may involve the chemical degradation resulting in the scission of the polymer chains such as their ester bonds [93], phosphonate groups [94] or by removing chlorine atoms and simultaneous release of the drug compounds that they carry [95]. These polymers must have the properties such as biocompatibility, elasticity (required for stent expansion) and adequate drug release properties. The researchers, in order to control the steady release of the drug and reduce the first burst release during the vascular healing, have explored many strategies. The “first burst” phenomenon is very common for the stents covered with one layer of polymer and drug. Many researchers [1, 96] have proposed a layer of polymer with drug and one or more free drug coatings as the top layers. Figure 2.7 shows the schematic of this conception. In their study, Li et al. [96] have investigated the performance of drug release with different thickness of the top layer (polymer layer without drug). They concluded that the top layer with medium or high thickness prevents the burst release of the drug, the top layer playing the role of a diffusion barrier and hindering the contact of the drug with the blood flow. They have also showed that adding plasticizers such as PEG in the top layer decreases the first burst release of the drug (shown in figure 2.8) [96].

The studies also show that rough coating surfaces achieve better hydrophilicity and produce faster polymer degradation, accelerating the drug release from the inner layer [96]. Table 2.1 shows a

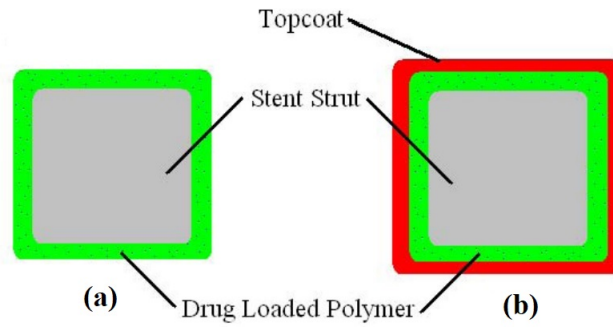


FIGURE 2.7 – Drug-eluting stent strut cross-sections, (a) is a DES strut with a drug loaded polymer matrix and stent strut (b) has a transport regulating topcoat [97]

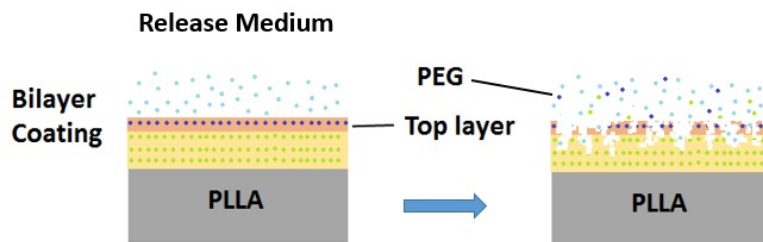


FIGURE 2.8 – Model proposed by Li et al. [96] for coating the stent with the polymer layers

2.2. DESIGN CONCEPTION OF DRUG-ELUTING STENTS

comparison of the amount of drug release in 4 weeks for different types of stents with different types of coatings [26]. The hydrophilicity and hydrophobicity of the polymer coatings are also important with regard to their biocompatibility. This factor is important for the adhesion of monocytes to the polymer layer. In some studies [98, 99] it is observed that the polymers with more hydrophobicity have more monocyte adhesion comparing to the polymers with more hydrophilicity, therefore considering this factor can help to better control local inflammation and cell proliferation after stent implantation. In a review study by Das et al. [100], different types of polymers are considered, more or less hydrophobic, to decrease the attachment of monocytes: hydrophobic polymers such as teflon, coatings with anticoagulant and anti-thrombosis drugs such as heparin or antimicrobial coatings such as silver. The difficulty of using hydrophilic polymers is the ability of these materials to absorb water; subsequently, these hydrophilic polymers experience a rapid degradation resulting in the increase of the drug release. In this case, degradation is much faster than the water penetration into the bulk of the polymer layer [101, 102].

From a general point of view in DES, neither the polymer nor the drug should have any chemical action with each other changing their properties and the structures, and also polymers should be diffusible enough for the drug [103]. The polymer and the drug can have two different configurations: first, the drug is distributed homogeneously into the polymer (matrix configuration); secondly the drug is contained inside small reservoirs in the form of microcapsules [104] (shown in figure 2.9) surrounded by the polymer layer. As the technology of the matrix is easier to fabricate and more effective in controlling the slow release of the drug, it is more popular in practice compared to the reservoir configuration [105].

Moreover, some DES are completely bioresorbable, meaning that they contain nonmetallic structure and only the polymer scaffold supports the mechanical properties of the stent. Evidently, the degradation products should be nontoxic, easily absorbed [1, 26]. The ideal bioresorbable vascular stents would support the vascular structure from 3 to 6 months and then completely disappear from 3 to 18 months after vascular healing. The polymers used in this kind of stents are for example: poly caprolactone (PCL) [88, 107], poly(L-lactide) (PLA) [108–111] (poly lactic acid is also made in our own blood and the body recognizes it and breaks it down to safe components such as water and oxygen); polyurethane (PU) [112] is also an attractive candidate for scaffold fabrication with moderate biocompatibility and excellent mechanical properties [1], poly(anhydride ester) [60], poly(D,L-lactide) (PDLLA) [113],

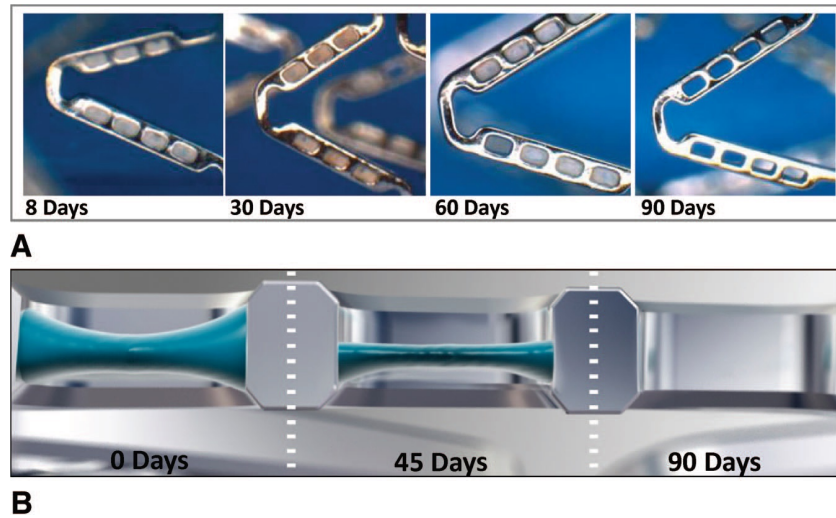


FIGURE 2.9 – (a) NEVO open-cell design. Multiple laser-cut reservoirs hold a blend of PLGA and sirolimus in mechanically stable stent struts. Sigmoidal bridge elements connect the circumferential strut rings. (b) Drawing shows a detailed view of the filled reservoirs. (c) Scanning electron micrograph of a reservoir [106]

polycarbonate polymer (PC) [60], chitosan (CS) [114] are among the most popular and most applied natural polymers used for drug delivery systems [115], polystatin (BPL) [116] is also suggested as it is not only bio-absorbable but it is also a drug as it is (it promotes re-endothelialization during its degradation and bio-absorption of the scaffold). The main weakness of these polymer scaffolds, compared to the metal structures, is that they are less mechanically capable to keep the vascular lumen open [13]. Moreover, some studies revealed that early or non-uniform degradation of these polymers might cause late-stent thrombosis and even heart attack to the patients [18, 30].

2.2.3 Drugs in the case of drug-eluting stents

Drug delivery kinetics and related mechanisms are firmly depending on the type of the active substance (physical and chemical properties of the active substance, such as molecular weight, water solubility, particle size ... [18, 36–38]). Hydrophilicity or hydrophobicity is also determinant for the drug release during the therapy. Hydrophobic active substances are more favorable, as hydrophilic active substances are rapidly washed away by the fluid followed by the burst release of the drug [117] and hydrophobic active substances are more prone to make binding with the receptors. This matter is very important in the cardiovascular cases. As shown in [118], hydrophobic drugs have a greater

2.3. CHARACTERISTICS OF THE TEST CONDITION

average variability than hydrophilic drugs and the former remain relatively closer to the intima than hydrophilic drugs at all Péclet numbers of drugs [118]. For this reason, the malapposition of the stent struts in the arterial tissue affects more negatively the hydrophilic drugs than the hydrophobic drugs. Moreover, it is mentioned in [119] that the physico-chemical properties of the active substance also affect its distribution in the polymer matrix (as a carrier): hydrophobic active substances are uniformly distributed in the matrix whereas hydrophilic active substances move towards the surface of the polymer. Consequently, the prevailing release mechanism for hydrophobic active substances is diffusion whereas for hydrophilic active ingredients, convection also plays a significant role. As mentioned earlier, hydrophilic active substances have tendency to move or to stay towards the surface of the polymer and consequently this type of molecules can easily generate the first burst phenomenon (the drug is rapidly released by desorption in the first periods of time [119]). In a comparison between paclitaxel and sirolimus drugs by Bozsak et al. [18], it is showed that the transport of paclitaxel in the arterial wall is dominated by convection while the transport of sirolimus is dominated by the binding process. Therefore, paclitaxel is efficient when used for drug-coated balloons but sirolimus is not a good choice.

Another key parameter related to the active substance is its water solubility and its physical state in the polymer matrix. Evidently, the kinetics of release is not the same when the active substance is dissolved by water absorption in the polymer matrix and when it is not water-soluble and remains dispersed in the polymer matrix. For instance in a study by Chakraborty et al. [120], the release kinetics of water-soluble and insoluble drugs from HPMC (hydroxypropyl methylcellulose) based matrix were studied. The study reveals that the release kinetics of the soluble drug is an anomalous non-Fickian diffusion transport whereas insoluble drug follows zero-order release kinetics.

2.3 Characteristics of the test condition

2.3.1 Release compartment

2.3.1.1 Artificial lumen

One of the most important parameters to achieve an accurate drug release from DES under in vitro conditions is the fluid medium: a wide range of solutions and fluids has been used for this purpose, trying to approach the body environment as close as possible. The water, phosphate buffered saline

2.3. CHARACTERISTICS OF THE TEST CONDITION

(PBS), organic component/PBS, and inorganic component/PBS are such commonly used solutions. In particular, the pH and viscosity of the medium are important parameters, which are affecting the drug release kinetics. In general, PBS with a pH of 7.4 is considered in many studies as a good medium to analyze the drug release [121] due to its ability to keep the pH constant and to the proximity of its ions with the ions of the body. However, using this medium to study the release of some drugs such as Sirolimus seems to be challenging. Indeed, some studies show that sirolimus has a very low stability in this buffer solution at pH 7.4 [122]. Thereafter, Naseerali et al. [123] have studied the influence of various media on the release profile of sirolimus from drug-eluting stent. Their results suggest that a 9:1 (v/v) of normal saline and isopropanol medium can be suitable for the investigation of in vitro release kinetics of sirolimus. Pruessmann et al. [124] have studied the impact of deionized water, PBS and phosphate buffered saline without sodium chloride (PB) as media to investigate the release kinetics of the triamterene drug from coated stents. According to their study, deionized water showed the best release efficiency compared to PBS and PB. This increase was justified due to the higher solubility of the triamterene in deionized water and PB compared to PBS. It is worth noting that according to the results of this study, the properties of the drug should always be considered as an important parameter in order to select the medium. Indeed, it clearly has an effect on the kinetics of drug release.

As mentioned above, the type of drug should be considered as an important parameter in choosing the medium. In particular, non-polar drugs that have a low solubility in an aqueous medium have attracted the attention of many studies. In fact, the '-olimus' group of drugs are not stable at alkaline or neutral pH. So lowering the pH to less than 7.4 could be a way to reduce the degradation of these drugs in the medium. Likewise, the solubility of these poorly water-soluble drugs in aqueous media can be improved using suitable solvents, such as surfactants.

Raval et al. [125] worked on the optimization of media for the release of sirolimus (SRL) from drug-eluting stents. They buffered the media at pH=4 to minimize the degradation of the drug and increased its solubility using a special amount of surfactant.

According to them, a release medium consisting in 0.1% P123 (kind of PEO-PPO-PEO block copolymers) in phosphate buffer pH=4 was most suitable for in vitro release of SRL from DES. In another study by Jelonek et al. [126], acetonitrile and methylene chloride as a media were used to analyze the SRL loaded in PLLA and PDLA. It is worth noting that the solutions used as media were

2.3. CHARACTERISTICS OF THE TEST CONDITION

good solvents for both the drug and the polymeric carrier. Because in most cases the drug released from the stent is trapped in the polymer coating, the use of solvents and surfactants can increase the rate of degradation of the polymer coating. Let us note that the use of surfactants can affect the separation and quantification of SRL by HPLC (High Performance Liquid Chromatography), which can lead to erroneous results when evaluating the SRL concentration in the medium.

In other studies [79, 80] analyzing the influence of the struts and also the distribution of the drug in the two media (artificial lumen and artificial tissue) the viscosity of the medium was studied. Therefore a mixture of glycerol-water (40/60 vol%, 0.01% surfactant) was used as an artificial blood. Merciadéz and his colleagues [127] have used a new medium containing an organic solvent prepared using 2% ultra pure sodium dodecyl sulfate (SDS), in high purity water with 10% gradient-grade acetonitrile (ACN), and buffered to pH=4.5 with phosphate. This allowed them to correlate their *in vitro* release profile with the *in vivo* one from the porcine. Moreover in a study by Chabi et al. [81] where the hemodynamic of the flow with the presence of stent was under consideration, a mixture of 87% of glycerol and 13% of water was used.

2.3.1.2 Artificial tissue

The influence of the fluid medium on the release of drug from DES is only one part of the story. The other part is: how much drug is diffused into the artery? This is certainly the main clinical goal and the most challenging domain to investigate. Clinicians advise that a uniform drug concentration should be attained across the arterial wall, and that the concentration should be maintained within some therapeutic window [128]. In this regard, studies are trying to measure the amount of drug that has penetrated the vessel using different gels that can simulate the vessel artery. Neubert et al. [129] considered the calcium alginate hydrogel for simulation of the vessel artery. The water content of the gel was approximately 96%. The main reasons to choose the calcium alginate hydrogel matrix are: its stability at 37 °C, the feasibility to adapt gel strength and elasticity, and the mild gelling conditions which allow for the incorporation of diverse substances such as proteins or living cells. The experimental procedure used to make the gel (concentration, temperature, additives...) also affects the gelling time and the drug diffusion into the gel.

Depending on the environmental conditions of setup for analyzing drug released from the stents, some properties of hydrogels such as mechanical properties, degradation and swelling are among the

2.3. CHARACTERISTICS OF THE TEST CONDITION

factors that will affect their selection.

In a study by Semmling et al. [130] the hydrogels of 2 wt.% agar, 2 wt.% agarose, 10 wt.% PAA and 15 wt.% PVA were selected. In order to find a measure for the long-term stability of the gels, the mechanical properties of the prepared gels were determined by texture analysis. In this regard, stress-strain curves of native gels, as well as gels that had been perfused with phosphate buffered saline (PBS) at pH=7.4 in their setup for 28 days, were studied. Their results showed that agarose gel seems to be the most suitable candidate for long-term dissolution testing since the target gel parameters are relevant for their use as a tissue simulating compartment. It should be noted that in addition to the desired physical and mechanical properties in order to select a hydrogel as a vessel wall, the drug penetration coefficient in the hydrogel has great importance and should be considered as a parameter with high status. In another study by Semmling et al. [131] the penetration coefficients of triamterene in the same hydrogels were examined. According to their results, the penetration coefficients in these gels were in the range of $2 \times 10^{-4} \text{ mm}^2/\text{s}$ (PVA) to $8 \times 10^{-4} \text{ mm}^2/\text{s}$ (agarose). The results of these studies showed that the hydrogel with the lowest diffusion coefficient had 4% of drug penetration to it. The comparison of these results is meaningful when the penetration coefficient of sirolimus in the human coronary arteries is reported to be $1.5\text{--}2.5 \times 10^{-4} \text{ mm}^2/\text{s}$ [132], which is close to the penetration coefficient of triamterene in hydrogels used in these experiments. Bandomir et al. [133] studied the amount of paclitaxel diffused in the calcium alginate, polyacrylamide (PAM) and poly(vinylethylimidazolium bromide) hydrogels from a drug-coated balloon. According to their study, the relevant parameters of synthetic hydrogels to consider when mimicking artificially a vessel wall are permeability, flexibility and long-term stability. The dissolution of the polymer network by monovalent cations such as Na^+ , as well as its susceptibility to microbial contamination, were among the disadvantages mentioned for calcium alginate hydrogel. In order to select the type of hydrogel, it is important to know the mechanism of drug transport to the hydrogel. Studies have shown that drug delivery from drug-impregnated stents is controlled by both penetration/diffusion and convection mechanisms. Given that the diffusion mechanism is based on the concentration gradient, the drug must be dissolved beforehand in the matrix and subsequently, it has to penetrate into the gel or medium [134].

For example, a study of a balloon impregnated with paclitaxel in contact with a hydrogel showed that due to the low solubility of the drug paclitaxel in the aqueous medium, the amount of drug transferred to the hydrogel was linked to the mechanical forces applied during balloon expansion [133].

2.3. CHARACTERISTICS OF THE TEST CONDITION

In addition, the researches [73, 118, 135–138] have shown that biological reactions, such as the binding of the drug particles with the receptors in the tissue affects the drug penetration. Consequently, in order to simulate the *in vivo* reactions, some proteins can be added to the hydrogel. The presence of proteins can cause the drug to deposit in the vessel wall, which after a while can allow the drug to penetrate into the tissue [139]. It is worth noting that when the drug has low solubility, after opening the stent by balloon, part of the drug is transferred into the gel by mechanical forces. But after that, the remaining amount of drug only washes off from the stent due to its inability to penetrate into the gel. This can cause an error in calculating the amount of drug that has penetrated into the gel. Semmling et al. [140] examined the effect of using different hydrophobic additives in hydrogel compartment simulating the vessel wall on release and distribution from model substance-coated stents. In this regard, four alginate-based gel formulations containing reversed-phase column microparticles LiChroprep[®] RP-18 or medium-chain triglycerides in the form of preprocessed oil-in-water emulsions Lipofundin[®] MCTin with different concentrations were chosen. In general, the use of additives was applied to improve the medium contact with the hydrogels used. It is worth mentioning that in this study, fluorescein and triamterene were used as hydrophilic and hydrophobic drug models, respectively. The results showed that the effect of gel improvement had no significant effect on the penetration of the hydrophilic drug into the hydrogel, while the improved gels were a more suitable substrate for the transfer of hydrophobic drug into the hydrogel. Another important and effective factor with hydrogels for the penetration of drugs through them is the suitable choice of the base agent in hydrogels. Pruessmann et al. [124] investigated the effect of deionized water, PBS and PB as the base for preparing hydrogels for the diffusion of triamterene in them. Their study showed that more drug was transferred to deionized water-based hydrogels than PBS and PB-based hydrogels. This effect was due to the absence of salt in deionized water, which was discussed in the previous section. It is notable that in all these tests whether they are *ex vivo*, *in vivo* or *in vitro*, stent positioning on the arterial tissue is very important and the malapposition of stents highly affects the results [118, 141].

2.3.2 Release test methods

Because *in vivo* tests are expensive and time-consuming, examinations by *in vitro* tests have been at the center of attention of many studies. Researchers have always been trying to increase the accuracy of the *in vitro* tests in order to provide the best estimate of their results in comparison to *in vivo*

2.3. CHARACTERISTICS OF THE TEST CONDITION

tests. In general, the methods used for this purpose are divided into static and dynamic conditions, the main difference between the two being the medium flow. Generally, the temperature used in these two methods is 37°C (body temperature).

2.3.2.1 Static condition

The static method has been used as a common method in measuring drug release from drug impregnated stents and other drug delivery systems. In general, in this method, the stent is immersed in a certain amount of medium, and then the sampling of the medium is done at certain periods. Temperature is kept constant during the drug release test. One of the important points for testing the drug release in the static state is the sampling of the medium. Some medium is removed from the system at different time intervals and must be replaced with fresh medium [142]. For example in the study of Khan et al. [143], the rapamycin released from drug-eluting stents was evaluated under static conditions. In order to evaluate the amount of drug released, each sample was immersed in 2 ml of medium and then, for sampling, 1.5 ml of medium was replaced with some fresh solution at the following times: 6 h, 1 day, 3 days, 5 days, 10 days and then weekly up to 75 days.

As mentioned earlier, the evaluation of drug release from stents is very important to determine the effectiveness of stents, and studies have always tried to keep the test conditions as close as possible to the body conditions.

An important question arises: how accurate are these tests under static conditions? Abbasnezhad et al. [144] showed the significant difference between the drug release under static and dynamic conditions (the next section will discuss more on the effect of flow on drug release). Likewise, since the release of the drug in static state has slower kinetics than in dynamic state [145], more time is required to perform the tests. However, due to the availability of this method, it seems that useful basic information can be obtained from this static approach.

2.3.2.2 Dynamic condition

Drug release from the drug-eluting stents has several drug release mechanisms. The most important mechanisms consist in the diffusion-controlled drug release, dissolution/degradation-controlled drug release, ion exchange-based drug release and osmosis-based controlled release [146]. Studies showed the effect of the presence of the flow rate on these mechanisms. It is worth noting that each mechanism

2.3. CHARACTERISTICS OF THE TEST CONDITION

provides a different kinetic release from the stent. For example, in some cases, the presence of degradation mechanism can increase the rate of drug release from the stent. The use of shakers has been amongst the common methods of measuring the amount of drug release under dynamic conditions. For this purpose, a certain number of stents (usually one stent) is placed in a container filled with the medium (screwed-glass vials [147], tubes [148], or flasks [149]), and then the test is performed at a certain agitation of the shaker. In most studies, the temperature intended for the experiment was kept constant at 37 °C by an incubator [150] or a water bath [147, 151]. The agitation speed of shaker in the studies are commonly of 50 [152, 153], 75 [57, 154], 80 [149], 100 [147, 150], 120 [151], 130 [155], 175 [148], 250 and 300 [156] rpm. One of the drawbacks of these studies is that they do not specifically justify the choice of the agitation speed to evaluate drug release. Consequently, the experimental conditions created by shakers are not easily comparable to the ones encountered in in vivo tests. The main advantage of this approach is to accelerate the drug release from the stent and reduce the time required to perform the test. To the best of our knowledge, the effect of shaker agitation on drug release has not been studied by numerical simulation. Sampling in these studies to check the amount of drug released consists in several methods. Generally, the methods of sampling are as follows: 1. Changing the special volume of medium with fresh medium (fresh medium is added to keep the test volume constant and avoid the saturation) [156]. 2. The medium is completely replaced with new medium at specific times [148, 150, 151]. 3. A specific portion of the medium is removed to analyze and returned to the test environment after analysis [154]. Apart from the shakers there is another method for the dynamic conditions which is the circulation of the flow at constant flow rate. This condition can have more similarities to the real case comparing to the shakers. For example in a study by Bandomir et al. [157], the flow rate of 35 ml/min was chosen for studying the drug delivery from the drug-coated balloon, whereas in a study by Zheng et al. [77] the flow rates of 3, 10, 30 ml/s were chosen for the sirolimus release from DES. Another study for the release of sirolimus from DES has been done by Merciadetz et al. [127] in which the flow rate of 25 ml/min was used. Another study [158] has considered the laminar flow rates of 6.8, 10, 11.6, 12.3 and 17.3 l/min based on the different laminar flow rates of an oscillating heart pulse.

In an investigation by Seidlitz et al. [159] the flow rate of 35 ml/min is used with reference to the flow rate in the coronary vessels, as well as the flow rate of 4 ml/s for two different types of drugs.

Their analysis indicated that the variation of the flow rate has not a distinct effect on the drug

2.3. CHARACTERISTICS OF THE TEST CONDITION

release and distribution but they concluded that the effect of the flow rate should be analyzed on a case-by-case basis by individual assessments.

In another study by Bernard et al. [160], the authors considered two flow rates of 60 and 140 ml/min as the minimum and maximum values of the blood flow in a right coronary artery. They have stated that an increase in the flow rate emphasizes fluid perturbations, and generates a wall shear stress rise except for inter-strut area. Moreover, in the case of dynamic conditions, pulsed flows and especially systolo-diastolic flow patterns are of great interest. In their study, Vijayaratnam et al. [80] performed CFD simulations to investigate the impact of luminal blood flow patterns on the drug transport behavior of stented arteries. They concluded that neither the pulsatility of the flow nor the viscosity of the fluid changes the results of the drug uptake. However, in Ku et al. [161], the comparison between the continuous and pulsed flows revealed some marked differences especially at the bifurcations.

2.3.3 Apparatus for release testing

As seen above, in vitro drug release from the DES is a big challenge and involves many researchers. In this regard, the design of an apparatus that can imitate in vivo conditions is very difficult. Indeed such a setup should be able to provide a systolo-diastolic flow pattern, mimic the various media (blood flow, polymer coating and arterial wall) and should be able to measure the drug transfers in these media as a function of time and space. We describe below the most commonly used apparatus to achieve some of these goals. In the static state, laboratory vials are generally used. However in the dynamic state, many studies use dissolution test apparatus like those commonly used in the pharmaceutical industry to evaluate the performance of a drug. In the USA, these devices are referred to as USP (United States Pharmacopeia) apparatus. USP apparatus 1 (basket) and 2 (paddle) were introduced in the 1970s for the purpose of providing a platform to evaluate the in vitro performance of dosage forms using standardized conditions. We can also cite the Reciprocating Cylinder USP 3 apparatus which was developed to mimic gastrointestinal test, the flow-through cell apparatus (USP 4) which has a continuous flow circulation and was designed for low soluble drugs, implants and suppositories, compendial. Apparatus 5 (paddle over disc) which is similar to the paddle system (USP 2) but with an additional disc mounted on it. Cylinder type or USP 6 resembles to the basket type but the basket and shaft are replaced by a cylindrical stirring element. USP 5 and USP 6 are normally destined for the

2.3. CHARACTERISTICS OF THE TEST CONDITION

drug release from the transdermal patches. Finally, the Reciprocating holder apparatus with agitation (USP 7) is the most recent apparatus destined for different types of drug carriers such as tablets, capsules, transdermals, osmotic pumps, and arterial stents, with different agitation speeds. Generally, in the case of DES studies, these devices are not sophisticated enough because they are not capable to reproduce the systolo-diastolic flow and the inherent pressure variation which are important parameters to account for as proved by various numerical studies [144, 162, 163]. The presence of an artificial arterial tissue is another important element affecting the release. In this regard, the development of the vFTC (vessel-simulating flow-through cell) method [164] was undertaken (shown in figure 2.10). However, so far, the simulated tissue does not accurately reproduce the characteristics of the real one [165, 166]. Among all these devices, the apparatus USP 2, USP 4, USP 7 and vFTC are mostly used in the study of drug delivery from DES. To evaluate the effect of some of these setups on the release profile, Medina et al. [167] have compared the release profile of ibuprofen using the USP 2 and USP 4 apparatus with the release profile of a reference. Their results have indicated that the release profile obtained by the USP 4 apparatus was similar to the profile of the reference. In another paper Pruessmann et al. [35] have studied the release of triamterene from a DES using three different test setups: USP 7 apparatus, USP 4 apparatus (FTC) and vessel-simulating flow through cell (vFTC). Their results stated that dissolution vessel geometry (USP apparatus) and medium volume had no influence on the release behavior, whereas flow through cell method had lower release rate than in the USP 7 apparatus. The vFTC method was also used by Seidlitz et al. [159] to study the dissolution and release of fluorescein sodium and triamterene from stent coatings. They compared their results with the ones obtained by the standard paddle (USP 2) and flow-through cell (USP 4) apparatus. The results showed that the release from the coating was decelerated in the USP 2 apparatus compared to the USP 4 (figure 2.11 (a)). However in another study by Pruessmann et al. [35] about the release of triamterene with the methods of FTC and vFTC, it is showed that the release of the drug was higher at the first stage with vFTC before being exceeded by the drug release obtained by FTC method (figure 2.11 (b)). To sum up, the studies in this field show that many attempts have already been done in order to study experimentally the drug release from drug-eluting stents, but these solutions are not completely satisfactory. Moreover, in vitro/in vivo correlations, accounting for the different parameters, in order to personalize the therapy and thus increase its efficiency, remain a challenging topic.

2.3. CHARACTERISTICS OF THE TEST CONDITION

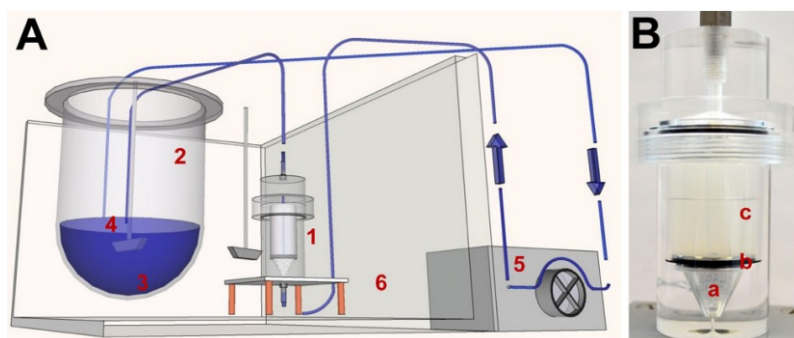


FIGURE 2.10 – Schematic overview of the in vitro test setup (A) and photograph of the vFTC equipped with a 2 wt% agarose gel (B); 1) vFTC, 2) media container, 3) PBS of pH 7.4, 4) paddle stirred at 50 rpm, 5) peristaltic pump, 6) heated water bath, a) glass beads, b) stainless steel disc, c) hydrogel [140]

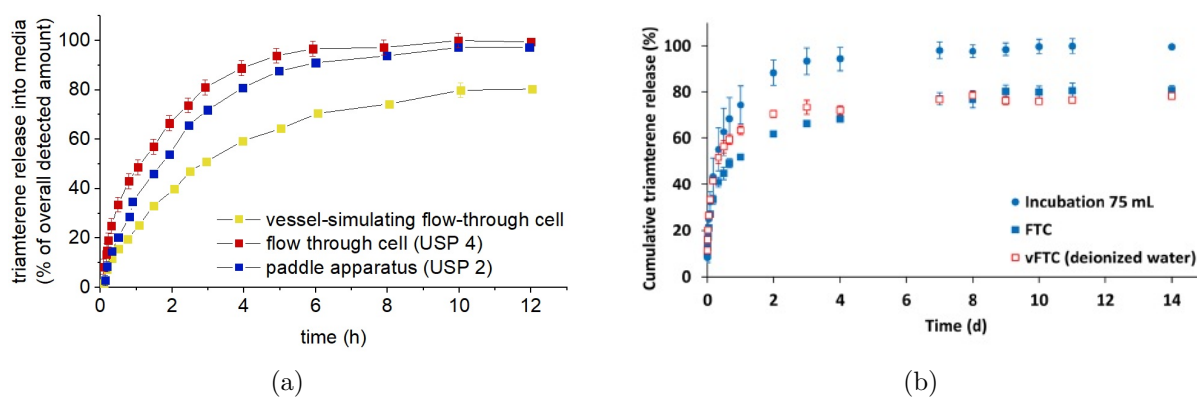


FIGURE 2.11 – (a) Incubation setup carried out in 100 ml glass flasks. Flow-through cells were equipped with an agarose hydrogel based on deionised water (vFTC (deionised water)) or run without a second compartment (FTC). (b) triamterene from stent coatings into media over time with vessel-simulating flow-through cell, flow-through cell (USP 4), or paddle apparatus (USP 2); flow rate 35 ml/min, paddle speed 50 rpm [35, 159]

2.3. CHARACTERISTICS OF THE TEST CONDITION

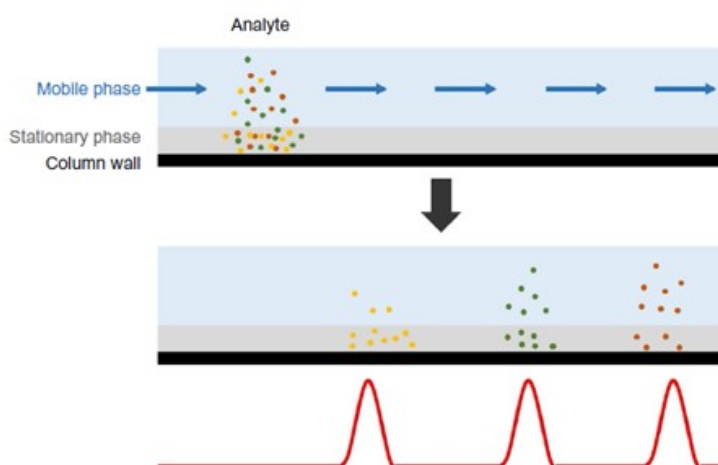


FIGURE 2.12 – Separation mechanism by HPLC [168]

2.3.4 Analytical tools to determine drug release

The first step to determine the efficiency of a drug delivery carrier is to evaluate the amount of drug released from the carrier at different times. The main technologies used for this task are: High-performance liquid chromatography, UV-Vis spectroscopy and Raman spectroscopy.

High-performance liquid chromatography

Liquid chromatography is a classical technique used to separate a sample into its individual parts. This separation occurs based on the chemical or physical interactions of the sample with the mobile and stationary phases. There are many different types of chromatography techniques and systems available for a wide range of applications all of which are defined as High Performance Liquid Chromatography (HPLC). HPLC analysis focuses on macromolecule isolation through chemical interaction, affinity or hydrodynamic volume. Because the molecules present in the mobile liquid phase interact differently with the stationary phase, they produce different signals on the detectors as schematically illustrated in figure 2.12. This technique is generally associated with other analytical techniques (optical detectors) such as UV detectors or fluorescence detectors.

UV/Vis-detector

UV/Vis spectrophotometry is a technique based on the absorption of photons belonging to the UV, visible or near IR regions of the electromagnetic spectrum. When submitted to such radiations, the substances are prone to electronic transitions. The signal consists in a series of peaks in an absorbance

vs wavelength spectrum. Compared to HPLC, UV-spectrophotometry method is much faster and less expansive (this technique was used in this work).

Fluorescence detector

Fluorescence detectors are probably the most sensitive among the existing modern HPLC detectors. It is possible to detect even a presence of a single analyte molecule in the flow cell. Typically, fluorescence sensitivity is 10 -1000 times higher than that of the UV detector for strong UV absorbing materials. Fluorescence detectors are very specific and selective among the others optical detectors. Compounds having specific functional groups are excited by shorter wavelength energy and emit higher wavelength radiation which is called fluorescence.

Raman spectroscopy

This technique consists in illuminating the sample with a monochromatic light (usually from a laser in the visible, near infrared, or near ultraviolet range, although X-rays can also be used). The interaction of this light with the molecules of the sample depends on their vibrations (this phenomenon is called inelastic diffusion or Raman scattering) and a shift in the energy spectrum of the diffused photons is observed. This method is more advanced compared to UV and HPLC. One of its advantages is the ability to use it in-situ during the experimentation, therefore it decreases the use of disposables, it is fast, precise and has less risk due to less transportation of test substances [169, 170].

2.4 Modelisation and simulation

2.4.1 Semi-empirical models

Mathematical models have always been one of the most effective ways to improve the design of different carriers for the drug delivery system. Also, it has always been important to determine the mechanism of drug release (which were discussed in physical mechanisms section) and moreover to identify kinetics of the release from various systems, such as osmotic systems, degradable, or non-degradable systems. This results in lower costs as well as lower laboratory tests.

Mathematical models commonly used to determine the drug release/dissolution profile are zero order kinetics, first order kinetics, Hixon-Crowell, Higuchi model, Weibull model, Baker-Lonsdale model, Korsmayer-Peppas model and Hopfenberg model. Apart from the physical mechanisms, the release from the surface of the particle leads to burst release effect. This part of release takes place at the

first stage of the release profile, which is not totally accepted to be categorized as a physical mechanism. This burst release can be avoided by washing the carriers with water or a proper solvent after crosslinking process, or by increasing the crosslinking density.

However, these methods reduce the encapsulation efficiency of the drug. The mathematical equation representing this phenomenon according to numerous studies is as [171]:

$$\frac{dC}{dt} = -k_b C \quad (2.1)$$

where k_b is the initial burst constant, and C is the concentration of the drug in the release environment at time t .

Diffusion based models:

The diffusion mechanism, present in all the DDSs, can account for different mathematical models.

- Fick's law

The most famous equation of diffusion mechanism is the Fick's law. Fick's first law corresponds to the mass diffusion across a unit area per unit of time (equation 2.2), and the Fick's second law corresponds the conservation of the concentration (equation 5.11) [172]:

$$\vec{J} = -D\vec{\nabla}C = -D \cdot \overrightarrow{\text{grad}} C \quad (2.2)$$

$$\frac{\partial C}{\partial t} = D\Delta C \quad (2.3)$$

where \vec{J} is the diffusion flux, D is the diffusion coefficient, C is the concentration. There are many studies that have modeled the drug release by modifying the Fick's law [23, 173–175]. In another study by Gudino et al. [175], a model describing the penetration of the plasma into the polymer layer is proposed:

$$\frac{\partial c_p}{\partial t} = \vec{\nabla} \cdot (D_p(c_p)\vec{\nabla}c_p + D_v\vec{\nabla}\sigma_p(c_p)) \quad (2.4)$$

here c_p and D_p are respectively the concentration and diffusion coefficient of the plasma in the polymer, D_v is a viscoelastic diffusion coefficient and σ_p the stress associated to solvent uptake and exerted

TABLE 2.2 – Comparing the results of carbidopa and levodopa release with different models [177]

Model Name	r ² (Carbidopa)	r ² (Levodopa)
Zero order model	0.933	0.9157
First order model	0.8322	0.9212
Higuchi model	0.9931	0.9916
Korsmeyer-Peppas model	-4.158	-4.09
Hixson-Crowell model	0.9586	0.9897

by the polymer.

- Higuchi's equation

The second famous diffusion equation derived from Fick's second law is Higuchi's equation [176]. It is used for the water soluble and poorly water soluble drugs, semisolids (include creams, ointments, and gels), solids and some transdermal patches. This model is:

$$Q = K_H t^{0.5} \quad (2.5)$$

Q is the cumulative amount of active substance release at time t , K_H is Higuchi's constant. In a study, Gouda et al. [177] have investigated the release kinetics of the carbidopa and levodopa drugs in the polymer matrix and have shown that they mostly correlated with the Higuchi's model. This implies that the drug release is controlled by the diffusion (shown in table 2.2 and figure 2.13).

- Baker-Lonsdale

Baker-Lonsdale [178] developed a model based on Higuchi's equation which describes the controlled release of drug from a spherical matrix and that can be represented as :

$$\frac{3}{2} \left[1 - \left(1 - \frac{Q_t}{Q_\infty} \right)^{\frac{2}{3}} \right] - \frac{Q_t}{Q_\infty} = Kt \quad (2.6)$$

where Q_t is the amount of drug released at time t and Q_∞ is the amount of drug released at an infinite time and K is the release constant.

Dissolution based models:

- Zero-order equation

This mechanism of release represents the dissolution of drug from a dosage form that does not

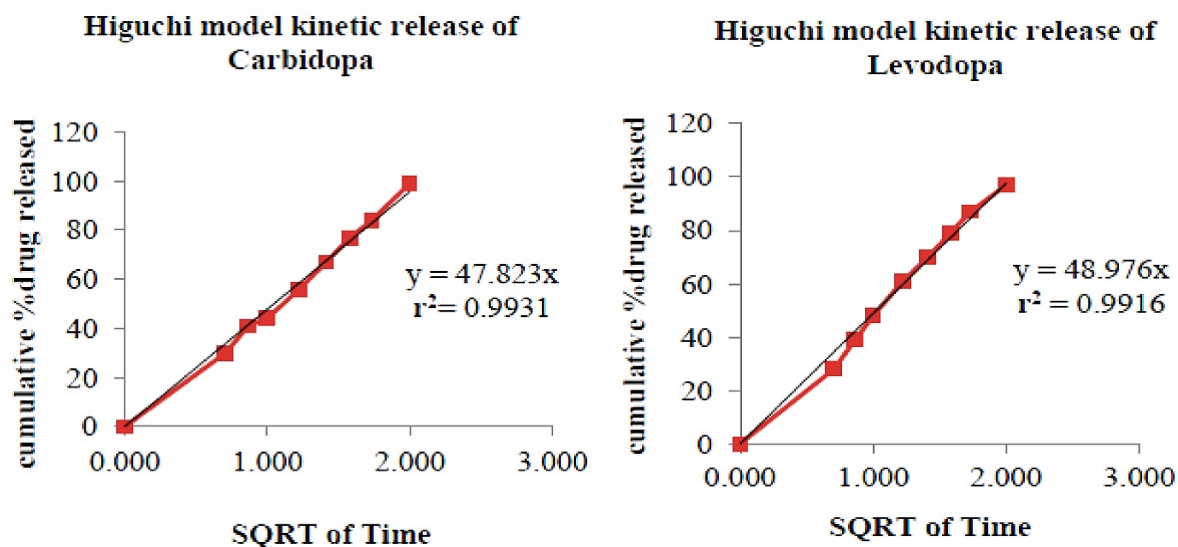


FIGURE 2.13 – Higuchi kinetics model of Levodopa and Carbidoopa [177]

disaggregate and releases the drug slowly. In this model, the drug release rate is independent of its concentration and can be represented as [179]:

$$Q_t = Q_0 + K_0 t \quad (2.7)$$

with Q_0 the initial amount of active substance, Q_t the cumulative amount of active substance released at time t (release occurs rapidly after drug dissolves) and K_0 the zero order release constant. Some examples of systems which give zero order release are: matrix tablet with low solubility drug, transdermal, implantable depot, suspension, oral control release and oral osmotic pressure. For instance, Zhang et al. [38] have studied the release behavior of the poorly water-soluble drugs from hydroxypropyl methylcellulose polymeric films (HPMC) and then have interpolated the results with the zero order equation with an excellent agreement. As performing the test for different polymer thicknesses they have observed that by increasing the thickness of the polymer the release mechanisms changed from Fickian diffusion to zero order release and also they discovered that the sample area and the sample thickness vary linearly with the drug release. In another study by Chinthaginjala et al. [180] on the release of eletriptan hydrobromide (hydrophile drug) from mucoadhesive buccal tablets, the results were best fitted with the zero order equation (shown in figure 2.14) and the mechanism of the release was non-Fickian.

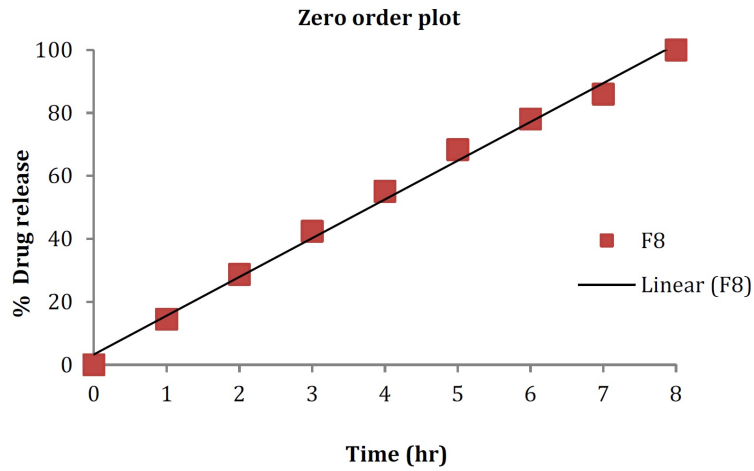


FIGURE 2.14 – Zero-order plot of F8 composed of: 20 *mg* Eletriptan Hydrobromide, 50mg Chitosan, 25 *mg* Sodium alginate, 52 *mg* Lactose, 2 *mg* Magnesium Stearate, 1 *mg* Talc; with the total weight of 150 *mg* as a tablet [180]

- First-order equation

In a first-order process, the rate of drug dissolution is directly proportional to concentration of a particular substance. This equation is broadly used for water soluble drugs in the porous matrix. For the first-order release kinetics, release equation is defined as :

$$Q_t = Q_0 e^{-Kt} \tag{2.8}$$

where Q_0 is the initial amount of active substance, Q_t the cumulative amount of active substance released at time t and K the first-order release constant. Some examples referring to the first-order release are: matrix dissolution controlled release or matrix diffusion controlled release. Ranjan et al. [181] have studied the drug release kinetics in the shakers with different shaking speeds. Their results were well interpreted by using a first-order equation (shown in figure 2.15).

-Hixson-Crowell equation

This model is used to study the release of particles or tablets whose surface or diameter change. Hixson-Crowell release equation is defined as:

$$\sqrt[3]{Q_0} - \sqrt[3]{Q_t} = K_{HC}t \tag{2.9}$$

2.4. MODELISATION AND SIMULATION

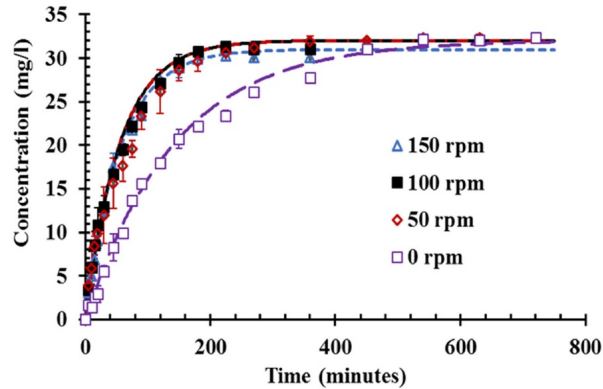


FIGURE 2.15 – Concentration versus time profile for the drug solution in the dialysis bag placed in the flask for a different shaking speeds for 0.03 g drug in 10 ml buffer ($C_0=32$ mg/l for 0, 50, 100 rpm and $C_0=31$ mg/l for 150 rpm) [181]

TABLE 2.3 – Release behavior for different mg of tablet components: Glycerylbehenate/ Hydroxypropylmethyl cellulose 1) 50/50 2) 25/75 3) 75/25 4) 100/0 5) 0/100 [182]

Formila no.	Zero order	First order	Higutchi	Hixson-Crowell
1	0.875	0.939	0.946	0.961
2	0.953	0.978	0.987	0.988
3	0.847	0.985	0.924	0.970
4	0.955	0.976	0.990	0.988
5	0.948	0.964	0.987	0.978

with Q_0 the initial amount of drug, Q_t the cumulative amount of active substance release at time t and K_{HC} the Hixson-Crowell release constant. K_{HC} is affected by the surface area and the diameter of the particles. In a study by Raslan et al. [182] on the dissolution of the theophylline from three different matrix tablet, the results are better fitted by the Hixson-Crowell equation rather than by the Higuchi, zero and first order equations as proved by the values of the coefficient of determination R^2 in table 2.3.

Besides these commonly used models, there exists many others like: the Weibull model [183], Nernst and Brunner model [184], Gompertz model [185], Danckwert model [186],...

Swelling based models:

- Flory-Rehner equation

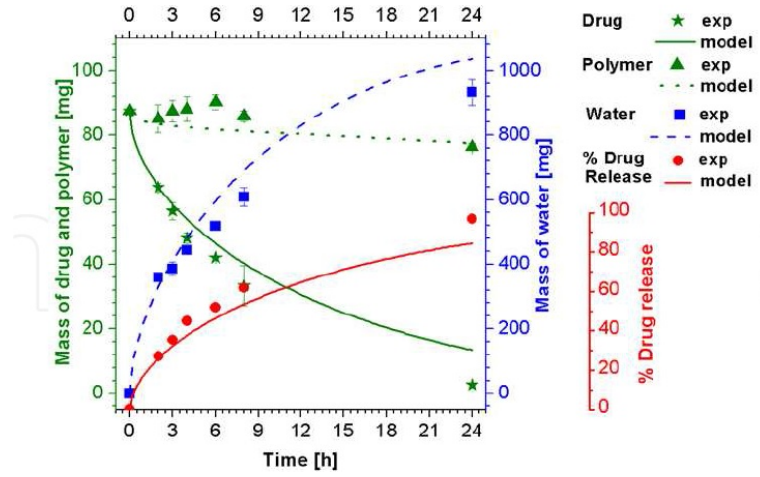


FIGURE 2.16 – Mass evolution inside the polymer matrix during dissolution time. Drug and polymer mass evolution are depicted in green and water mass evolution is depicted in blue, and the red color shows the percentage of the drug released [188]

Equation 2.10 is used in the case of swelling of the polymers (microgel swelling) in presence of liquid molecules. It describes the equilibrium swelling of a lightly crosslinked polymer in terms of crosslink density and the quality of the solvent. Equation 2.10 shows how the swelling is related to the molecular weight of chains between crosslinks [187]:

$$-[\ln(1 - \nu_2) + \nu_2 + \chi_1\nu_2^2] = \frac{V_1}{\bar{\nu}M_c} \left(1 - \frac{2M_c}{M}\right) \left[\nu_2^{\frac{1}{3}} - \frac{\nu_2}{2}\right] \quad (2.10)$$

where ν_2 is the volume fraction of polymer in the swollen mass, χ_1 is the Flory-Huggins interaction parameter, V_1 is the molar volume of the solvent, $\bar{\nu}$ is the specific volume of the polymer, M is the primary molecular mass, and M_c is the molecular weight of chains between crosslinks. This model was used by Caccavo et al. [188] for drug delivery systems based on the swelling of a hydrogel to compare their experimental results.

- Korsmeyer – Peppas equation

This equation is used mostly when the release is controlled by relaxation mechanisms (swelling, erosion...) and diffusion. This phenomenon is called anomalous or non-Fickian diffusion and is generally observed for microcapsules, microspheres and hydrophilic polymeric matrix. It is described by

2.4. MODELISATION AND SIMULATION

TABLE 2.4 – R^2 values for the release kinetics of in vitro drug release from Moxifloxacin-loaded PLGA nanoparticles. MNx means 1 drug: x polymer [191]

Formulation code	Zero-order	First-order	Higuchi	Korsmeyer-Peppas
MN1	0.867	0.961	0.967	0.978
MN2	0.950	0.988	0.990	0.992
MN3	0.956	0.948	0.955	0.964
MN4	0.888	0.935	0.970	0.979
MN5	0.938	0.977	0.981	0.986

the following equation [189]:

$$\frac{M_t}{M_0} = K_m t^n \quad (2.11)$$

where M_t is the amount of active substance released at time t , M_0 is the total amount of active substance in dosage form, K_m is the kinetic constant and n is the diffusion or release exponent, where n is estimated from linear regression of $\text{Log}(M_t/M)$ versus $\text{Log} t$. For n equals to the 0.5, it conforms to the Fick's diffusion release. For $n = 1$, it follows the zero order release mechanism, and for other n values, it follows non-Fickian law related to the existence of several simultaneous release mechanisms such as diffusion, erosion, swelling, osmosis... [190]. For example, Udgil et al. [191] have studied the release behavior of moxifloxacin from the PLGA and obtained results well fitted by the Korsmeyer-Peppas release kinetics (see the R^2 in table 2.4).

A modification of the Korsmeyer's semi-empirical equation by incorporating the concept of lag time was introduced by Kim and Fassihi [192] and Ford et al. [193]. Having accounted for the burst effect, the modified equation is given by:

$$\frac{M_t}{M_0} = K_m (t - t_{lag})^n + b \quad (2.12)$$

where K_m is a constant and b is the total fractional drug released from the burst effect.

- Peppas & Sahlin equation

This model, like the previous one, accounts for both diffusion and relaxation mechanisms.

$$\frac{M_t}{M_0} = K_1 t^m + K_2 t^{2m} \quad (2.13)$$

2.4. MODELISATION AND SIMULATION

wherein K_1 is the diffusion constant, K_2 the relaxation constant, m the purely Fickian diffusion exponent for device of any geometrical shape. Table 2.5 shows the values of m for different shapes and the related mechanisms. In a study by Argin et al. [194], the release kinetics and swelling behavior of physically crosslinked xanthan-chitosan hydrogels as microcarriers in simulated gastric fluid was studied. The release profile has better fitted the Peppas-Sahlin equation (shown in table 2.6).

TABLE 2.5 – Comparison of the value of “m” with shape of the matrix and related mechanisms [195]

Shape	Diffusion exponent (m)		
Film	0.5	$0.5 < m < 1$	1
Cylinder	0.45	$0.45 < m < 0.89$	0.89
Sphere	0.43	$0.43 < m < 0.85$	0.85
Mechanism	Fickian diffusion	Anomalous transport	Case-II transport

TABLE 2.6 – Analysis of dynamic swelling data for xanthanechitosan capsules using Higuchi, Korsmeyere-Peppas, and Peppas-Sahlin [194]

Capsule combinations with 0.7% chitosan	Higutchi	Korsmeyer- Peppas	Peppas- Sahlin
	R ²		
pH=6.2; X=0.7%	0.9792	0.9926	0.9971
pH=6.2; X=1.0%	0.9537	0.9467	0.9859

Physical degradation/erosion models:

- Hopfenberg model

This is a model, used for the drug release from slabs, spheres and infinite cylinder when they are exposed to heterogeneous erosion. It follows the following equation:

$$\frac{M_t}{M_\infty} = 1 - [1 - (K_0 t)/(C_0 a_0)]^n \quad (2.14)$$

where M_t is the amount of drug dissolved at time t , M_∞ is the total amount of drug dissolved, K_0 is erosion rate constant, C_0 the initial concentration of drug in the matrix and a_0 measured as the radius of the sphere or cylinder or the half-thickness for a slab [196]. Katzhendler et al. [197] have studied the release of the hydroxypropyl methylcellulose and amoxicillin from erodible tablets and have used the Hopfenberg model to fit their experimental results with a good accordance (shown in figure 2.17).

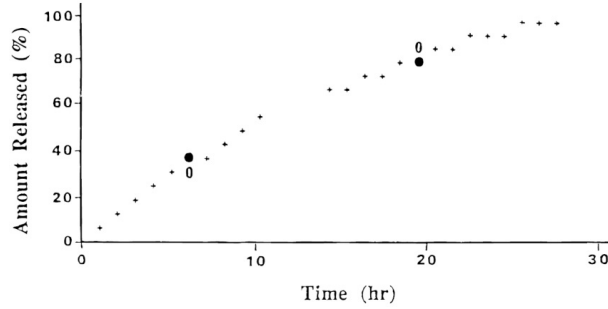


FIGURE 2.17 – Release of Amoxicillin from whole tablet surface plotted according to Hopfenberg equation: (●) predicted values calculated according to Hopfenberg equation; (○) observed data; (+) predicted and observed (when the two points overlap), Tablet composition; 15% Methocel K4M+5% PEG 4000 [197]

- Zhu model

This is a model, used for the drug release from polymer matrix exposed to the erosion. It is an analytical model proposed for describing mass loss in polymer thin films [162] adapted for the drug release. It follows the below equation:

$$\frac{M_t}{M_\infty} = 1 + e^{-2kt} - 2e^{-kt} \quad (2.15)$$

where M_t is the amount of drug released by mass loss of polymer, M_∞ is the total amount of drug, k is the reaction rate constant, and t is the time.

Osmotic model:

The usual equation for the release rate of a drug across a semipermeable membrane due to osmosis is expressed by [198]:

$$\frac{dM_t}{dt} = \frac{A}{h} K' (\Delta\pi S) \quad (2.16)$$

where A and h are respectively the area and the thickness of the membrane, K' is a constant related to the membrane permeability, $\Delta\pi$ is the osmotic pressure gradient across the membrane and S the saturation solubility of the drug in the dissolution medium.

2.4.2 Mechanistic model of drug release profile

In drug delivery systems, mathematical modeling plays an important role in clarifying the important drug release mechanisms, thus facilitating the development of new pharmaceutical products by a systematic, rather than trial-and-error, approach. Predicting the spatio-temporal profile of drug delivery systems by the improvement of mathematical models and simulations will increase the efficacy of the therapy and will reduce the development time of the DDSs [128, 166, 199–201]. In this regard, a set of physical mechanisms are involved (mathematical models discussed in section 2.4.1), where the diffusion normally is present in all of them. For some approaches, such as numerical simulation, some characteristics of the drug carriers and of the environmental conditions are sufficient to predict the drug release profile. On the other hand, some empirical models are developed for a family of drug carriers based on a set of experimental data. In order to remain efficient, these empirical models must be also able to predict release profiles even if these profiles do not belong to the experimental data used to obtain it.

To develop these mathematical models, some boundary conditions are required and of course, some assumptions must be applied in order to make the models more applicable. For example, we can assume that the drug is uniformly distributed in the polymeric matrix of the DDS. Likewise the shape of the drug carrier affects the drug release through the geometrical boundary conditions. Moreover, the state of the drug in the DDS can lead to two possibilities: (i) the initial drug loading is lower than the solubility of the drug inside the polymer matrix ($C_0 < C_s$), which implies a dissolved drug system, and (ii) the initial drug loading is higher than the solubility of the drug inside the polymer matrix ($C_0 > C_s$), which implies a dispersed drug system. Therefore all the boundary conditions of the mathematical models should be carefully taken into consideration [202]. For this reason, the release profile from these two DDS may not be the same. However, it does not mean that the more complex the mathematical model is, the better it is. The most ideal model is the simplest model that is able to satisfy the theory of step-by-step drug release mechanisms for general cases and highlight the important process affecting the drug release profile.

Depending on the aim and complexity of the models, each of these three regions (polymer film, tissue artery, lumen) can be take into consideration as shown in figure 2.18. Improving the model accuracy requires an appropriate description of the fundamental mechanisms involved behind the

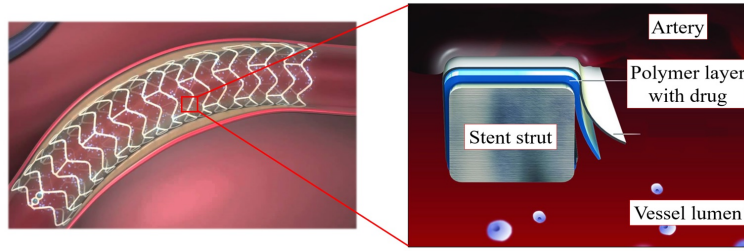


FIGURE 2.18 – Schematic of a drug-eluting stent and its different layers and the contact mediums

physical processes. Mathematical models for the estimation of drug release profiles follow two distinct approaches: either by solving the equations of the physical mechanisms involved [181, 203]; or by taking into account the appropriate kinetics [165, 204–206]. It is necessary to identify the main impact of many factors affecting the release profile to ensure the success of any form of modeling. Since many factors govern the release kinetics, the mathematical models are usually formed by the sum of the models associated to the mechanisms, supposedly independent from each other [207]. Of course the difficulty here is to carefully identify every mechanism involved in the release. In this regard, in a study by Lucero-Acuna et al. [208] studying the effect of the temperature variation on the drug release from the nanoparticles of PLGA in a solution of PBS, the temperature effect was applied to the drug release data with two different models. The first model consisted in the simultaneous burst release and degradation-relaxation mechanism (BR model). The second model consisted in the diffusion in addition to the former mechanisms (BRD model). Figure 2.19 shows the comparison of the experimental results with the BR and BRD models. The curves indicate that both models fit well the experimental data but considering in addition the mechanism of diffusion, the accuracy of the model has increased.

In their study, Zhu et al. [162] have investigated a mechanistic model for in vitro sirolimus release (data from the literature) from PLGA biodegradable stent coatings coupled with polymer degradation and erosion. For this aim, the drug transport in the PLGA coating is based on a varying effective diffusivity D_e accounting for the variation of the molecular weight M_w of PLGA, its porosity ϕ and drug partitioning in the solid and liquid-filled pores (κ). The coupled degradation-erosion model and the drug release model are solved and validated using in vitro sirolimus release data (equation 2.17):

$$\frac{\partial C}{\partial t} = \frac{\partial}{\partial x} \left(D_e(M_w, \phi) \frac{\partial C}{\partial x} \right) \quad (2.17)$$

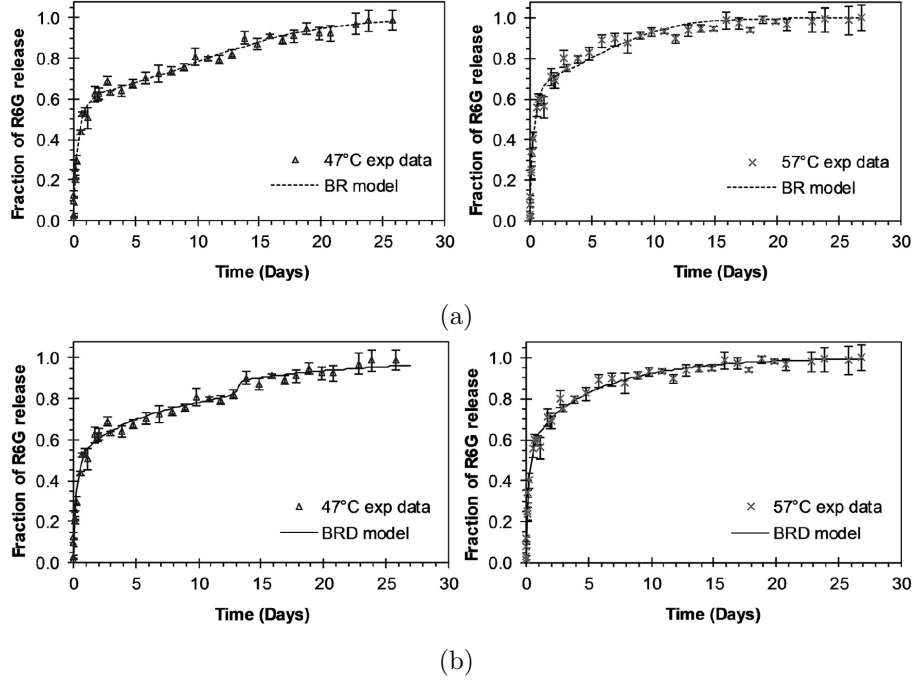


FIGURE 2.19 – (a) Experimental and theoretical (BR model) R6G release profile from PEGylated nanoparticles at different temperatures, (b) experimental and theoretical (BRD model) drug release profile from PLGA nanoparticles at different temperatures [208]

in this model, the effective drug diffusivity D_e is derived from the diffusivity in the polymer phase D_s , the diffusivity in the liquid-filled pores D_l , porosity ϕ , and drug partitioning between the liquid-filled pores and solid PLGA phase κ :

$$D_e = \frac{(1 - \phi)D_s + \kappa\phi D_l}{1 - \phi + \kappa\phi} \quad (2.18)$$

the diffusivity in the polymer phase D_s further depends on the change of M_w , and according to the reptation theory in polymer physics, this diffusivity correlates with the average of M_w

$$D_s = D_{s0} \left(\frac{M_w}{M_{w,0}} \right)^2 \quad (2.19)$$

where $M_{w,0}$ is the initial weight-average molecular weight to model the drug release, the effective drug diffusivity in equation 2.18 requires the value of the porosity, which is related to the mass loss via the following expression:

$$\phi = \phi_0 + (1 - \phi_0)(1 + e^{-2kt} - 2e^{-kt}) \quad (2.20)$$

where ϕ_0 is the initial porosity in the PLGA coating and k is the degradation rate constant. From the

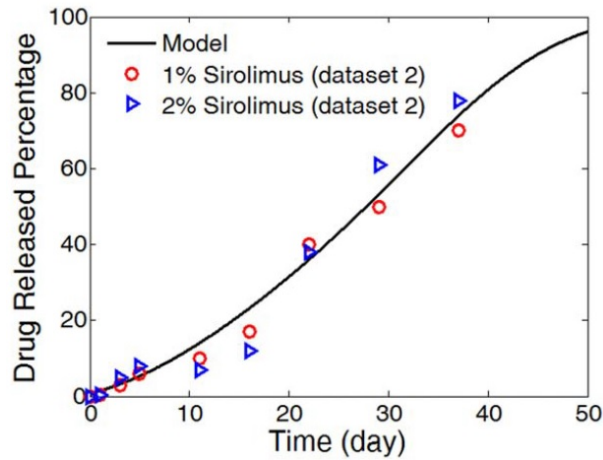


FIGURE 2.20 – Model simulation matches experimental data of sirolimus release from PLGA coating [162]

above mentioned model, the sirolimus release from the PLGA stent was predicted. The experimental results and the model are compared in figure 2.20. There is a good match between both approaches.

2.4.3 Simulation of drug release profile

Apart from the mathematical modeling, numerical simulations are very helpful tools in the prediction of the drug release profile. In this case some studies have performed the calculation in one-dimensional [209], some in two-dimensional [210, 211] and also three-dimensional [199, 212]. In this regard, there is the possibility to calculate the drug concentration in all the three regions in contact with the stent. Some studies have predicted the drug release in the lumen and blood domain. On the other side, some studies have focused on the drug content in the artery tissue (for the purpose of therapy). Finally, some studies have focused on the drug release from the polymeric film coating the stents [81, 213, 214]. In some studies, the initial concentration of the drug is considered to remain constant during the release, which does not fit the reality [214–217]. Like for the mathematical modeling, we also commonly find in the numerical simulations some assumptions and simplifications. For example, in some studies, steady flow is considered instead of pulsed flow, because they have stated that the effect of the pulsatility on the release of the drug from DES is negligible [79, 80]. However, some other studies talk about the importance of the pulsed flow rate. In the aim of stent optimization, several numerical studies focused on the influence of some geometrical parameters and on the polymer and drug

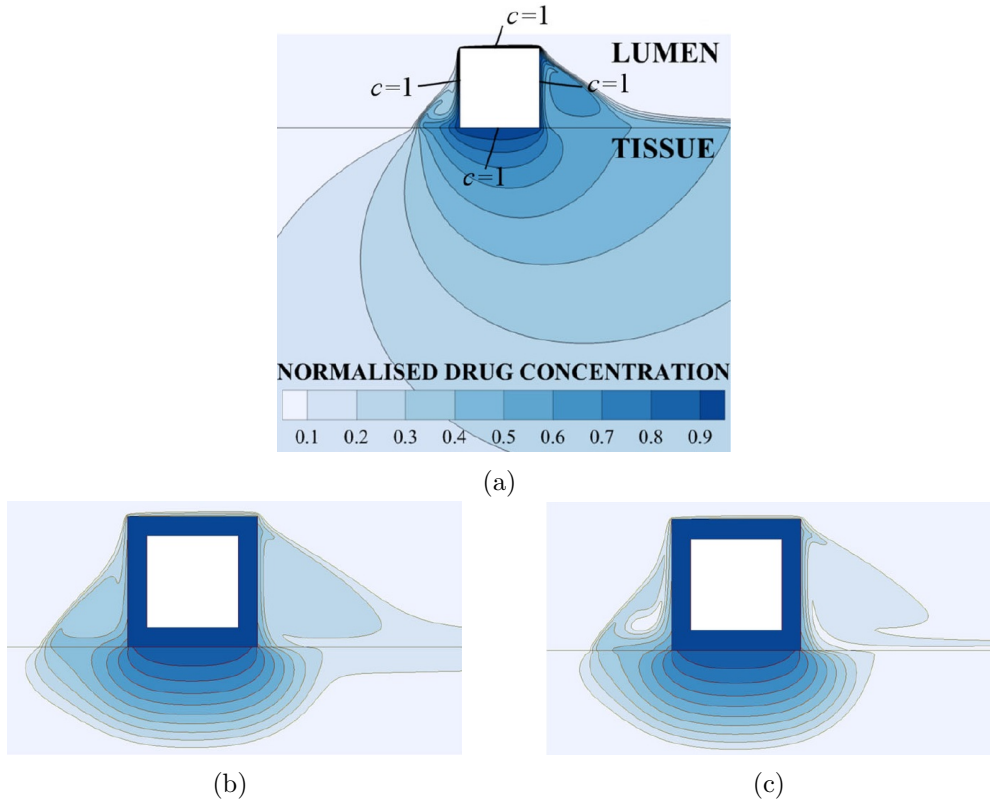


FIGURE 2.21 – Normalized drug concentration distribution (a) in the premier study with considering constant drug concentration, at the second study with varying concentration (b) at steady-state flow rate and (c) pulsed flow pattern [80]

properties (diffusion coefficient, strut spacing, effect of the plaque in the stenosed artery) [218–220]. For instance, Barakat et al. [18, 32] have studied the drug concentration in the tissue for two different types of drug and they have analyzed the kinetics of the drug uptake. One of the advantages of the numerical simulation is its ability to provide quantitatively and qualitatively the drug distribution in the different regions (lumen, tissue and polymer). In a study by Vijayaratnam et al. [211] they have studied qualitatively the drug distribution around the stent and in the tissue. In this first work in 2D, they consider the flow as steady and also the drug content in the polymer as constant during the time. They have obtained the qualitative distribution of the drug in the tissue which was firmly affected by the flow rate. However, in another study [80] time varying depletion of the drug from the coated stent was modelled at the steady and pulsed flow. The simulation results showed that changing the luminal blood flow pattern, the non-Newtonian properties of blood and its complex near-wall behavior has negligible effect on the drug uptake. Figure 2.21 shows these results.

In another study by Ferreira et al. [221] the effects of the stent geometry (due to the atherosclerosis plaque eccentricity) on blood hemodynamics and drug release in a stented artery is investigated. Figure 2.22 (a) shows the results of the simulation. Their results showed that medial segments, R3 in the eccentric case and R5 in the concentric case, exhibit simultaneously low wall shear stress and low drug concentration. These findings suggest that restenosis and thrombosis can occur with higher likelihood. Moreover, in the eccentric wall (bottom) the drug diffuses very quickly, due to the higher diffusion coefficient in the healthy part of the vessel wall.

2.4.4 In vitro-in vivo correlations and acceleration method

The in vitro tests, as long as they are representative or close to the in vivo tests, are particularly important. One of the challenges of this decade is therefore to develop reliable correlations between in vitro and in vivo tests. An in vivo/in vitro correlation (IVIVC) is described by the US Food and Drug Administration (FDA) as a predictive mathematical model that describes the relationship between an in vitro property of an extended release profile (usually the rate or extent of release of the drug) and a related in vivo response, for example, plasma drug concentration or amount of drug absorbed [222, 223]. This relationship may be qualitative or semi-quantitative, such as the mechanism of the release. This method is more developed and used for the oral administration, where it permits to develop the drug carrier and to control the dosage of the drug in the window therapy. Therefore, a validated predictive IVIVC will have a substantial positive effect on the consistency of the commodity, and increased productivity and decreased costs. To develop an IVIVC model, both in vitro and in vivo results are requested. According to some studies [224–226], to develop IVIVC mathematical models, relating the entire release of the drug in vitro and predicting the drug absorbed or the concentration of the drug in plasma, the mathematical correlation is applied in both one stage or two-stage procedure. For the single stage IVIVC procedure, the in vitro release data are used considering the pharmacokinetic parameters such as C_{max} , T_{max} , absorption lag time, to predict the plasma drug profile. An example for such a one-stage process is the study by Jacobs et al. [227] where an IVIVC model was developed for the oral delivery of components of galantamine by combining the immediate-release and extended-release and integrating the pharmacokinetic profiles of them. The second type is a two-stage procedure, which is more common to build the IVIVC. It is more straightforward because the in vitro released drug and the in vivo absorbed drug can be directly compared. An example of a two-stage approach is shown in

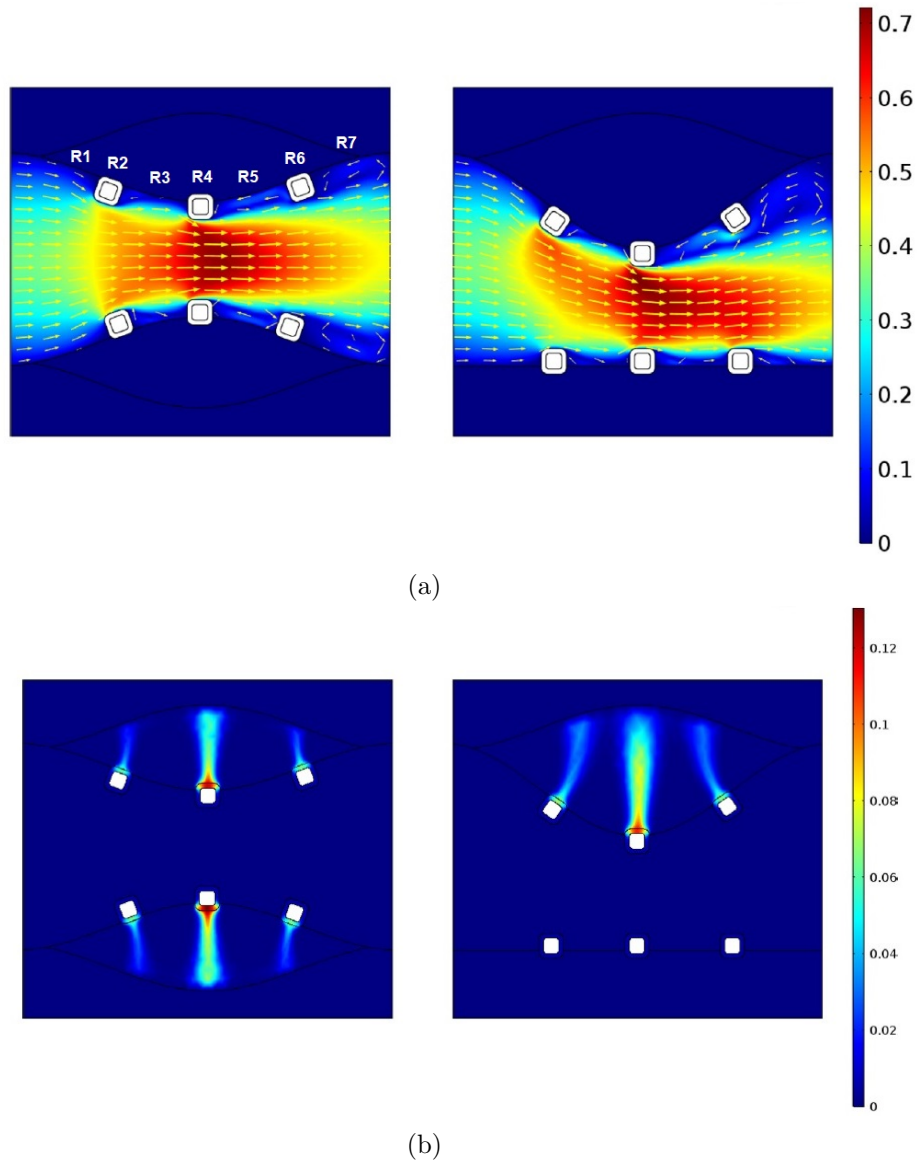


FIGURE 2.22 – (a) velocity field [m/s] in concentric (left) and eccentric (right) stenosis models, (b) Normalized drug concentration distribution into the arterial wall in concentric (left) and eccentric (right) stenosis models after one month [221]

2.4. MODELISATION AND SIMULATION

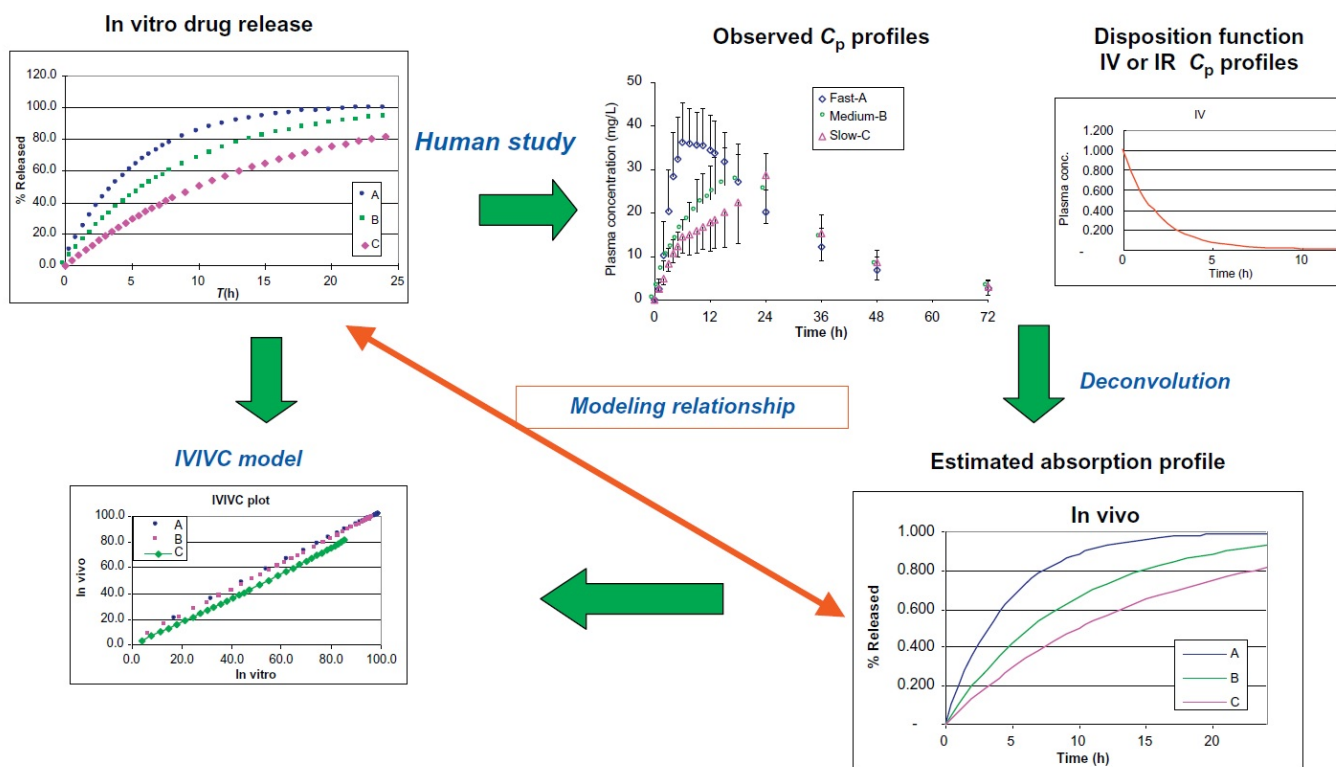


FIGURE 2.23 – Illustration of convolution and deconvolution in IVIVC development [224]

figure 2.23 [224].

Several failures in attempts to achieve IVIVC for drug administration can typically be due to the discrepancy between experimental conditions of the in vitro and in vivo tests. It is therefore important to consider how in vitro and in vivo results can be influenced by various parameters such as the physico-chemical and biopharmaceutical properties of the drug, the administration technology, the formulation of a drug and its interactions with the in vivo and in vitro environment [224]. In this regard, a qualitatively and quantitatively relationship should be established between the drug release profiles, considering different parameters of in vitro tests. The latter will help to better choose the in vitro experimental methods and conditions in order to better correlate with the kinetics and the mechanisms of the in vivo release. For example, Ma et al. [154] investigated the release profile of the combinations of two drugs of paclitaxel/sirolimus in vitro (measuring the drug content in PBS) and in vivo on a model of rat aorta. The results from these experimentations showed that both drugs at both in vitro and in vivo conditions had a two-phase release profile. The results are shown in figure

2.4. MODELISATION AND SIMULATION

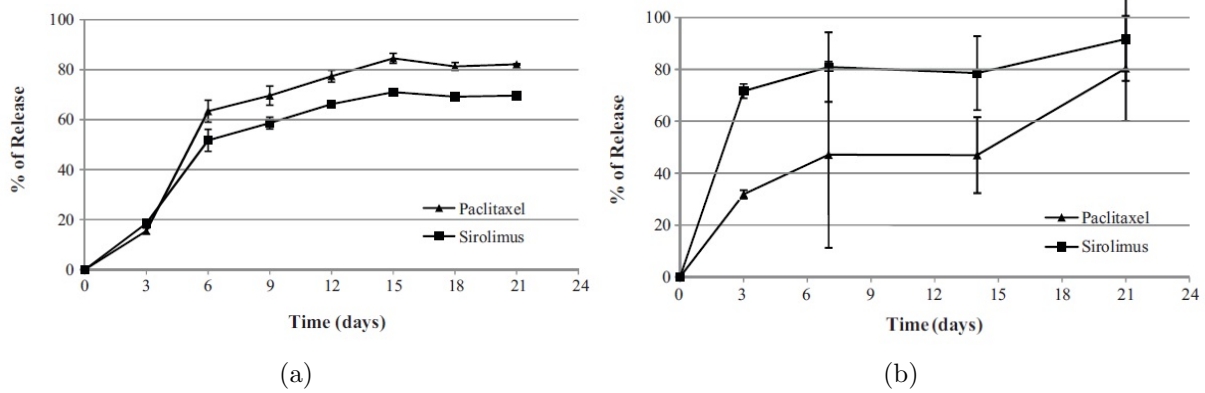


FIGURE 2.24 – (a) In vitro and (b) in vivo, release profiles of paclitaxel and sirolimus from PLGA/ACP coated stents [154]

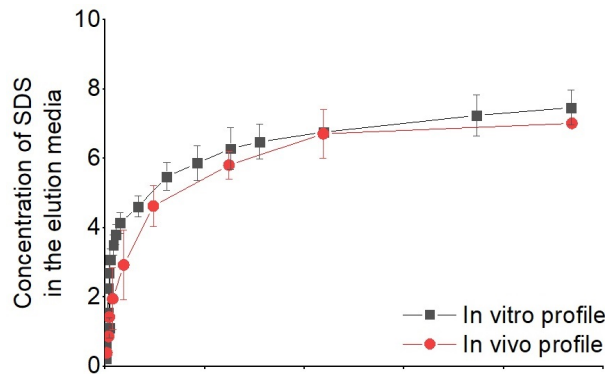


FIGURE 2.25 – Comparison of the in vitro and in vivo profiles with time-scaling factor [127]

2.24.

If the in vitro results are not correlative with in vivo results, the in vitro conditions should be improved to get closer to the in vivo conditions and therefore to the in vivo results. In a study by Sako et al. [228], the in vitro release of acetaminophen from different compositions of a hydrophilic matrix was evaluated but did not correspond to the in vivo tests. Thereafter by modifying the in vitro test conditions, the results became more consistent with the in vivo results. One of the difficulties in this method is that each IVIVC is valid only for a specific set of parameters. Therefore by changing one of these parameters (e.g. with or without excipients), it is necessary to develop a new IVIVC [229, 230]. Therefore developing a IVIVC should be studied case by case, referring to the different types of the DDS and considering different effective parameters, and their adaptability to the in vitro conditions. In the case of drug-eluting stents there is high enough parameters for adapting. In this regard, some

2.5. SUMMARY

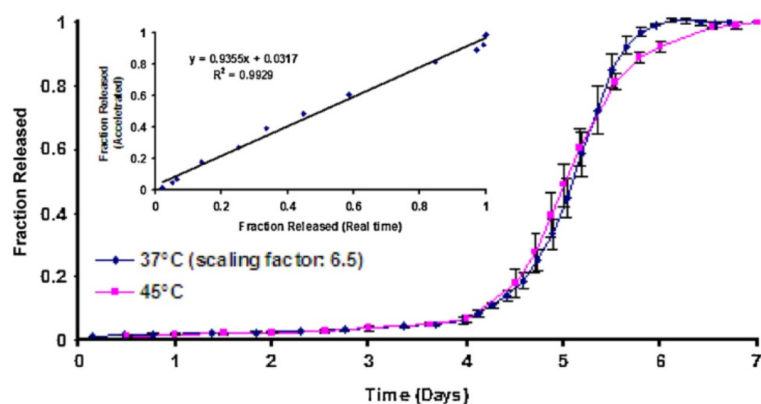


FIGURE 2.26 – In vitro release profiles of Risperdal Consta 25 *mg* long acting injection (risperidone microspheres) in 0.05 *M* PBS pH 7.4 at 37°C (time scaled) and 45°C ($n = 3$). Insert shows linear correlation between real time (37°C) and accelerated (45°C) fraction released [231]

researchers focus on one parameter, such as the strut thickness, dosage, type of the drug or type of the material, etc, whereas some others focus on multiple parameters.

The accelerated in vitro tests are also in the center of the attention. In a study by Rawat et al. [231] they have performed the in vitro release tests from microspheres at different temperatures, which was a parameter for accelerating drug release (shown in figure 2.26). Finally, they have made a correlation with the in vivo release profile.

In another study by Merciadiez et al. [127], they have modified different parameters of the in vitro release tests from DES in order to bring the in vitro release profiles close to the in vivo release profiles. In this aim, they have obtained an in vitro release profile from USP apparatus 4 in 24 hours, which corresponds to the in vivo release profile of 30 days in porcine artery. Figure 2.25 shows this correlation. The parameters chosen for the in vitro test were as follows: test apparatus (USP 4), elution medium was an organic solvent, flow circulation of 25 *ml/min*, pH about 4.5 and the temperature of 37°C. According to the current state of the art, there is no universal method for in vitro tests that can mimic the complexity of the in vivo tests.

2.5 Summary

According to the bibliography, a lot of work has been done in the field of drug delivery. It can be deduced from these studies that, due to the great importance of intrinsic properties of the compounds

2.5. SUMMARY

of drug carriers in the release profile, researchers have recently begin to study and analyze more precisely the stent materials rather than directly examine drug release profile from a final commodity. This approach is very helpful in choosing the design parameters. Compared to oral drug delivery, for which the advances are highly significant, the improvements in the case of stents are still rather slow. Among the elements to progress in this area, a bio-relevant device that can simulate real conditions is required; this device can be helpful to properly analyze the behavior of the compounds subject to the variation of miscellaneous parameters. The lack of these points in studies on drug-eluting stents has led us to design a bio-relevant test bench that can approach to real conditions. This device is able to simulate both the lumen and the tissue of the artery. Moreover, this test bench can reproduce the systolo-diastolic flow patterns encountered in blood flows.

This bibliographical review also points out the lack of information concerning the evolution of the main mechanical properties of the polymer. For this reason, two different types of polymers have been investigated mechanically before and during drug release in addition to the main physico-chemical properties.

Besides, mathematical models, which can predict drug release behavior by considering physical and chemical mechanisms associated to the used compounds, can be effective in this regard. To do so, a model to predict the release profile based on the mechanisms associated with release from the different types of polymers was developed. Moreover, an accelerated two-parameter kinetic model, considering the flow rate and the initial drug load, was elaborated.

Finally, many models and simulations are available among the literature but validations based on bio-relevant in vitro tests are missing. In this study, we present also a comparison between a numerical simulation, a mathematical model and experimental results.

Chapitre 3

Materials and methods

Content

3.1	Materials	90
3.2	Samples preparation	91
3.3	Bio-Relevant Apparatus (BRA)	93
3.3.1	Specification and description of the BRA	93
3.3.2	Generation pulsed circulation	96
3.3.3	Mimicking arterial system	99
3.4	In vitro drug release procedure and associated measurement	102
3.4.1	Protocol of the UV-Vis method	102
3.4.2	Protocol of the gravimetry method	104
3.5	Characterization methods	106
3.5.1	Microscopic observations	106
3.5.2	Differential Scanning Calorimetry (DSC)	106
3.5.3	Thermo Gravimetric Analysis (TGA)	106
3.5.4	Dynamic Mechanical Thermal Analysis (DMTA)	107
3.5.5	Fourier-Transform InfraRed spectroscopy (FTIR)	107
3.5.6	Drug solubility	107
3.5.7	Tensile testing	107
3.5.8	Permeability measurement of the hydrogel	107
3.5.9	Fluorescence spectroscopy	108

This chapter presents the experimental materials and methods developed during this thesis. In the first section, we explain our choices concerning the materials used to model the polymer-matrix and the selected drugs. The second section presents the bio-relevant apparatus designed to perform the tests. The third section describes the procedure adopted for samples manufacturing. We present in the fourth section the methods implemented for the determination of the release kinetic-profiles. The description of the other physical and mechanical characterization tools, allowing more robust analysis and explanation of the mechanisms involved, is the subject of the fifth section.

3.1 Materials

In this study, two kinds of polymers, degradable and non-degradable, and two kinds of drugs, hydrophile and hydrophobe, were used. The non-degradable polymer Polyurethane (PU) results from the synthesis of the hardener, isocyanate type 4,4-diphenylmethylenediisocyanate (MDI) with a resin Gyrothane 639. This resin is composed of polyol, dye, and a catalyst. The related items were supplied by the RAIGI company.

PLGA (Poly(lactic-co-glycolic acid)) is the second type of the polymer used in this study. It is a biodegradable polymer with a 50-50 molar ratio of D,L-lactic to glycolic acid and a molar weight $MW = 38 - 54 kDa$. The solvent used for the synthesis of PLGA is ethyl acetate, purchased from Sigma Aldrich, France. This solvent was chosen because it also dissolves the drug without degrading it, therefore it distributes the drug homogeneously in the polymer carrier. Figure 3.1 shows the chemical formula of two polymers.

Concerning the hydrophobic drug, we chose the diclofenac sodium (DS) [232] purchased from Sigma-Aldrich, France. It is a nonsteroidal anti-inflammatory drug used to treat pain and inflammatory diseases. It has the molecular weight of $318.13 g/mol$ and its water solubility is of about $0.014 mg/ml$ at room temperature. As for the hydrophilic drug, diclofenac epolamine (DE) supplied by the Genevrier laboratory in granular form is used. In $65 mg$ of this active substance, $50 mg$ of diclofenac sodium and $15 mg$ of epolamine and excipient are identified. Its density is about $450.7 mg/ml$ and its water solubility at $37^{\circ}C$ was measured to be about $5.554 g/l$. Figure 3.2 shows the chemical formula of the two drugs. To perform the medium mimicking the arterial wall, an agarose gel, purchased from Sigma-Aldrich, was used. This choice is motivated by the long-term stability of this gel, its mechanical

3.2. SAMPLES PREPARATION

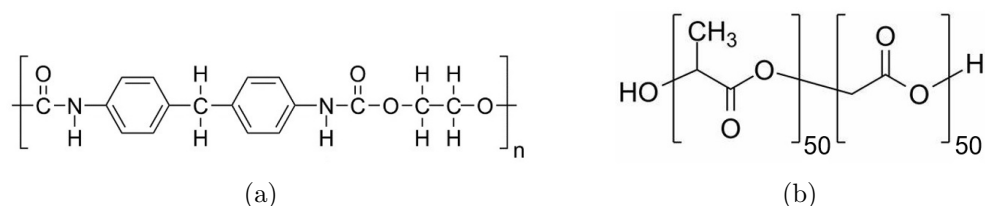


FIGURE 3.1 – Chemical formula of (a) PU and (b) PLGA

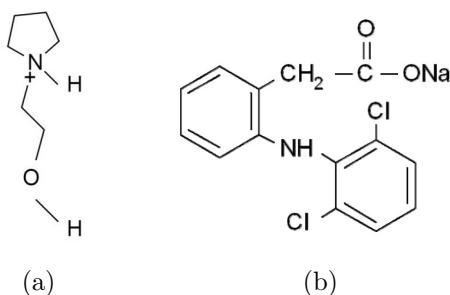


FIGURE 3.2 – Chemical formula of (a) epolamine and (b) diclofenac sodium

properties and its permeability to the chosen drugs.

A Phosphate Buffered Saline (PBS) is used to mimic the blood. This fluid was chosen due to the proximity of its ions to those of the blood and its ability to keep the pH close to 7.4, during the release test. The PBS is also a suitable solvent for the chosen drugs. This substance was purchased from Sigma-Aldrich, France. Distilled water was the second type of the fluid used in this study, where it was provided in the laboratory.

Finally, to study qualitatively the drug distribution in the artificial gel, phosphorescent micro-particles, because of their long lifetime, were purchased from Luminetic, Deutschland Germany.

3.2 Samples preparation

PU-DE

Two types of samples, loaded and unloaded, are manufactured. Process is:

- i) A solution combining the hardener and resin in a proportion of 2/5 following the recommendations of the technical data sheet is prepared. For loaded samples, the resin is premixed with the drug in mass ratios, drug mass / polymer mass, in a range of 10% to 30%.
- ii) The homogenization of the mixture in a beaker is carried out by magnetic stirring for approximately 30 minutes at 600 rpm and

3.2. SAMPLES PREPARATION

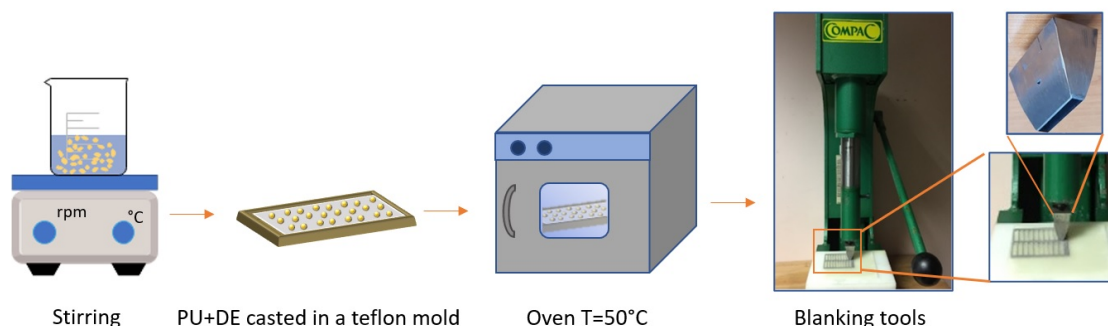


FIGURE 3.3 – Fabrication process of PU samples loaded with DE

the ambient temperature. iii) The mixture thus prepared is poured into a mold covered with Teflon. Particular care is taken to collect all the prepared mixture using a stick. iv) The loaded mold is heated in an oven regulated at 50°C for about 30 min . v) Finally, the plates taken out mold are cut using a punch, shown in figure 3.3 on the right, into rectangular samples of $5 \times 30\text{ mm}^2$ and thicknesses 0.3 and 2 mm . A precision caliper is used (precision $\pm 0.001\text{ mm}$). All the equipment (beaker, magnet, wooden sticks...) were covered with Teflon films in order to prevent the ingredients to stick to them.

PLGA-DS

Two types of samples, loaded and unloaded, are manufactured. Process is:

i) A mixture of $20\%w/v$ polymer in solvent (ethyl acetate) was prepared. For loaded samples, two different percentages ($5\text{ wt.}\%$ and $10\text{ wt.}\%$) of DS were considered; this means that for 1 g of PLGA, 0.05 g and 0.1 g respectively of drug was added. A solution of the drug and the solvent was prepared in a screwed glass vial. ii) The homogenization of the mixture in a beaker is carried out by magnetic stirring for approximately 60 minutes at 100 rpm and near to 70°C . Then the weighted PLGA was added into this solution and finally we kept agitating at 600 rpm for about 1 hour at 40°C .

iii) The mixture thus prepared is poured into a mold covered with Teflon and dried at room temperature for 24 hours . iv) The loaded mold is placed in a vacuum oven regulated at 40°C for 24 hours . v) Finally, the films taken out mold are cut using a punch into rectangular samples of $0.3 \times 5 \times 30\text{ mm}^3$.

Hydrogel

To perform the tests with the artificial tissue layer, agarose gels were prepared in 1% (w/w) of

3.3. BIO-RELEVANT APPARATUS (BRA)

concentration. This means that for 0.1 g of agarose powder, 10 ml of PBS were used. The agarose was dissolved in PBS at about 100°C, stirred with a magnetic stirrer until optically clear solutions were obtained. During this period, the container was firmly closed in order to avoid the evaporation and change the concentration. Then the temperature is lowered to 60°C and the solution is poured into the container molds where they are cooled until gelation.

3.3 Bio-Relevant Apparatus (BRA)

3.3.1 Specification and description of the BRA

Specification

Designing a Bio-Relevant Apparatus (BRA) is a complex task that requires knowledge to develop the mechanical and physico-chemical environment to make the system as close as possible to the environment of the *in vivo* tests. In this study, two biochemical and biomechanical parameters were considered in order to achieve an ideal BRA. Biomechanical parameters are:

- Flow rate
- Pressure

And the biochemical parameters include:

- pH
- Temperature

The objectives of this work is to develop a BRA that can provide static, steady or unsteady flow conditions. To generate the unsteady flow patterns, this apparatus should be equipped with an electronic circuit connected to a pulsed pump that can produce a systolo-diastolic flow. It also should contain a pressure sensor, a flow-meter and a thermometer; the apparatus should also contain a regulating system to control the flow rate, the pressure and the temperature of the medium in real-time. This BRA should be able to perform the tests with or without the artificial tissue. In the latter case, it should allow to measure the amount of drug released from the polymeric carrier into the flow or/and into the artificial tissue.

Pulsed pressure and flow rate

The levels of blood pressure and the shape of the pulses vary with age and people. We therefore

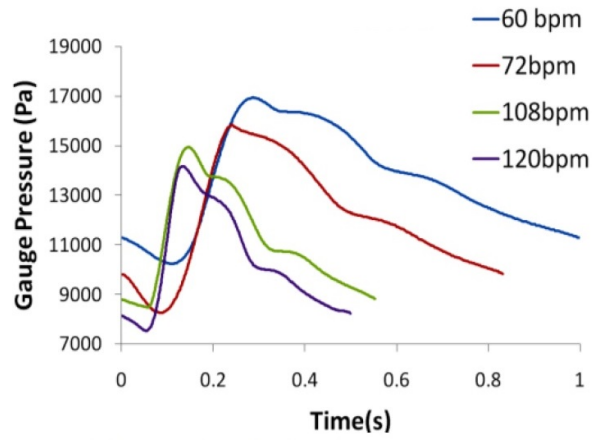


FIGURE 3.4 – Pressure waveforms at different heart rates [233]

studied the typical arterial pulse among the patients. Figure 3.4 shows the systolo-diastolic waveforms in a human carotid of different people at different heart rates. Blood pressure has the following characteristics:

- 110 to 140 *mm Hg* for systole
- 60 to 80 *mm Hg* for diastole
- 70 to 95 *mm Hg* for the average
- 60 to 80 beats per minute

In figure 3.5, we see the corresponding variations of the flow rate for the same patients. It varies between 5 *ml/s* and 35 *ml/s* (the average flow rate at rest is about 5 *l/min* in the heart).

General view of BRA

A general view of the apparatus is shown in figure 3.6. The apparatus is composed of two floors. At the first floor, we have two pumps, a reservoir and the water heater. The test chamber was placed at the second floor. A pressure sensor, a flow-meter and a thermometer to monitor the pressure, the flow and the temperature of the circuit in the real-time are also connected to specific points shown in figure 3.6.

In this study, a one-liter cubic reservoir in plastic (1) was used to store the fluid that is used to simulate the blood. The apparatus being a closed loop, the capacity of the reservoir was chosen to avoid the saturation of the solution during the time of release.

3.3. BIO-RELEVANT APPARATUS (BRA)

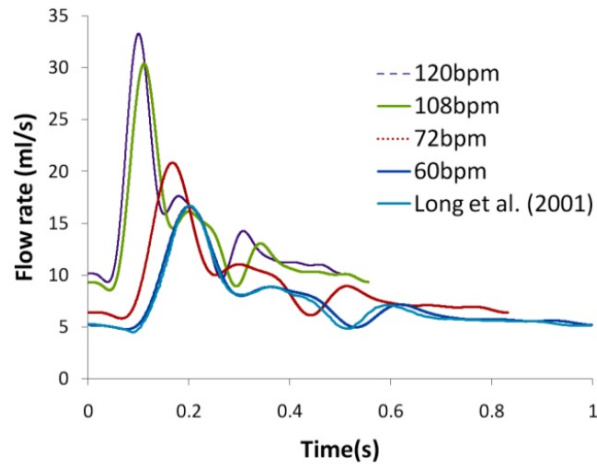


FIGURE 3.5 – Flow rate waveforms for different pulse rates [233]

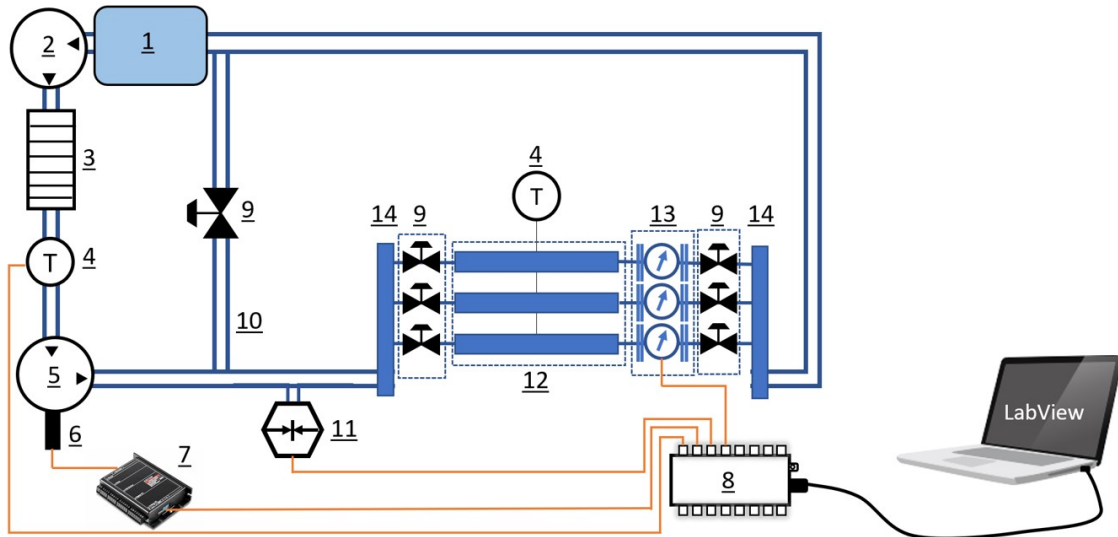


FIGURE 3.6 – Schematic of the bio-relevant apparatus

3.3. BIO-RELEVANT APPARATUS (BRA)

A magnetic-drive centrifugal pump model VM-D20T-SP (2) was connected to the outlet of the reservoir in order to push the solution towards the electric heater (3) and thereafter towards the system. This pump was used in the case where the steady flow in the system was needed. To regulate the flow rate, the valves at the entrance and a by-pass were used. In order to simulate the body temperature, an adjustable electric heater (3) was used to regulate the temperature efficiently and maintain it always at a constant value. The temperature of the fluid in the system was verified (4) to be always in the range of $37\pm 0.5^{\circ}C$.

The two important characteristics of the BRA, generating the pulsed flow and simulating the artificial artery are explained below:

3.3.2 Generation pulsed circulation

Pulsed pump

To generate the fluid circulation in pulsed regime particularly, we have adopted the solution of the centrifugal pump controlled by a variable speed. The impeller and volute design were carried out following the method of centrifugal pumps design and performances analysis and the CFD procedure developed in [234]. The design point specified, the geometric parameters and the hydraulic design for the impeller and the volute are given respectively in figure 3.7 (a) and (b). Figure 3.8 shows the characteristics of the pressure-flow rate for diverse speed of rotation of the impeller and the time setpoint for this rotational speed provides access to the pulsed signal, as explained below. The CAD of the pump and its shaft line is shown in figure 3.9. Manufacturing the impeller and volute was subcontracted to MDP, and the other parts were carried out at the prototyping center in ENSAM. To drive the impeller of the centrifugal pump, we have used a DC motor, Maxon EC-4-pole motor (5). This motor was selected considering the power to be supplied to the fluid. It is connected to an ESCON-Maxon servo controller (6). This controller is linked to a National Instruments acquisition card (7). This card, controlled by LabView, generates the commands of the pulsed wave patterns and the number of pulses per minute received by the servo controller (figure 3.10 shows the program written in LabView to generate the pulsed flow). A coupling connects the motor and pump shafts. Figure 3.9 shows these parts.

Electronic parts

The electronic circuit is a major part to control the relation between the elements of the apparatus

3.3. BIO-RELEVANT APPARATUS (BRA)

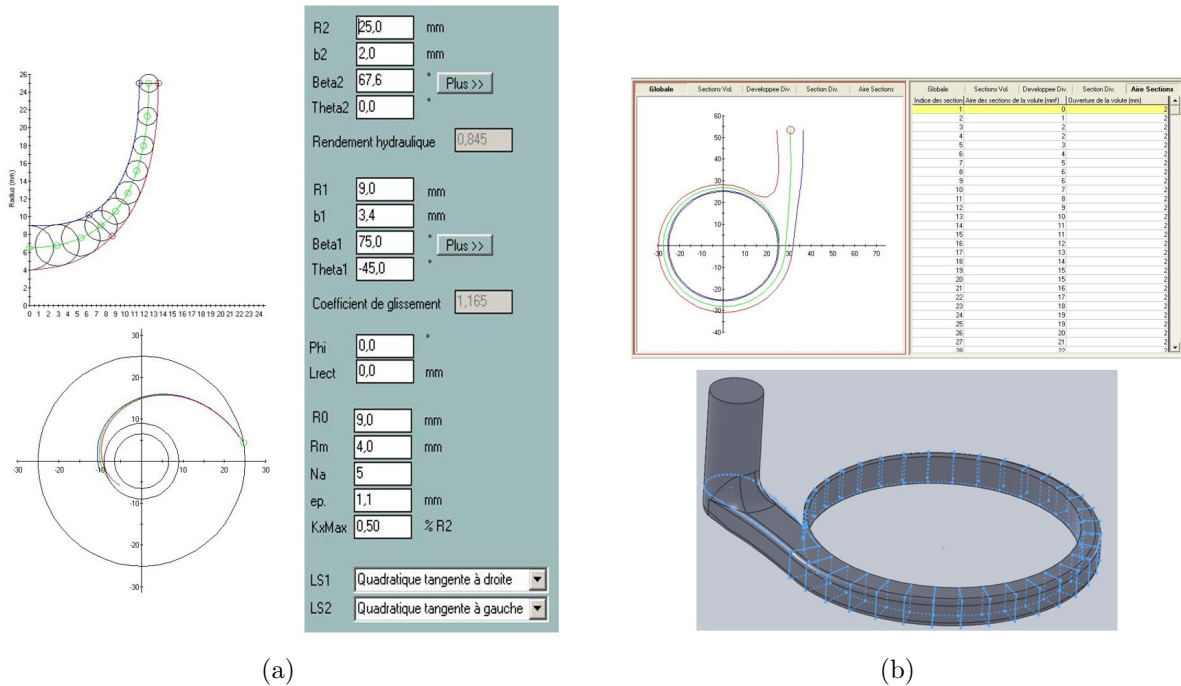


FIGURE 3.7 – Geometric parameters and the hydraulic design of (a) the impeller and (b) the volute [235]

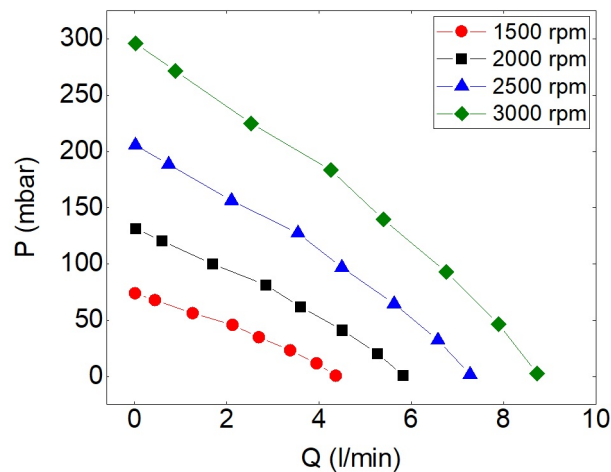


FIGURE 3.8 – Characteristics of the pressure-flow rate for diverse speed of rotation of the impeller [235]

3.3. BIO-RELEVANT APPARATUS (BRA)

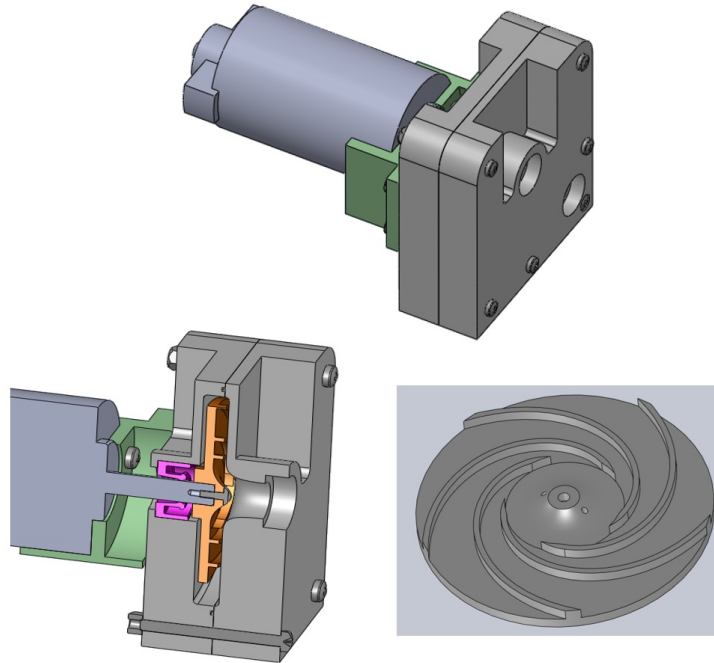


FIGURE 3.9 – Centrifugal pump for generating the pulsed flow [235]

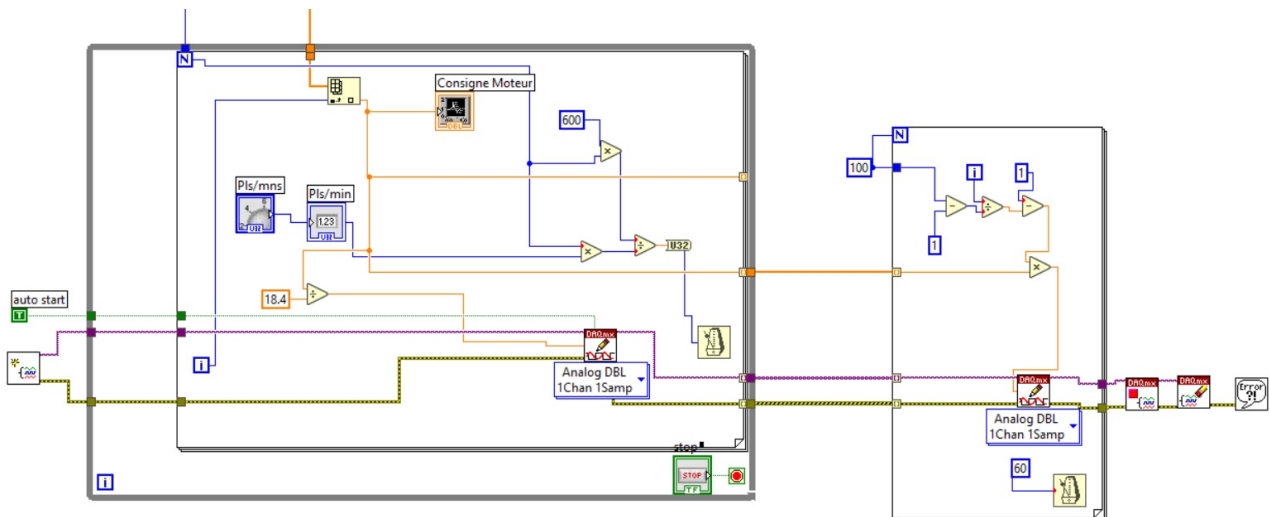


FIGURE 3.10 – Loop of the command of pulsed flow and regulator of the number of pulses per minute

3.3. BIO-RELEVANT APPARATUS (BRA)

(motor, flow-meter, pressure sensor, and thermometer) and the acquisition card. The acquisition card is responsible for the communication between the control system (computer with Labview software) and the electronic components. In this study, the NI USB-6008 acquisition card (8) was used and was connected to all the sensors. A flow-meter of a FT-110 Series–TurboFlow (13) and a pressure sensor (11) of the type JUMO MIDAS SI were used. For the monitoring of temperature, a Class A PT100 resistive probe (4) was used (this probe is deemed to be more accurate than thermocouples). Figure 3.11 shows the program written using the Labview programming language to display the values obtained by the three sensors (pressure, flow-meter and temperature). The pressure and the flow generated by the motor and the pump were adjusted with the valves (9) at the entrance of the chamber and the valve of the by-pass (10). Figure 3.12 shows the waveform conveyed to the motor and the corresponding signals from the flow-meter and the pressure sensor. Moreover, the value of the test temperature and the number of pulses per minute for the unsteady flow tests are also presented in this figure. To launch the test, LabView requires a text file of the amplitude of waveform, to transfer the command. In this aim, the waveform of the blood flow in the carotid was obtained from the literature [233, 236]. The frequency of the waveform was adjusted directly in LabView (see the rotary knob at the bottom left in figure 3.12).

3.3.3 Mimicking arterial system

Drug release test chamber

In this test apparatus, three chambers (12) were designed to examine the drug release simultaneously from the polymeric films. The chambers were made from transparent plexiglas to easily control the test conditions. Figure 3.13 shows these test chambers. The channels are equipped on their bottom wall with an extra compartment in order to contain the agarose gel simulating the tissue artery. After fixing this part, a plexiglas cover sheet was placed on the surface of the chambers to insure adequate test conditions. The dimensions of each chamber are of $30 \times 30 \times 130 \text{ mm}^3$. The hydraulic diameter of the chambers is 4 times larger than the normal diameter of the carotid artery.

Procedure of apposition

In this section, the procedure to perform the drug release from the polymeric samples in the artery (hydrogel) and lumen (PBS) in static, steady and unsteady conditions (systolo-diastolic flow) is explained. In the presence of a flow (whether steady or unsteady), the liquid medium was first

3.3. BIO-RELEVANT APPARATUS (BRA)

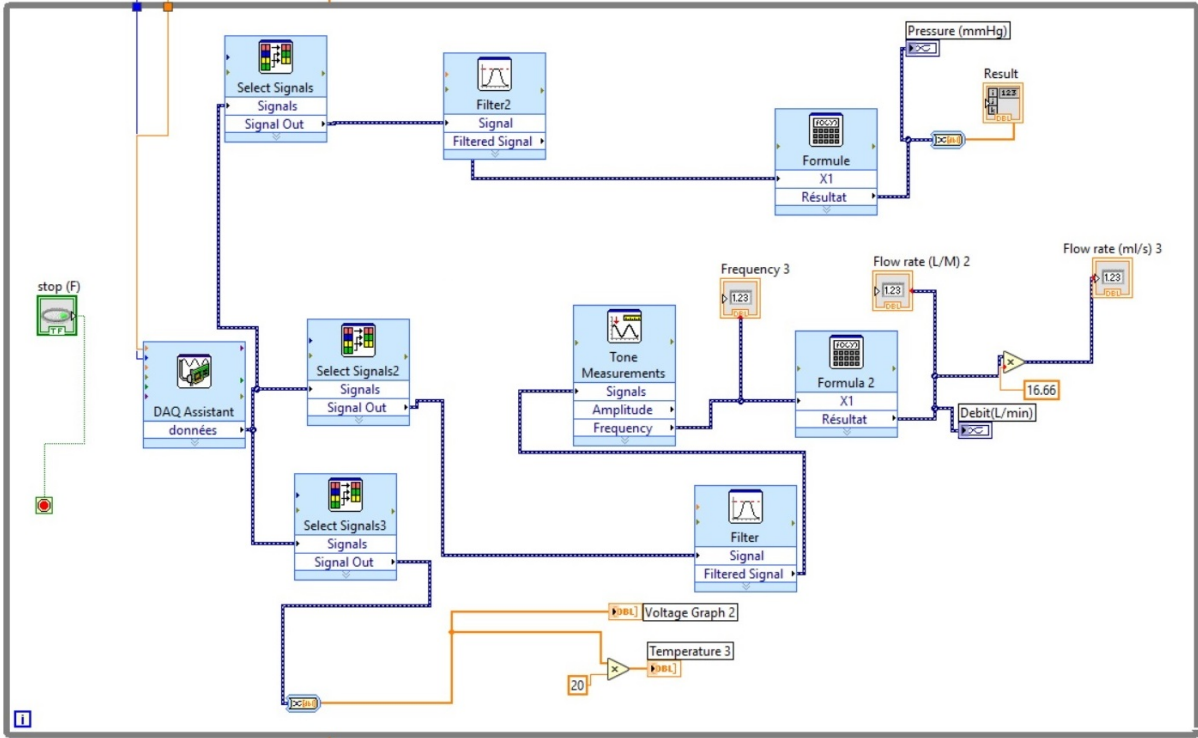


FIGURE 3.11 – Loop for capturing the values of pressure, flow rate and temperature in Labview

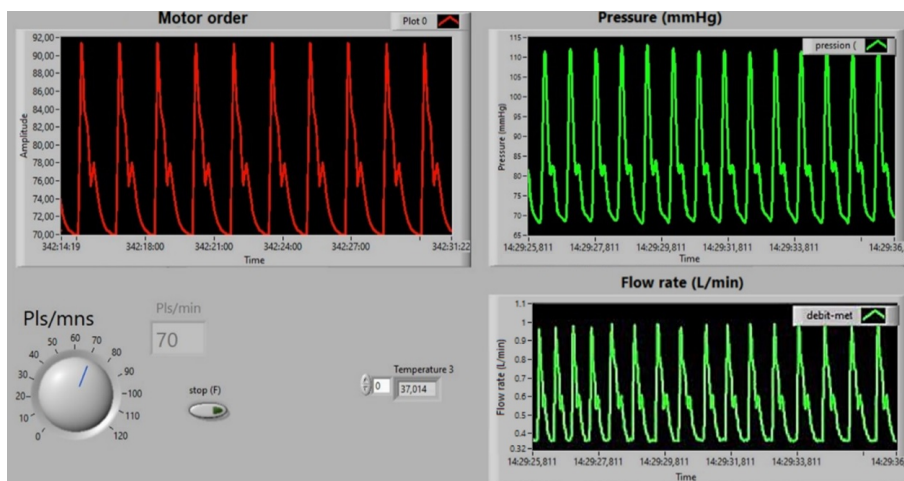


FIGURE 3.12 – LabView program showing the command of the pulse to the pump (on the left) and acquisition of the flow rate and pressure during a pulsed test (on the right)

3.3. BIO-RELEVANT APPARATUS (BRA)

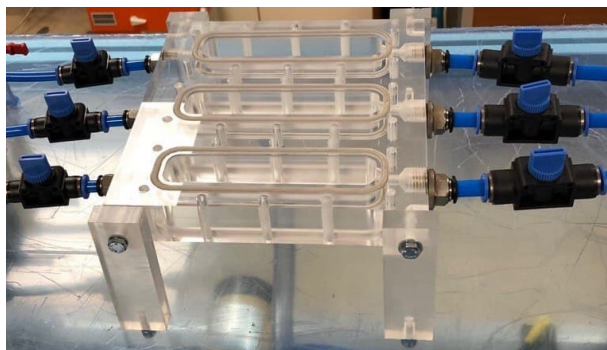


FIGURE 3.13 – Schematic of the chambers

transferred into the reservoir. The temperature was kept at $37\pm 0.5^{\circ}C$. Polymeric films with different percentages of drug were prepared beforehand. In the absence of hydrogel (considering just the lumen compartment), the samples were fixed on a non-diffusible surface replacing the hydrogel. To perform the tests considering the artificial tissue layer, agarose gel was prepared according to the procedure explained in section 3.2. The hydrogel was placed in a compartment situated in the bottom wall of the test chamber; then the polymeric samples were placed on the gel (figure 3.14). In both cases (with or without gel), the polymer samples were fixed with small clips on the surface, in order not to move with the flow. In one case study, a metal sheet (stainless-steel) as a holder was also placed on the polymer film. Once the samples have been placed, the tests were implemented in steady (constant flow rate) and unsteady (pulsed mode) conditions. In order to evaluate the drug released from the polymer films into the medium and also the concentration penetrated into the gel, sampling was performed at specific time steps. To determine the amount of drug that has diffused into the gel, at each time step, the gel in the chamber was removed for analysis and replaced with a new pre-prepared gel. Then the removed hydrogel was dissolved using microwaves and was quantified by UV-Vis spectrometry. Moreover, at the same moment, 4 ml of PBS were sampled from the system (from the reservoir) and the concentration of the drug in the liquid medium was also evaluated with the UV-Vis technique. In the static conditions (no flow rate), the prepared polymeric films with or without drug were immersed in a 10 ml of phosphate buffered saline (PBS) solution at a concentration of $60\text{ mg}\cdot\text{ml}^{-1}$ or distilled water (depending on the type of the test). The tests were conducted in the screwed glass vial at the temperature of $37^{\circ}C$ in an incubator. The results of the release were obtained for different time intervals. For the UV-Vis method, at each time step, 4 ml of the solution were sampled for analysis

3.4. IN VITRO DRUG RELEASE PROCEDURE AND ASSOCIATED MEASUREMENT

and 4 ml of fresh medium was added.

3.4 In vitro drug release procedure and associated measurement

Among the aims of this thesis study of the quantities of drug released, as a function of time, in the two media, the circulating fluid and the hydrogel. For this, two measurement protocols based on the techniques of ultraviolet-visible spectroscopy (UV-Vis) and gravimetry were implemented.

3.4.1 Protocol of the UV-Vis method

The Perkin Elmer lambda 35 UV-Vis spectrophotometer was used to determine the concentration of the drug in the PBS/distilled water solution. To calculate the cumulative release percentage of the drug, the total amount of drug loaded in the polymeric carrier was also measured. In this aim, PLGA samples were completely degraded into a PBS solution at the temperature of 90°C for about 4 hours, and PU films were dissolved in the dimethylformamide solvent at 90°C for about one day. Prior to perform these measurements, some calibration curves need to be obtained for each drug in each medium. For example, the calibration curves obtained for the diclofenac sodium in PBS are shown in figure 3.15 on the right. In this case, the calibration curves for diclofenac sodium in PBS and gel give respectively the following equations:

$$C_{PBS} (\mu g/ml) = -2.766 + 29.371 \times \text{absorbance (counts)} \quad (3.1)$$

$$C_{gel} (\mu g/ml) = -0.429 + 24.535 \times \text{absorbance (counts)} \quad (3.2)$$

and the equations obtained for diclofenac epolamine in PBS and gel are respectively :

$$C_{PBS} (\mu g/ml) = -57.271 + 863.65 \times \text{absorbance (counts)} \quad (3.3)$$

$$C_{gel} (\mu g/ml) = -10.528 + 475.12 \times \text{absorbance (counts)} \quad (3.4)$$

The mentioned calibration equations are in good accordance to the famous Beer-Lambert law.

3.4. IN VITRO DRUG RELEASE PROCEDURE AND ASSOCIATED MEASUREMENT

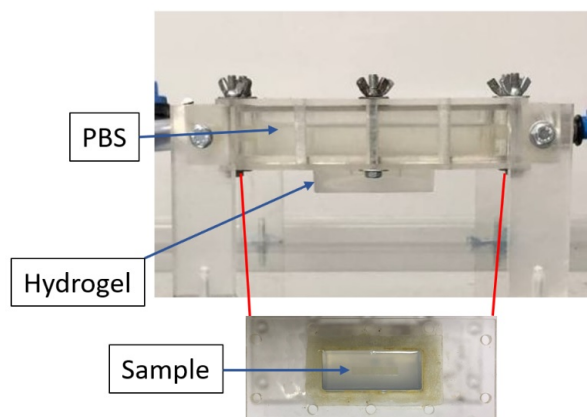


FIGURE 3.14 – Compartement containing the hydrogel and the polymeric samples

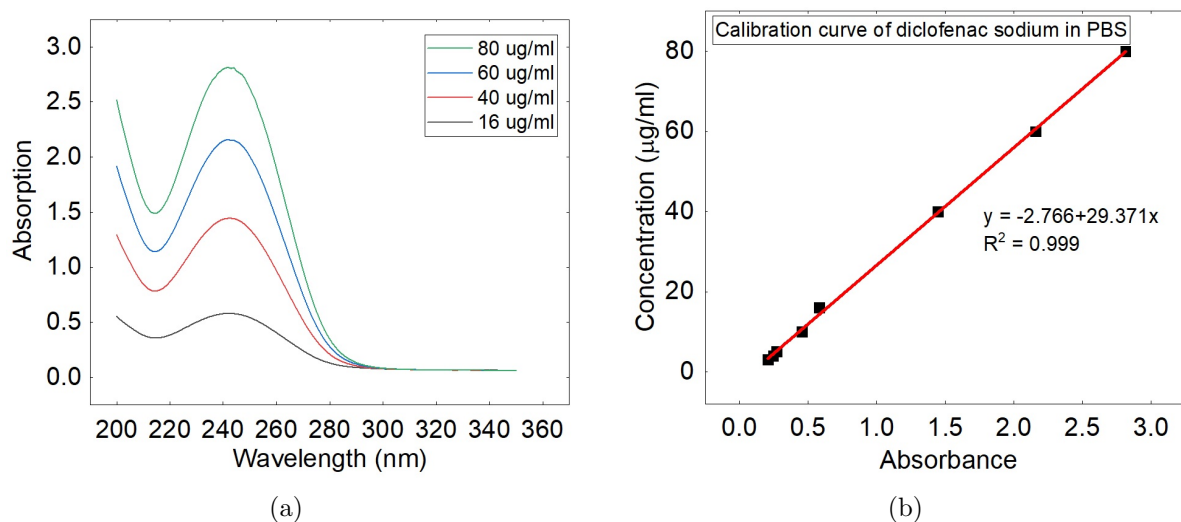


FIGURE 3.15 – (a) Absorption peaks obtained from some of the diclofenac sodium concentration in PBS with UV-Vis, (b) Calibration curve obtained for diclofenac sodium in PBS

3.4.2 Protocol of the gravimetry method

The main steps of the protocol to measure the amounts of drug released and the quantity of absorbed water are based on the gravimetric method described below. This method was used in order to take into account all the components of the drug such as the amount of the excipients released from the non-degradable PU. In this method, the mass of the pure (non-loaded) PU samples was measured before and after each test in order to verify that its value remains constant. At the first step, before starting the test, each sample is dried in the oven at 50°C for 30 minutes to remove any absorbed moisture. Then it is placed into a desiccator to cool. Immediately after cooling, each specimen is weighed (m_0) using a balance (Kern, PNJ 600-3M) with the accuracy: 0.001 g . In the second step, we place the sample into the test chamber. After a given time, the sample is removed from the test chamber and wiped with a dry cloth to remove any water present at the surface. The sample is weighed again (m_1) and placed in an oven at 50°C to extract the absorbed water during the in vitro test. It is maintained in the oven until the mass of the sample is stabilized. At this time, the mass of each sample is recorded again (m_2). Figure 3.16 schematizes this measuring protocol. The experiments were repeated three times and the mean value \pm standard deviation is reported in the results. In this method, each point on the curve is related to one sample. The percentages of wet mass, water absorption and released drug are presented as follows:

$$\text{Wet mass (\%)} = \frac{(m_1 - m_0)}{m_0} \times 100 \quad (3.5)$$

$$\text{Water absorption (\%)} = \frac{(m_2 - m_1)}{m_0} \times 100 \quad (3.6)$$

$$\text{Drug release (\%)} = \frac{(m_2 - m_0)}{(\text{initial mass of drug})} \times 100 \quad (3.7)$$

3.4. IN VITRO DRUG RELEASE PROCEDURE AND ASSOCIATED MEASUREMENT

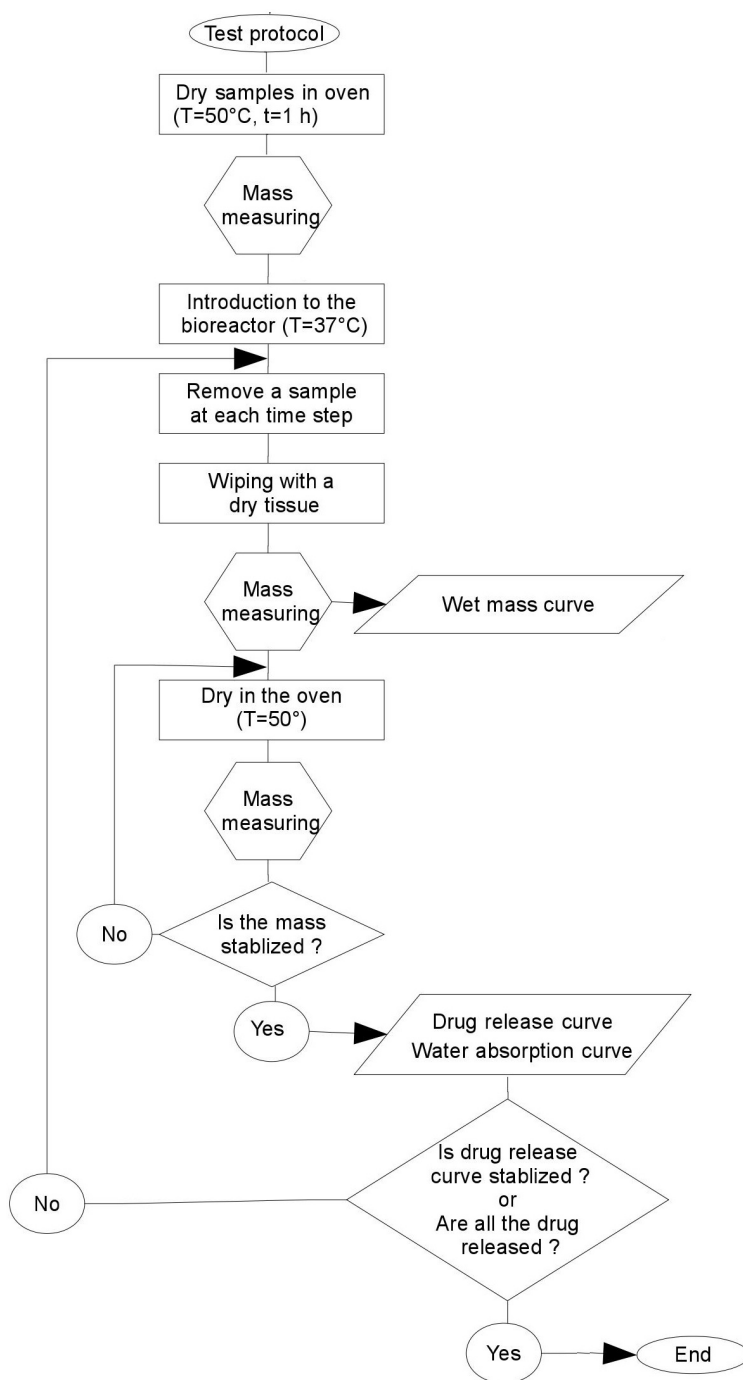


FIGURE 3.16 – Algorithm showing the protocol of the gravimetry method

3.5 Characterization methods

Physico-chemical and mechanical properties were measured for the samples in this study by different characterization methods.

3.5.1 Microscopic observations

An optical microscope (OM) and an electronic microscope (HITACHI 4800 SEM) were used to investigate qualitatively the material micro-structure and especially the evolution of the sample structure before, during and after the release and tensile tests.

3.5.2 Differential Scanning Calorimetry (DSC)

DSC Q1000 V9.0 apparatus was utilized to find out the heat exchange evolution, in the range between the glassy temperature up to the melting point. A slight piece of each sample was placed in a hermetic aluminum capsule. For PU (respectively PLGA), the apparatus was calibrated at -60°C (respectively at 25°C). Then the samples were heated at a rate of $5^{\circ}\text{C}/\text{min}$ up to 200°C (for PU) and 250°C (for PLGA). A three-cycle process was applied to eliminate the thermal history effect of the material.

3.5.3 Thermo Gravimetric Analysis (TGA)

TGA tests were carried out using a Q50 TGA instrument (TA instruments, USA), in order to study the solvent evaporation effect on the quality of the films and on the drug release. Polymer films of PLGA with 0 and 10% DS following the same process (explained in section 3.2) were prepared. They were cut into the small parts, then they were placed in the center of the platinum sample pan and heated isothermally at different temperatures of 23, 40, 45, 50°C over a period of time in a mixed atmosphere of nitrogen/oxygen (60/40); the weight loss was then determined. Further, to study the effect of sample drying on the released drug, the samples were dried in the oven at the mentioned temperatures instead of using the TGA technique.

3.5. CHARACTERIZATION METHODS

3.5.4 Dynamic Mechanical Thermal Analysis (DMTA)

To analyze the storage and loss modulus, as well as T_g of the samples, DMTA tests with the apparatus Dynamic Mechanical Analyzer type Q800 V21.2 were performed. Moreover, multi-frequency tests at a constant amplitude (PU and PLGA) over a temperature range (from -70°C to -20°C for PU and from 30°C to 55°C for PLGA) with the rate of $2^{\circ}\text{C}/\text{min}$ were performed. The dimensions of the rectangular specimens were $30 \times 5 \times 2 \text{ mm}^3$ and $30 \times 5 \times 0.3 \text{ mm}^3$ respectively for PU and PLGA samples.

3.5.5 Fourier-Transform InfraRed spectroscopy (FTIR)

A Perkin-Elmer FTIR Spectrometer was used to determine the chemical composition of the samples to study their degradation by examining the changes in area or disappearances of certain characteristic peaks. The technique used to produce the infrared spectra of the drug granules was the transmission method whereas for the film samples loaded/not loaded with drug, reflection method was used.

3.5.6 Drug solubility

The solubility (S) of the diclofenac epolamine was measured in the laboratory on the hot-plate magnetic stirrer at the temperature of 37°C and stirring rate of 800 rpm . The drug was added into distilled water until saturation occurs; then the amount of the drug dissolved in the media was obtained by the aid of the UV-Vis spectroscopy.

3.5.7 Tensile testing

Quasi-static tensile tests with the velocity of $5 \text{ mm}/\text{min}$ were performed with an electromechanical and hydraulic system. Instron 4301 machine was used to identify the effects of drug percentage, flow rate and the release on the mechanical behavior of the polymeric supports at different time intervals. The tensile tests were performed at the ambient temperature.

3.5.8 Permeability measurement of the hydrogel

The permeability of the agarose-gel is evaluated experimentally under the static-flow condition. For this, a volume of (4 ml) of agarose 1% weight/volume (w/v) was prepared (the same procedure

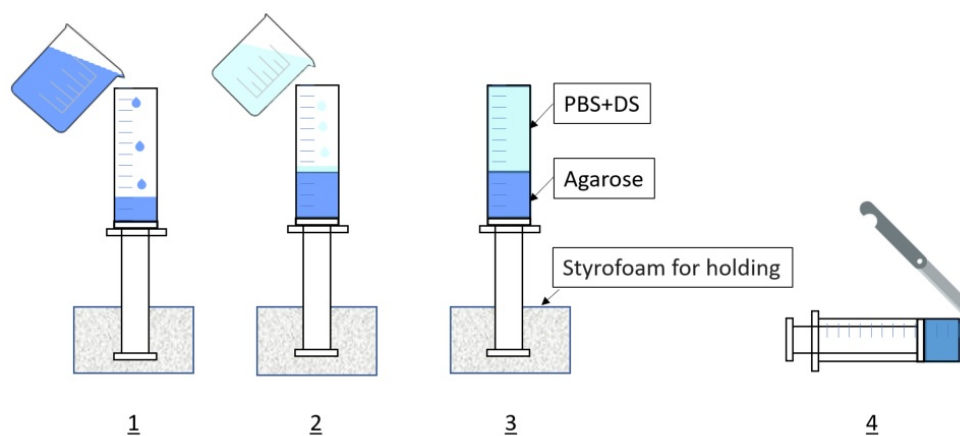


FIGURE 3.17 – Procedure to measure the diffusion coefficient of drug in gel

that was used for the hydrogel preparation) and then poured into a syringe of 12 ml of capacity, the part of which on the needle side has been cut (shown in figure 3.17). The remaining volume of the syringe is filled, after gelation of the agarose in the syringe, with a solution containing a precise dose of drug (50 mg of DS per 1 ml PBS solution). These syringes are withdrawn at three various times and each time the non-diffused solution is emptied. Next the drug-soaked hydrogel is cut into slices 4 mm thickness so that they are employed to quantify, by the UV-Vis technique, the amount of drugs that it contains.

3.5.9 Fluorescence spectroscopy

Fluorescence spectroscopy was used to analyze the spatiotemporal distribution of phosphorescent particles in the hydrogel during drug release. The CL-1000 ultraviolet apparatus was used to excite the phosphorescent particles. The drug-loaded polymer samples and of scattering phosphorescent particles are first made with 30, wt.% with the same procedure explained in 3.2. Then, at each time step, the hydrogel is removed from the test apparatus and is cut into lamellas with a thickness of 5 mm. These lamellas are then illuminated in the ultraviolet apparatus for about 40 seconds until the clarity of the scattering phosphorescent particles is sufficient.

Chapitre 4

Experimental results - In vitro drug release

Content

4.1 Primary characterization of materials	110
4.1.1 Polyurethane	110
4.1.2 PLGA	112
4.1.3 Hydrogel	116
4.2 Drug release in artificial lumen	119
4.2.1 Factors influencing the in vitro drug release	119
4.2.2 Investigation of drug release mechanisms	138
4.2.3 Evaluation of the mechanical, physical and chemical properties of the polymeric drug carriers during release	147
4.3 Drug release in artificial lumen and tissue	165
4.3.1 Presence of artificial tissue in drug release system	165
4.3.2 Steady and non-steady flow rates	167
4.3.3 Presence of the metal layer on the polymer layer	171
4.3.4 Distribution pattern of luminescence particles in the gel	173

This chapter presents the experimental in vitro release tests performed at different conditions in order to investigate the effect of these factors on the polymer carriers and in consequence on the release behavior. The first section discusses about the primary characterization of materials used in this study. The second section presents the effect of the different factors influencing the in vitro drug release in the artificial lumen, their mechanisms of the release and also evaluation of the mechanical, physical and chemical properties of the polymeric drug carrier during the release. Finally the last section represents the effect of some parameters such as pulsed flow and artificial tissue layer in the release profile.

4.1 Primary characterization of materials

This section presents the initial characterization of the polymer samples and used drugs. The physico-chemical and mechanical characterisations have been performed to evaluate some material characteristics such as glass transition temperature, material composition, tensile modulus, and microstructure. These characterizations can be used to identify and get the knowledge of the used materials and also serve as the references for comparing their evolution during drug release.

4.1.1 Polyurethane

The PU samples were investigated before using in drug release system. Figure 4.1 shows the thermal analysis of the PU and DE. Figure 4.1 (a) shows a glass transition temperature of about -43°C for the PU sample, where diclofenac epolamine (figure 4.1 (b)) shows three endothermic phase transition, a very important near to 100°C . The results confirms that PU and DE have not the transition temperature near to the application temperature ($T = 37^{\circ}\text{C}$).

As the exact glass transition temperature of PU was not clear in the DSC test, thermo-mechanical analysis (DMTA test) was performed. Figure 4.2 shows that the T_g of PU is -43°C which is very below the application temperature, this polymer is in its rubbery state. Beside physico-chemical characterizations, figure 4.3 illustrates the mechanical properties of this polymer. One can note that there is a good repeatability of tensile curves. PU presents the Young modulus of about 6.6 MPa with tensile strain and stress of about 500% and 4.7 MPa, respectively. The chemical composition of this polymer and DE are investigated by FTIR test (shown in figure 4.4). The band at 1070 is related to the stretching bonds of C-O-C. The bands in the range of $1535\text{-}1230\text{ cm}^{-1}$ are assigned to C-N and bending bands of N-H, bending vibration of urethane linkages. The bands 1703, 2870, 2960 and 3313 are respectively related to the stretching bands of C=O, CH₂, C-H and N-H. The important peaks related to DE are as follow: 3392 cm^{-1} related to the N-H amine stretching bound, 1419 cm^{-1} relates to C=O carboxyl ion and 644 cm^{-1} for C-Cl stretching movement. Figure 4.4 (c) shows the comparison of the FTIR spectrum of PU-Pure, DE and PU-DE sample, the results show that DE shows a lot of common peaks with PU and as the density of the peaks are rather low, therefore the peaks of DE is not clearly distinguishable in the mix of PU-DE sample but it confirms that as there is no evidence of the created or disappeared peaks, therefore is no interaction between the drug and the polymer materials used.

4.1. PRIMARY CHARACTERIZATION OF MATERIALS

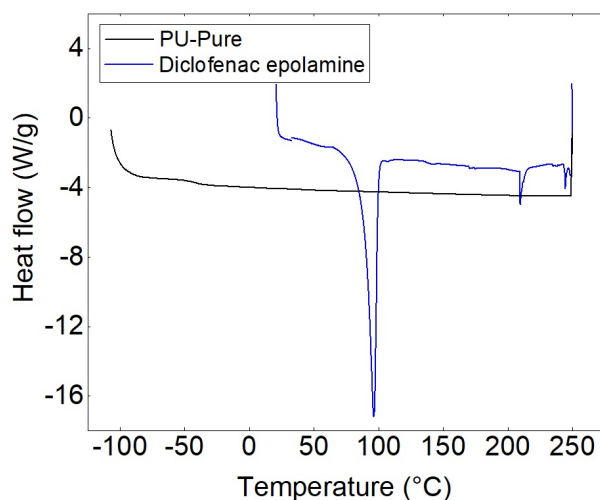


FIGURE 4.1 – DSC results of polyurethane and DE

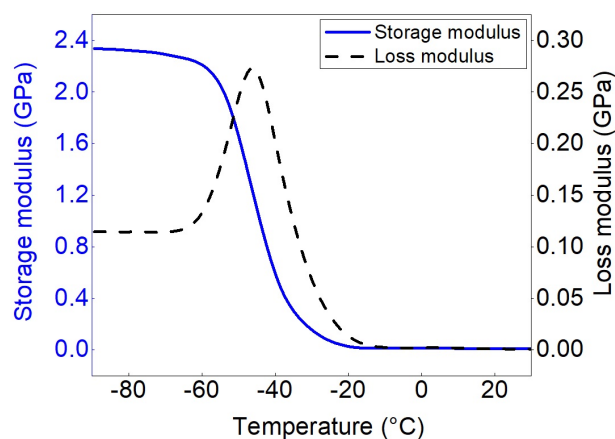


FIGURE 4.2 – DMTA curve of pure PU

Finally, microstructure observation of the PU-Pure, DE and PU-DE sample, are shown respectively in figures 4.5 (a), (b), (c). Figure 4.5 (a) shows the microstructure of the sample from the edge, where it can be seen that a suitable surface of the sample is obtained. Figure 4.5 (b) shows the DE particles are in the range of 40-160 μm . The PU sample mixed with 10% of DE is shown in figure 4.5 (c) where the presence of some small inevitable pores are observed in this figure, which indicate probably entrapping of the drug particles.

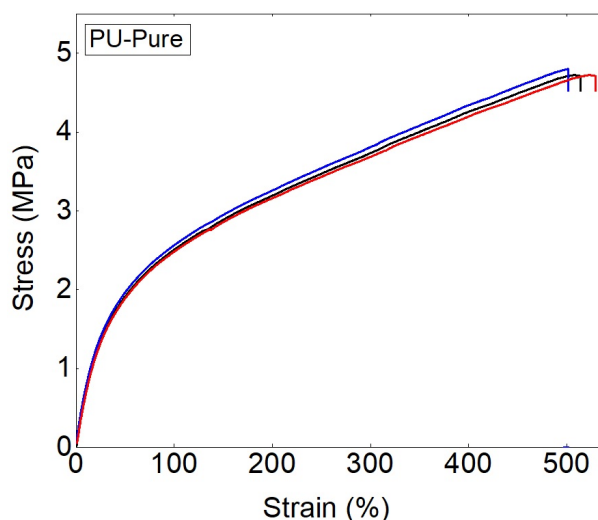


FIGURE 4.3 – Tensile properties of three non-charged PU samples

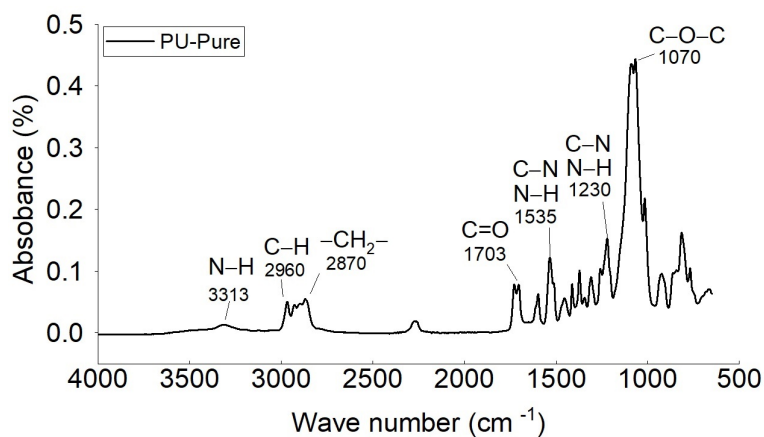
4.1.2 PLGA

Concerning the second mixture, figure 4.1 shows the DSC pattern of PLGA and DS. This figure indicates that there is no transition for DS around 37°C , however PLGA presents a glass transition temperature of about 45°C . This value is near to the application temperature which should be taken into account. Moreover, the figure shows that PLGA is a semi-crystalline polymer with melting point of about 345°C .

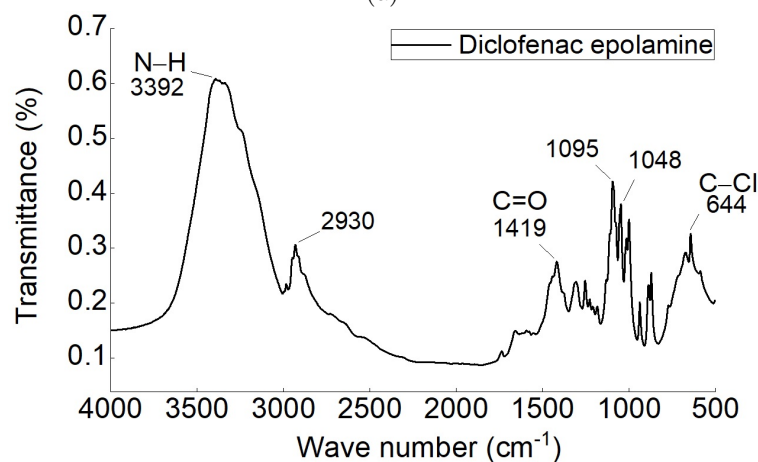
Figure 4.7 shows that the transition temperature of the PLGA from the glassy state to the rubbery state is about at 39°C . It is notable that the transition region is rather wide and it is in the range of application temperature (37°C) therefore, much attention should be given to the behaviour of this polymer during the test.

Figure 4.8 shows the mechanical properties of this polymer, one can observe from this figure PLGA has a low modulus (lower than the PU) but it has a rather higher failure strain at about 600%. The chemical composition of this polymer is investigated by FTIR test (shown in figure 4.4 (a)). The peaks between the range of the $1000\text{-}1500$ and the peak between the $1500\text{-}2000\text{ cm}^{-1}$ are the characteristic peaks for the PLGA [237]. The bands of the CH_2 and CH_3 are observed in the region of the $1500\text{-}1300\text{ cm}^{-1}$. The band 1452 cm^{-1} corresponds to the anti-symmetric vibration of CH_3 from the lactic unit and the 1422 cm^{-1} represents the bending of the CH_2 from the glycolic unit [238]. In the $1300\text{-}1000\text{ cm}^{-1}$ region of the infrared spectra, the initial peak observed at 1163 is assigned to the anti-symmetric

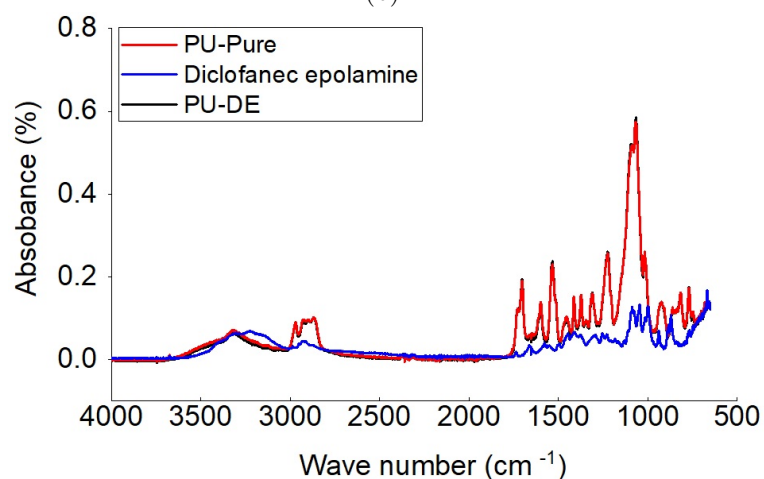
4.1. PRIMARY CHARACTERIZATION OF MATERIALS



(a)



(b)



(c)

FIGURE 4.4 – FTIR spectra of (a) PU and (b) diclofenac epolamine and (c) PU-DE sample

4.1. PRIMARY CHARACTERIZATION OF MATERIALS

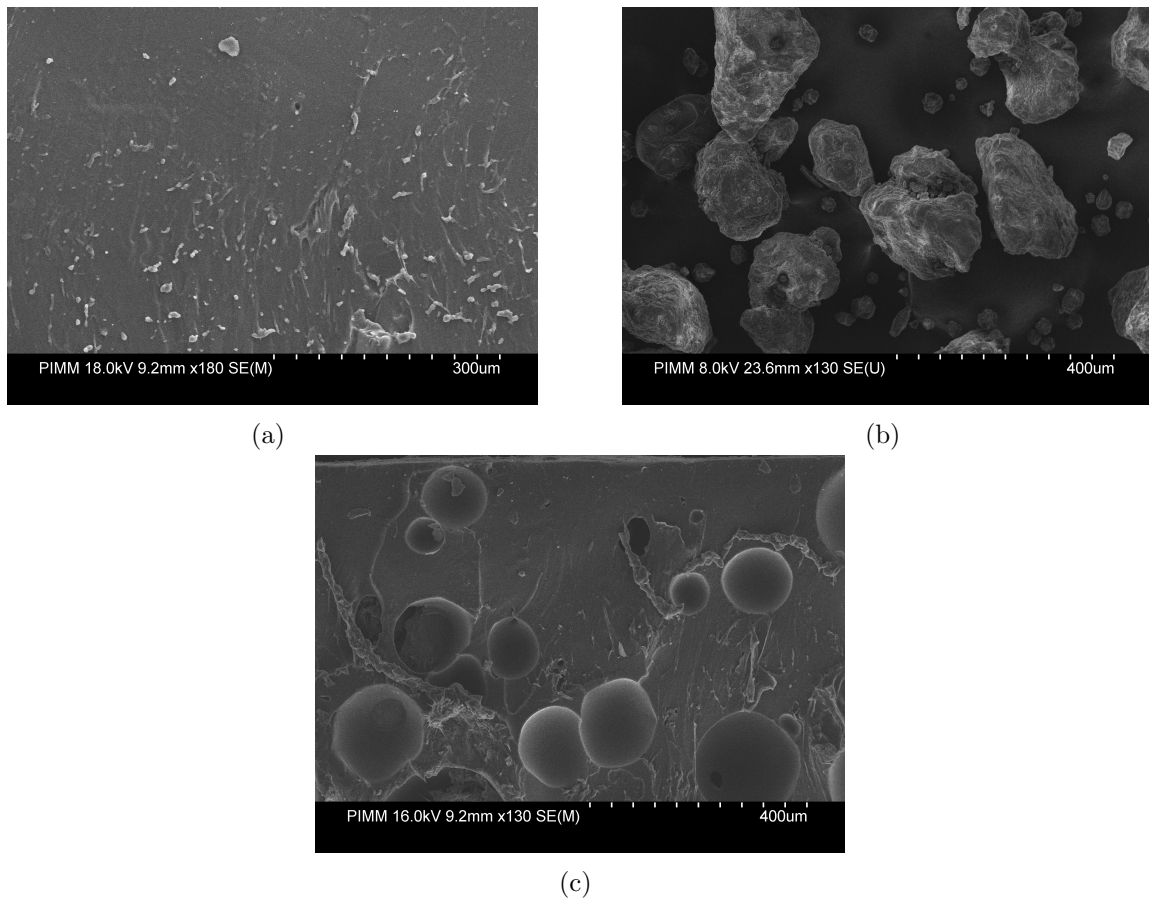


FIGURE 4.5 – SEM images of (a) non-loaded PU from the side of the sample (b) diclofenac epolamine and (c) PU sample loaded with 10%DE

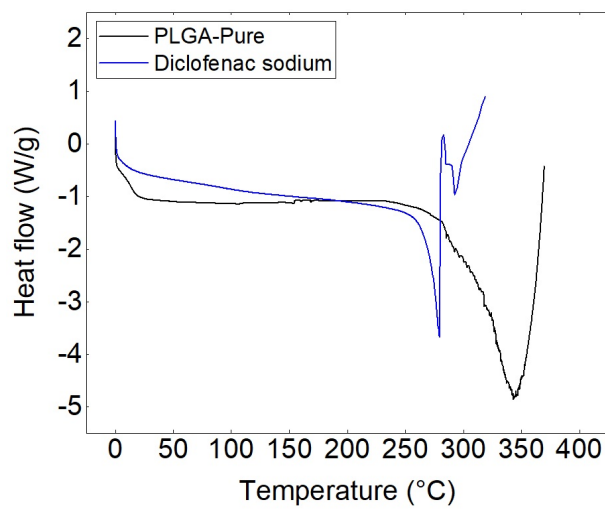


FIGURE 4.6 – DSC of PLGA-pure and diclofenac sodium

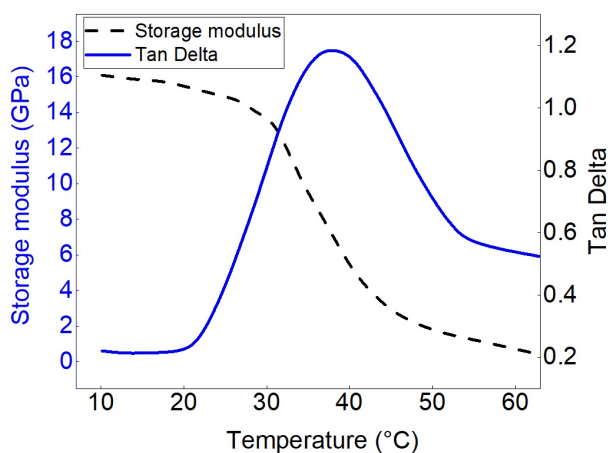


FIGURE 4.7 – DMTA results of pure PLGA

stretching of COC for glycolic and lactic units. The symmetric stretching of COC is observed at 1082 cm^{-1} for both glycolic and lactic units. The two other peaks observed in this region at 1129 and 1047 cm^{-1} are assigned to the vibration of CH_3 from the lactic units. In PLGA, the band at 890 cm^{-1} is assigned to C-COO of the glycolic units. Figure 4.9 (b) shows the IR spectra of diclofenac sodium. It exhibits a characteristic peak at 3384.80 cm^{-1} because of NH extending of the secondary amine, 1575.75 cm^{-1} attributable to $-\text{C}=\text{O}$ extending of the carboxyl particle and at 747.66 cm^{-1} in view of C-Cl extending. Figure 4.9 (c) shows the FTIR spectrum of PLGA-Pure, DS and PLGA-DS sample, the results show that DS shows the common peaks with PLGA and as the density of the peaks are rather low, therefore the peaks of DS is not clearly evident in the mix of PLGA-DS. In addition as there is no evidence of the created or disappeared peaks, therefore it is confirming no interaction between the drug and the polymer materials are happening.

Finally microscopic observation of the PLGA-Pure samples and the diclofenac sodium particles are shown in figure 4.10. Figure 4.10 (a) which is from the surface of the PLGA sample without drug shows rather a smooth surface. Figure 4.10 (b) shows the DS particles (drug particles poured on an adhesive paper) which are in the range of $4\text{-}20\text{ }\mu\text{m}$. Figure 4.10 (c) shows the prepared sample of PLGA loaded with 10% of DS. This figure shows the loaded drug particles in the round shape on the polymeric samples.

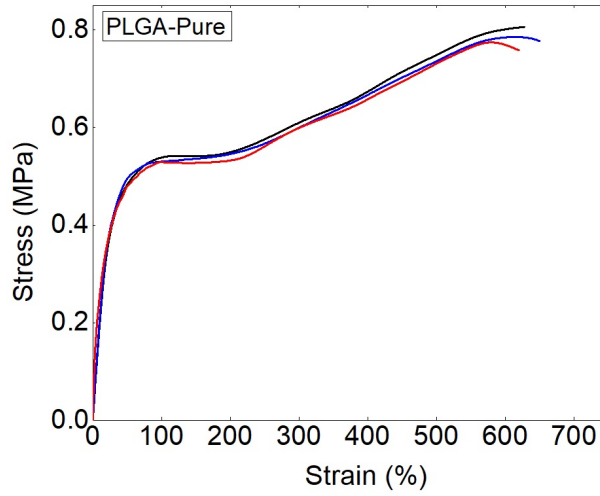


FIGURE 4.8 – Tensile test curve of pure PLGA

4.1.3 Hydrogel

The hydrogel used in this study was characterized physically. The value of the diffusion coefficient was calculated by following the procedure explained in the materials and methods (section 3.5.8), then by considering the Fick's second law, equation 4.1 [239, 240].

$$\frac{\partial C}{\partial t} = D \frac{\partial^2 C}{\partial x^2} \quad (4.1)$$

with mentioning that no swelling of the gel was observed during the experimental. By considering the coordinate position $x = 0$ for the interface between the gel and the drug solution, where x is the length of gel, we have the initial boundary conditions of: $c(0, t) = C_0$, $t \geq 0$, $c(x, 0) = 0$, $x > 0$ and knowing that $erfc(z) = 1 - erf(z)$ therefore, the Fick's second law is transformed to:

$$c(x, t) = C_0 \operatorname{erfc}\left(\frac{x}{2\sqrt{Dt}}\right) \quad (4.2)$$

where $c(x, t)$ is the concentration diffused in the gel at the distance of x at time t , C_0 is the initial concentration of the drug in the solution. The calculation was discretely obtained for each slices for the three time steps of 3h, 24h, 48h. Figure 4.11 shows the concentration of the drug diffused in the hydrogel versus to the x , for different time intervals. The average value was obtained about $1.12 \times 10^{-4} \text{ mm}^2/\text{s}$. This is where the diffusion coefficient of the sirolimus drug across the vessel wall is reported to be about $1.5\text{-}2.5 \times 10^{-4} \text{ mm}^2/\text{s}$ [241]. It is reported in the literature that a 1% agarose

4.1. PRIMARY CHARACTERIZATION OF MATERIALS

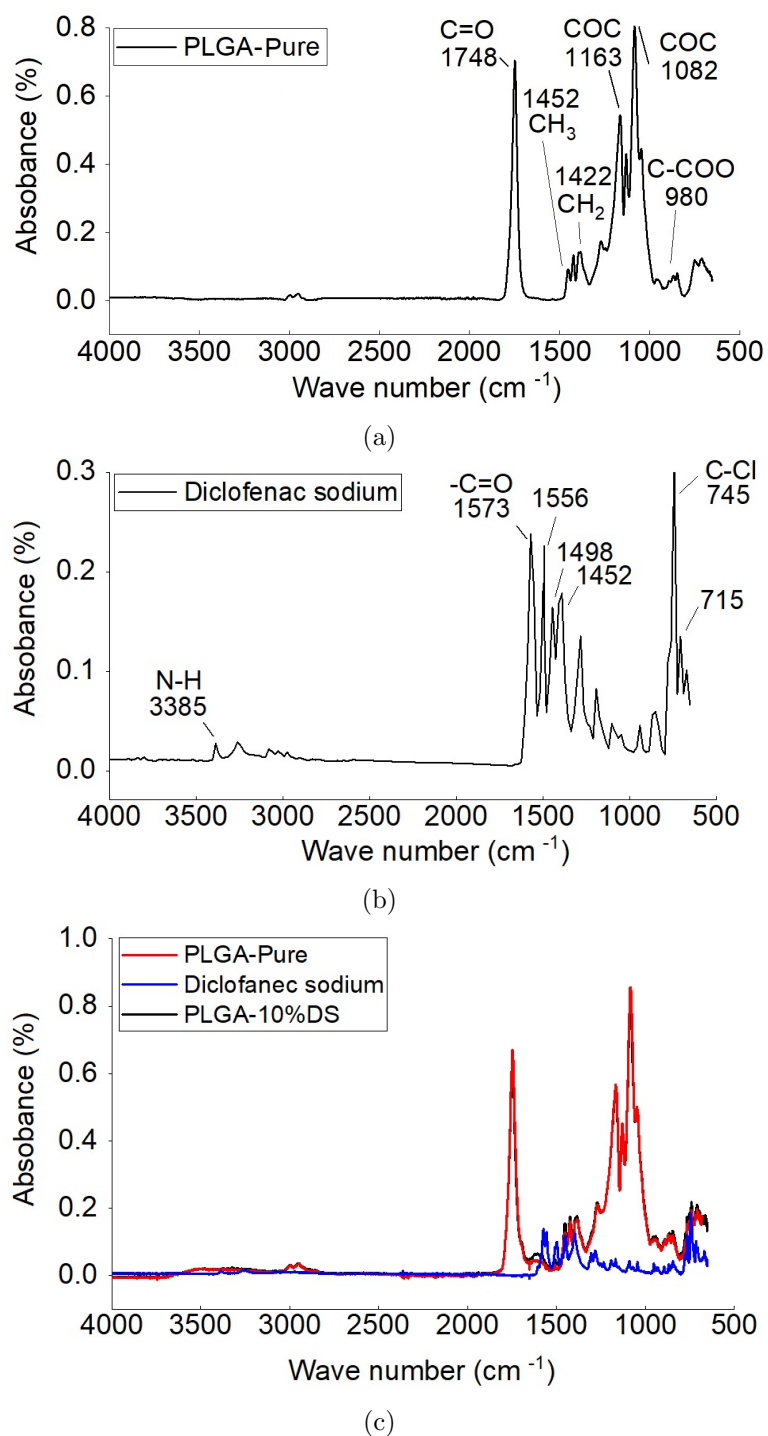


FIGURE 4.9 – FTIR results of (a) pure PLGA and (b) diclofenac sodium (c) PLGA-DS film

4.1. PRIMARY CHARACTERIZATION OF MATERIALS

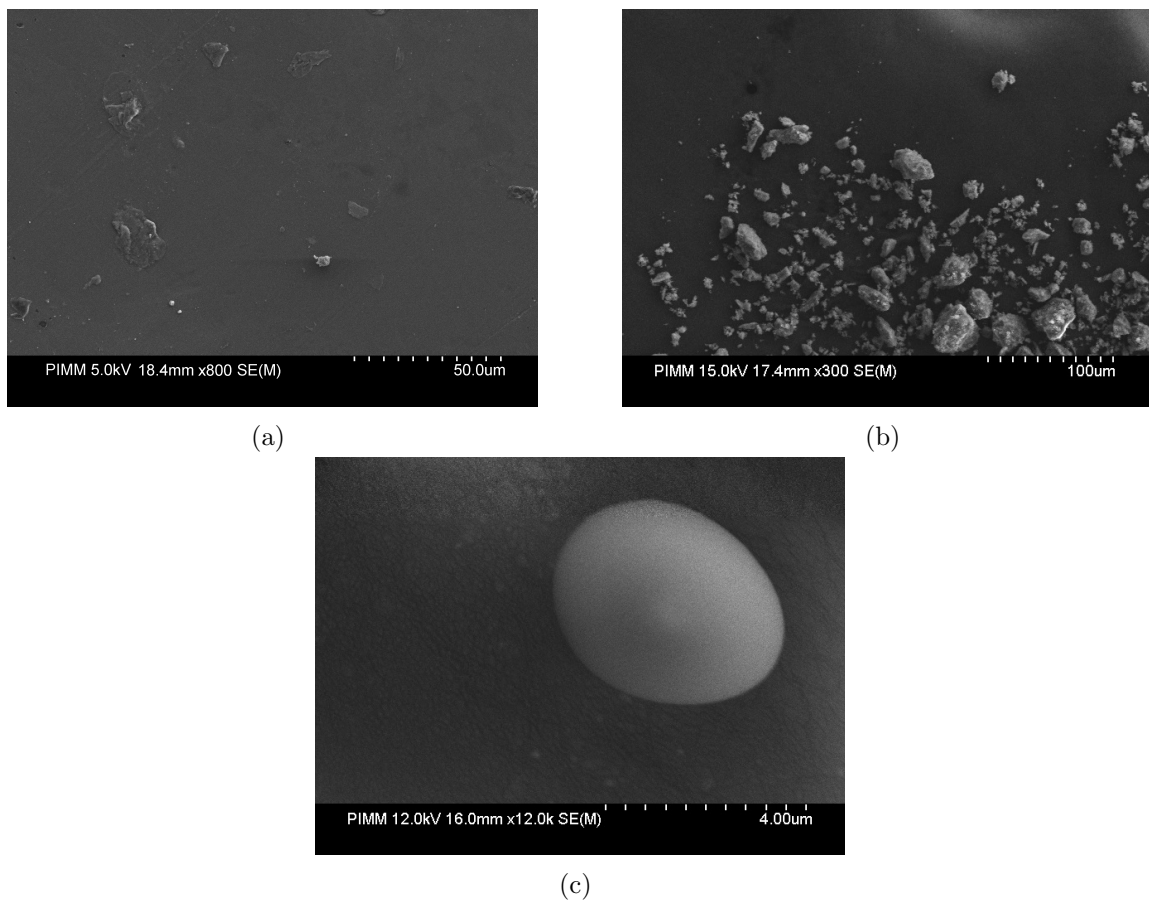


FIGURE 4.10 – DSC of (a) PLGA-pure, (b) diclofenac sodium powder and (c) diclofenac sodium in the PLGA-10%DS film after sample preparation

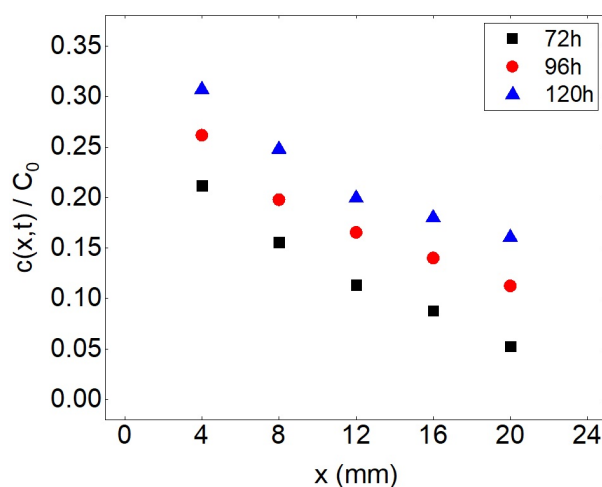


FIGURE 4.11 – Concentration profiles of DS in hydrogel at different distances of diffusion after different time intervals at static state

gel has a median pore size of roughly 100 *nm*.

One can conclude from primary analysis, we tried to consider two types of polymers : 1) PU which is an elastomer produced by mixing of polyols and isocyanate, and 2) PLGA which is a semi-crystalline thermoplastic. In this way the effect of polymer morphology on the drug release can be analyzed. Moreover, in terms of drug choice the hydrophobe and hydrophile type have been considered. The application temperature (37°C) should be considered in the case of PLGA-DS system due to the glass transition temperature of PLGA (45°C). These features confirm the importance of physico-chemical and mechanical characterisation of used materials in drug delivery systems. The importance of some influencing parameters will be presented in the next section for these two systems: PU-DE and PLGA-DS.

4.2 Drug release in artificial lumen

4.2.1 Factors influencing the in vitro drug release

In this section the lumen part of artery has been considered to study the effect of some parameters on the drug release from polymeric carriers.

4.2.1.1 Effect of solvent evaporation

Drying thin polymer films is an important process that influences the film structure and its stability [242]. In this part the effect of the solvent evaporation of the PLGA samples during the fabrication process on the release profile have been investigated. After drying one day in the ambient temperature, the effect of the further drying at the temperatures of 23°C, 45°C and 50°C for 24 hours was considered on the release of DS from PLGA. The chosen temperatures were respectively at below glass transition, the glass transition zone and above the glass transition temperature. Figure 4.12 shows the mass loss of the PLGA-10%DS films during the drying in the TGA apparatus, versus the time of drying. The results show that at the temperature of 23°C the rate of the solvent evaporation is very slow, where by increasing the temperature the rate of the evaporation increases. It is notable that drying above the glass transition temperature (50°C) significantly affect the kinetic of evaporation.

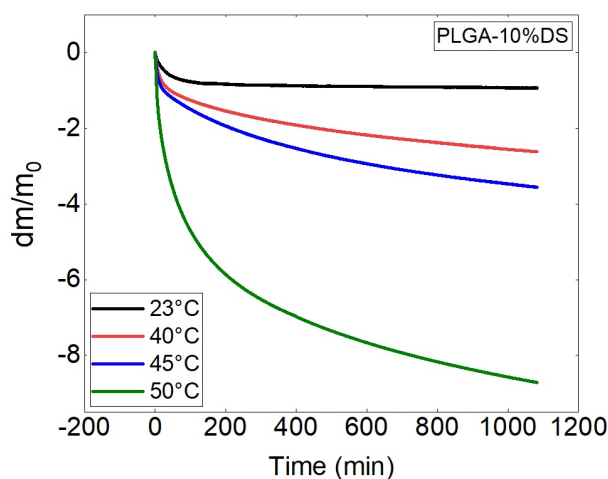


FIGURE 4.12 – Mass loss of the polymeric samples of PLGA-10%DS during the drying in the TGA versus the time of drying

Further investigations on the microscopic images are shown in figure 4.13. From these figures one can note that by increasing the temperature of drying from 23°C to 40°C the solvent trapped in the polymeric films are evaporated slowly. To analyse the effect of the drying temperature and the effect of solvent evaporation the release tests have been performed after the sample preparation at the temperature of 37°C in the PBS at the flow rate of 7.5 ml/s. Figure 4.14 shows that the drug release was significantly influenced by the drying temperature and consequently the solvent evaporation rate, where by decreasing the temperature of drying the release rate was more faster. The reason for the fast

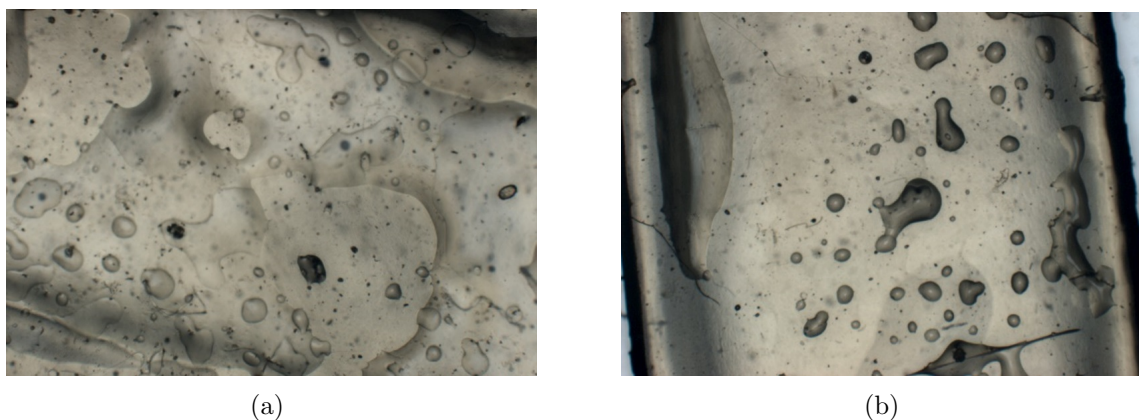


FIGURE 4.13 – Optical images of the PLGA films after drying of 300 minutes at the temperatures of (a) 23°C and (b) 40°C

release from the samples dried at the temperature of 23°C can be due to the presence of the solvent in the polymeric samples. The former can result in an incomplete polymerisation, therefore the polymer chains would be loose and have more space between their chains which may free the drug easily from it. Moreover, decrease in the release of the drug from the samples dried at 50°C can be due to the amount of the crystallized phases in the PLGA [243, 244]. As discussed before, the drug charged in the polymer can more easily liberate from the amorphous phase than the crystalline phase. The results show that the release curve is accelerated especially in the second phase of release which shows the contribution of the mechanisms of diffusion, swelling and the erosion which will be more discussed in the following sections. Moreover, it is obtained from figure 4.14 that the optimum temperature of drying is around the glass transition temperature. This temperature has less effect on the polymer structure and the drug is released in an uninfluenced manner. Therefore, the effect of the other parameters on the drug release in the following sections was continued with the samples which were dried at 40°C.

4.2.1.2 Effect of polymer thickness

The thickness of the polymeric samples was amongst the other important parameters which worth to be investigated. In this regard the drug release from the PU samples loaded with 10% of drug with two different thickness of 0.3 and 2 mm was evaluated (figure 4.15). The tests were performed in the PBS solution at the temperature of 37°C and UV-Vis method was used for quantification of drug. The results signify that for the samples of 0.3 mm in thickness, kinetic of the release during the first period is higher compared to the 2 mm. The first period of the release is normally related to the burst release

4.2. DRUG RELEASE IN ARTIFICIAL LUMEN

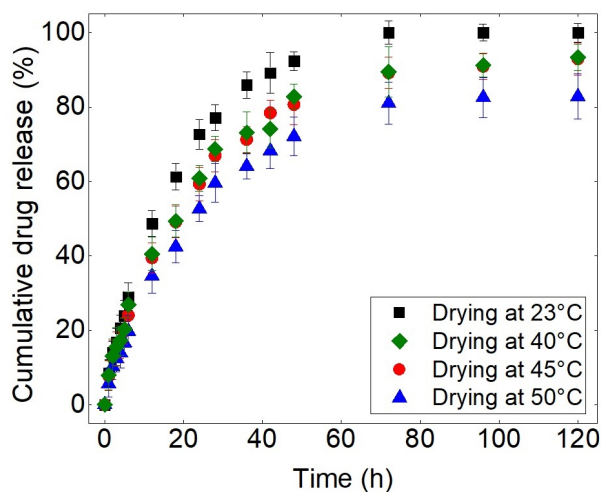


FIGURE 4.14 – Drug release results of the PLGA-10%DS prepared at different drying temperatures of 23°C, 40°C, 45°C and 50°C, and released at the temperature of 37°C in PBS at the flow rate of 7.5 *ml/s*

where drug particles connected with the release medium are liberated. The second part of the release has more deviation, it is evident that decreasing the thickness of the samples has led to less migration distance for the drug particles. It is notable that, this part of the release is more controlled by the diffusion, which is highly thickness dependent. It is worth noting that the release profile may obtain by the contribution of the same mechanisms of release (as they are following the same rhythm), but the kinetic of the release is more faster which results in the fast depleting of the drug from the carrier.

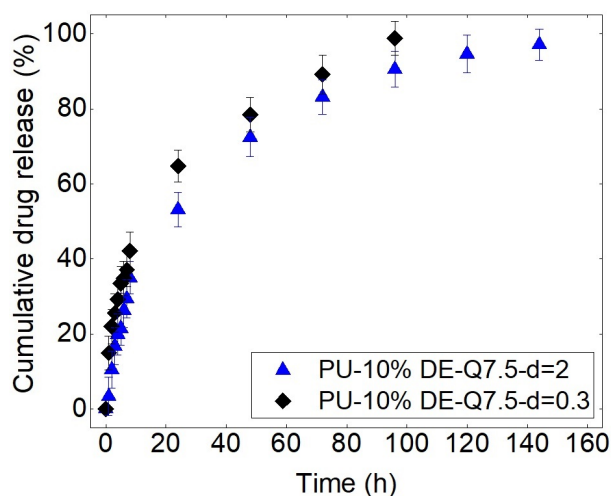


FIGURE 4.15 – Cumulative drug release curves from PU-10%DE at the flow rate of 7.5 *ml/s* for two different thickness of samples, 2 and 0.3 *mm*, in accordance to the release time

4.2.1.3 Effect of the initial percentage of the loaded drug

According to the literature review regarding to the importance of this parameter, the influence of the initial drug load was studied. This parameter was investigated for the (a) DE from the PU samples in distilled water medium (b) DE from the PU samples in PBS medium (c) DS from PLGA samples in PBS medium, which are discussed respectively in this section.

(a) DE release from PU in distilled water

In drug delivery system when we are talking about the polymeric carrier, it is noticeable that the release is happening due to a driving force, in this study this driving force can be related to the water absorption, therefore it is necessary to investigate the effect of the drug percentage on this phenomenon. Figure 4.16 (a) shows the water absorption rates for four various cases, pure PU and PU with drug loading 10, 20 and 30% mass of DE. It is notable that the water penetrates even in the pure PU, but with a lower value, close to 5%. In contrast, for the drug loaded PU samples this rate increases with the initial percentage, where for the samples of 30%DE it reaches to about 70%. The presence of the drug, therefore, plays a leading role in the absorption of water. This is due to the the hydrophilic property of the chosen drug. One can note that this value is affected by the difference of the density of the drug (450.7 mg/l) and water (997 mg/l) where they are substituted in the same area. In this part the measuring method was the method of gravimetry, therefore, in the calculation of drug release all the components of the drug (epolamine, excipients) are taken into consideration. For the release of the drug from non-degradable PU samples three different percentages of the drug (10, 20, 30%) were loaded in the polymer. Figure 4.16 (b) shows the drug release percentage for three different DE loaded PU samples. It is notable that increasing the initial drug did not resulted in the prolonged release. In contrast, comparing the three curves of the PU with 10, 20, and 30% of drug, it is apparent that by increasing the drug content there is a decrease in the maximum time of the release. In addition the kinetic and amount of the release is increased. We can get from figure 4.16 (b) that the release is commenced with an initial burst release. Further, the release is followed with a higher kinetic of the release with increasing the drug percentage. In this aim knowing the mechanisms of the release are important to analyze the reason of the phenomena. As it is obtained from the figure 4.16 (a) It is notable that in the case of hydrophilic drug increasing the drug content has increased the absorbed water content. Polyurethane is almost known to be hydrophobic polymer. Therefore, the diffusion of the water to the polymer is most probably through the pores. In this case contacting with

4.2. DRUG RELEASE IN ARTIFICIAL LUMEN

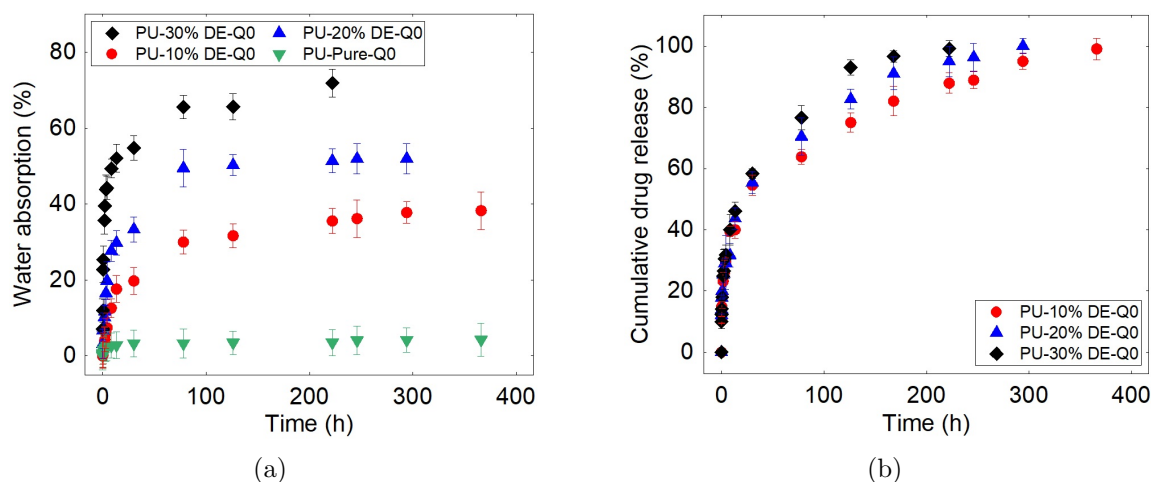


FIGURE 4.16 – (a) Water absorption and (b) Drug release percentage for PU with different percentage of DE in flow-less state

the hydrophilic drug results in the fast dissolution of the drug and release of them through the water filled pores. Therefore, one can note the importance of the mechanism of the diffusion in this system. On the other hand, absorption of a large amount of the water due to the presence of the hydrophilic drug in a porous structure of a matrix results in the osmotic pressure. The created pressure results in pushing out the dissolved drug with the water solution through the pores, where it shows an increase in the kinetic of the release. It is notable that the released drug and then the free space left in the samples helps to more water absorption and free space for releasing the remained drug. Knowing that the swelling mechanism can result in the dimension variation of the samples, therefore we have measured the geometry of the samples before and after tests. The results showed that the polymeric samples didn't have any dimension change.

Moreover, the effect of the drug percentage was investigated in the case of steady flow at the flow rate of 7.5 ml/s . The results of water absorption and drug release for continuous condition, $Q = 7.5 \text{ ml/s}$ are presented in figure 4.17. In this figure, one can note the effect of the initial drug load on the release results. Comparing the results of the water absorption for the tests with the flow rate of 7.5 ml/s and with different percentages of drug, one can note that water can penetrate into the polymer about 32% in the case of PU with 10% drug, and it is slowly increasing by the drug percentage to 56% PU with 30% drug. Figure 4.17 (b) shows that from the slope of second part of the curve, one can note the same mechanism of drug release in this condition at different drug percentages. Globally, the same behavior of water absorption and drug release can be seen in continuous case and flow-less

4.2. DRUG RELEASE IN ARTIFICIAL LUMEN

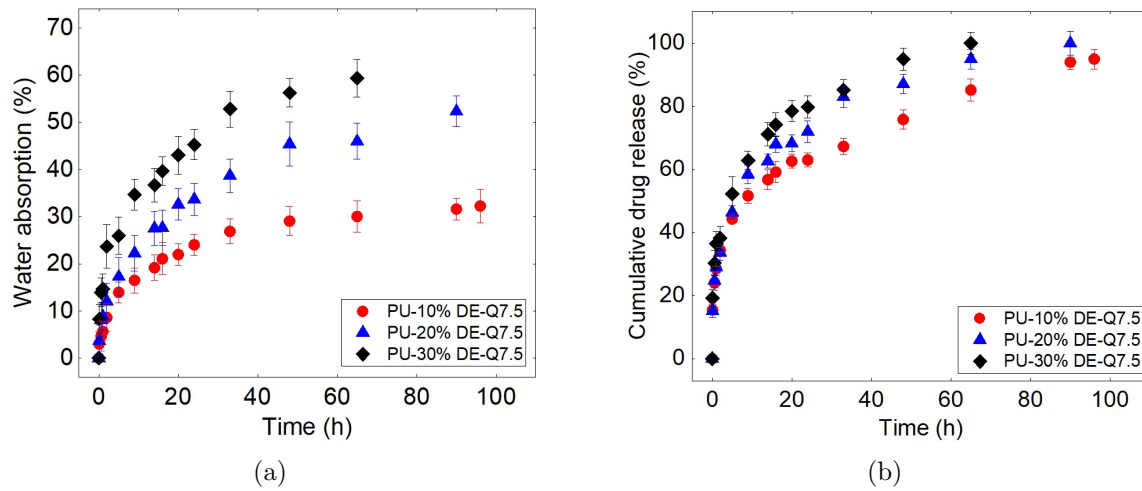


FIGURE 4.17 – (a) Water absorption and (b) Drug release for different percentage of drug at steady flow with flow rate of $Q=7.5 \text{ ml/s}$

state with different drug percentages.

Figure 4.18 shows the micrographs of DE, pore sizes in the PU-10%DE and polyurethane loaded samples after 1h of the release test at the flow rate of 7.5 ml/s . Figure 4.18 (a) shows that the average size of the DE particles is about $40 \mu\text{m}$. Comparing figure 4.18 (a) and (b) indicates that the size of the pores is rather equal or bigger than the DE particles. By analysing the micro-graphs shown in figure 4.18 (b), (c), (d) and (e), the following observations can be obtained:

- For very low concentrations of drug, some particles may be isolated in the matrix and so not ever come into contact with the water;
- By increasing the drug percentage the connection between the pores are increased;
- For the higher percentage of the drug higher amount of the pores are observed;
- A risk of percolation exists for the samples of higher drug content. Moreover, the voids are closer, and the possibility of a connection between them may establish the connection for the circulation of the fluid, which causes the rapid release of the drug. In conclusion, the size, concentration and distribution of the drug particles in the matrix represent factors that can affect the drug release.
- However, the porous matrix is helping release of the drug from the matrix [145] but its optimized content depends to the aim of the therapy.

(b) DE release from PU in PBS

4.2. DRUG RELEASE IN ARTIFICIAL LUMEN

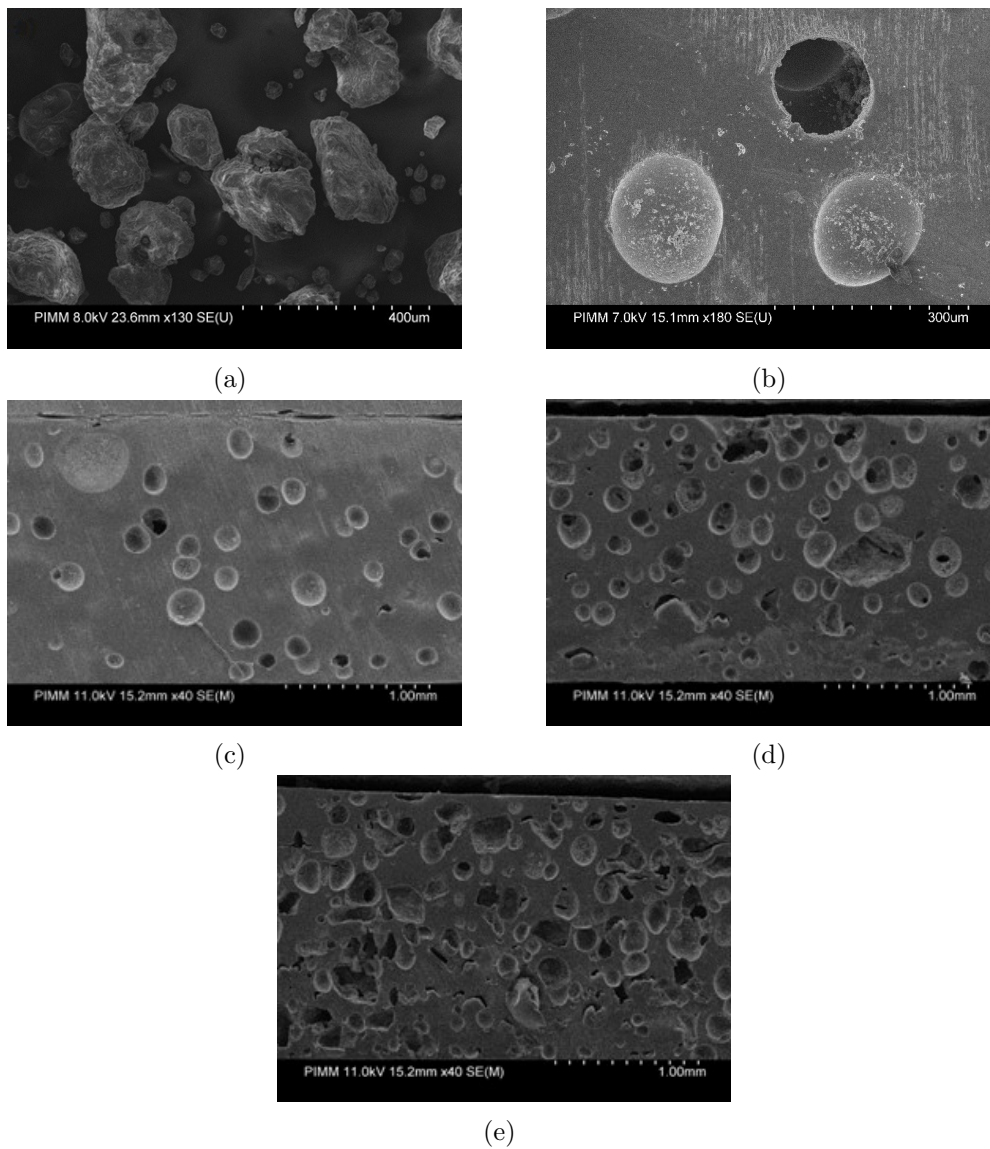


FIGURE 4.18 – SEM micrographs: (a) DE (b) PU-10%DE ($300\ \mu\text{m}$) (c) PU-10%DE ($1\ \text{mm}$) (d) PU-20%DE ($1\ \text{mm}$) and (e) PU-30%DE ($1\ \text{mm}$) from the thickness side of the samples after one hour of the test at the flow rate of $7.5\ \text{ml/s}$

In this section the DE release is measured from PU samples in the PBS by the measuring method of UV-Vis. Figure 4.19 shows the drug release from the PU samples loaded with 10% and 20% DE at the flow rate of 7.5 *ml/s*. The results indicate that by increasing the initial load, the drug release percentage is higher almost during the entire period of release. Several mechanisms can account for the increment in relative release rates with increasing drug load such as burst release due to the presence of more drug particles on the surface during the initial period. As mentioned in [66] that the physico-chemical properties of the active substance affect their distribution in the polymeric matrix, wherein it is more probable for the hydrophilic active substance to move to the surface of the polymer. So the hydrophilic active substance that have more tendency to stay towards the surface have more willing of first burst release wherein the drug is released by desorption in the first periods of time. Moreover, increasing the hydrophilic drug particles increase the water absorption which is the requirement of the drug release from the polymeric films. Therefore, fast water absorption and hence rapid dissolution of drug at higher drug loading, causes high amount of osmotic pressure, which is another reason of the increase in the kinetic of the release. The other reason can be due to the increase in the number of the pores created on the surface and especially along the thickness of samples (shown in figure 4.20). However, one can note from figure 4.19 that finally the kinetic of the release decreases for both PU-10%DE and PU-20%DE and they are depleted of the drug nearly at the same time. In another words it is observed from the release profiles that after the burst release, where the release is controlled by the diffusion phenomenon, the release kinetic decreases. It can be due to the higher initial burst release where after that the gradient of concentration decreases and results in the slower kinetic of diffusion.

4.2. DRUG RELEASE IN ARTIFICIAL LUMEN

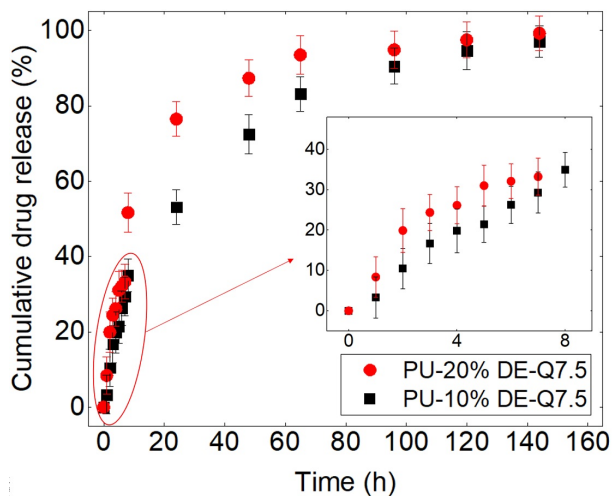


FIGURE 4.19 – Cumulative drug release curves from PU-10%DE at the flow rate of 7.5 ml/s for two different percentages of 10% and 20% DE versus to the release time

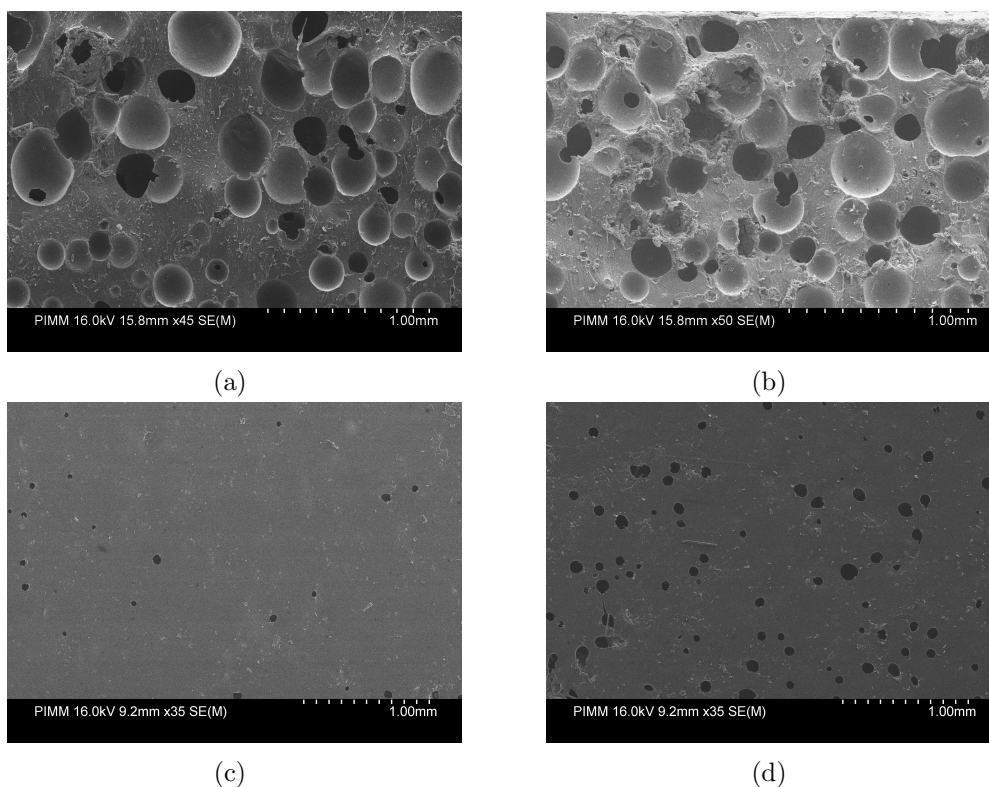


FIGURE 4.20 – Micrographs of the (a) PU-10%DE and (b) PU-20%DE at Q7.5 after drug release of 96h from the side and (c) PU-10%wt and (d) PU-20%wt from the surface side

- Comparing the results by the measuring methods of gravimetry and UV-Vis

4.2. DRUG RELEASE IN ARTIFICIAL LUMEN

The comparison between the results of the method of UV-Vis with the method of gravimetry (shown in figure 4.21) indicates that the release at the first region is more accelerated in the method of gravimetry. This can be explained by two reasons: 1) the effect of the PBS which decrease the solution of the drug compared to distilled water (remembering that in the method of gravimetry distilled water and in the method of UV-Vis PBS was chosen as a solution medium) 2) consideration of the excipients release in the gravimetry method which is not totally considered in the method of UV-Vis. As this difference is observed at the first period of the release it seems that the reason is due to the taking into account the excipients release which normally liberate during the first period. It is notable that the same observations were found for PU-20%DE-Q7.5.

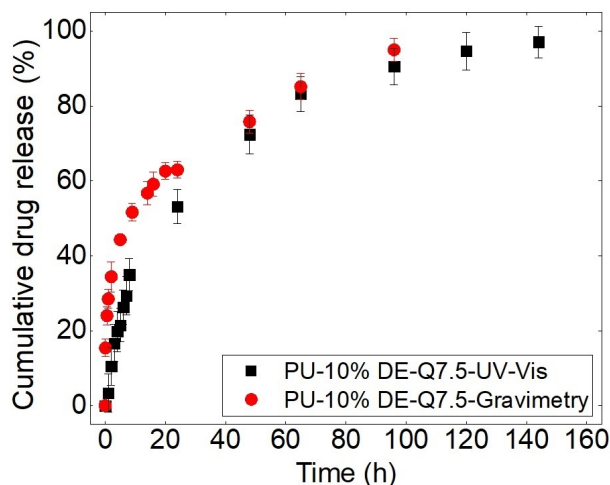


FIGURE 4.21 – Comparison of the gravimetry method with UV-Vis method for PU-10%DE-Q7.5

(c) DS release from PLGA in PBS

In this section drug delivery from PLGA loaded with various percentages of active substance, diclofenac sodium (DS: 5%, and 10%) at the static state in phosphate buffered saline (PBS) for different release intervals has been studied at the release temperature of 37°C. The measuring method used was UV-Vis spectroscopy.

Figure 4.22 shows the drug release profiles from the PLGA-5%DS and PLGA-10%DS films in above mentioned conditions. The results indicate that increasing the drug load from 5 to 10% at the first 12 hours does not indicate significant variations in the drug release. However, by moving forward in time, the variance is becoming more evident. Understanding the importance of the amount of water absorption in drug carriers in order to release the drug, leads to analyze the water absorption data

(shown in figure 4.23). The results obtained from the amount of water absorbed by the two polymer films with 5 and 10% of the drug do not significantly difference until 24 hours. In a period of 24 to 48 hours, the results show an increase in the amount of absorbed water in the polymer with 10% of drug compared to 5% of drug. This increase in water absorption results in accelerating the possible mechanisms for the release of the drug from the polymer. In this aim, one can note that initially the film is dry then it is exposed to the aquas environment of test medium. It is there that an initial amount of drug which are contacted with the surface is released. It is notable that in this case the amount of the burst release comparing to the PU samples loaded with DE at the static state is very lower. This can be due to the nature of the polymer in resulting an structure different to the other one. PU samples normally before exposition to the test environment have more porous structure than the PLGA samples. Thereafter, diffusion of the water to the polymer films starts to happen where the film starts the swelling since the dry core of the film induce a compressing stress to the wet side, results in reducing the water diffusion and increase the drug release. However due to the initial thin thickness of the samples it is not a long time process. When the samples are completely wet due to the water absorption the swelling continue in all the direction and increase the width, length and thickness of the films. In this case the polymer chains are distancing from each other and this makes the entrapped drug molecules free to release. In this case diffusion will also increase until a decrease in the drug concentration [245]. However, increase in the dimension of the samples due to the swelling can decrease the release because of the high distance of migration. Mechanism of the erosion because of the absence of the flow seems to be negligible in the release from these samples. This matter will be discussed in details in chapter 5.

Figure 4.24 shows the optical microscopic images of PLGA samples with 5 and 10% of drug (PLGA-5%DS, PLGA-10%DS) after certain intervals of the release test.

These images show that by passing the time of the release, the number of the pores created in the samples increases where the pores [246] created in the PLGA samples during the release is the main reason for the release. In addition higher quantity of the small pores in the PLGA-10%DS is the reason for higher release rate of the PLGA-10%DS to the PLGA-5%DS.

Figure 4.24 (e) is taken from the surface edge of the same sample as figure 4.24 (c) by comparing these two figures it is evident that the high quantity of the pores are formed near to the edge of the samples. Therefore, the water absorption of the samples is not homogeneous in the entire surface of

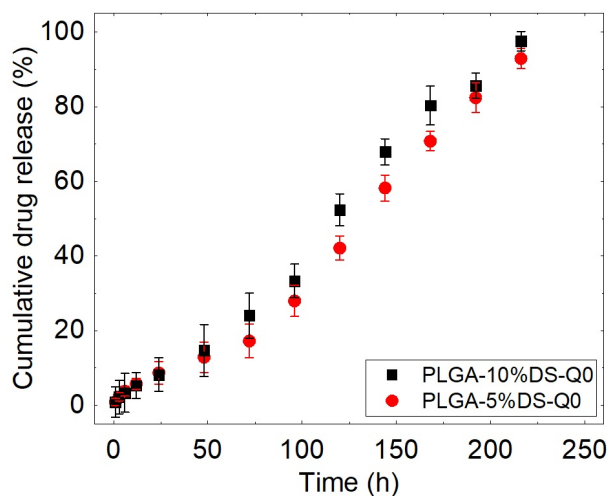
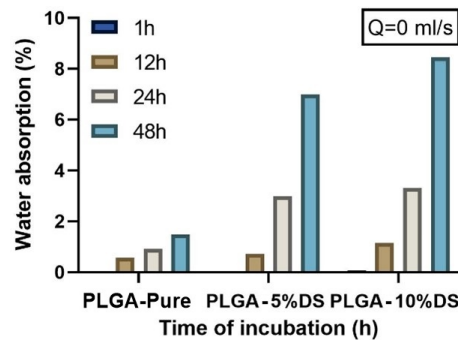


FIGURE 4.22 – Cumulative drug release from PLGA films with 5% and 10% DS at $Q=0$ ml/s

the samples. Moreover, the effect of the drug percentage is noteworthy. The calculation of the number of pores by the ImageJ software for the samples of PLGA-10%DS and PLGA-5%DS after 48 hours of release showed that the number of pores in the 10% sample is two times more than the samples with 5% of DS, this is where the surface area of the PLGA-5%DS is occupied by 22% of the pores whereas it is 28% for the PLGA-10%DS. One can note that higher percentages of the pores in PLGA-10%DS can be the reason for the high release kinetic from these samples compared to PLGA-5%DS. According to the calculation by ImageJ software from the high magnification micro graphs, the PLGA-5%DS polymer film contains pores of 3–140 μm in size, with a mean size of 12.42 μm and pores of 3–120 μm in size with a mean size of 9.92 μm for the PLGA-10%DS after 48 hours of release. One can note that by increasing the initial drug load for the samples, the number of the pores created during the release increases however mean size of the created pores is smaller compared to the low initial drug loaded samples. As a reason one may note that because each particle of the drug is absorbing the water, therefore as there are more drug particles more pores are formed. This is the necessity of the drug release where the water penetrates around particles and helps them to release. Once the particles absorbed the water, they form the bubbles, some small bubbles grow and some other isolated bubbles blast and results in the pores, where in the consequence the drug is released.



(a)

FIGURE 4.23 – Water absorption percentages for PLGA-Pure, 5% and 10% DS at the static state

4.2.1.4 Effect of flow rate

Due to the presence of flow in the study of drug delivery in the case of stents, it is important to investigate the effect of this parameter. In this section the influence of the flow rate on the release of (a) DE from the PU samples in distilled water medium (b) DE from the PU samples in PBS medium (c) DS from PLGA samples in PBS medium was studied.

(a) DE release from PU samples

In this section drug (DE) release from PU samples at three different flow rates of 0, 7.5 (flow rate of the healthy internal carotid artery) and 23.5 ml/s (flow rate of the healthy internal carotid artery during the exercise) in the distilled water at the temperature of 37°C was tested. The measuring method was the method of gravimetry.

Figure 4.25 is representing the effect of flow rate on water absorption and the drug release from the samples with 10% of drug. Figure 4.25 (a) illustrates there is not high differences in water absorption of the numerous samples at various flow rates for PU with 10% drug. Figure 4.25 (b) indicates the effect of the flow rate on the drug release. One can note that by increasing the flow rate the rate of the released drug at the initial period does not show a high difference, whereas the second part of the curve shows a significant difference in the kinetic of the release. The former can be due to driving force, such as increase in the pressure. Moreover, decreasing the mass boundary layer, induces high concentration gradients which leads to high diffusive flux.

(b) DE release from PU samples

4.2. DRUG RELEASE IN ARTIFICIAL LUMEN

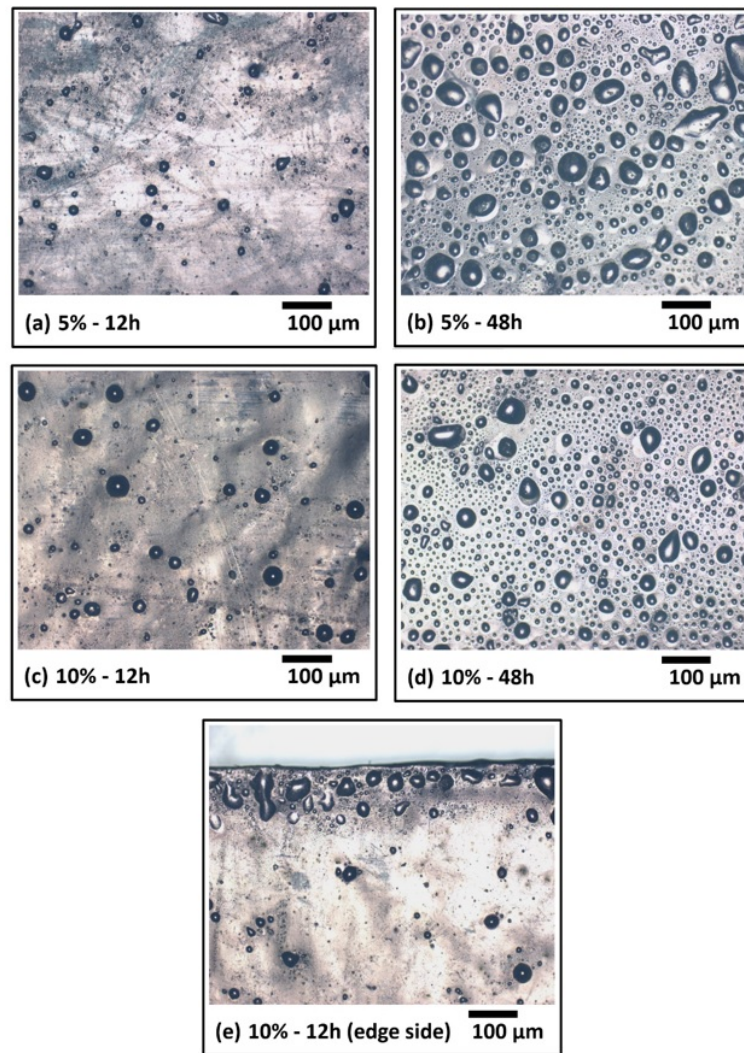


FIGURE 4.24 – Optical microscopic observations of the samples (a) PLGA-5%DS after 12 hours, (b) PLGA-5%DS after 48 hours, (c) PLGA-10%DS after 12 hours, (d) PLGA-10%DS after 48 hours, (e) PLGA-10%DS after 12 hours from the edge of the sample, of drug release test in the static state

4.2. DRUG RELEASE IN ARTIFICIAL LUMEN

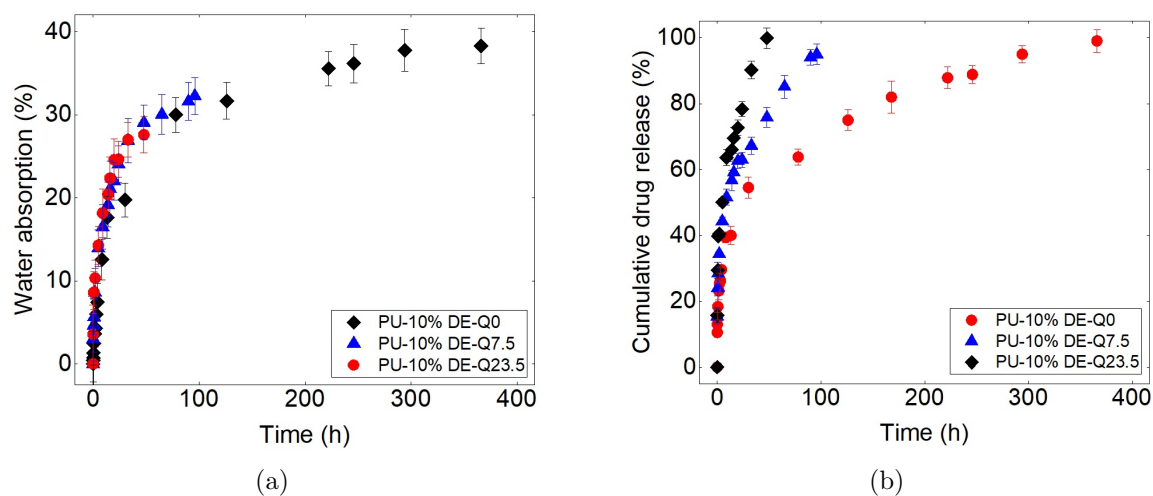


FIGURE 4.25 – (a) Water absorption and (b) drug release for PU with 10% of DE at different flow rates

In this section drug (DE) release from PU samples at the flow rates of 0 and 7.5 ml/s was examined in the PBS medium at the temperature of 37°C. The drug measuring method was the UV-Vis method.

Figure 4.26 shows that increasing the flow rate decreases the overall time of the release, however the first region of the release (burst release) is slightly higher for the continuous flow, but it does not have a remarkable difference of the release kinetic. The second stage of the release which is almost continued with the mechanism of diffusion is slower for the flow rate of zero compared to 7.5 ml/s . Former results reveals that the mechanism of diffusion is not irrelevant with the flow rate. It is notable that, even in the static state the method was the incubation method, and two surfaces of the samples were in contact with the dissolution medium, but in the continuous state just one side was contacted with the dissolution medium. Therefore, it emphasizes the importance of the flow rate on the release. This difference implies the effect of the gradient of the concentration. One can consider the release at the time t (shown in figure 4.27) for the static and continuous state, where in the circulating medium the gradient stays always high between the samples and the medium. However in the static although the medium is not saturated, but the gradient of concentration will be low at the time of $t+\varepsilon$. Specially comparing the continuous state to the static state, it is noticeable that there is an additional pressure of the circulating fluid over to the atmospheric pressure. The results indicate that the same phenomenon of release is occurring for the cases with different flow rates, where accelerating the flow, increase the kinetic.

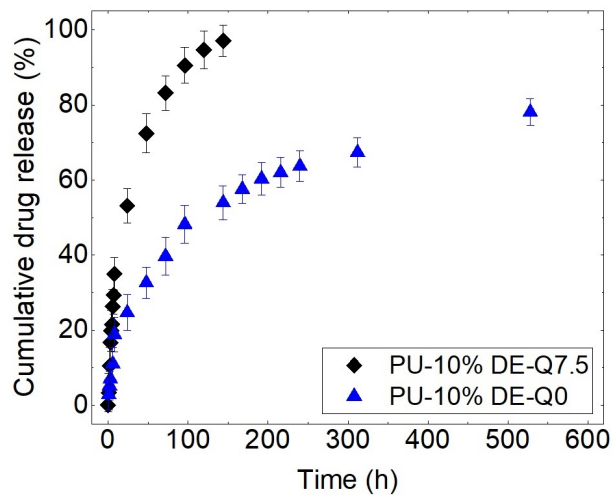


FIGURE 4.26 – Cumulative drug release curves from PU-10% DS at the flow rate of 0 and 7.5 ml/s

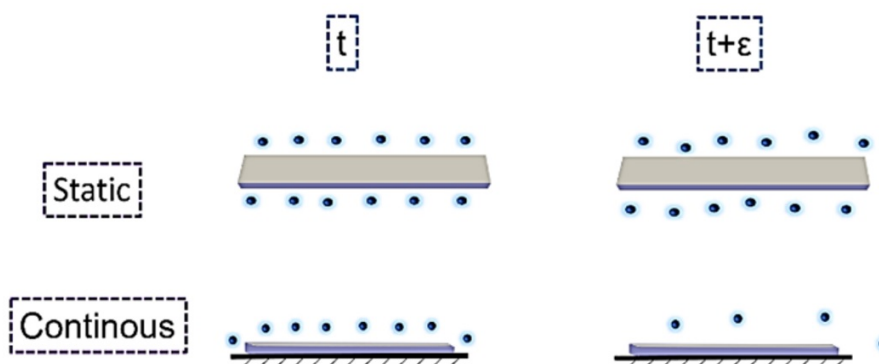


FIGURE 4.27 – Gradient of concentration at t and $t+\epsilon$ for the static and continuous flow rate

(c) DS release from PLGA samples

In this section drug (DS) release from PLGA samples loaded with 10% of DS at different flow rates of 0, 6.5, 7.5 and 23.5 ml/s in PBS at the temperature of 37°C were studied.

Figure 4.28 shows the drug release profiles of PLGA-10%DS films at different flow rates of 0, 6.5, 7.5 and 15 ml/s . The results show that by increasing the flow rate the kinetic of the release is increased (as discussed for the PU-DE samples). However, it is obtained from figure 4.28 that from the flow rate of 0 to 6.5 ml/s this difference is significant. While, from 6.5 to 15 there is not a large difference in the kinetic of the release. This emphasizes that the effect of flow type is more considerable in this type of the polymer carrier. The former can be due to the contribution of the mechanisms of release.

It is notable that the samples at different flow types and flow rates are depleted from the drug at nearly the same time. Moreover, results show that nearly the same kinetic and mechanisms for the release from the samples at different flow rates in the continuous state are happening. Understanding the importance of the amount of water absorption in drug carriers in order to release the drug, leads us to analyze the water absorption data (shown in figure 4.30). Comparing the effect of the flow rate on the water absorption of PLGA-Pure and PLGA-10% DS showed that by increasing the flow rate the amount of the water absorbed is increased (notice the time intervals for two different types of flow. It was chosen regarding to the stability of the polymer films for further analysis).

Analysing the mechanisms happening during the release in these systems are important for further investigations. The results shown in figure 4.28 indicate the presence of the burst release significantly for the samples exposed in the continuous state of flow with different flow rates. In this regard, initially the film is dry then it is exposed to the aquas environment, after the initial burst release due to the gradient of the concentration between the films and the aquas environment the mechanism of diffusion is occurring. Two other mechanisms that was observed during the test, are swelling and erosion of the samples. Swelling of the samples was highly observed after one hour of the test for the samples exposed in the continuous flow. Moreover, observation of the small crumbs in the test chamber during the release is indicating the presence of the erosion (physical degradation) resulting in the mass loss of the polymer.

Considering figure 4.28, about 78.8% of drug was released from PLGA-10%DS at the flow rate of 7.5 ml/s in the first 48 hours, while PLGA sample with 10% of drug at 48 hours releases only

4.2. DRUG RELEASE IN ARTIFICIAL LUMEN

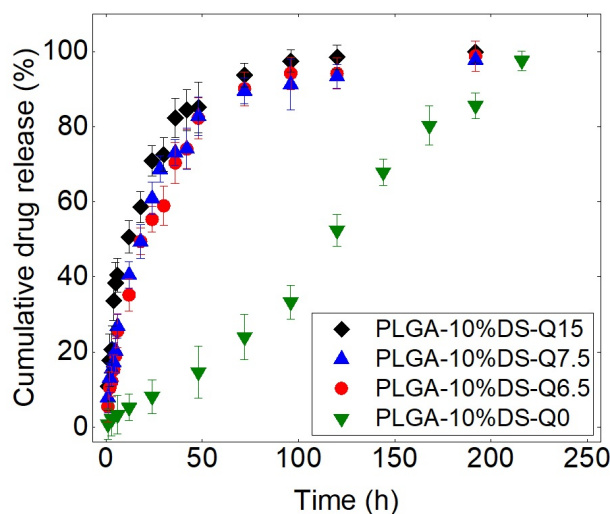


FIGURE 4.28 – Cumulative drug release from PLGA films with 10% DS at the flow rates of 0, 6.5, 7.5 and 15 ml/s

17.8% of drug at the static state. It is worth noting that the time needed for the release of the 80% of the drug in the static state is about four times more than the continuous state. One can mention that according to studies, the presence of flow rate has increased the penetration of the fluid into the carrier which will increase the amount of the absorbed water. The water penetrated to the polymer films results in the dissolution of the drug particles and also swelling of the polymer layer, thereafter the active substance leaves the polymer layer by the probable mechanism of diffusion. Degradation is another important mechanism for this type of polymer but according to the literature studies the incidence of the chemical degradation in the short duration of the test is far from the expect. However the physical degradation such as erosion or environmental stress results in the cracking can be another reason of the release, notably with the presence of the flow. Further explanation of the mechanisms will be discussed in chapter 4.

Figure 4.29 shows the SEM micrographs of the PLGA-10%DS after 48 hours of release test at two different flow rates of 0 and 7.5 ml/s . The effect of the flow rate on the structure of the PLGA films is evident from these figures. It is observed that in the release condition without flow (shown in figure 4.29 (a) and (c)) the bubbles are created by water absorption, however in the case with flow (shown in figure 4.29 (b) and (d)) the bubbles seem to be already exploded and the porous structure is seen which results in more release of the drug and of course decreasing the mechanical properties of the samples. Moreover, figure 4.29 (b) clearly shows the presence of the swelling of the polymer in

4.2. DRUG RELEASE IN ARTIFICIAL LUMEN

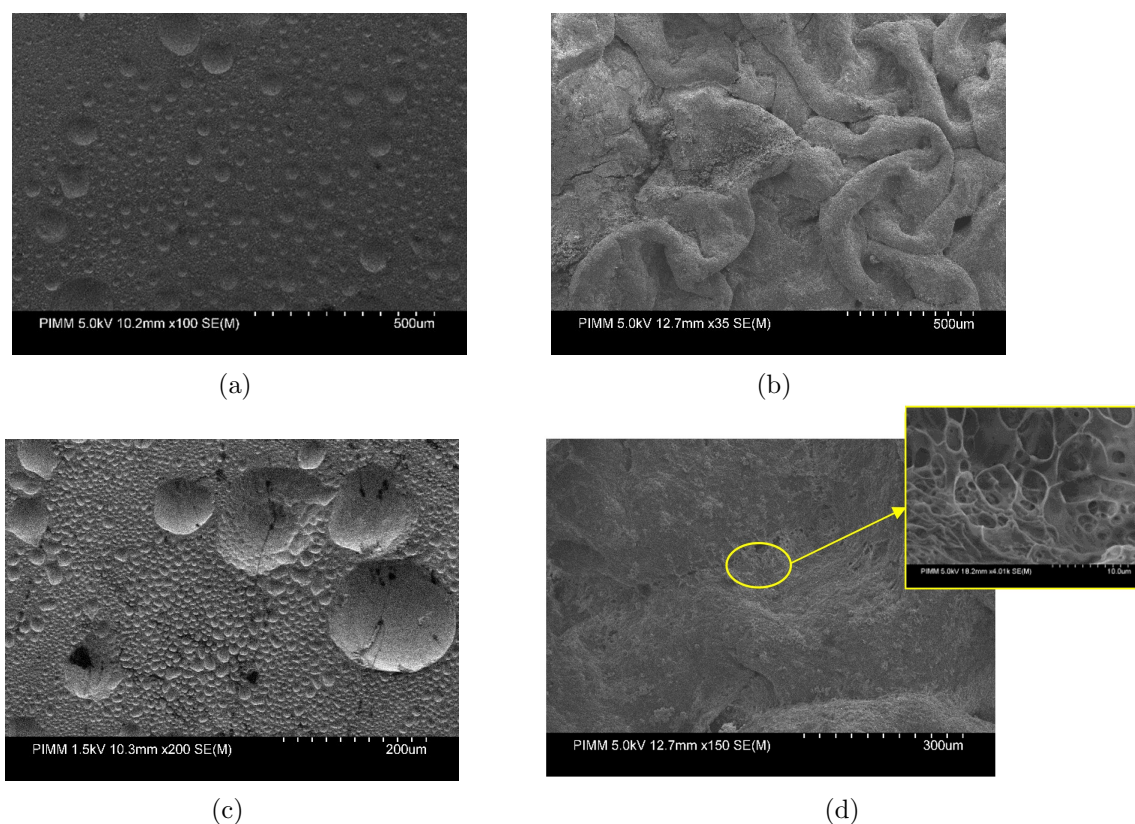


FIGURE 4.29 – SEM micrographs of PLGA-10%DS after 48 hours of drug release at (a), and (c) the flow rate of 0, (b), and (d) flow rate of 7.5 ml/s , but at different magnifications

the continuous state. The results show that the flow rate significantly changes the morphology of the polymer, where it increases the roughness of the samples in the mesoscale. It is notable from figure 4.29 (d) which is the larger scale of the figure 4.29 (b) that how the swelling results in the increase of the detachment of the polymer chains and increases the molecular spacing. The latter results in the liberation of the drug from the polymer chains and also causes a fragile structure of the polymer.

4.2.2 Investigation of drug release mechanisms

(a) PU-DE drug delivery system

In order to investigate the mechanisms, first finding the steps of the release profile is considered. The experimental data was investigated using Higuchi model, which has been used extensively in several studies to evaluate the stages of drug release from carries. The Higuchi equation 2.5 was described previously.

4.2. DRUG RELEASE IN ARTIFICIAL LUMEN

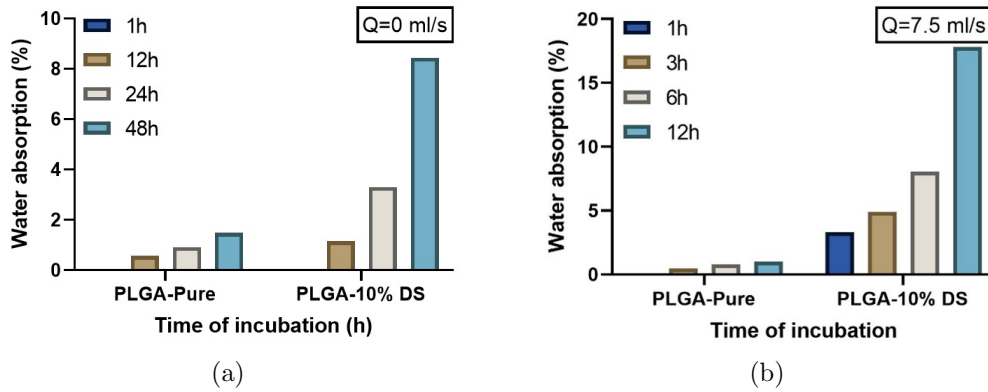


FIGURE 4.30 – Water absorption percentages for PLGA pure, 5% and 10% at flow rates of (a) 0 and (b) 7.5 ml/s

After identifying the steps, Korsmeyer-Peppas was applied to each curve in order to detect the mechanisms whether it is diffusion or degradation and swelling controlled. For this purpose, the Peppas equation 2.11 was first evaluated. To further investigate the mechanism of drug release from carriers; zero-order, first-order, and Peppas-Sahlin models were examined. Moreover, Peppas-Sahlin model is used to calculate the percentage of the contribution of the mechanism of diffusion during the release. In Peppas-Sahlin equation, by considering the following relation [195]:

$$F = \frac{1}{1 + \left(\frac{k_2}{k_1}\right)^m} \quad (4.3)$$

where k_1 and k_2 are constants obtained from equation 2.13, the contribution of the diffusion mechanism at different times can be investigated. Figure 4.31 shows the algorithm for following this strategy.

The experimental results have been analyzed by Higuchi equation (figure 4.32 and table 4.1). Fitting the experimental data at the static and dynamic conditions with different dosages by Higuchi model, presented two-step drug release from the PU films. The regression results of the Higuchi model for each step are presented in table 4.1. The correlation coefficients for all the samples were high and near to 0.99. In general, comparing the values of the K_H from table 4.1, show that the kinetic constants in the first and second steps are increased by the drug load. From these curves, the below conclusion can be drawn:

- The number of steps seems to be independent of the considered parameters.
- Second step gives another kinetic of the release lower than the first step. It notes the presence of the other mechanism(s), or it can be the same mechanism as first step but with different kinetics due

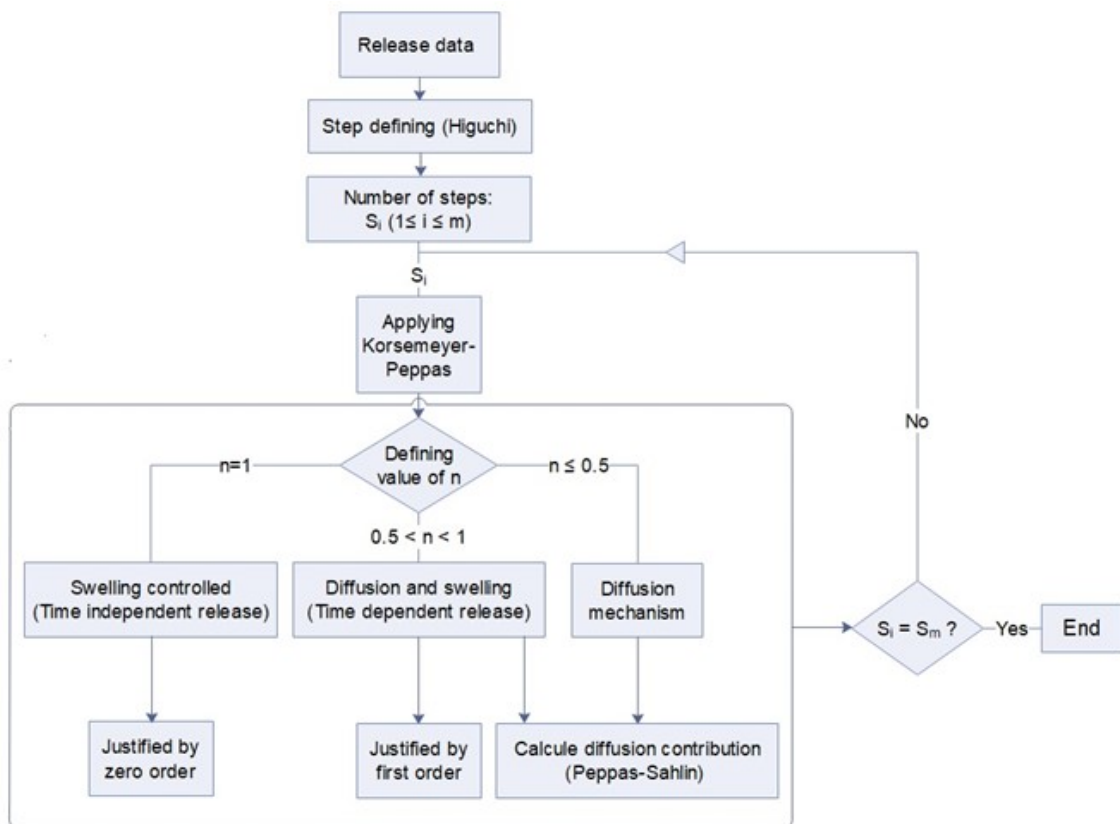


FIGURE 4.31 – Algorithm for defining the mechanisms contributed during the release from a drug loaded carrier

4.2. DRUG RELEASE IN ARTIFICIAL LUMEN

TABLE 4.1 – Values related to the Higuchi model by fitting the experimental results

Test conditions	K		R^2	
	Step 1	Step 2	Step 1	Step 2
PU-10%DE-Q0	0.108	0.037	0.98	0.99
PU-20%DE-Q0	0.108	0.049	0.98	0.99
PU-30%DE-Q0	0.108	0.064	0.99	0.98
PU-10%DE-Q7.5	0.175	0.071	0.98	0.99
PU-20%DE-Q7.5	0.175	0.071	0.98	0.98
PU-30%DE-Q7.5	0.175	0.071	0.97	0.98
PU-10%DE-Q23.5	0.285	0.106	0.98	0.99
PU-20%DE-Q23.5	0.285	0.106	0.98	0.99

to certain reasons.

- One can define that the threshold time, which is the time where the kinetic changes, are different for dynamic flow rates; however, it is the same for the static state. The later indicates that when the drug content is increased at dynamic state more particles can participate in the release at first step.

- However, the release kinetics of the first step is increasing with drug percentages but with a high regression they are nearly the same, comparing to the second step.

- In static state, the rate of drug release in the second step increases by increasing the drug dosage. However, it is constant for continuous flow rates, (shown in figure 4.32). One can note that the influence of drug dosage is more evident in the case of static compared to the continuous flow. Comparing to the figure 4.32 (a) in the static state the influence of the drug percentage is more significant in the second part of the release. In these release curves the first part of the release profile is mostly related to the burst release and the second part is almost related to the diffusion. Therefore, one can note that the effect of the drug percentage on the mechanisms of the release can be dependent at the same time to the flow rate.

To investigate and intuition the mechanisms of drug release from carriers, equations 2.11, 2.7 and 2.4.1 were fitted. The fittings were applied to each step; the results of these models are presented in table 4.2. Figure 4.33 shows the curves related to the fitting of the Korsmeyer- Peppas model.

The constants related to the fitting of equations 2.11, 2.7 and 2.4.1 related to Korsmeyer- Peppas, zero-order, and first-order models, respectively, are presented in table 4.2 for the PU samples charged with different percentages of drug at the static and continuous flow. The unfavorable fit of equations

4.2. DRUG RELEASE IN ARTIFICIAL LUMEN

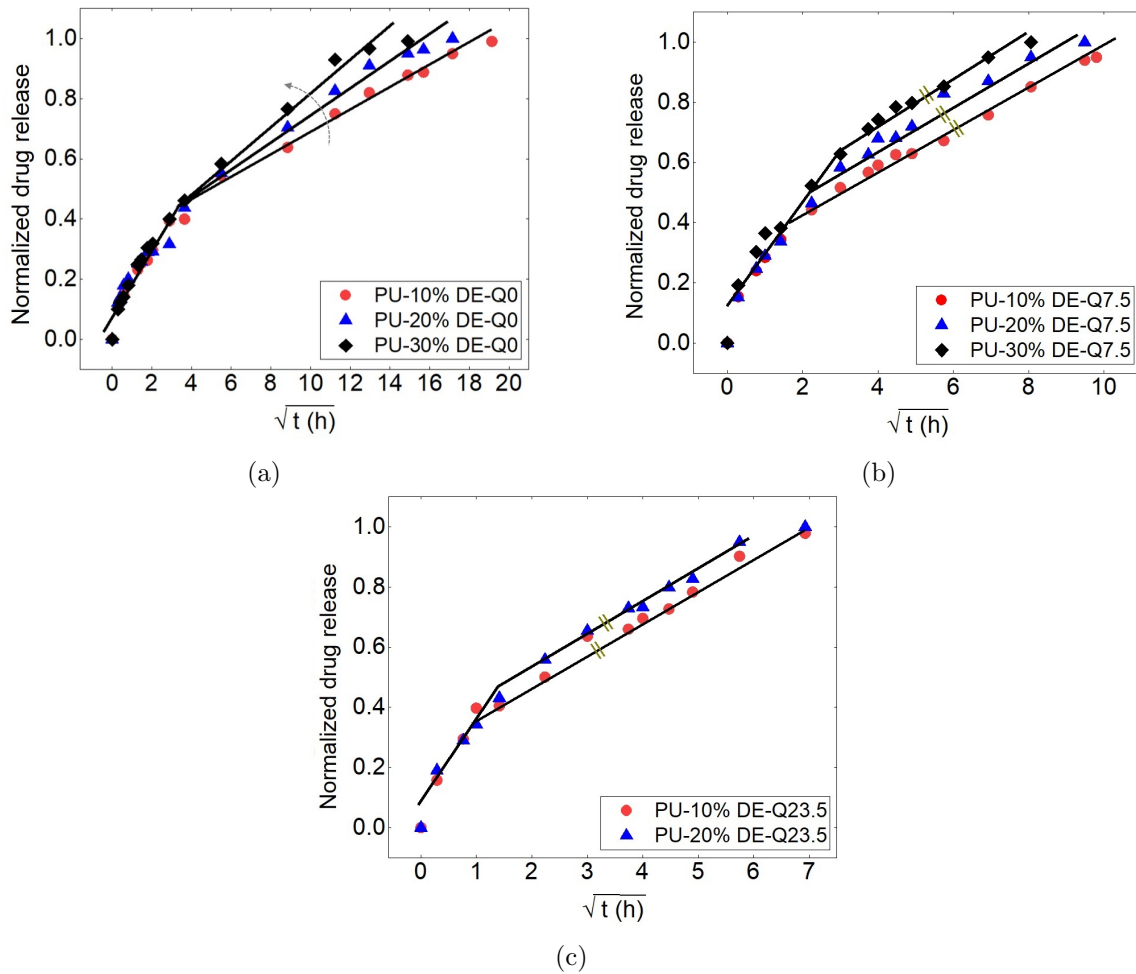


FIGURE 4.32 – Step analyzing by Higuchi model for the experimental tests of drug release with different drug loads (10, 20, and 30%) at the (a) static condition, (b) continuous state with the flow rate of 7.5 ml/s and (c) continuous state with the flow rate 23.5 ml/s

4.2. DRUG RELEASE IN ARTIFICIAL LUMEN

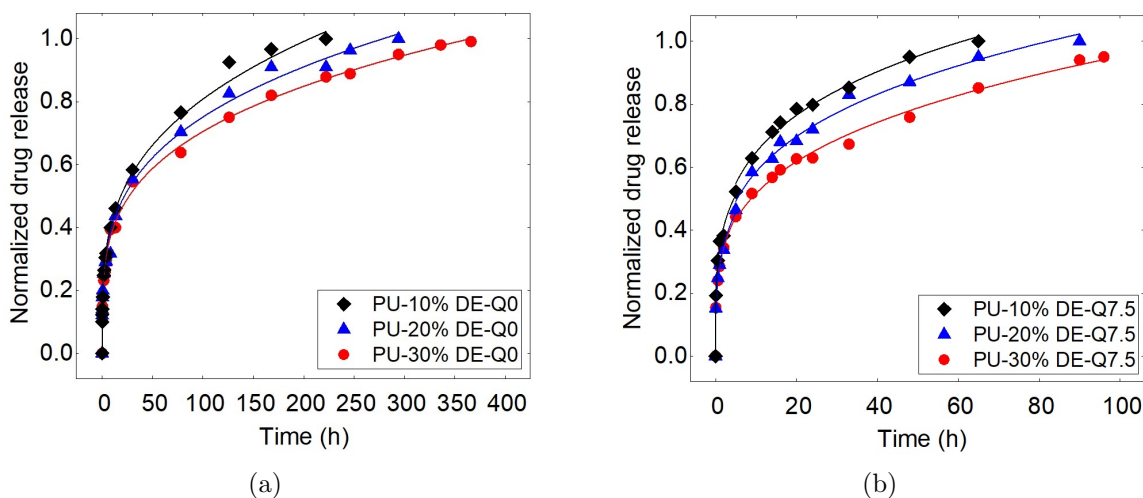


FIGURE 4.33 – Regression results of (a) PU-10, 20, 30%DE-Q0 and (b) PU-10, 20, 30%DE-Q7.5 in two steps with Korsmeyer- Peppas model

2.7 and 2.4.1 indicates the non-integration of polymer degradation and the dissolution, respectively. The regression results of the Korsmeyer- Peppas model presented in table 4.2 show the correlation coefficients for all tested samples were higher than 0.98. The n values are less than 0.5. It is noteworthy that, the amount of n value less than 0.5 indicates the pseudo-Fickian mechanism [247, 248] for drug release from the loaded PU. Therefore, in the case of the static and continuous state at two steps for three different percentages, diffusion is the involved mechanism but it is not the only mechanism intervened.

However, for considering the degradation in the test situation degradation test were conducted in the continuous flow state where, the three pure polyurethane samples were immersed in the aquatic environment for 28 days. The results demonstrated no mass loss during this test. As the mass loss is an indicator of the degradation, the material is facing the first type of degradation where it experiences a decrease in mechanical properties but no weight loss during the test period [176, 249]. Therefore, referring to the experimental degradation test of polyurethane samples, no degradation was observed.

Figure 4.34 shows the contribution of diffusion mechanisms for the samples with different drug percentages at the flow rates of 0 and 7.5 ml/s by equations 2.13 and 4.3. As shown in figure 4.34, the contribution of the diffusion mechanism decreases over time for all three cases. Furthermore, the non-equilibrium coefficients n and m obtained from equations Korsmeyer- Peppas and Peppas-Sahlin

4.2. DRUG RELEASE IN ARTIFICIAL LUMEN

TABLE 4.2 – Regression constants for different mathematical models for PU-10%DE, 20%DE, 30%DE-Q0

Polymeric films	Korsmeyer-Peppas						Zero-order				First order			
	K		n		R ²		K		R ²		K		R ²	
	Step 1	Step 2	Step 1	Step 2	Step 1	Step 2	Step 1	Step 2	Step 1	Step 2	Step 1	Step 2	Step 1	Step 2
PU-10 %DE-Q0	0.19	0.23	0.29	0.25	0.99	0.99	0.042	0.002	0.12	0.95	0.063	0.015	0.29	0.78
PU-20 %DE-Q0	0.16	0.51	0.30	0.18	0.98	0.99	0.042	0.002	0.12	0.95	0.062	0.022	0.25	0.87
PU-30 %DE-Q0	0.21	0.60	0.31	0.16	0.99	0.98	0.046	0.002	0.19	0.91	0.072	0.029	0.57	0.93
PU-10%DE-Q7.5	0.28	0.08	0.27	0.46	1	1	0.11	0.005	0.28	0.98	0.17	0.05	0.59	0.71
PU-20%DE-Q7.5	0.29	1.11	0.28	0.12	1	0.99	0.113	0.006	0.40	0.93	0.18	0.07	0.64	0.84
PU-30%DE-Q7.5	0.35	4.16	0.24	0.04	0.99	1	0.13	0.007	0.11	0.93	0.22	0.88	0.71	0.84

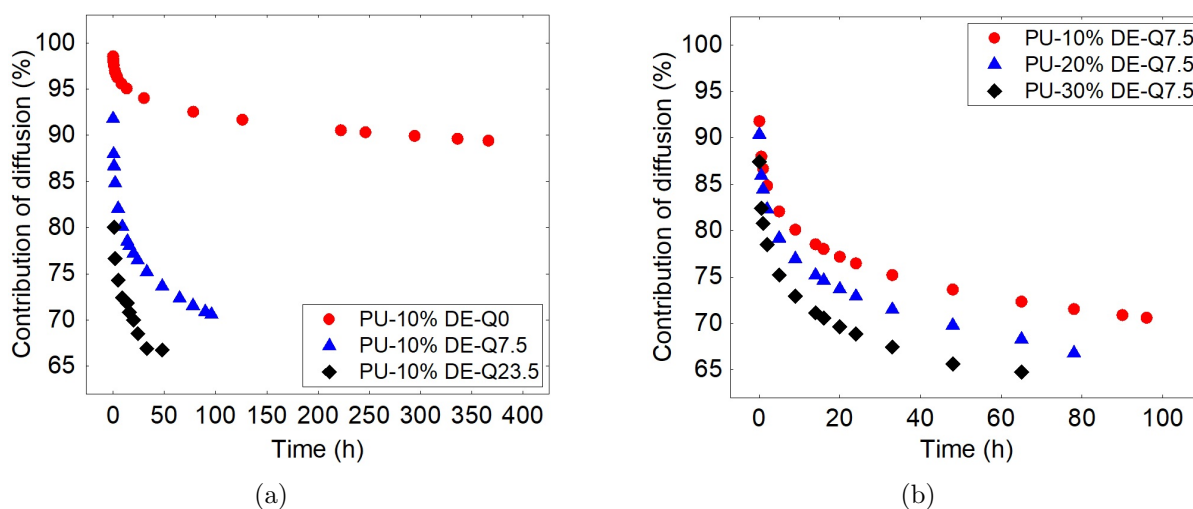


FIGURE 4.34 – Contribution of diffusion versus the time of release at (a) different flow rates for the PU-10%DE (b) different initial drug percentages at the flow rate of 7.5 ml/s

showed that drug release was not affected only by diffusion.

Figure 4.34 (a) shows that the portion of the diffusion mechanism decreased along with increasing the time for all three samples and also it is clear that an increase of flow rate from 0, 7.5 ml/s to 23.5 ml/s, causes a decrease in the portion of the diffusion mechanism in drug release. The decrease in the contribution of the diffusion mechanism over time will be justified by the decrease in the concentration gradient by the time because the diffusion mechanism is controlled by the potential chemical gradient. As mentioned, drug release can involve a variety of mechanisms, common mechanism for drug delivery based on polyurethanes can be diffusion [250]. In the previous section, the contribution of the diffusion mechanism was obtained by equation 2.13 and it was shown that the diffusion mechanism was the dominant mechanism throughout the drug release period, but according to figure 4.34 (a), all the

drugs were not released just by this mechanism. It is also noteworthy that if the mechanism of drug release was uniquely based on diffusion, the n value obtained from equation 2.11 should be equal to the m value obtained from equation 2.13 [250] which in accordance to the calculations, these values were not equal. Therefore, the contribution of the other mechanisms takes attention. The results of the degradation of polyurethane at different times showed no degradation. Therefore, drug release cannot be attributed to the carrier's degradation or dissolution. In the first step for the matrix carrier especially with the undissolved drug particles, the first moments of the release are probably related to the phenomena of burst release. As the studies of the burst-release have shown this mechanism inevitably occurs at the first liberation period and will continue until the release of the drug is stable [145, 171]. Referring to the initial values of the burst release obtained from the figure 4.34 (a) indicate that burst release is increased by changing the state of the flow from static to continuous, whereas it shows less differences for two cases with the flow rates. For the second step, another mechanism in which the drug can be released is based on osmotic pump, this mechanism can be created by osmotic pressure and it is not based on diffusion. One of the reasons for this mechanism is the absorption of water into the polymer. Also, the polymer degradation must be negligible and the porous structure of the matrix is necessary, moreover the presence of the hydrophilic drug favors this phenomenon [52–54].

The results of water absorption showed the amount of water absorbed by PU-10%-Q0, PU-10%-Q7.5 and PU-10%-Q23.5 increased with time. Moreover, increasing the flow rate increases water penetration into the polymer channels and pores. On the other hand, the osmotic pumping is based on the osmotic pressure resulting from water absorption and the solutes dissolved in it. Thus, one can note that increasing the rate of water uptake over time and increasing the flow rate causes the release of the drug through osmotic pressure [52–54]. Consequently, the contribution of the diffusion mechanism to the drug release is decreased by increasing the flow rate and the time of the incubation.

As for the different percentages of drug at the flow rates of 0 and 7.5 ml/s , step analysing by the equation of Higuchi was performed for the flow rate of 23.5 ml/s , shown in figure 4.32. The results show that equally for the flow rate of 7.5 for the flow rate of 23.5 ml/s , also the effect of the flow rate overcomes to the effect of the drug percentage where the second stage of the release shows the constant kinetic of the release for different drug concentrations. One can note that the state of the flow is more significant than the flow rate, where by changing the state of the flow from static to continuous the release behaviour changes this variance is more than the condition where the different flow rates at

the same state of flow (continuous state) is applied.

Referring to the figure 4.34 (b) at the first step as the contribution of the diffusion is decreased at the starting point of release for the samples with 10, 20 and 30 percentages of drug. Therefore release related to the contribution of other phenomena at the first period of the release respectively for 10, 20 and 30 percentages of drug increase. As mentioned above for the polymeric sample at the first moments of the release the probable phenomenon is the burst release which is less related to the water absorption. As the percentage of the drug increases the probability of the drug particles to stay on the surface of the polymer matrix increases. It is therefore by increasing the drug percentage the value related to the burst release increases. In the second step, the other contributed mechanism is the osmotic pressure which is increased by the water absorption and increasing the free space by releasing the more drugs. It is notable more the drug percentage, more the contribution of the osmotic pressure. The system is more non-equilibrium where the drug percentage increases, therefore activation energy for contributing of the mechanisms increases. Moreover, hydrophilicity of the sample due to the more hydrophilic drug increases, hence water absorption increases, and vapor pressure would be another reason for commencing the osmotic pressure. Additionally, another parameter affecting the osmotic pressure is the permeability of the matrix, where increasing the drug content increases the permeability of the matrix. Therefore, the release of the drug through osmotic pressure will depend on the amount of drug loaded and consequently water absorbed into the polymer. Moreover, verifying experimentally the mass of the non-loaded polymers and the dimensions of the loaded and non-loaded PU samples after different test times showed no variation in these values. The latter has proved that respectively degradation and swelling mechanisms do not exist in this type of samples.

One can conclude that the results allowed the identification of three mechanisms of drug delivery; burst-release, diffusion and osmotic pressure mechanisms. The diffusion represents the dominant mechanism in all periods of delivery. However, the contribution of the burst-release throughout the initial time and the osmotic pressure during the second step is accompanied by the diffusion. The proportion of drugs delivered in accordance to time for each of these mechanisms changes during the release period. In addition, the contribution of the other mechanisms apart from diffusion increases with the flow rate which is discussed deeply in section 5.2.1.

(b) PLGA-DS drug delivery system

Applying different release mechanisms to DS release profiles from PLGA films showed that the

4.2. DRUG RELEASE IN ARTIFICIAL LUMEN

TABLE 4.3 – Values related to the Peppas model by fitting the experimental results

Model	Korsemeyer- Peppas			Zero-order		First order		Higuchi	
	K	n	R^2	K	R^2	K	R^2	K	R^2
PLGA-5%-Q0	0.06	1.36	0.99	0.42	0.99	0.022	0.81	4.69	0.88
PLGA-10%-Q0	0.17	1.18	0.99	0.46	0.99	0.022	0.56	5.22	0.9
PLGA-10%-Q7.5	6.66	0.73	0.99	2.54	1	0.16	0.32	12.4	0.95

release profiles in the static state with two different percentages of drug are following the zero order release with the R^2 of 0.99 (stated in table 4.3). It is drawn from the release curve that the release is happening with a rather constant rate in which the rate does not change with the increase or decrease in the concentration of the drug during the release [251, 252]. In addition, when the percentage of the initial drug load is increased the kinetic of the release for zero order is increased, but it is not significant, therefore, it is notable that even by increasing the initial concentration of the drug, release from these samples follow the same mechanism with almost the same rate of release. However, the regression results with Korsemeyer-Peppas shows good correlation where for the $n > 1$ obtained in the static state indicates super case II transport, which describes the rapid increase in the absorption of the solvent in the polymer where it results in the forces exerted by the material with the swelling property [253]. One can note that rather the same conclusion was drawn (in section 4.2.1.3) for the PU samples with different drug percentages at the static state release, the kinetic of the release was not significantly changed during the first period of the release.

Referring to the same table (4.3) the value $n = 0.73$ for the 10% of the drug at continuous state shows the degradation of the polymer film during the release period, where it seems that contribution of the erosion has intensified the kinetic of the degradation.

4.2.3 Evaluation of the mechanical, physical and chemical properties of the polymeric drug carriers during release

The studies show the importance of the properties of polymeric drug carriers used as a cover or a scaffold of the stents for determining their behavior on the release. Literature showed that the force applied to the polymer during the inflation of the stents and also in their fabrication, change their behavior upon drug release and further may results in the incidence of heart attack or had to go through another medical intervention. Better understanding the evolution of the properties of these carriers will allow to assess their behavior and may allow to the improve their functionalization. In this

work, the aim is to characterize the physico-chemical and mechanical properties of the polymeric films with two parameters consistent to the test conditions. The films were loaded with different percentages of drug. Two flow rates of 0 *ml/s* at the static state and 7.5 *ml/s* (simulating the circulation in the healthy internal carotid artery) were considered. In vitro release tests have been performed in the PBS medium at the temperature of 37 °C for PU and PLGA drug incorporated samples. In fact, two drug delivery systems of polyurethane loaded with diclofenac epolamine and PLGA loaded with diclofenac sodium have been considered.

4.2.3.1 PU loaded with diclofenac epolamine

In this section physico-chemical and mechanical properties of the PU samples charged with 0, 10 and 20% DE before and after the tests at the flow rates of 0 and 7.5 *ml/s* were evaluated. The tests were performed in PBS solution at the temperature of 37°C. The properties studied are such as glass transition temperature (T_g), free volume fraction and mechanical properties before or during test.

Glass transition temperature evaluation during drug release

One of the important physico-chemical properties is the glass transition temperature where around it the polymer chains have not the same arrangement and this can change the drug release from the polymers. For clearly observing the evolution of the T_g value DMTA tests have been performed before and after release tests at different time intervals for the samples of PU-10%DE at the static flow condition (shown in figure 4.35). This figure shows that the glass transition temperature is about -43°C showed that the glass transition temperature did not change during the release tests. It indicates the fact that the water absorption and drug release have not any effect on the glass transition temperature of PU during release tests.

Free volume fraction calculation of PU

In a polymer, free volume can be determined by the volume of the total mass, which is not occupied by polymer chains and therefore can be a favorable place for the diffusing molecules, which can affect the permeability of the polymer membrane. Normally the space or pores formed between the polymer chains are assumed to be as the free volume in the polymer. These free volumes are randomly distributed in the polymer which reflects the movements of the polymer chains and therefore the transport of the molecules and on the whole the performance of the polymer membrane. It is difficult to analyze the pore directly in the membrane since the differences exist on a molecular scale. It is an

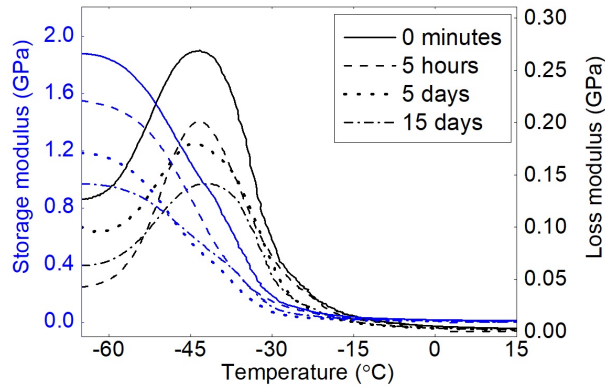


FIGURE 4.35 – DMTA curve of PU loaded 10% mass of DE at various times and flow-less state

inherent property, temporary, and variable, where the polymer's physical state and density significantly impact its value. The mechanism of reducing the extra free volume of the membrane can be linked to physical ageing, arising from the contraction of the lattice and the migration and diffusion of the free volume from the inside of the membrane to the surface [246]. These explanations reveal the importance of the polymer structure in the kinetic of the drug release. There are some studies which showed the effect of the pore structure and the importance of the free volume fraction in the drug release. The polyurethane used in this study was an elastomer where in the structure small holes as the free volume are created. Change of this parameter is investigated for the PU films without drug and with 10%, and 20% of drug.

The Williams–Landel–Ferry equation (WLF) equation is one of the most used equations in polymer systems to calculate the free volume fraction in the polymer membranes. It is principally utilized to predict the mechanical properties of material out of the time range of the experimental test. The visco-elastic behavior of the polymer is related on the frequency of applied loading. This dependence between temperature and viscosity which is proportional to frequency and also correlating relation which describes the temperature dependence of the molecular relaxation times in glass forming substances at the glass transition temperature T_g [254], is explained by Williams-Landel-Ferry (WLF) equation:

$$\ln \frac{F}{F_r} = -\frac{(C_1(T - T_g))}{(C_2 + (T - T_g))} \quad (4.4)$$

The increase of glass transition temperature during multi frequency DMTA tests (figure 4.36 (a))

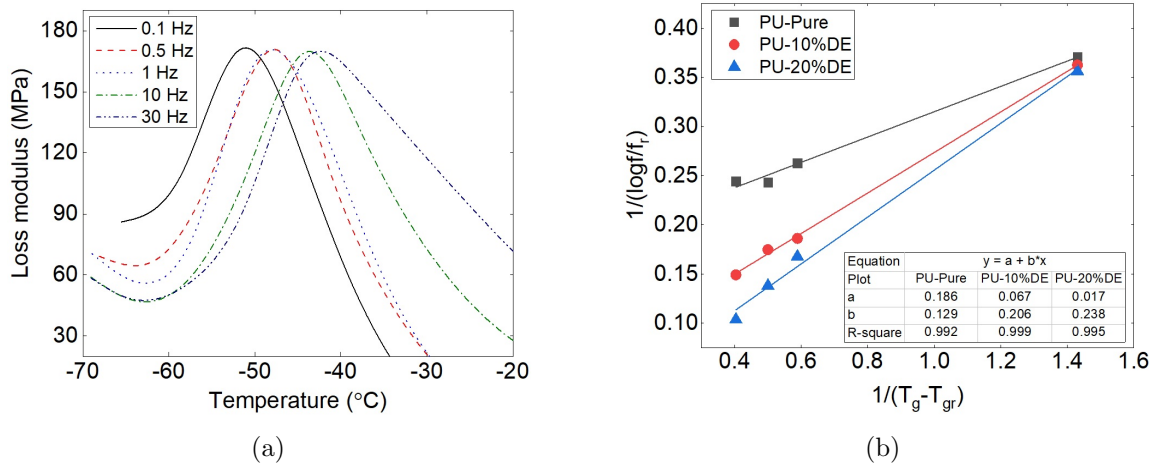


FIGURE 4.36 – (a) Multi frequency DMTA tests: glass transition temperature evolution of PU-10%DE sample and (b) linear regression of WLF equation for PU-Pure, PU-10%DE, PU-20%DE

obeys the WLF theory. The linear regression coefficient was almost 1 (figure 4.36 (b)).

Therefore, the value of free volume fraction coefficient by using $(f_g = \sqrt{(B \cdot \Delta\alpha \cdot A) / 2.303})$ for PU PU-10%DE, PU-20%DE is calculated about 0.37×10^{-2} , 0.47×10^{-2} , and 0.5×10^{-2} , respectively. It is notable from the results, that the drug percentages change the free volume fraction of the polymer, as by increasing the drug percentage free volume fraction slightly increases. One can conclude that the effect of the drug concentration on the variation of polymer molecules in mixing should be considered. Where it needs to be combined with the effect of the free volumes of the constituent solvent, polymer and drug in a polymer carrier film, in determination of its thermodynamic properties.

Mechanical properties of PU

Figure 4.37 (a), (b) shows the tensile curves of the PU samples with 0 and 10% of drug at different time of incubation in the static state. Results show that the effect of drug in the mechanical properties of the polymeric samples are significant. Figure 4.37 (a) shows that the immersion time for the pure PU samples does not change significantly the tensile properties. However, shown in figure 4.37 (b) indicates that increasing 10% of the drug decreased the mechanical properties to about half. Moreover, presence of the drug causes the variation of the mechanical properties during the release time compared to the pure polymer.

Figure 4.37 (c), (d) and (e) shows the tensile behavior of the PU samples with 0, 10 and 20% of the drug at the flow rate of 7.5 ml/s . The results from these figures show that adding 10% of drug, decrease

4.2. DRUG RELEASE IN ARTIFICIAL LUMEN

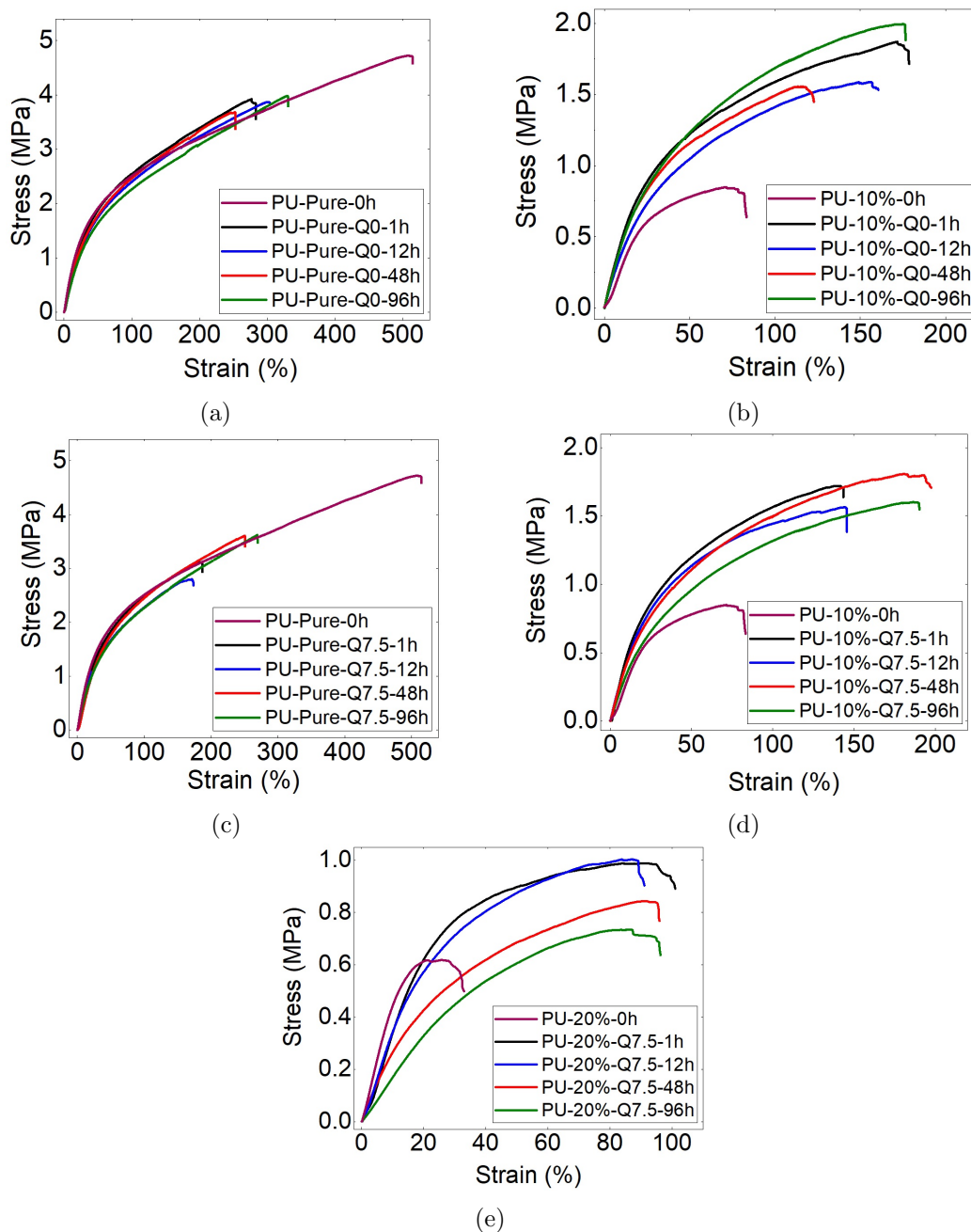


FIGURE 4.37 – Stress-strain curves of PU samples with (a) 0 and (b) 10%DE, at the flow rate of zero and (c) 0, (d) 10%DE and (e) 20%DE at the flow of 7.5 ml/s, at different time intervals

4.2. DRUG RELEASE IN ARTIFICIAL LUMEN

the mechanical properties to about half and adding 20% drug decrease it to about quarter compared to the pure PU. While one can note from the figures 4.37 (a) with 4.37 (c) and 4.37 (b) with 4.37 (d) that comparing the flow rate of 0 and 7.5 ml/s for PU-Pure stress and strain drops from 3.95 to 3.36 MPa and from 330 to 269 which shows that the effect of the flow rate on the mechanical behavior is not highly noticeable for this kind of polymer. Additionally, mechanical properties of the PU samples with 0, 10 and 20% of the active substance before positioning in the fluid, showed the high effect of the drug load in the properties of the carriers (shown in figure 4.37 (c), (d), and (e)). It indicates that adding the active substance results to the low elasticity of the polymer carrier. Where after the initial contact of the drug charged samples with the aquas medium (1h) and the water absorption of the active substance and the polymer, the carrier becomes more deformable (shown in figures 4.37 (d), and (e)). Figures 4.38 (a)-(f) show the comparison of the modulus, ultimate strength and strain at break values for the different percentages of the drug (0, 10%, and 20%) at different time intervals of the static and continuous release tests. The results from the figures 4.38 (a), (b) show the effect of the drug percentage in the mechanical behavior of the samples is more significant compared to the flow rate, where the increase in the drug percentage, decrease the Young modulus value. The results show that the time of incubation slightly decreases the value of the modulus, where this effect is more visible for the charged polymers than the pure polymers. Figures 4.38 (c), (d) show the ultimate strength of the PU with different percentages of drug at the flow rates of 0 and 7.5 ml/s . By comparing these values, the impact of the flow rate and time of incubation is not significant however increasing the initial load of the drug decreases highly the ultimate strength of the PU samples. The variance in the strength during the initial incubation time can be due to the plasticizing effect of the water molecules on the components of the DDS. Figures 4.38 (e) and (f) show the strain at break for the PU with a different percentage of drug at the flow rates of 0 and 7.5, respectively. Comparing the results of the strain at break for the PU shows that increasing the drug percentage decreases the elongation of the polymeric samples. However, elongation of the samples along with the incubation time does not differ significantly but because of the plasticizing after 96hours it has a slight increase.

From the mechanical results one can observe that the highest modulus, stress and elongation at break among all the results with/without drug, before or after test refers to the virgin pure PU. While PU-20%DE before the incubation test has the lowest value of the stress and strain. This can be explained as the percentages of the drug increases the number of the pores in the samples increases,

4.2. DRUG RELEASE IN ARTIFICIAL LUMEN

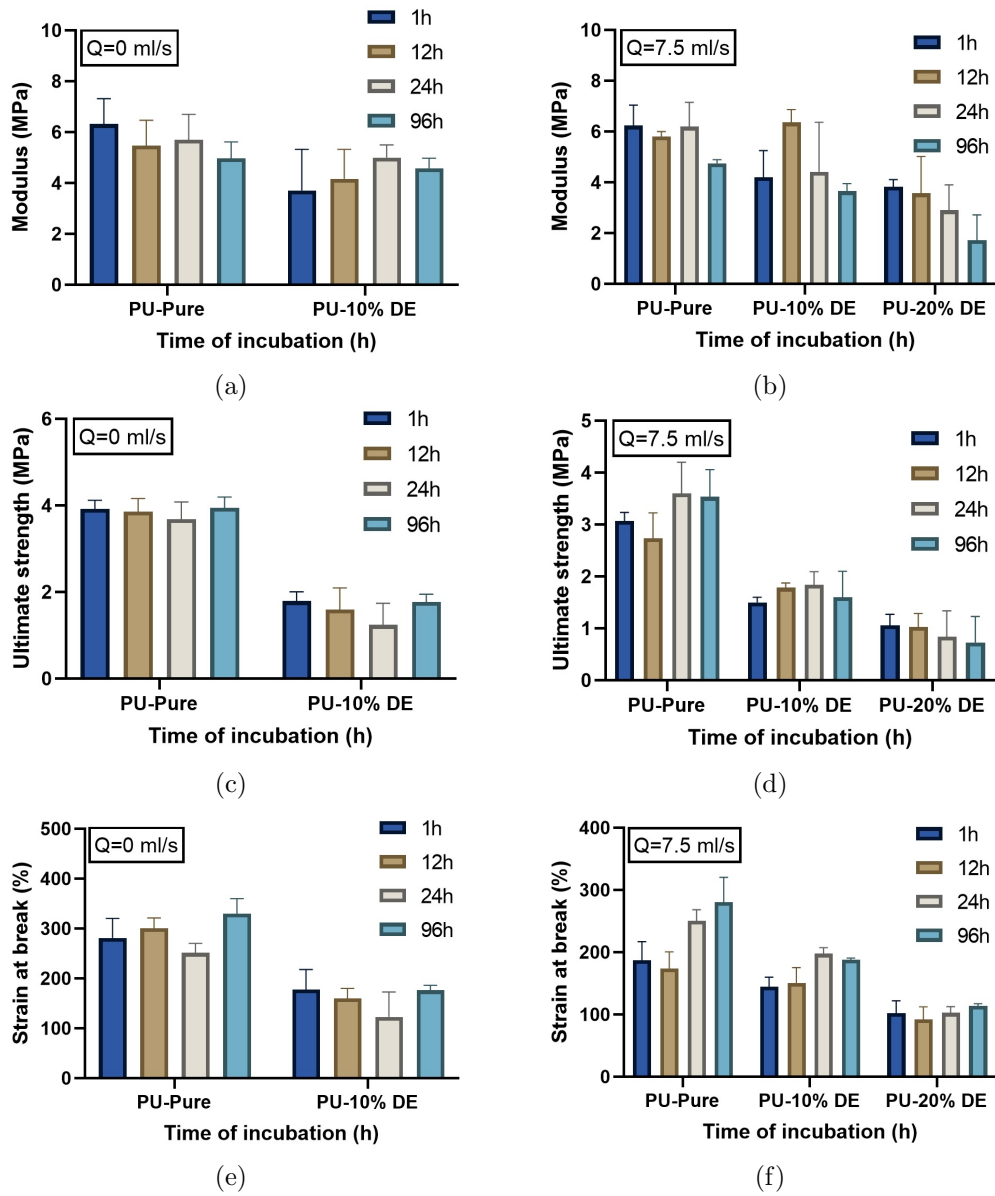


FIGURE 4.38 – Material characteristics of the PU samples with different percentages of DE after release test in the static and continuous state

which results in the decrease of the mechanical properties. Whereas, the flow rate does not affect remarkably the mechanical properties of the samples. The results showed that by increasing the flow rate the kinetic of the drug release is increased however this parameter did not change significantly the intrinsic properties of the material like as the T_g and modulus. Where, the drug percentages change the mechanical properties of the polymer and increases the free volume fraction in the samples however the glass transition of the polymer stays rather constant (comparing figures 4.2 and 4.35).

4.2.3.2 PLGA loaded with diclofenac sodium

Drug delivery from PLGA loaded with various percentages of active substance, diclofenac sodium (DS: 0, 5%, and 10%) at different flow rates of 0 and 7.5 ml/s in phosphate buffered saline (PBS) for different release intervals has been studied. The effect of the flow rate and the drug percentage on the variation of some physical properties such as glass transition temperature (T_g), free volume fraction, and mechanical properties before or during test have been investigated. In vitro release tests have been performed in the PBS medium at the temperature of 37°C.

Glass transition temperature evaluation during drug release

Amorphous phase of polymers are identified by a glass transition temperature (T_g), which is the point of the transformation between a highly viscous brittle material called glass and a less viscous, more elastic rubbery state. The rubbery state (above the T_g) is a structure with high molecular mobility and is thus more susceptible than the glassy state to physical, chemical, and mechanical changes. It is interesting to investigate the glass transition temperature during drug release. The latter could help to analyze the ductile-fragile transition [255–257]. Figure 4.39 shows the variation of the glass transition temperature versus the time of the incubation in the PBS solution for the samples of PLGA, PLGA-5%DS and PLGA-10%DS. The results show that increasing the drug percentages in the polymer films increase the T_g value, where the drug particles are acting as the anti-plasticizer. In this regard by increasing the drug percentages, PLGA films become more brittle. However, by increasing the time of the release, water molecules are acting as the plasticizers and decrease the glass transition temperature [255]. The decrease in T_g during the time of the release is normally related to the hydrolysis of the PLGA films due to the increasing of the water absorption [257]. One can notice that the release rate in PLGA can be related to glass transition temperature due to the higher macromolecular chain mobility of the polymer above its T_g . In this respects T_g of the samples during the release decreases,

however initially the test temperature (37°C) is below the T_g of the samples. Where during the test, T_g of the samples decreases therefore, they are exposed at the temperature above their T_g and helps to the release. One can notice that the release rate from the PLGA samples which are exposed to the temperature above their T_g can be related to the higher macromolecular chain mobility and the drug diffusion through it. On the other side it decreases their mechanical properties because when the material is exposed to the glass transition temperature for some time, then is cooled slowly to room temperature that makes the material more brittle [258]. On the other hand there is the effect of the aging of the material during the time of the release. This is another reason where affects the toughness of the polymer, demonstrated in the mechanical analysis part.

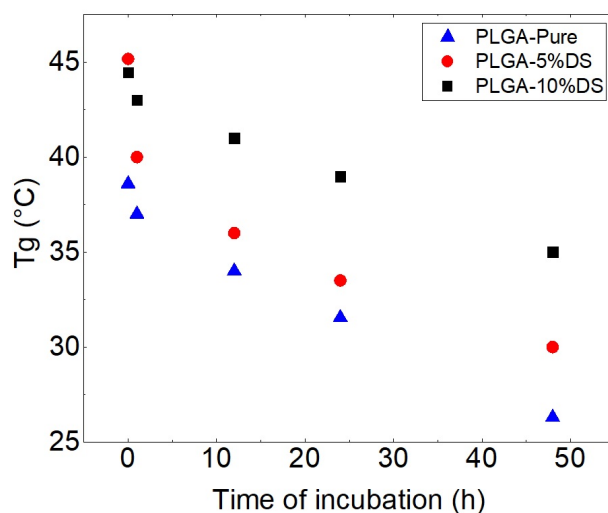


FIGURE 4.39 – Glass transition temperature of the PLGA-Pure, PLGA-5%DS and PLGA-10%DS after different time intervals of incubation tests

Free volume fraction calculation of PLGA

The porous structure and free volume fraction give the loaded PLGA films their properties upon drug release. In the amorphous phase small holes as the free volume are created. Effect of this parameter is investigated for the PLGA films without drug and with 5%, and 10% of drug and its influence on the release behavior. One can note that when increasing frequency, the glass transition temperature has an increasing trend to high temperatures. The increase of glass transition temperature during multi frequency DMTA tests is shown in figure 4.40.

As described in the previous section the free volume fraction explained by the Williams-Landel-

4.2. DRUG RELEASE IN ARTIFICIAL LUMEN

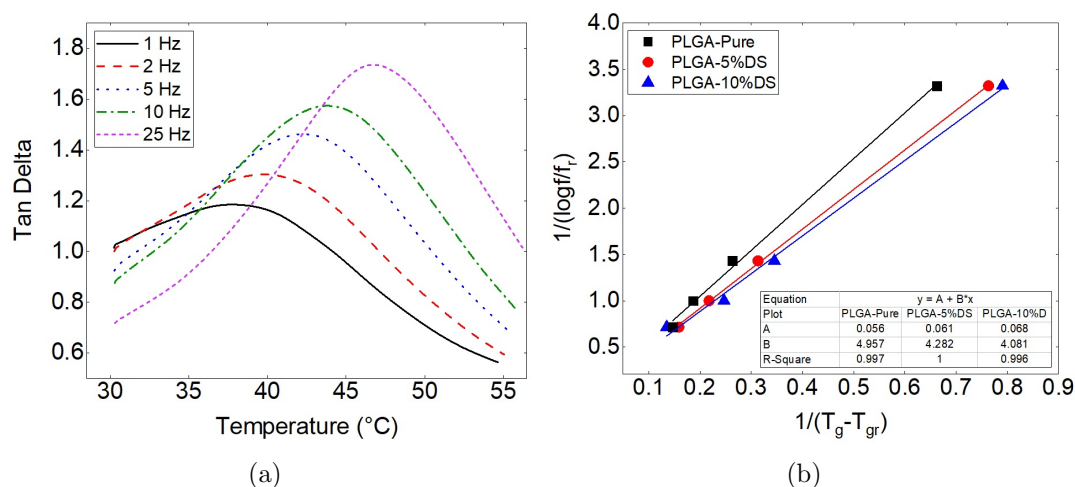


FIGURE 4.40 – Multi frequency DMTA tests: glass transition temperature evolution of pure PLGA and (b) linear regression of WLF equation on the results obtained from DMTA tests for the PLGA samples

Ferry equation was calculated for the PLGA-Pure, PLGA-5%DS and PLGA-10%DS samples and are presented in table 4.4.

TABLE 4.4 – The values related to the free volume fraction parameters for the samples of PLGA-Pure, PLGA-5% and PLGA-10% DS

Parameters	C_1	C_2	f_g
PLGA-Pure	5.42	22.11	0.0192
PLGA-5%	4.76	19.77	0.0195
PLGA-10%	4.43	20.59	0.0206

One can note the effect of the drug percentage on increasing the free volume fraction of the polymeric samples. However this dependence to the drug percentage is less than the for the PU samples with DE.

Polymer degradation

In order to analyse the chemical and physical degradation of the polymer carriers FTIR spectra and SEM observations were respectively utilized. For the PLGA-Pure samples at the flow rate of 0 and 7.5 ml/s at different time intervals FTIR results are presented in the figure 4.41. Relatively same decrease in the size of the peaks during the release are shown in the figure 4.41, it is related to the decrease in the thickness of the samples because of the dilatation observed in the width and length of

4.2. DRUG RELEASE IN ARTIFICIAL LUMEN

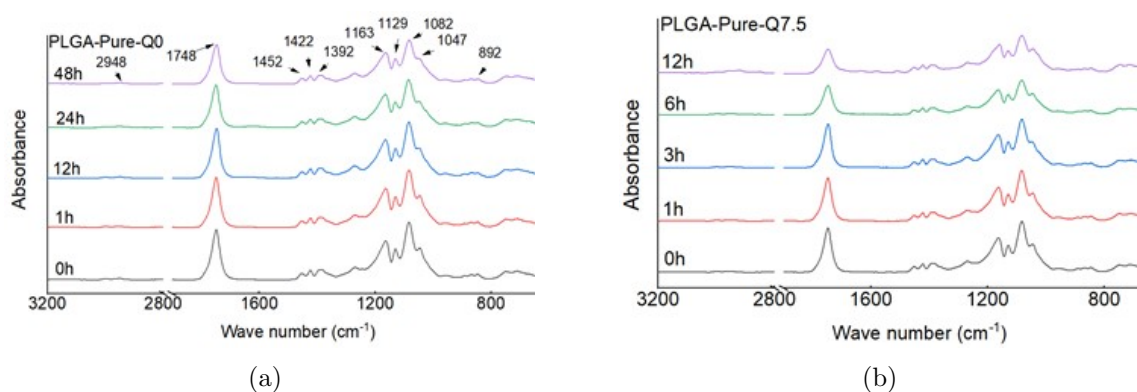


FIGURE 4.41 – FTIR spectroscopy after (a) static and (b) continuous drug release for PLGA pure after certain time of incubation

the samples during the immersion time. The results showed that there is no chemical degradation after 48 hours of immersion, in the static state. However, it is necessary to perform the test after several immersion time to confirm if there is the chemical degradation phenomenon.

Microscopic of the surface morphology of the PLGA-Pure films before and after 1, 12, 24, 48 hours of incubation in PBS at the flow rate of zero are presented in figure 4.42. The surface of the samples before incubation is smooth. By getting in the time of release, the samples gets an opaque white and rough surface consisting of the microscopic bubbles because of the water absorption and starting the phenomenon of physical degradation which is evident in the figure 4.42 (c). As shown in this figure by getting in the time, the bubbles will be changed to the pores. Finally, the pores are connected to each other and results in the weakness of the mechanical properties of the samples and results in their fracture.

Mechanical properties of PLGA

Using PLGA films as an example, the stress–strain curve can be divided into an elastic, yielding and strain-hardening region. Figure 4.43 shows that in all the samples the plasticity of the polymer after 1-hour immersion in the PBS increases where they have high strain compared to the virgin ones. This is for the plasticizing effect of the water on the PLGA samples. However, after one hour the effect of the test temperature, 37°C which is near to the transition temperature of the polymer used and also anti-plasticizer effect of the drug substance in the polymer [255], the effect of the swelling and erosion, moreover the creation of the pores decrease the elongation of the samples. It is obtained from the figure 4.43 that by increasing the immersion time of the samples, the polymer becomes brittle,

4.2. DRUG RELEASE IN ARTIFICIAL LUMEN

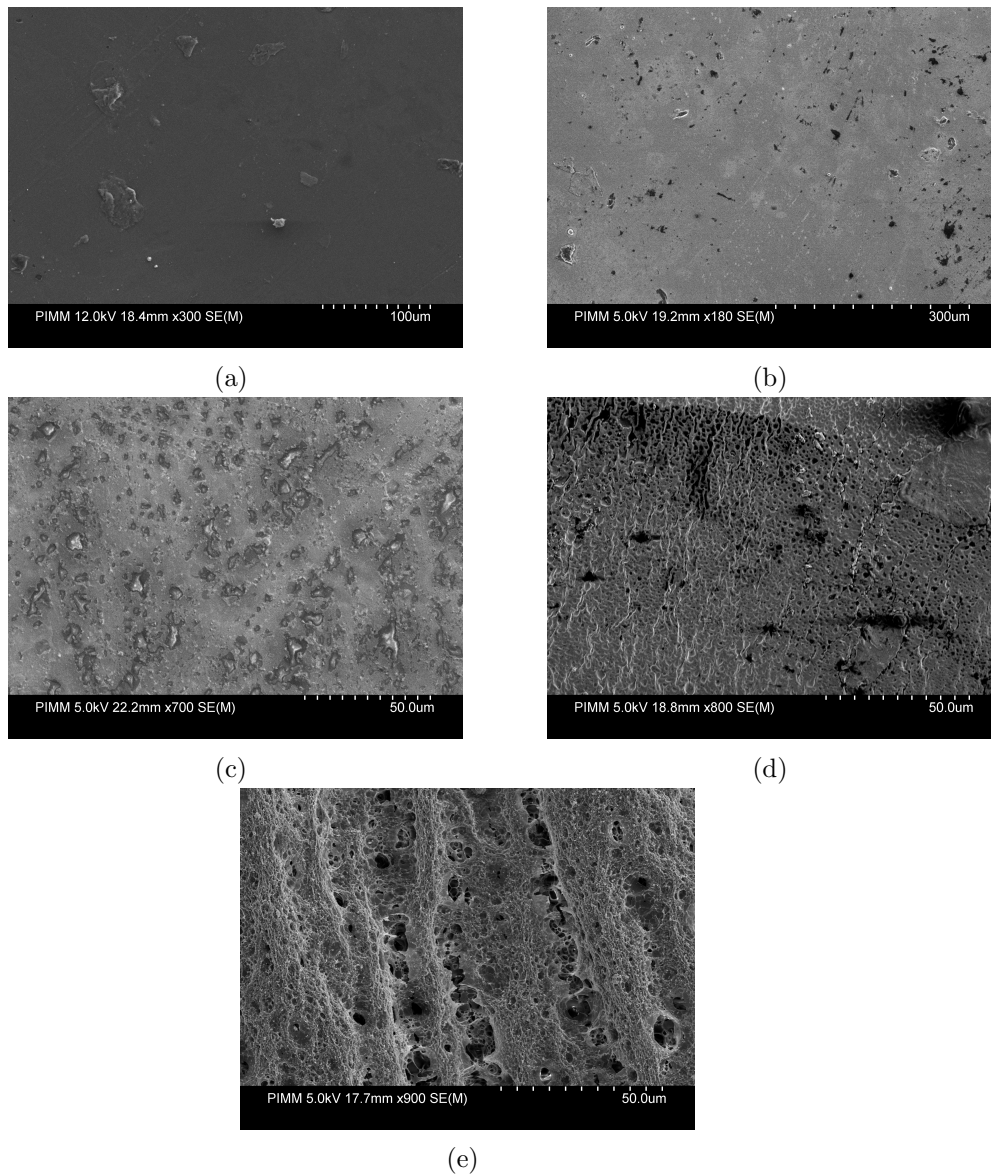


FIGURE 4.42 – Micrographs of the PLGA samples in PBS at zero flow rate after (a) 0, (b) 1, (c) 12, (d) 24, (e) 48 hours

4.2. DRUG RELEASE IN ARTIFICIAL LUMEN

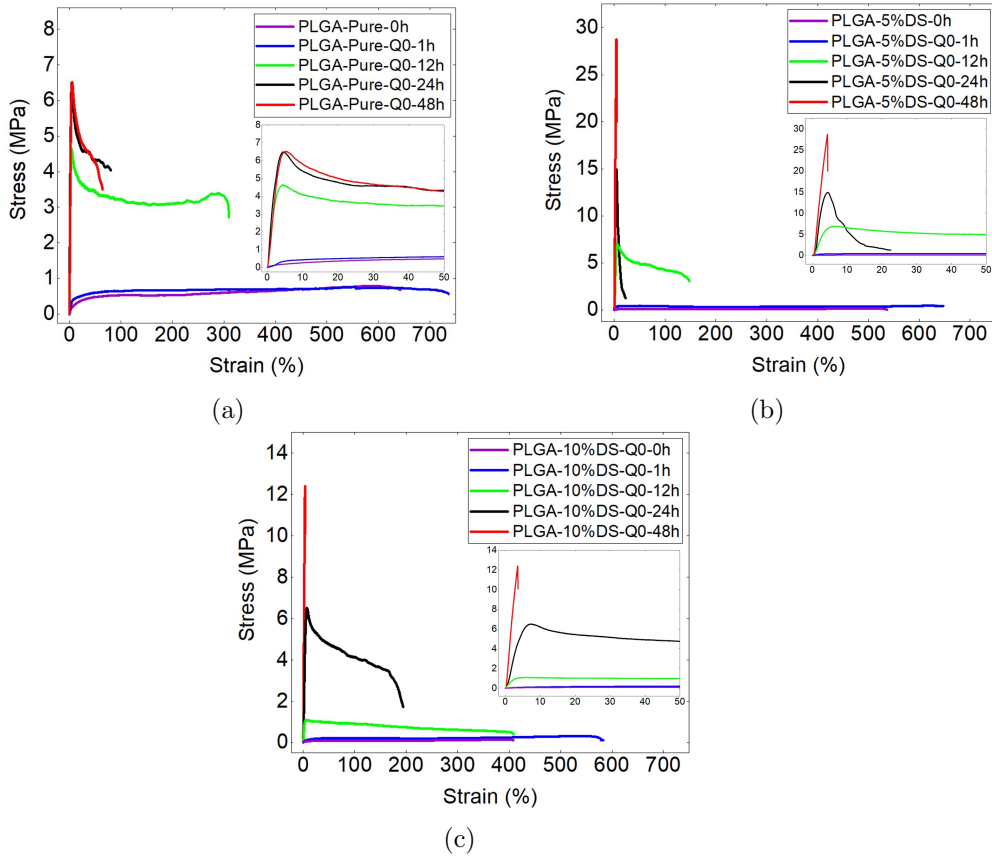


FIGURE 4.43 – Stress-strain curves of the tensile test for the samples of PLGA (a) pure, (b) 5%, and (c) 10%DS after incubation in the static state

where the Young's modulus and the maximum stress of the samples increases.

This difference is more remarkable when certain percentages of the drug were added to the polymer films. However, by increasing the percentage of the drug from 5% to 10%, an increase in the elongation, decrease in the Young's modulus and maximum stress is observed. One can note that the more elongation for the samples of PLGA-10%DS compared to the PLGA-5%DS can be due to the small-sized pores which were observed in the optical microscopic observations (shown in figure 4.24). In the case of the continuous state with the flow rate of the 7.5 ml/s , the effect of the drug percentages was not highly detectable on the maximum stress of the polymer. However, the elongation at the break has decreased to about half (shown in figure 4.44).

Figures 4.45 (a)-(f) show the comparison of the Young's modulus, ultimate stress and strain at break values for the different percentages of the drug (0, 5%, and 10%) at different time intervals of

4.2. DRUG RELEASE IN ARTIFICIAL LUMEN

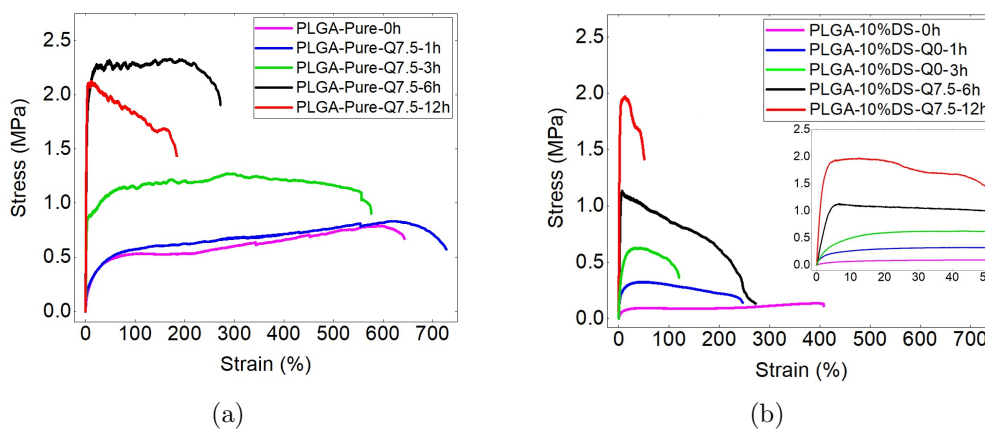


FIGURE 4.44 – Stress-strain curves of the PLGA (a) pure and (b) 10% DS after release test at the flow rate of 7.5 ml/s

the static and continuous release tests. The results from the figures 4.45 (a) and (b) show that by increasing the flow rate from 0 to 7.5 ml/s the Young's modulus of the samples have decreased to unless half. This decrease was much higher significant for the samples with 10% of the drug. Another remark is that by comparing these two graphs one can note that variation of the drug percentage makes more variance in the mechanical properties than the variation of the flow rate. Presence of the drug has increased the Young's modulus of the polymeric samples, in contrast increasing the flow rate has decreased them.

Figures 4.45 (c) and (d) show the maximum stress of the PLGA with different percentages of drug at the flow rates of 0 and 7.5 ml/s , respectively. From the figure 4.45 (c), it is evident that increasing the drug percentage to the 5% of diclofenac sodium increase the maximum stress, however in the case of 10% this value is decreased. The later can be explained by the higher swelling of the samples of PLGA-10%DS compared to PLGA-5%DS. By comparing figures 4.45 (c) and (d), the effect of the flow rate on the maximum stress is evident. Where by changing the flow rate from 0 to 7.5 ml/s , the maximum stress has decreased from about 5 MPa to 2.5 MPa for the samples of PLGA-Pure after 12 hours of release test. Whereas this difference is more notable for the samples of PLGA-10%DS. Figures 4.45 (e) and (f) show the strain at break for the PLGA with different percentages of drug at the flow rates of 0 and 7.5 , respectively. Comparing the results of the strain at break show that, increasing the initial drug load and flow rate have decreased the elongation at break. Where the effect of the flow rate is much notable when the samples are loaded with drug. Moreover, the effect of the flow rate and drug percentage is more significant by increasing the time of the release.

4.2. DRUG RELEASE IN ARTIFICIAL LUMEN

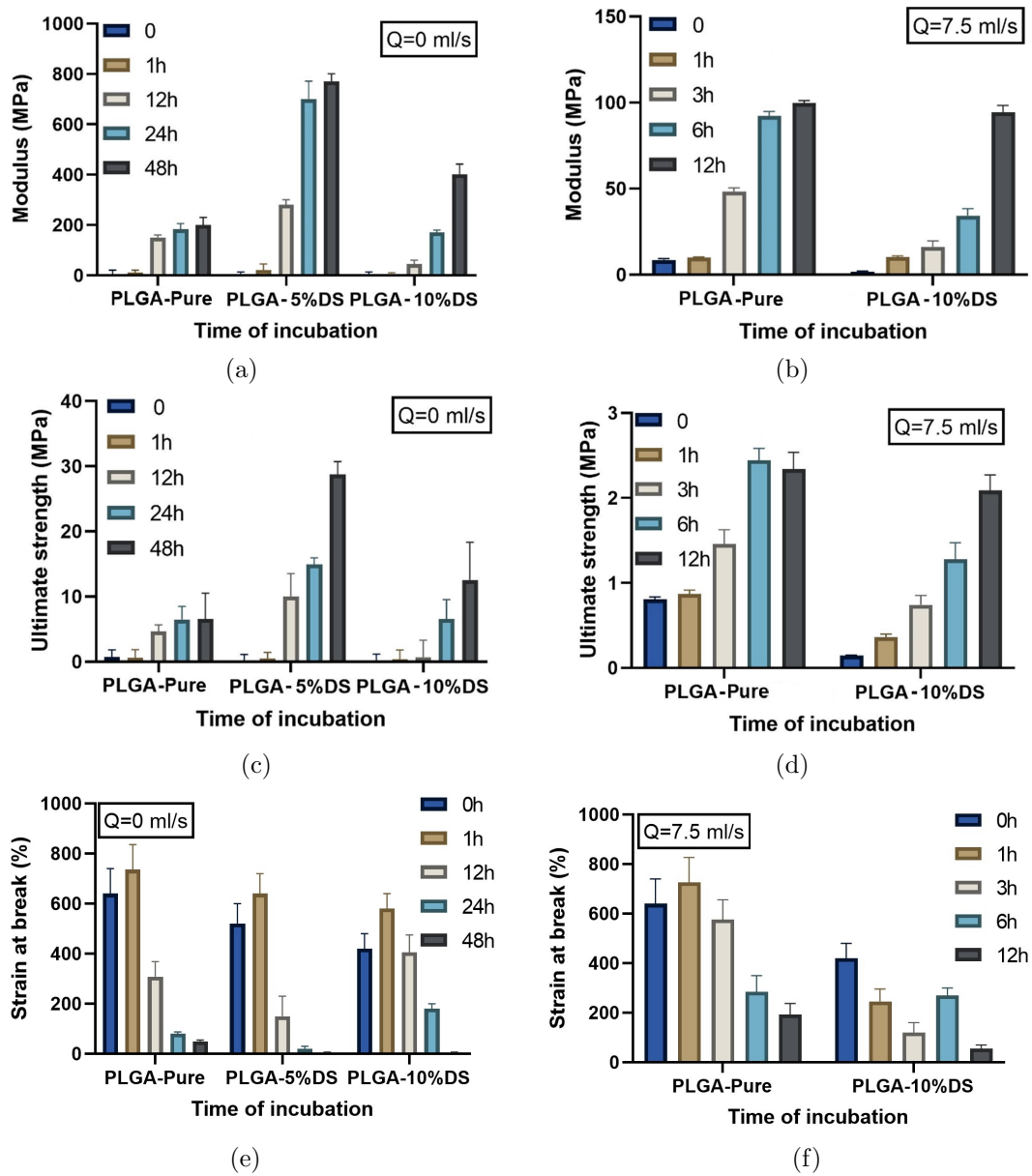


FIGURE 4.45 – Material characteristics of PLGA samples with different percentages of DS after drug release test in the static and continuous state

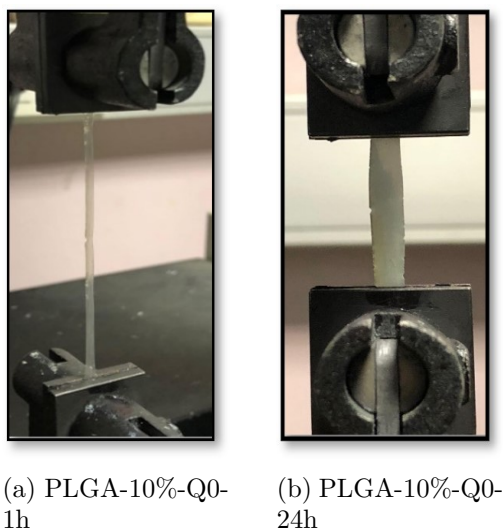


FIGURE 4.46 – Tensile test of the PLGA with 10% of DS after 1 and 24 hours of drug release test at static state

Moreover, one can see from figure 4.46, the difference between two samples in contact with PBS after 1 and 24 hours. The elongation is notable after 1 hour of immersion; however, the bulking phenomenon is observed for the samples of PLGA-10%DS after 24h of immersion due to the swelling. Indeed, the deformation of PLGA samples are decreased with the time of release.

From the mechanical results one can observe that the higher modulus and maximum stress is for the samples of PLGA-5%DS. This can be explained by more homogeneity of samples in this case. This means the drug can be a role of the reinforcement for PLGA, but not for all percentages. However, when the percentage of the drug is increased, the loss of properties can be due to less homogeneity. Figure 4.47 shows the presence of the drug particles in the polymer film. This figure reveals how the presence of the drug in the polymer film can change the structure of the samples and in consequence their behavior during the tensile test. Drug particles change the softness of the samples in the scale of micron. It is observed from the figure 4.47 that the drug particles in the polymer cause the small cracks which can affect the mechanical and physical properties and, in the consequence, change the release properties. This is a bidirectional phenomenon where changing the physical and mechanical properties will change the mechanism of the release and the release rate.

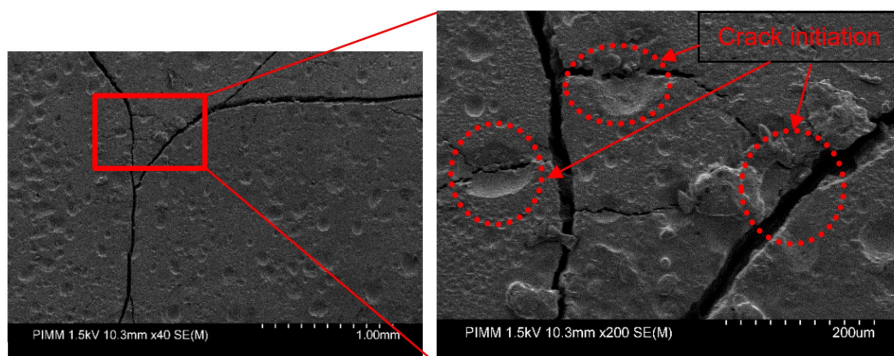


FIGURE 4.48 – SEM micrographs of the PLGA-10%DS after drug release of 48h in the static state after tensile test with the magnification of (left) 1 *mm* and (right) 200 μm

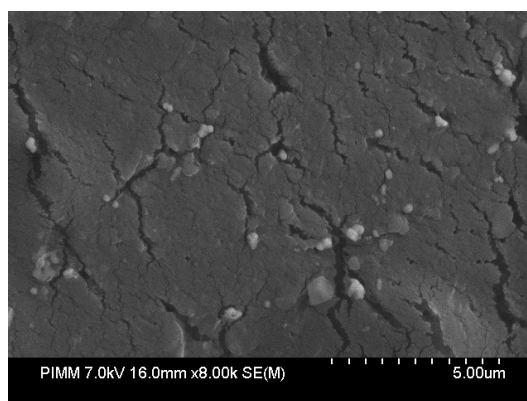


FIGURE 4.47 – SEM micrograph of the PLGA-10%DS before release test

Figure 4.48 (a) shows the crack propagated after the tensile test for the samples of PLGA-10%DS after 48h of drug release. As it is highlighted with the circles in figure 4.48 (b) it was found that the large-sized pores can be the origin of the crack initiation and the fracture of the samples. By analyzing the fractography of the samples, it can be noted that these micro-cracks, which are the origin of the phenomenon of local damage, further, their coalescence can result in the final rupture of the sample. Hence according to the tensile results, the samples of the PLGA-5%DS had lower strain at break compared to the PLGA-10%DS.

In fact in drug delivery systems several aspects should be considered. The presented results showed the relationship of all the characteristics of the material with together and with the drug release. The term of material refers to the polymers and here in this study PLGA. As it is evident all the polymers

4.2. DRUG RELEASE IN ARTIFICIAL LUMEN

have glass transition temperature range where the polymer shifts from a rigid glassy material to a soft (not melted) material, and is usually measured in terms of the stiffness or modulus. This glass transition temperature range could be varied when the polymer is exposed to water or etc. The latter can change some physical and mechanical properties of the used polymer. In fact, during drug release studies the interaction between the polymer and fluid such as PBS medium or water should be considered. The results confirm that by increasing the time of immersion, the glass transition temperature is decreased (presented in figure 4.49). One can note that the physical and mechanical properties are changed. For example, by increasing the time of incubation and consequently the drug release time, molecular mobility, and flexibility of PLGA are decreased. However, PLGA presents high strength and Young's modulus. Figure 4.49 shows the schematic of the variation of the polymer properties during and after drug release. In this figure the applied test temperature and the zone of the variation of the glass transition temperature, moreover some mechanical and physical properties were illustrated.

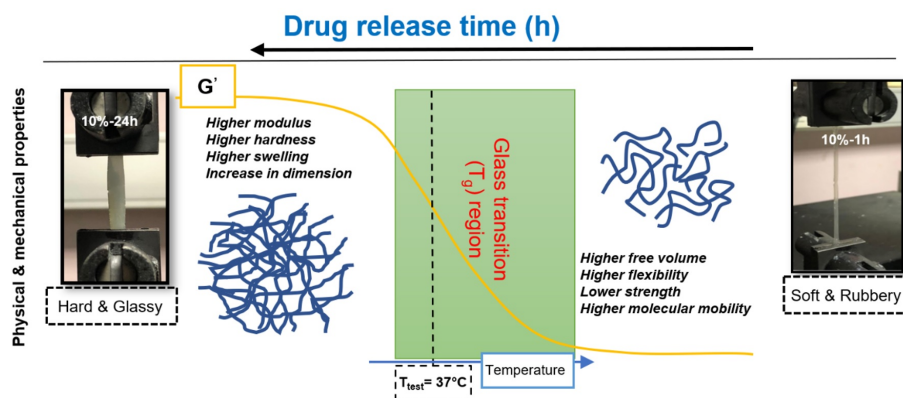


FIGURE 4.49 – Schematic of the variation of the polymer properties during and after drug release

One can notice that the relation of micro-structure and properties of PLGA plays an important role in drug delivery systems which use polymer as a drug carrier. Therefore, referring to the case of utilisation, the type of the polymer and its properties should be well understood. The results proved the relationship between the characteristics of the material with the drug release. Increasing the drug percentage in the PLGA film, water absorption has increased and as a result quantity of the pores created are also augmented, therefore an increase in the kinetic of the release is observed. This evolution was also similar with increasing the flow rate. T_g is amongst the important parameters in this regard, where by getting in the time of release T_g of the samples decreases which helps to more movements of

the polymer chains and liberation of the drug particles. Another critical factor which was examined here represents the mechanical strength of the films to analyze its durability. The results presented that by increasing the drug percentage the polymer films become more brittle, importantly by the time of the release. This behaviour is much more significant when the flow rate is rising. As a result, this study revealed us substantial information about the relationship of indicators such as T_g , free volume fraction, modulus, the stress of the polymer and their variation during release time. These results may encourage in developing a drug release prediction model for this type of drug carrier.

It is notable to indicate that the results showed that the kinetic of the release have changed with the variance of the different parameters such as drug percentage and flow rate but to note about the effect of these parameters on the whole objective which is the therapy of the diseased area, it is better to further study it in the tissue area for seeing the biological effect of these parameters. In a study by McKittrick et al. [199] they have resulted that although the medicament in high dose stents don't stay a long time in the stent comparing to the low dose, but it stays longer time binded to the receptors in the tissue, which are evidently depending to the biological characters of the drug and the tissue.

4.3 Drug release in artificial lumen and tissue

In this part the effect of some parameters on the drug release from polymeric samples into the artificial lumen part and into the artificial tissue part (in order to simulate the artery) is investigated.

4.3.1 Presence of artificial tissue in drug release system

In this section the effect of the presence of the hydrogel as an artificial tissue layer is investigated for the drug release from PU and PLGA samples. Figure 4.50 shows the drug release profile from PU and PLGA samples with 10% of drug where the samples are placed on the hydrogel. Therefore from one side they are contacted with PBS fluid and the other side with hydrogel, used as a vessel simulator (shown in figure 4.51). From figure 4.50, one can note that there is an increase in the total release of the drug from the polymer in both cases for PU and PLGA samples. It is notable that presence of another hydrophilic environment contacted with the drug carrier, creates an additional concentration gradient in addition to the concentration gradient which was between sample and the flow medium. Therefore, it is obvious that the total amount of the drug released and the kinetics increase. The latter

4.3. DRUG RELEASE IN ARTIFICIAL LUMEN AND TISSUE

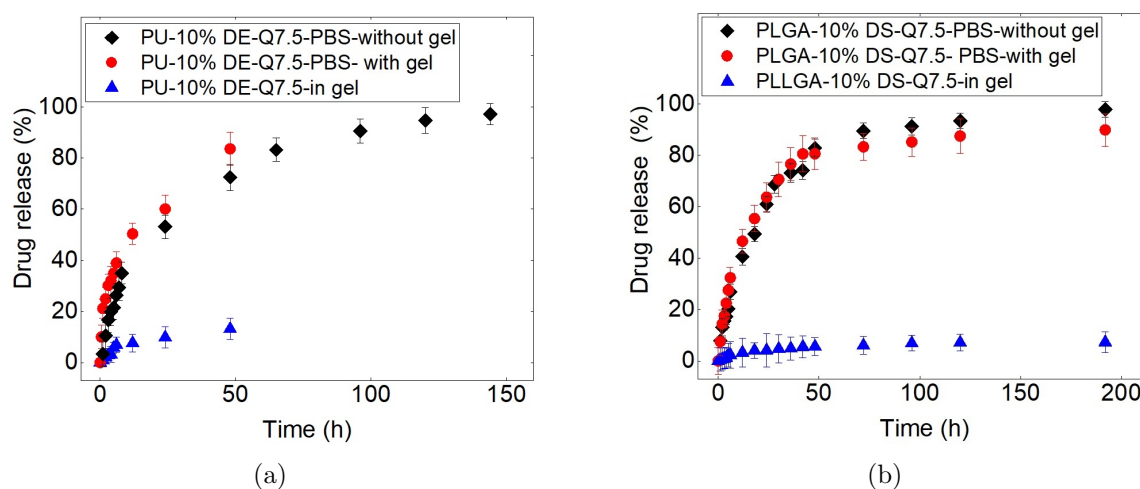


FIGURE 4.50 – Cumulative drug release curves in media and hydrogel from (a) PU-10%DE (b) PLGA-10%DS at at the flow rate of 7.5 ml/s in accordance to the release time,

phenomenon is observed at the first period of the release, where PU-DE samples are more affected. After a while, the gradient of concentration decreases so the release into the both side continue with lower kinetic of release. Studies have shown agarose 1% gel is mostly occupied by water, and the linkage in its network are so far [259], therefore, the gel compartment can be considered like as an aquas environment. Contacting both sides with the aquas medium helps to the fast dissolution of the drug particles and their release. One can note that PU samples have been more affected by the presence of the hydrogel, compared to the PLGA samples. The former can be explained by the difference in the mechanisms associated to the release. One can note that the presence of the hydrogel can influence on the mechanism of diffusion due to the gradient of concentration, and hydration of the samples due to the aquas nature of the hydrogel (shown in figure 4.52). Therefore, one can note that the release from the PU samples are more controlled by the mechanism of diffusion than the PLGA samples (this subject is discussed in section 5.2). On the other hand, the results show that the DE diffusion from the PU samples into the hydrogel is more than the diffusion of the DS from the PLGA samples. Porous structure of the PU and hydrophilic property of the drug can be the reason for this result. Therefore, one can conclude that for the DDS with hydrophilic drug and controlling mechanism of diffusion, liberation of drug is more affected by the presence of the aquas hydrogel compartment.

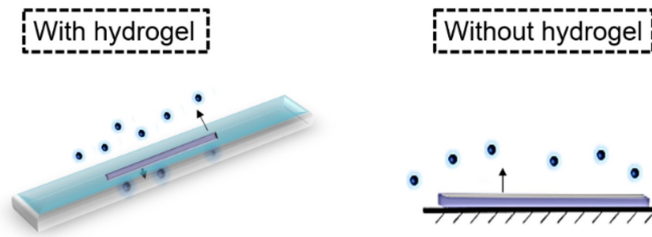


FIGURE 4.51 – Polymer film contacted (right) from one side with a gel and the other side with the lumen flow, (left) from one side with impermeable surface and the other side with the lumen flow

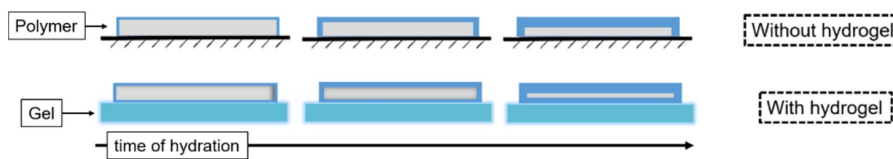


FIGURE 4.52 – Schematic of the hydration of the polymeric samples in the contact with or without the hydrogel and the fluid circulating in the system

4.3.2 Steady and non-steady flow rates

As an important example over the last few decades, hemodynamics for the diseased arteries has been extensively investigated and the effect of the continuous flow on the release of the drug is not hidden anymore [81]. However several factors still have not been thoroughly explored relatively to the pulsating behavior of blood flow and its effect on the arterial drug release. To characterize the influence of the luminal flow on the drug diffusion in the arterial wall, it is important to consider many aspects associated with the blood flow. In fact systolic-diastolic blood flow patterns induced by the cardiac pulse produce a complex flow nature that can affect overall profile of drug release [260]. The governing mechanisms in the pulsed flow that regulate the drug release still remain partially unravelled. A pulsed flow is characterized by its frequency and amplitude. It is a time dependent phenomenon for which the flow patterns depend on the geometry, the Reynolds number, the compliance of the arterial wall and non-Newtonian viscosity of blood. According to literature, blood flows may vary from one region of an artery to another: close to the heart the flows are highly pulsating with high velocities, the arterial walls are very compliant,... . Close to bifurcations, the flow patterns are also very complex, potentially non-laminar, with recirculation,... [161]. Compared to steady flow conditions, the pulsed properties of blood flow might provide much complex situation to investigate [261].

In this section we study how the flow pulsatility affects the drug release from the drug-eluting

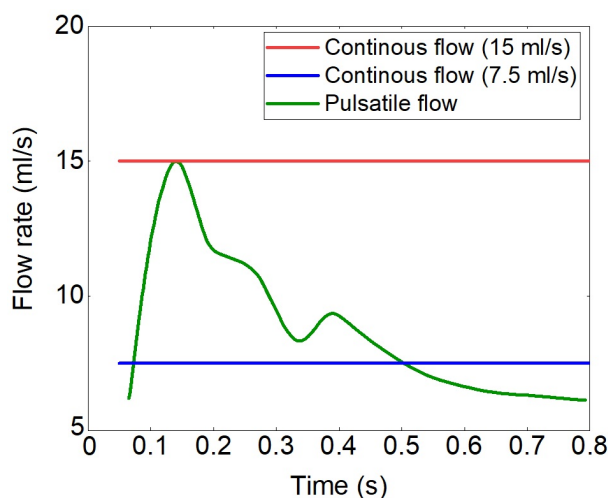


FIGURE 4.53 – Flow rates related to the three patterns of the flow performed in this study (corresponding to the flow in the carotid artery)

stents in the lumen area and also in the tissue component and we compare these effects to the case when the flow rate is constant. This effect was analyzed by the comparison of the release results from two steady state flows at 7.5 and 15 ml/s (corresponding respectively to the pressures of 75 and 112 $mmHg$), and the pulsed flow that varies between these values (shown in figure 4.53) at 70 heart beats per minute. The experiments were conducted considering one strut of a stent, modeled by a polymer film of PLGA (50:50) loaded with 10% of drug and agarose gel (1%) as the artificial tissue layer. To mimic blood, the chosen circulating medium is PBS at 37°C. Figure 3.12 shows the waveform conveyed to the motor and received by the flow-meter, the measured pressure waveform, the temperature and the number of pulses per minute for this type of release test.

Figure 4.54 (a), (b) show the results of the release of DS from the PLGA samples into the PBS medium and into the gel compartment. Figure 4.54 (a) shows that, by increasing the flow rate from 7.5 to 15 ml/s the release rate of the drug in the PBS is increased, however this difference is not much notable. Besides comparing the drug release results, in the steady state (flow rates: 7.5 and 15 ml/s) with the pulsed flow, we note a meaningful difference in the release rate. In the case of pulsed flow, the release rate is much higher than in the steady flow especially at the second period of the release after the burst phenomenon. It is also notable that by changing the state of the flow from steady to pulsed, the burst phenomenon increases. The second related mechanism is diffusion which, beside the drug solubility, also depends on the flow rate and on the steady/unsteady property of the flow: one

4.3. DRUG RELEASE IN ARTIFICIAL LUMEN AND TISSUE

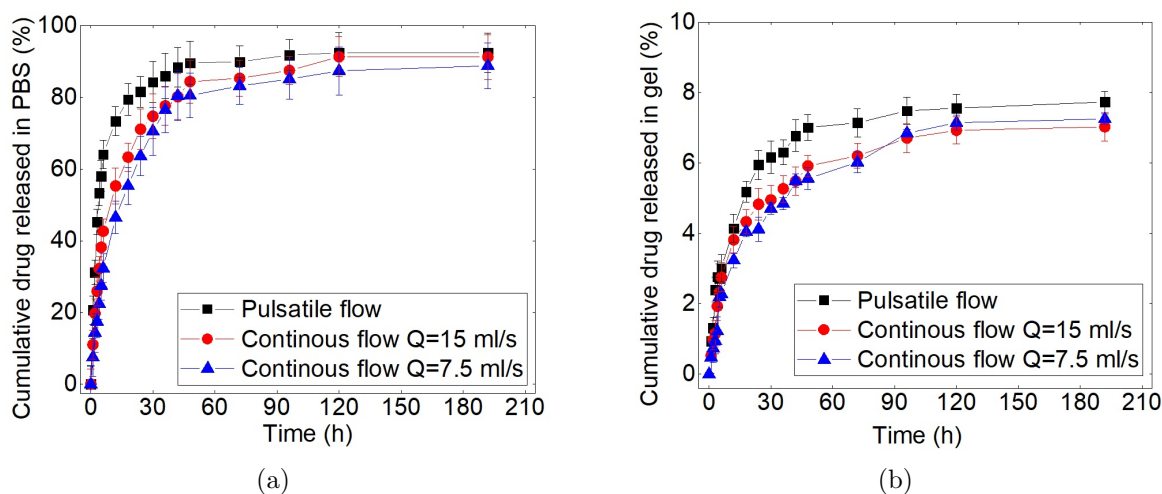


FIGURE 4.54 – Drug release from the PLGA films with 10% DS at different flow rates in (a) PBS, (b) gel

can note that for the steady state cases, increasing the flow rate of the fluid increases the diffusion of the drug from the polymer. Moreover, diffusion is enhanced in the pulsed flow compared to the steady flows. The results show that for all the flow rates, around 90% of the drug are released in the PBS at the time of 192h. To analyze these results more deeply, the microstructure of the samples has been observed under SEM microscopy. Figure 4.55 shows the SEM micrographs of the PLGA samples with 10% of DS at (a) the steady flow of 7.5 ml/s and (b) unsteady flow after 48 hours. From this figure, one can note in both situations (steady and unsteady) the creation of pores and the wrinkling of the polymer during the release. Thus it denotes the presence of the swelling and diffusion mechanisms in both cases. It is evident that diffusion is affected by the swelling phenomenon (change in the microstructure of the polymer matrix, modifications of the porosity of the material and of the dimensions of the samples...). From the mechanistic standpoint, it is also notable that by increasing the flow rate, the thickness of the hydrodynamic and mass boundary layers are getting smaller (figure 4.56). Thus the convective part of the drug flux in the lumen increases with the flow rate. This causes higher concentration gradients of the drug between the polymer sample and the fluid leading to higher diffusive flux. Thus, higher flow rate results in more drug released from the polymeric samples. It is noteworthy that the analysis about the boundary layer in the case of pulsed flow is not as easy. One can note that the drug release from the polymeric films in the case of unsteady pulsed flow is always higher than in the steady case. This is an effect of the flow pulsatility on the enhancement of the drug transfer as already noted in the Ph.D work of Chabi [81]. Another mechanism contributing to

4.3. DRUG RELEASE IN ARTIFICIAL LUMEN AND TISSUE

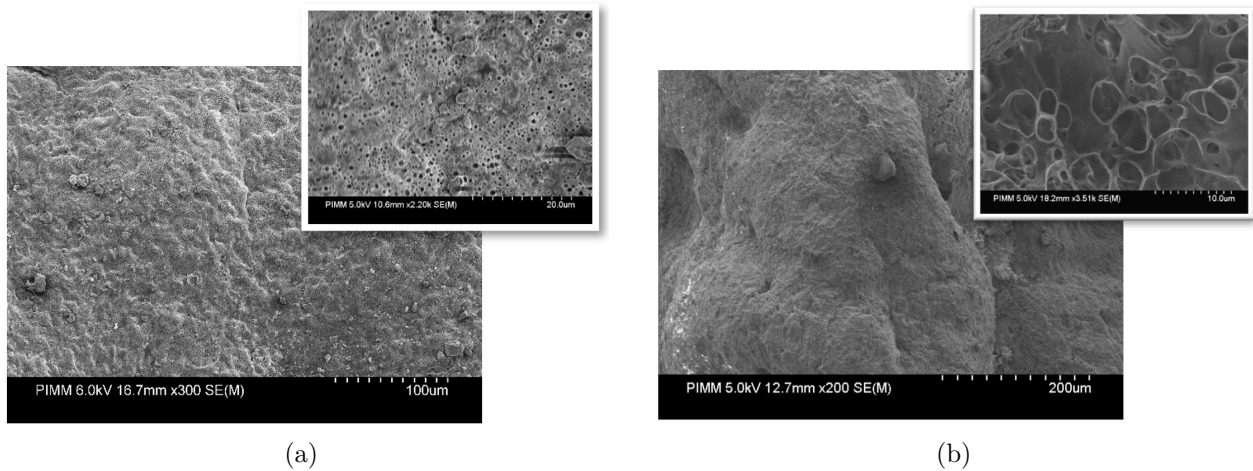


FIGURE 4.55 – SEM micrographs of PLGA-10%DS samples after 48h for (a) pulsed flow and (b) steady flow at 7.5 ml/s

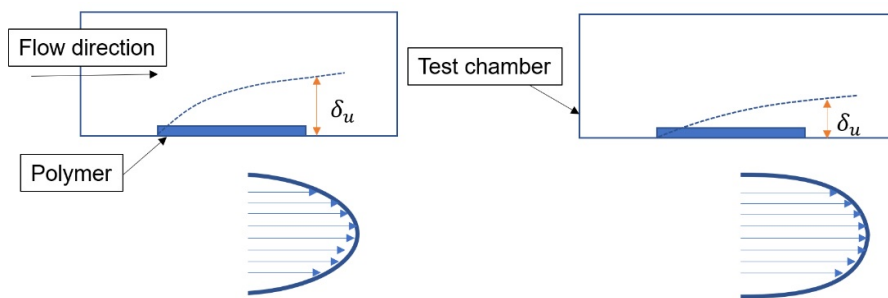


FIGURE 4.56 – Schematic representing the thickness of boundary layers created at two different flow rate (right figure is for the case with higher flow rate than the left figure)

the drug release from the PLGA polymeric films is the mechanism of the degradation/erosion which results in the cleavage of polymer chains and can help to the drug release. In this regard, it seems evident that increasing the flow rate results in higher velocity gradients especially near to the surface of the polymer, thus giving more friction between the fluid and the polymer. This is a reason for the mechanical weakening of the polymer and the increase of the rate of erosion. Of course in the unsteady flow, the wall shear stress and the wall friction will be higher than in the steady situation [262].

The other most probable mechanism for the drug release from PLGA carriers is swelling, which is the result of a high water absorption. PLGA 50:50 is a polymer which absorbs enough water to swell. In this regard, small bubbles are also created, depending on the other environmental conditions such as pressure or the contribution of other mechanisms such as erosion. These bubbles can blast and make the polymer surface more porous and suitable for the drug release. Figure 4.54 (b) shows the drug

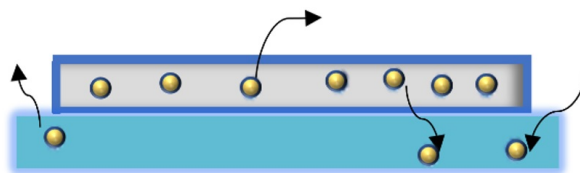


FIGURE 4.57 – Probable pathways of the drug to the release medium

concentration absorbed by the hydrogel in accordance to the release time. The controlling mechanism of the drug transport from the polymer into the gel is diffusion. At first, the existence of high drug concentration gradients explain the rapid growth of the curves. In the steady state, an increase in the flow rate induces a slight increase of the drug diffused into the hydrogel. The values at the 15 ml/s are only slightly higher than those at the lower 7.5 ml/s flow rate. In contrast, the results for the pulsed flow show that the amount of drug diffused into the hydrogel is higher than in the steady cases.

Figure 4.57 can give an explanation for this result: As it is evident, drug from the polymer transports to the flow medium and also hydrogel medium. Apart from that, there is the phenomenon of the wash-off [263] drug from the hydrogel to the flow medium. Besides, the drug that has just released into the flow medium near to the vicinity of the hydrogel can be pushed into the hydrogel by the sudden decrease of the flow at the pulsed flow state. This can be a reason for pushing in the drug which is released from the polymer carrier.

Another reason can be due to the different sizes of the vortices at the proximal and distal regions near the polymeric samples at the pulsed flow state. The former results at the elevated turbulence compared to the steady state flow. It can be the reason why in the pulsed state more drug is released in the flow and diffused in the hydrogel. Generally, the results show the higher depletion of the drug from the polymer carriers in the case of unsteady state comparing to, even higher value of the flow rate at the steady state.

4.3.3 Presence of the metal layer on the polymer layer

In the previous sections, we have studied the drug transfer from the polymer exclusively without the presence of a metallic scaffold. However, most of DESs contain a metallic structure which may support the polymeric layer. In this section, we investigate the influence of a metallic sheet, stainless steel with the thickness of 0.3 mm , simulating the presence of the metallic scaffold of a real stent, on

the drug release (DS) from a PLGA 50:50 film. Figure 4.58 shows the drug release comparison in the case of pulsed flow rate with and without considering the metal layer on the polymeric drug carrier. Figure 4.58 (a) shows the drug release in the PBS fluid. The results show a large difference in the release profiles with or without the metal layer. In order to compare them, the ratio of the drug released in the PBS without the metal layer to the one with the metal sheet varies in the range $1.1 < R < 2.8$ with an average value around 2. The influence of the metal layer is therefore clearly notable: covering the upper face of the polymer with the metal sheet, we deprive it with its largest surface in contact with the PBS flow. This effect is particularly strong at the beginning of the release (certainly because of the absence of burst), reaches a maximum at $t = 5h$ and then slowly decreases. This shield on the polymer can also decrease the effects of the erosion mechanism. Consequently, the release is mainly controlled by the mechanisms of diffusion and swelling. Figure 4.59 shows approximately the hydration of the polymeric samples with and without the presence of the metal layer. From this figure, one can note that presence of the metal layer decreases the contact of the polymer at the top surface with the aqueous medium and therefore decreases the rate of the water absorption on this side, compared to the hydrogel side. As the mechanisms of diffusion and swelling highly depend on the hydration and water absorption of the polymeric samples, the drug transported to the hydrogel is increased in the case with the presence of the metal layer.

One can propose the following explanation to this fact: initially the polymer layer is dry and starts to absorb the water. It is notable that when there is a metal layer, the hydration kinetics is a slower. Water absorption and swelling start from the sides of the polymer film and evolve inwards. At this time, the non-swollen part of the film impose a compressing stress on the swollen part that pushes out the drug towards the swollen part of the sample in contact with the hydrogel. In this case, a high quantity of drug is directed towards the hydrogel (as it is the side which is well wetted). Moreover, a metal barrier at the other side prevents the release of the drug into the fluid medium, contributing to keep high concentration gradients of drug in the polymer film and resulting in high diffusive transport. It is noteworthy that when the sample is entirely wet, the compressing stress reduces and the drug can easily diffuse in all directions [245]. However, it is evident that the swollen sample increases its dimensions and that larger distances reduce the kinetics of the release. This effect is less important in the presence of the metallic layer because swelling is slower. Figure 4.60 schematically summarizes these mechanisms during the initial steps of swelling and at the time when the entire sample is swollen.

4.3. DRUG RELEASE IN ARTIFICIAL LUMEN AND TISSUE

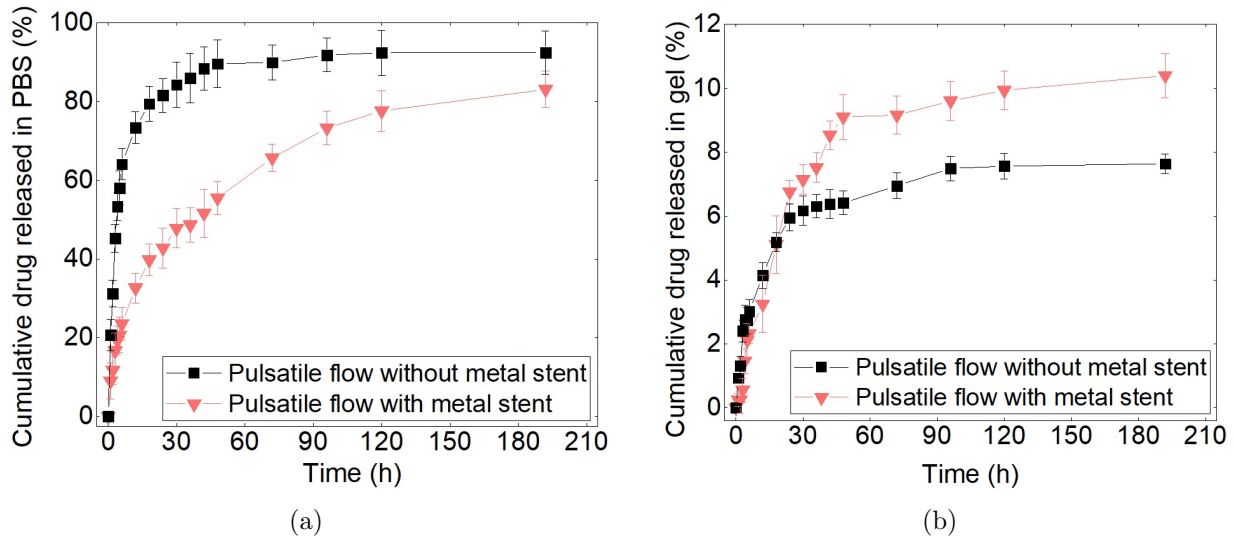


FIGURE 4.58 – Drug release results from PLGA-10% DS to the (a) PBS medium, (b) hydrogel, at the pulsed flow with and without presence of metal layer

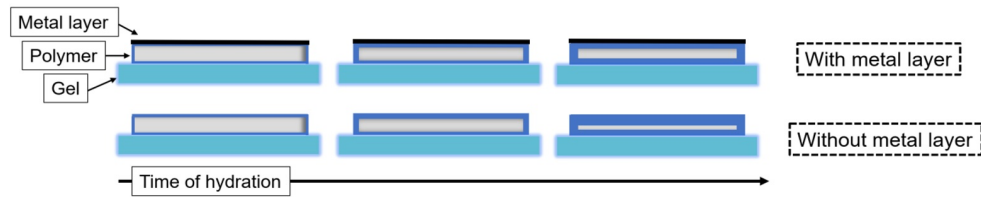


FIGURE 4.59 – Hydration of the polymeric samples in contact with fluid and hydrogel with and without the presence of metal layer

The obtained results denote that the presence of a metal barrier is important in the drug-eluting stents. Therefore, the replacement of a metallic scaffold by a polymer one should be carefully considered in terms of this “barrier effect” of the metal layer on the release.

4.3.4 Distribution pattern of luminescence particles in the gel

Until now, the results showed the effect of the different parameters on the release into the fluid medium and into the hydrogel. In addition to the amount of drug diffused into the hydrogel as in figure 4.58, it is also important to observe the spatial distribution of the drug particles in the hydrogel. This can be helpful in the design of the stents especially for the geometry of the struts. In this section, to qualitatively observe the diffusion of the active substance into the hydrogel, the drug particles were replaced by phosphorescent particles (the technique used here is described in chapter 3). The tests

4.3. DRUG RELEASE IN ARTIFICIAL LUMEN AND TISSUE

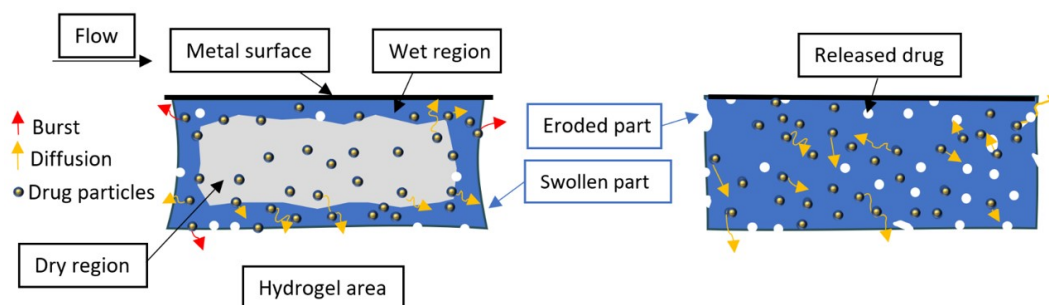


FIGURE 4.60 – Representing the mechanisms contributed to the drug release at the (a) initial and (b) late time of hydration of the polymeric samples

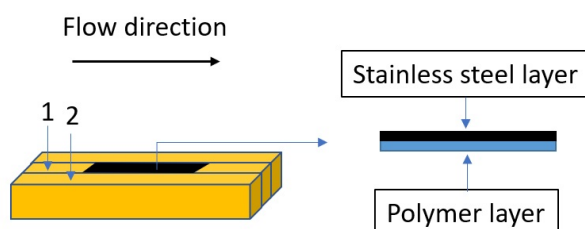


FIGURE 4.61 – Schematic of the position of the polymer + metal layer on the hydrogel and the two slices chosen for the analysis

were performed in pulsed flow conditions (as shown in figure 3.12) in the PBS medium and hydrogel compartment in the presence of a metallic sheet (stainless steel) above a PLGA polymeric film charged with 30%(w/w) of luminescent particles. Figure 4.61 is a schematic that shows how the samples are placed on the hydrogel and which slices are chosen for analyzing qualitatively the phosphorescence diffusion into the hydrogel. Figure 4.62 shows the qualitative phosphorescence distribution in the hydrogel in slice 1, which is the vertical slice placed below the polymeric sample. The results show the diffusive spreading with time of the phosphorescent particles into the hydrogel. These pictures highlight the rapid diffusion in the vertical direction (in the depth of the hydrogel) compared to the slow diffusion in the horizontal directions (in the length of the hydrogel). One can note that the particle distribution is slightly asymmetrical in the distal position due the convective effects. Figure 4.63 shows the phosphorescence distribution in the hydrogel after defined time steps in the slice 2. We can see that even at long times, the phosphorescent particles are very few in this slice. This highlights the weak diffusion into the hydrogel in the regions not directly in contact with the polymeric film and the weak diffusion in the transverse direction from slice 1 to slice 2.

4.3. DRUG RELEASE IN ARTIFICIAL LUMEN AND TISSUE



FIGURE 4.62 – Qualitative distribution of phosphorescence in the hydrogel (slice 1 shown in figure 4.61)

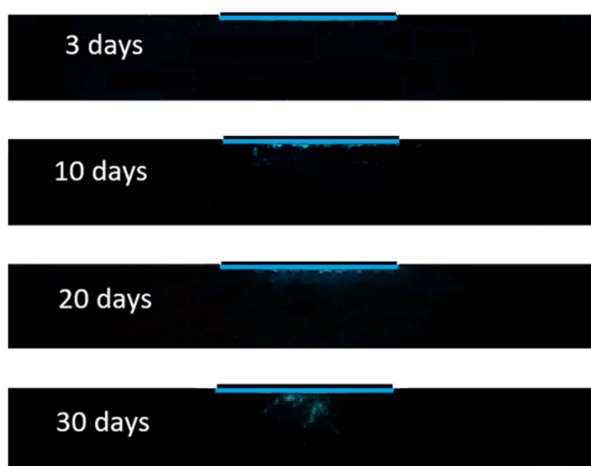


FIGURE 4.63 – Qualitative distribution of phosphorescence in the hydrogel (from the slice 2 shown in figure 4.61)

4.3. DRUG RELEASE IN ARTIFICIAL LUMEN AND TISSUE

Chapitre 5

Modeling and simulation - (in-silico modeling of drug release)

Content

5.1 Kinetic and accelerating model	177
5.2 Mechanism-based model	191
5.2.1 Application of the mechanism-based model for PU-DE	192
5.2.2 Application of the mechanism-based model for PLGA-DS	205
5.3 Numerical simulation	212

The improvement of mathematical models simulating the spatio-temporal behavior of drug delivery systems will make it possible to reduce their development time. Therefore, in this chapter we have focused on different types of modeling: empirical, mechanistic and also numerical simulation. The first section of this chapter is related to a mathematical model based on the release kinetics. This predictive model considers two parameters: the flow rate and the initial concentration. The second part proposes a mechanistic model based on the physical mechanisms involved in the release from the drug delivery carriers. Finally, the third part is devoted to a numerical simulation and a comparison of their results with the experimental results used in the first section for the kinetic model.

5.1 Kinetic and accelerating model

Generally speaking, the empirical models are developed for a family of drug carriers based on experimental data. To preserve all their interest, they must stay precise in predicting the release profile out of the data set used for the adjustment. Moreover, the complexity of drug delivery systems

makes it difficult to understand their underlying mechanisms, particularly in vivo. The alternative is to adopt fitting approaches to capture the experimental data sets. These fitting models typically contain fewer factors than purely mechanistic models. The advantage of this type of models concerns the simplicity of usage allowing their dissemination across the scientific community [264]. However, their validity is limited to the milieu utilized to define its setting data. For a family of drug carriers, it is necessary to properly adjust the precision of the model with identifying the number of the most influencing factors. Referring to earlier studies and researches, drug release profiles can contain various stages of the kinetics of release, the main of them being:

- Burst release (figure 5.1 (a)): normally short-lived, delivers high liberation rates that can be achieved in the initial stages after activation.
- Lag release (figure 5.1 (b)): represents the delay in the release of the drug.
- Fast release (figure 5.1 (b)): a consistent amount of drug is released over a limited period.
- Slow release (figure 5.1 (a)): drug release takes place slowly over an extended period.
- Extended release (figure 5.1): the release profile typically tries mimicking zero-order release.

In this section, an innovative predictive mathematical model based on the kinetics is proposed. This model should be applicable to various modes of administration like tablets, patches, drug-eluting stents, etc. The aim of this novel model is to formulate a function to calculate the cumulative drug-release for a group of drug delivery agents with similar properties. This model, should in fine:

- Take into account the influence of the design settings and the operating conditions on the amount of drug released from drug-carriers. These settings or conditions are for example: the flow rate of the fluid in circulation, the initial drug load; the type of the polymer carrier and etc.
- Allow taking into account changes in the kinetics of the drug release as a function of time throughout the period of release.

Equation 5.1, based on the Korsmeyer-Peppas equation, describes this model:

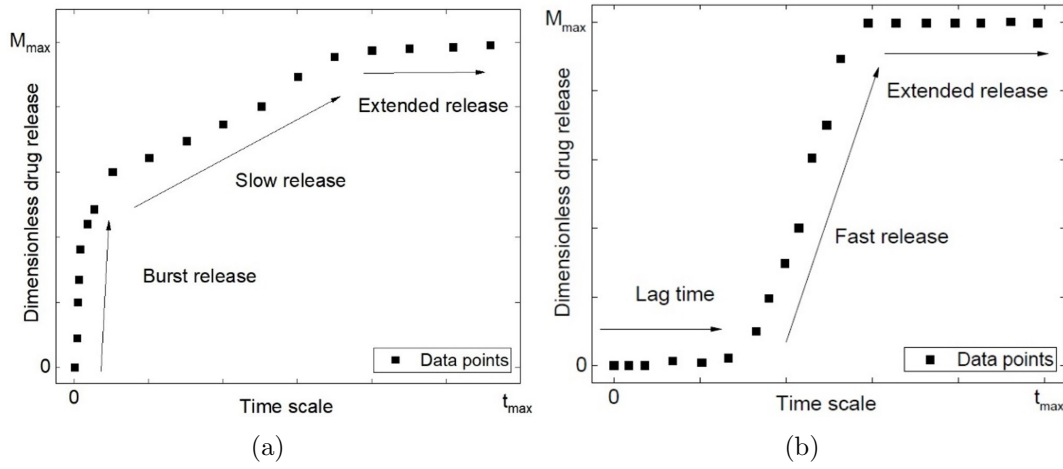


FIGURE 5.1 – Common release profiles and steps during the release

$$\text{Log}M_t = \text{Log}K + n_i \text{Log}t \quad (5.1)$$

where K is a constant which is different for each stage of the release profile and which depends on both concentration and time. Therefore, it can be easily obtained by the maximum values of the concentration and time in that particular stage. Therefore, the model will be presented in the form below:

$$\text{Log}M_t = \text{Log}\left(\frac{M_i}{t_i^{n_i}}\right) + n_i \text{Log}t \quad (5.2)$$

where M_t is the drug released at time t , M_i and t_i are respectively the maximum amount of the drug released, and maximum time of the release, at the i^{th} stage. This equation to whatever the dimensions of the drug carriers and the variables is applicable. The power coefficients n_i corresponds to the slopes of the straight lines identified in the Log-Log coordinate system. Their distinction demonstrates the presence of various kinetics and the other two settings t_i and M_i can depend on many factors such as the concentration of the active substance in the carriers, the thickness of the matrix layers, the physiochemical properties of the used drug and polymer (solubility, hydrophilicity, hydrophobicity, particles-size of drug, porosity, durability of the polymer, etc). To effectively reproduce any drug release profile, it is enough to accurately calculate the values of the set n_i , t_i and M_i . The Douglas-Peucker [265] algorithm is adapted to this purpose. More explanation is given in the first example of the results section.

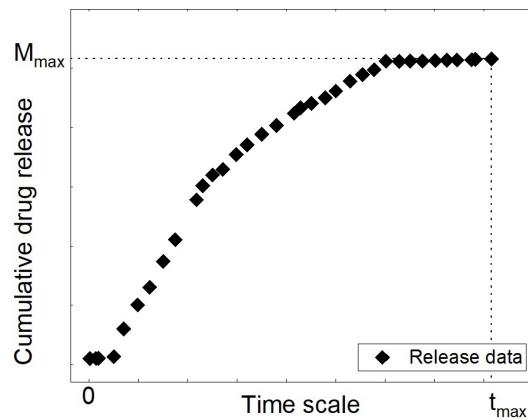


FIGURE 5.2 – Release profile of a certain drug in a certain polymeric matrix

Examining a generic drug-release profile

In order to test this model, we have generated an artificial release profile based on the various stages described above (figure 5.2). This profile is based on the following stages: lag-time, fast release, extended release, and slow release. Then the capacity of the main available empirical models to adjust this generic profile is evaluated. The failure of these assessments led to propose the present alternative mathematical model. The kinetics of drug release from the generic profile was analyzed using the zero-order and first-order, as well as the Korsmeyer-Peppas, Weibull, Higuchi and Hixon-Crowell models. The results in figure 5.3 indicate that none of these one-stage kinetics models can fit the whole data of the multi-stage generic release profile. It is therefore necessary that the mathematical model considers these aspects to correctly respond to the problem.

Application in multistage of Higuchi model and comparison with our proposed model

Figure 5.4 represents the results of the Higuchi model applied to the proposed generic profile using a three-stage approach. For each of the three chosen stages, we applied the modified Higuchi model:

$$M_t = M_i + K\sqrt{t} \quad (5.3)$$

The disadvantages in this approach are that only three out of the four stages are captured and that the power function is identical over the three stages (the coefficient n is invariably equal to 0.5). These limits lead to significant differences in the comparison, as it is clearly visible in figure 5.4. To overcome these difficulties, the simultaneous use of the power function proposed by Korsmeyer-Peppas and the stage's detection algorithm would represent an alternative. The main advantages of this model is its

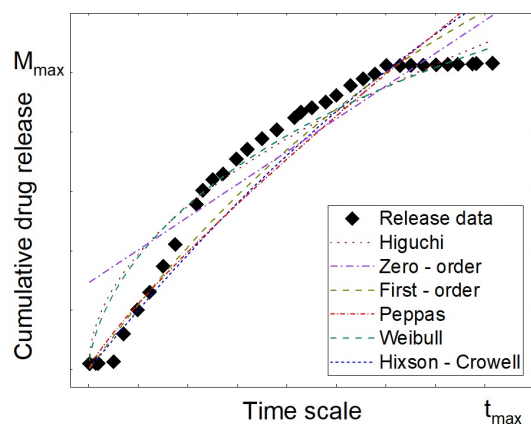


FIGURE 5.3 – One step fitting of data results with different mathematical models

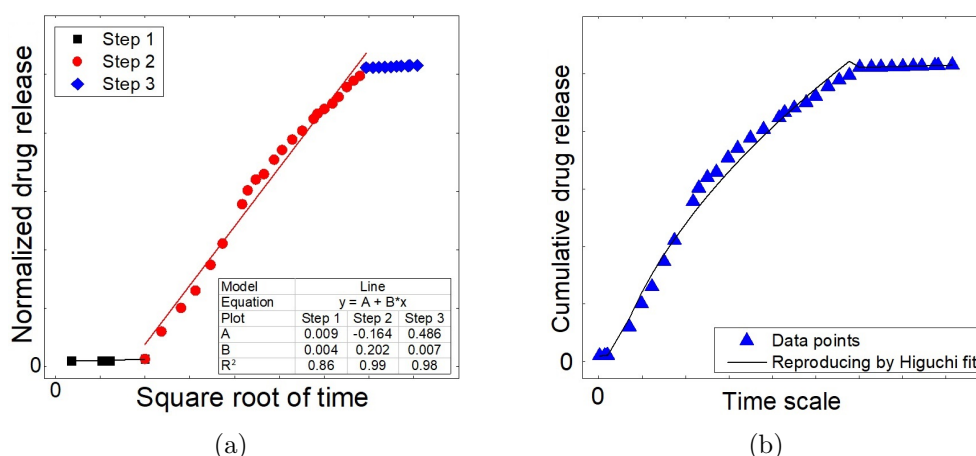


FIGURE 5.4 – (a) Step defining for the release profile of the figure 5.2 by the aid of the Higuchi model (b) Reconstruction the data points by using Higuchi fit

ability to restore all the stages that describe the kinetics of the drug-release profile and to adapt to the change in kinetics by adequately differentiating the power coefficients of the various stages. Figure 5.5 exposes the data calculated with the proposed model, in comparison with those of the generic profile. This figure clearly illustrates the relevance of the correlation between the data in the generic profile and the values calculated using equation 5.1.

Assessment of the model on the experimental data of PU loaded with DE and from the literature

This section deals with experimental data obtained in this PhD work and with data found by the authors and in the literature. Concerning our experimental data, we study the simultaneous effect of the flow rate and of the drug concentration for a single-stage release profile. Concerning the data from

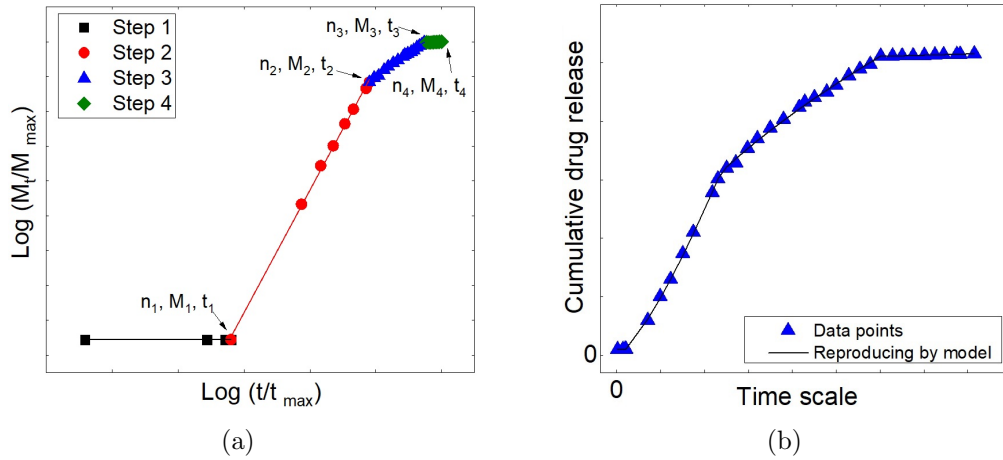


FIGURE 5.5 – (a) Step defining by the aide of Douglas-Peucker algorithm and the constants needs for defining the model (b) reconstruction the data points by using model

the bibliography, a study by [266] was used: where they studied the effect of the drug concentration for a two-stage release profile.

Taking into account the simultaneous effect of the flow rate and concentration in the model

In our in vitro experimental results, we have observed the influence of the flow rate and of the drug concentration on the kinetics of diclofenac epolamine released from polyurethane films. Then these parameters are employed in the model developed in the previous section. As a reminder, these data relate to three separate flow rates: 0 ml/s , 7.5 ml/s and 23.5 ml/s , and three drug concentrations: 10%, 20% and 30%. Figure 5.6 illustrates all of these results.

In figure 5.7, in a Log-Log coordinate system, we have plotted the mass of the drug M_t normalized by the mass $M_{95\%}$ (corresponding to a release of 95% of the initial mass) as a function of the time normalized by the $t_{95\%}$ (the time at which 95% of the initial mass is released). These data are correctly fitted by a single linear interpolation suggesting in consequence a one-stage kinetic of release.

Figure 5.8 shows the evolution of the slopes of these linear regressions at the DE concentration of 10% (these slopes give access to the values of the power coefficients $n_i = n_1$ in equation 4.2) as a function of the flow rate, represented by a reduced Reynolds:

$$\overline{Re} = \frac{Re}{Re_c} \quad (5.4)$$

with $Re_c = 2300$ (the accepted laminar-turbulent transition Reynolds number for flow in a pipe) and

5.1. KINETIC AND ACCELERATING MODEL

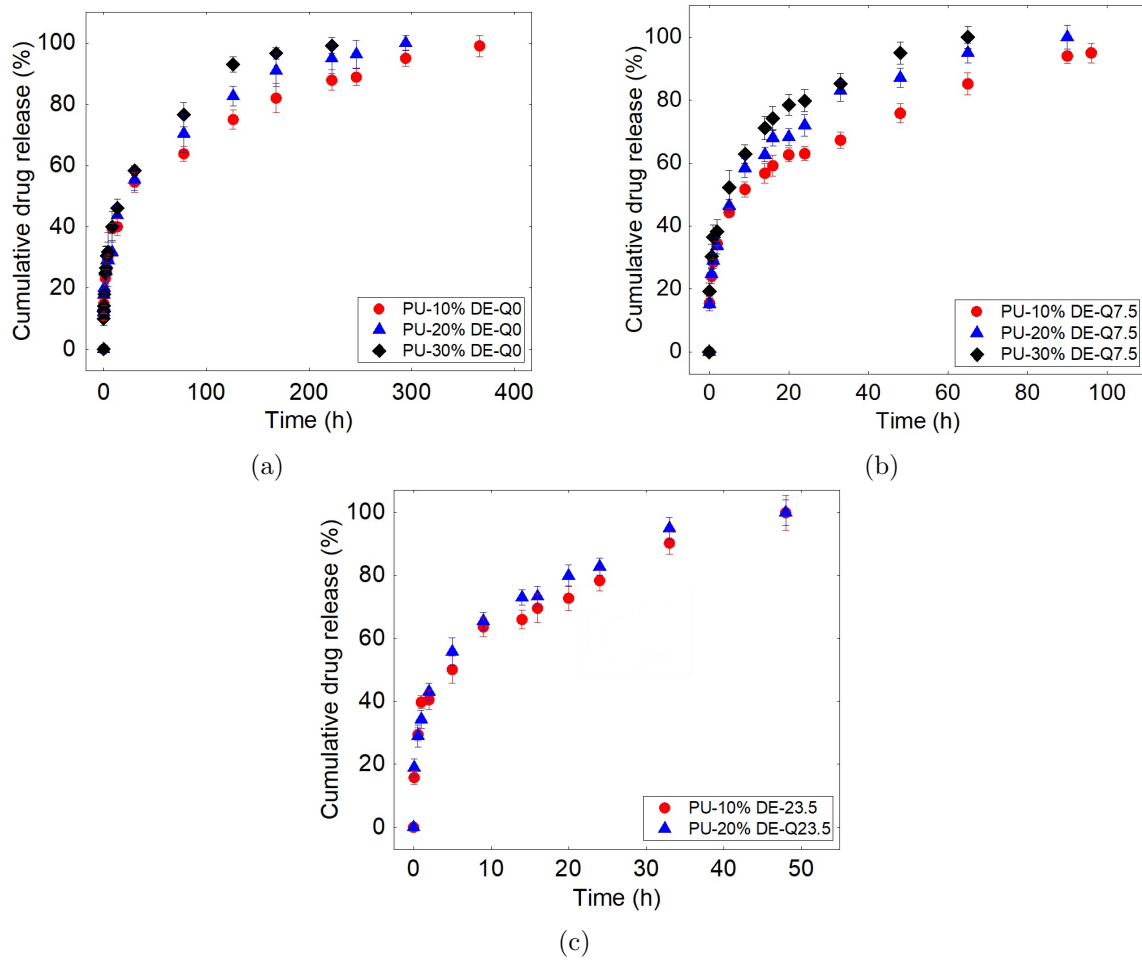


FIGURE 5.6 – Cumulative release of DE from PU matrix in (a) $Q = 0 \text{ ml/s}$ (b) $Q = 7.5 \text{ ml/s}$ and (c) $Q = 23.5 \text{ ml/s}$

5.1. KINETIC AND ACCELERATING MODEL

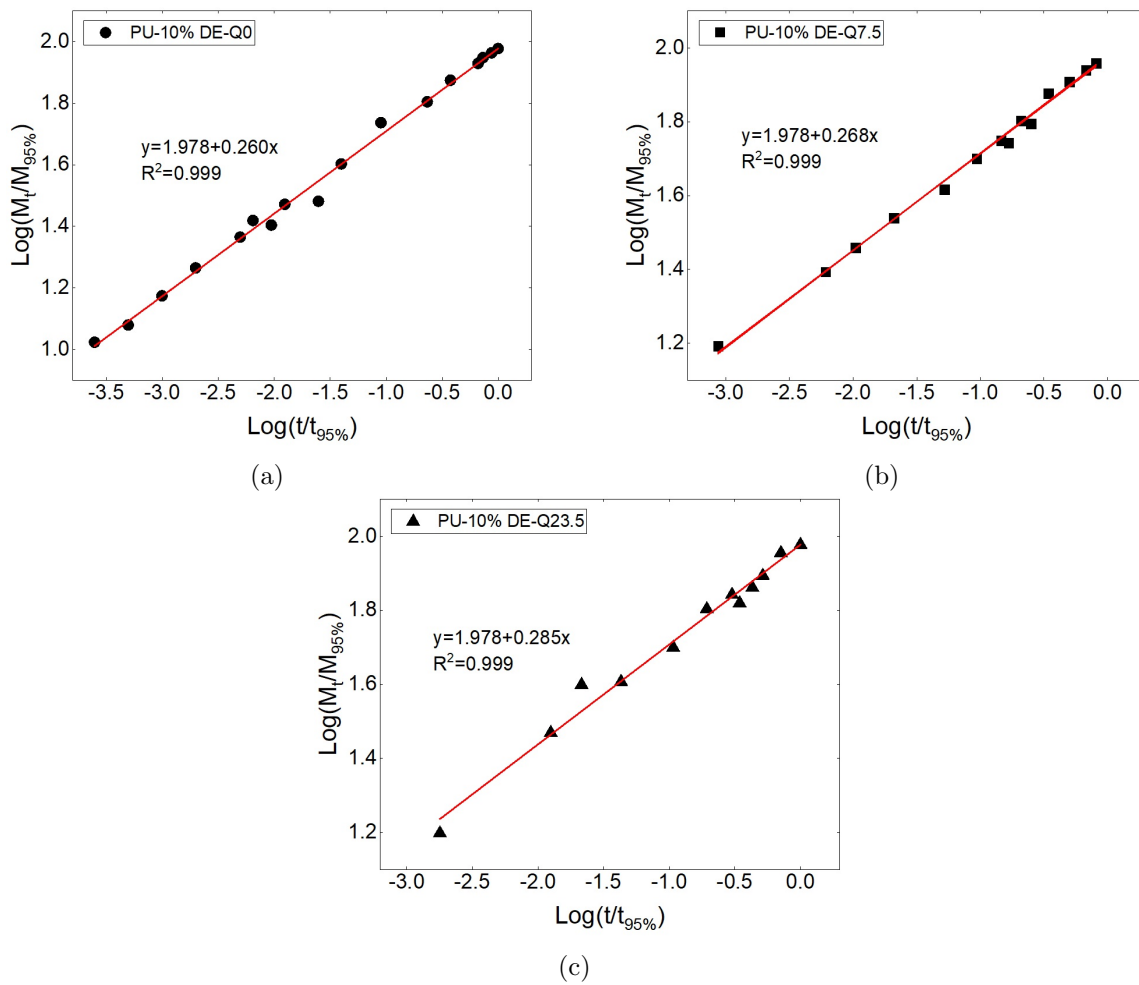


FIGURE 5.7 – Experimental results obtained from PU-10%DE at (a) $Q = 0 \text{ ml/s}$, (b) $Q = 7.5 \text{ ml/s}$, (c) $Q = 23.5 \text{ ml/s}$, and traced in the form of $\text{Log}(M_t/M_{95\%})$ versus to the $\text{Log}(t/t_{95\%})$

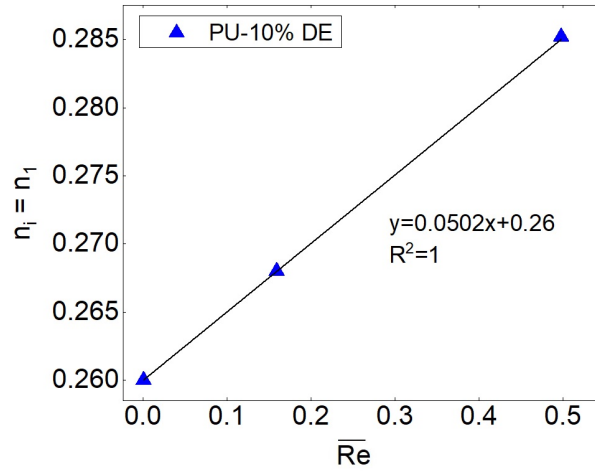


FIGURE 5.8 – Correlation between the values of $n_i = n_1$ and reduced Reynolds number

the Reynolds number:

$$Re = \frac{VD_H}{\nu} \quad (5.5)$$

with $V = Q/S$ the average velocity. We notice, in this case, that $n_i = n_1$ slightly increases with the flow rate. Figure 5.9 (a) shows, for the three flow rates, the evolution of the parameter $t_i = t_{95\%}$ as a function of the concentration. In this figure we have also plotted the point (0;100%), corresponding to the theoretical experiment for which there would be any polymer carrier and for which the release of the entire drug would be practically instantaneous ($t_i = 0$). Figure 5.9 (b) gives the values of the coefficients A and B, extracted from the regressions proposed in figure 5.9 (a) as a function of the reduced-Reynolds number. Once these parameters are obtained, it is possible to evaluate the robustness of our model for various experimental settings. As a first example, we compare in figure 5.10 (a) our model to the experimental data for the flow rate of 6.5 ml/s and the concentrations of 10% and 20% of DE in PU. Likewise in figure 5.10 (b), we have plotted the prediction for the flow rate of 7.5 ml/s and the concentration of 15% together with the experimental values. In both cases, the comparisons with the experimental data are satisfactory. Finally, figure 5.11 shows the prediction of our model for a flow rate of 7.5 ml/s and various concentrations ranging from 5% to 80%. One can note that the variant parameters chosen in this study, flow rate and drug concentration, can be considered as a parameter of acceleration for the release kinetics. Therefore, the model developed

5.1. KINETIC AND ACCELERATING MODEL

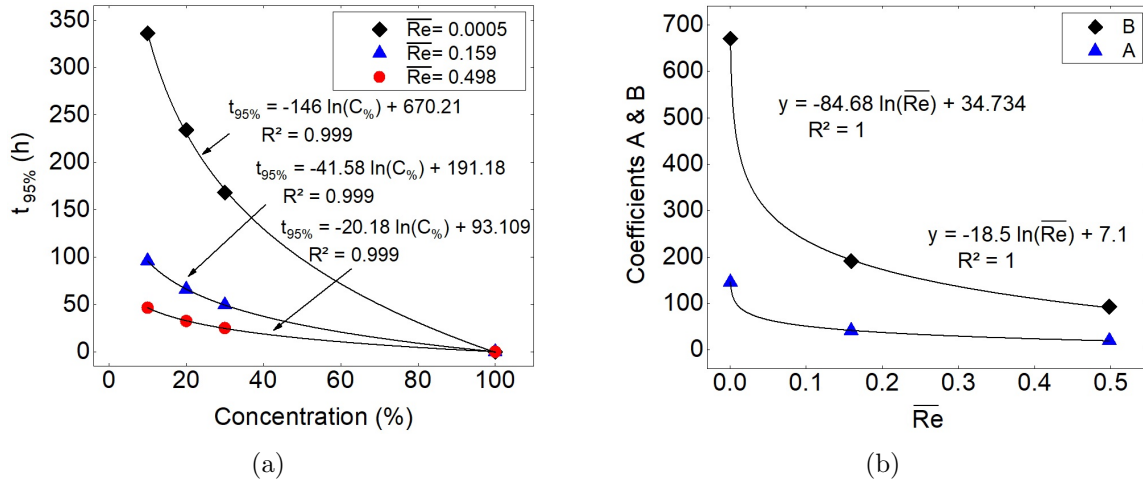


FIGURE 5.9 – (a) Correlation between the values of the maximum time of the release in accordance to the drug concentration (fitting equation: $y = -A \times \ln(C\%) + B$) (b) Values of coefficients obtained from figure 5.9 (a) versus to the \overline{Re} number

here is an accelerating model where figure 5.11 with considering the accelerated parameter of drug concentration, showed the predicted release profiles.

Influence of the drug concentration in two stages

As another trial, data available in the study by Bode et al. [266] have been selected to test the model for a multistage kinetics. This study considers the release of dexamethasone from PLGA samples in the form of cylindrical implants 5 millimeter in length and approximately 1.2 mm in diameter. All the experiments were carried out in glass flasks containing 80 ml of phosphate buffer at pH=7.4 under gyrosopic agitation at 80 rpm and 37°C. They studied six concentrations of dexamethasone: 15%, 10%, 7.5%, 5%, 2.5% and 1%. Figure 5.12 shows the data from these six dexamethasone release experiments. We used the data for 3 concentrations (10%, 5% and 2.5%) to calculate the parameters of our model for this family of drug carriers. From these release curves, two-stage kinetics were identified. The data of the remaining three concentrations (15%, 7.5% and 1%) are reserved to assess the validity of the approach as before.

For identifying the number of steps, the release results were plotted in the form of $\text{Log}(M_t/M_i)$ versus $\text{Log}(t/t_i)$ as shown in figure 5.13. This figure clearly shows that the release kinetics is two-step process.

From the correlation obtained for the set of the parameters (n_1 , n_2 , t_1 , t_2 , M_1 and M_2), shown

5.1. KINETIC AND ACCELERATING MODEL

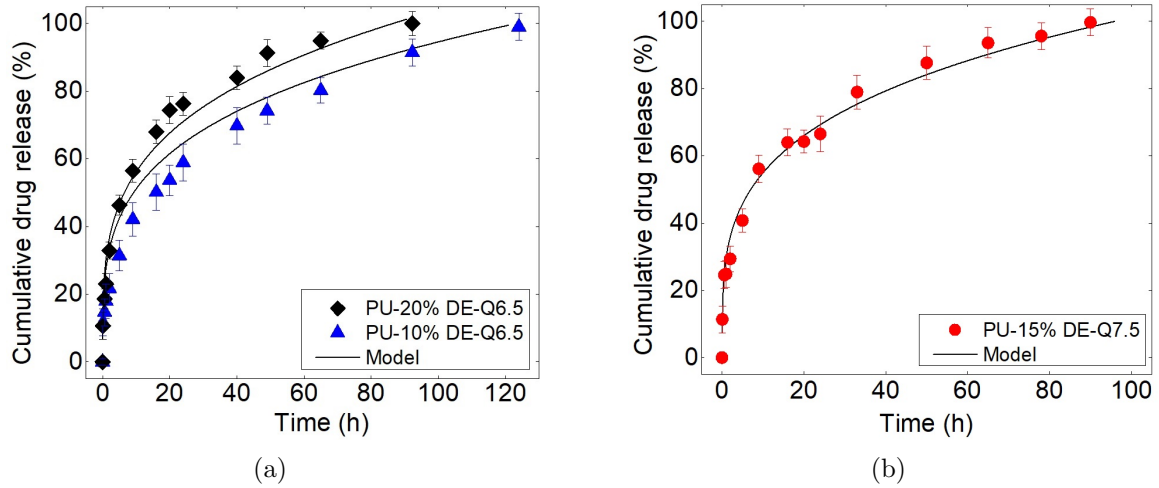


FIGURE 5.10 – Experimental data obtained with (a) PU-10 and 20% DE at the flow rate of 6.5 ml/s , R^2 are respectively 0.99 and 0.98 (b) PU-15%DE at the flow rate of 7.5 ml/s , $R^2 = 0.98$; at $T=37^\circ\text{C}$

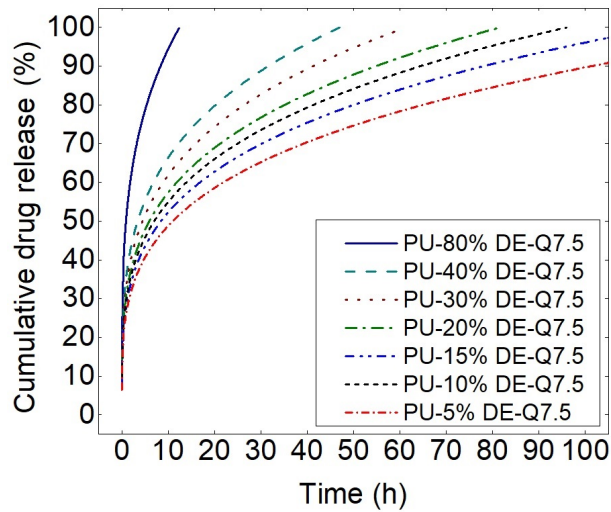


FIGURE 5.11 – Results for predicting the release behavior of different percentage of DE in the matrix of the PU at the flow rate of 7.5 ml/s

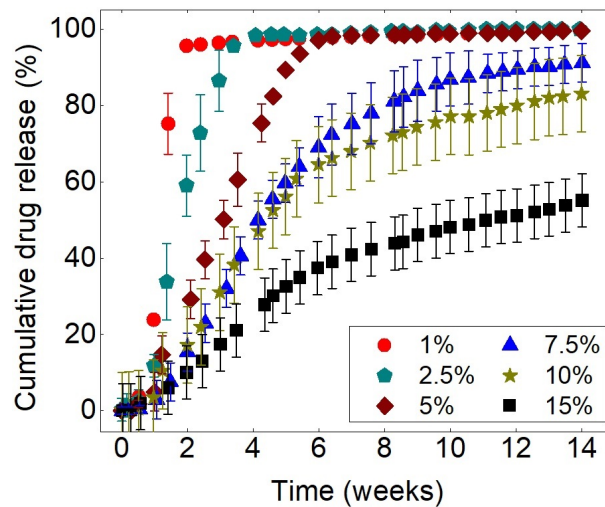


FIGURE 5.12 – Impact of the initial drug loading of PLGA: relative dexamethasone release kinetics [266]

in figure 5.14, some release profiles were traced for the PLGA-1%, PLGA-7.5% and PLGA-15%. Figure 5.15 shows the calculated model in comparison with the experimental data for these three concentrations.

The prediction procedure of the proposed model indicates a significant agreement with experimental data. Finally, we have assessed the robustness of our model considering the parameters from the previous study of Bode et al. for the experimental data from the study of Westedt et al. [267]. In this second proof case, contrary to the previous case, the experiments were performed under static conditions. This study concerns the release of paclitaxel from PLGA samples, for a concentration of 5%.

Figure 5.16 illustrates the release profile predicted by the model in comparison with the experimental data from the study by Westedt et al. We note that the results predicted by our model show an agreement for the first period but there is a deviation for the final part of the curve. The reason for these differences could be chiefly attributed to the stirring speed (static conditions in Westedt et al. vs dynamic conditions (80 *rpm*) for Bode et al.). One can note that this model can be helpful to predict the release profile for a family of the drug delivery systems with considering the variation of different parameters. However one should pay attention to the differences in the parameters which may vary from an experiment to another. Indeed, the parameters such as drug type, flow type, method

5.1. KINETIC AND ACCELERATING MODEL

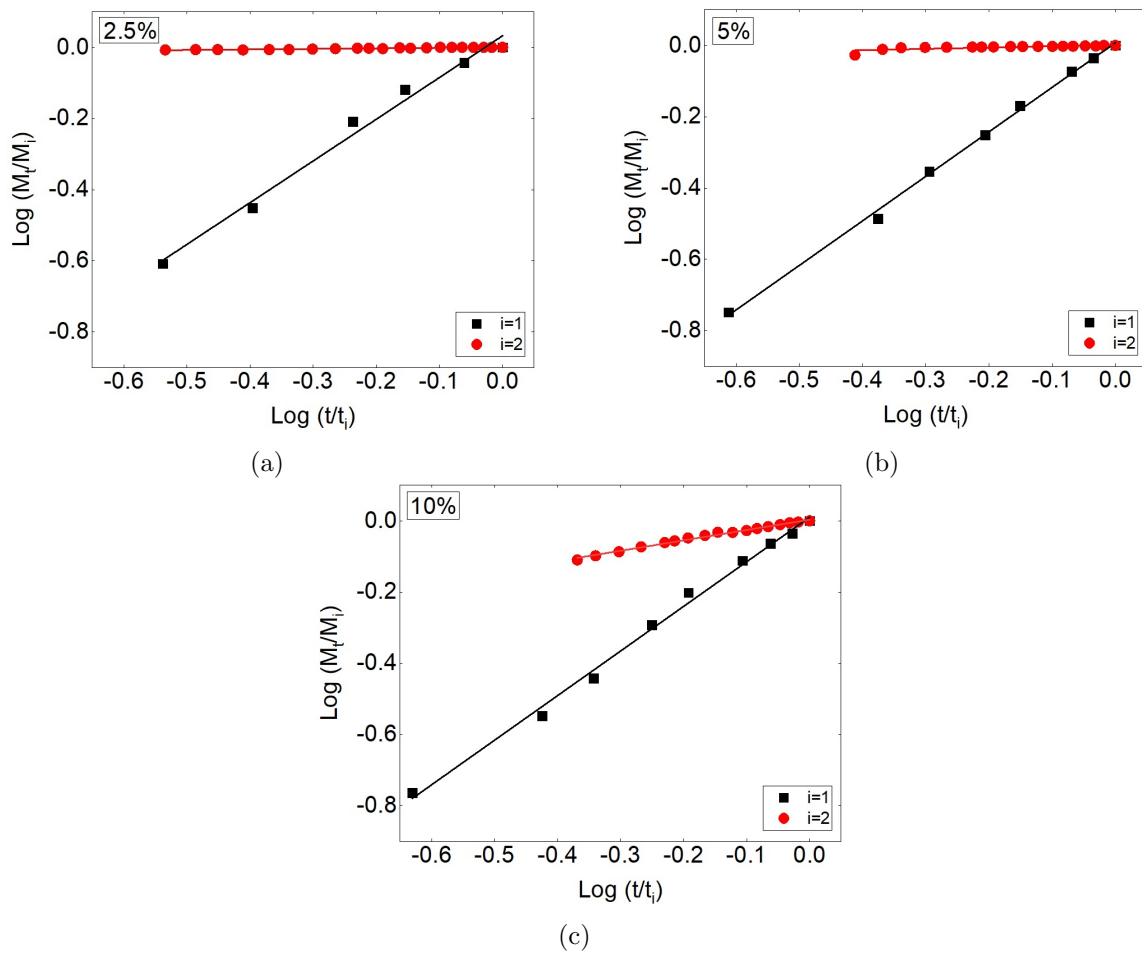


FIGURE 5.13 – Experimental results obtained from dexamethasone release from PLGA (a) 2.5 %, (b) 5%, (c) 10% of drug, traced in the form of $\text{Log } M_t/M_i$ versus to the $\text{Log } t/t_i$

5.1. KINETIC AND ACCELERATING MODEL

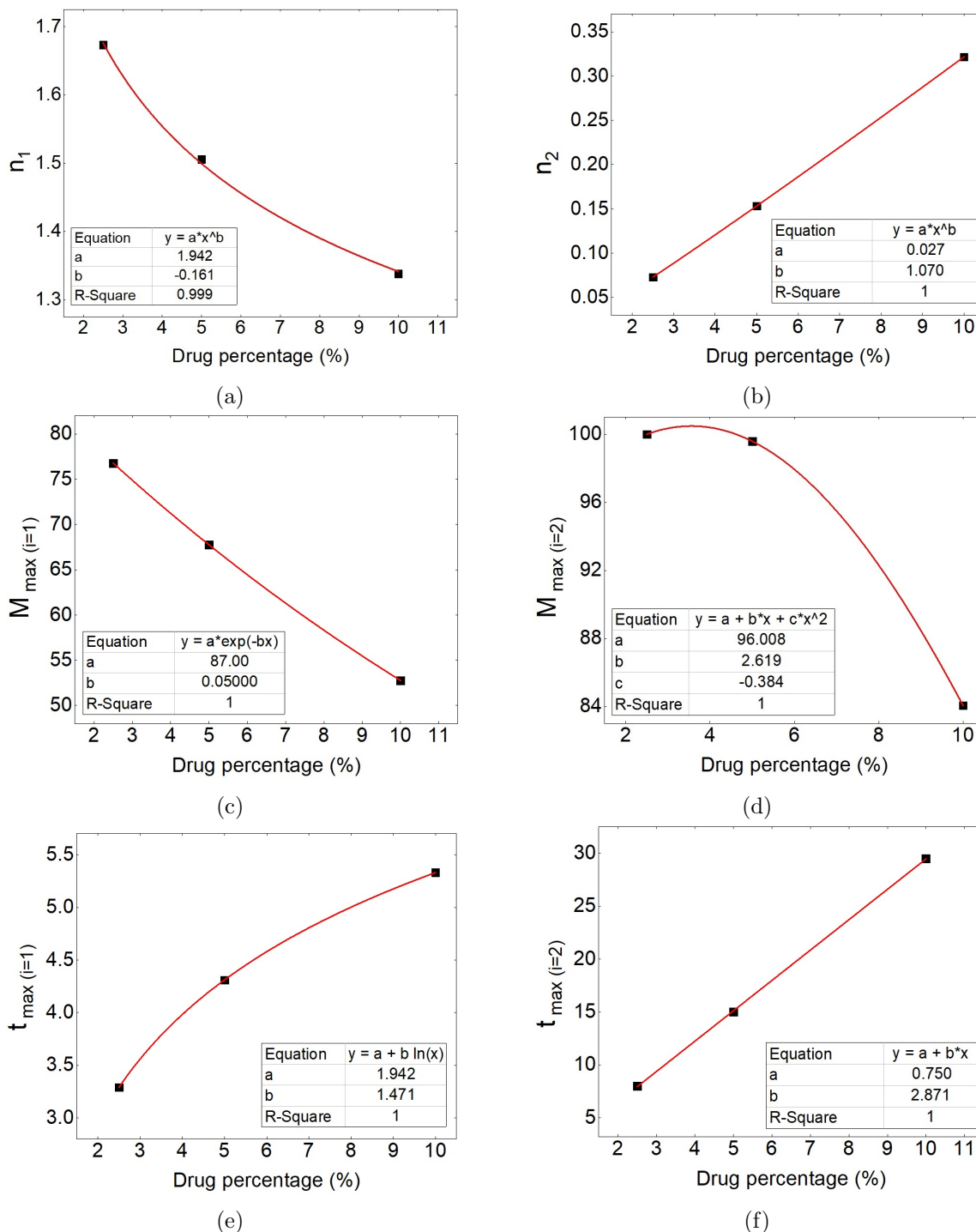


FIGURE 5.14 – Correlation between the values of (a) n_1 , (b) n_2 , (c) $M_{\max(i=1)}$, (d) $M_{\max(i=2)}$, (e) $t_{\max(i=1)}$, (f) $t_{\max(i=2)}$, versus to the concentrations of 2.5%, 5% and 10% of dexamethasone

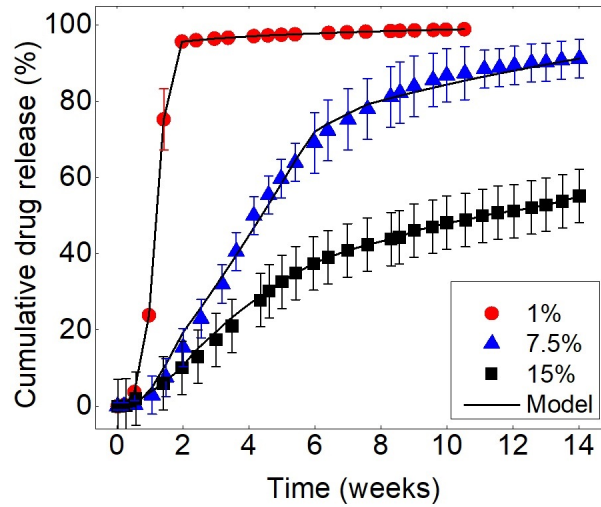


FIGURE 5.15 – Data experimental of the study [266] and the predicted curves of the model

of fabrication of the samples, drug load can play a role in the disagreement of the results with the predictive model.

5.2 Mechanism-based model

In this section, we present a method to predict the drug release profile based on the physical mechanisms that can intervene in the drug release from a drug-carrier. The application presented here incorporates the effects of drug concentration and flow rates based on the circulating flow in the test chamber. The method developed in this work is illustrated in the flowchart given in figure 5.17. It involves:

- i) Determining, from a database of well-documented trials, the mechanisms involved in the release.
- ii) Solving a system of non-linear equations, modeling the optimization problem and calculating the unknowns for this database.
- iii) Developing from these results a specific model predicting the release profile.
- iv) Applying the model to the data reserved to validate the constructed model. In fact, we try to adjust the experimental results with a model of the type:

$$\frac{M_t}{M_\infty} = \sum_{i=1}^{i=N} \mu_i \times F_i \quad (5.6)$$

where F_i is the equation related to a specific release mechanism (burst-release, diffusion, swelling, osmosis...) and μ_i the relative contribution of each release mechanism. In order to obtain the μ_i and

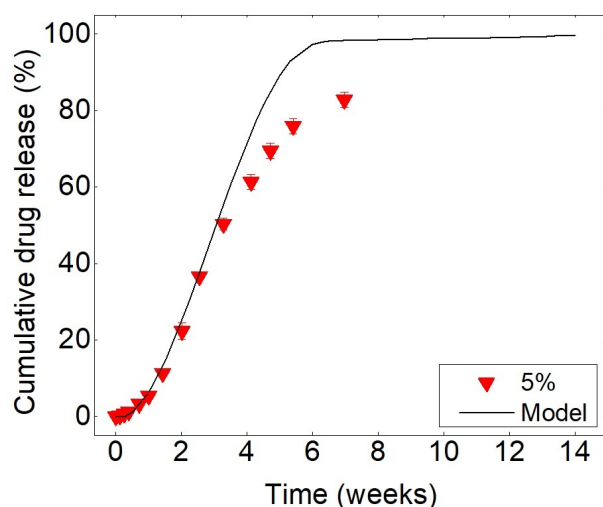


FIGURE 5.16 – Comparing the data release of [267] with the model

the parameters of each i equation, we used the Sequential Quadratic Programming algorithm. This algorithm is known as one of the most effective procedures for solving non-linear optimization problems [268].

5.2.1 Application of the mechanism-based model for PU-DE

The experimental data used here relate to the release of DE from samples of non-degradable polyurethane subjected to various flow and drug concentration conditions: the experimental data used to develop the mathematical model are based on release studies carried out in distilled water at 37°C, for three concentrations of DE and three different flow rates. These cases include simultaneously three mechanisms: burst-release, diffusion and osmotic pressure, identified beforehand (see chapter 4, section 4.2) here as being able to contribute to the drug liberation. Figure 5.18 shows the schematic of the mechanisms occurring during the release. At first, the fluid carries the drug particles on the surface of the sample (burst phenomenon, equation F_1); then water penetrates into the sample and dissolves the particles; finally, the dissolved drug particles release by the diffusion (equation F_2) and/or osmotic pressure (equation F_3) mechanisms.

The general equation employed in this case study related to the three phenomena (burst release,

5.2. MECHANISM-BASED MODEL

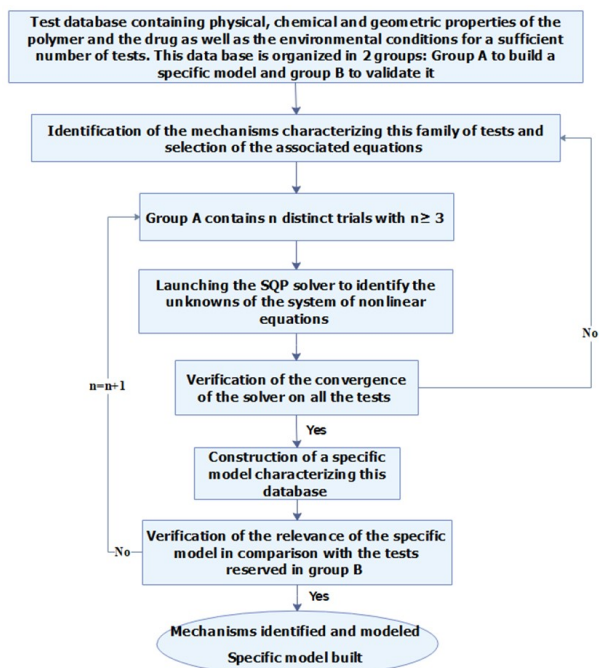


FIGURE 5.17 – Flowchart of the proposed method

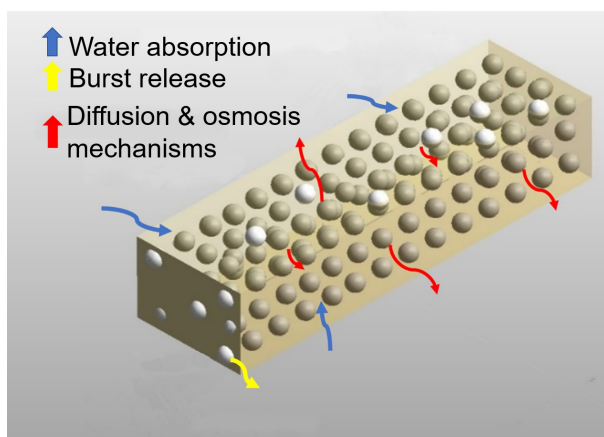


FIGURE 5.18 – Schematic of the phenomena occurring during the release. Yellow prism is the polymer matrix, white spheres are the drug particles on the surface contact in fluid medium, golden spheres are inside the polymeric matrix and the arrows show the direction of the flow from inside out or inverse to the matrix

diffusion and osmosis) is then written as:

$$\frac{M_t}{M_\infty} = \sum_{i=1}^{i=3} \mu_i \times F_i \quad (5.7)$$

With

$$\sum_{i=1}^{i=3} \mu_i = 1 \quad (5.8)$$

where M_t represents the quantity of drug released at time t , M_∞ is the amount initially loaded, μ_i the contribution of each of the 3 mechanisms involved and F_i is the corresponding equations.

According to the numerous studies, burst is normally related to the drugs on the surface of the samples. It can be related to the diffusion from the water-filled pores which are connected to the surface of the samples. Its release can be defined as [171]:

$$\frac{dC}{dt} = -k_b C \quad (5.9)$$

where the mass of the drug released at the beginning of the experiment ($t = 0$) is considered equal to the zero. The model is reformulated as the equation below:

$$F_1 = \frac{M_t}{M_\infty} = 1 - \exp(-k_b t) \quad (5.10)$$

here k_b represents the initial burst constant and t is the time of release.

Diffusive drug release is happening through the polymer matrix containing small pores. It is derived from the Fick's second law [269]:

$$\frac{\partial C}{\partial t} = D \Delta C \quad (5.11)$$

where D is the drug diffusion coefficient inside the polymeric matrix, C corresponds to the concentration of the drug in the polymer network. The initial presumption is that at the beginning of the trial, the drug is dispersed evenly in the film. Moreover, we suppose that the film thickness is very small compared to its other dimensions. Consequently, edge effects are insignificant, and the study can be confined to one dimension. Under these conditions, the simplified equation of diffusion gives the following release kinetics [269–272]:

$$F_2 = 1 - \frac{8}{\pi^2} \sum_{n=1}^{\infty} \frac{1}{n^2} \exp\left(\frac{-\pi^2 n^2 D t}{h^2}\right) \quad (5.12)$$

with h is the thickness of the matrix. This solution, corresponding to the late-time approximation of the diffusion equation, holds for the final part of the drug release, i.e. $0.4 \leq M_t/M_\infty \leq 0.6$.

The last phenomenon considered here is osmosis. The representative equation for this phenomenon [273–278] is given by 5.13:

$$\frac{dM_t}{dt} = \frac{AK'S}{h}(\sigma\Delta\pi - \Delta P) \quad (5.13)$$

where A and h are the surface and thickness of the polymer film (under the condition that the polymeric carrier is porous and the drug hydrophilic), K' accounts for the permeability of the porous membrane, S is the saturation solubility of the drug in the dissolution medium, $\Delta\pi$ represents the osmotic pressure difference across the membrane, ΔP is the hydrostatic pressure jump and σ the reflection coefficient. Generally, ΔP is negligibly small compared to $\Delta\pi$. Integrating this equation with this initial condition $M_{t=0} = 0$ leads to:

$$F_3 = \frac{M_t}{M_\infty} = \frac{AK'S\sigma\Delta\pi}{hM_\infty}t \quad (5.14)$$

The value of K' can be evaluated using a capillary bundle model for the porous membrane. Assuming a laminar flow in each pore of the membrane and supposing that the pore radii are the same, the pressure drop across membrane is the following:

$$\Delta P = \frac{(8\eta hU)}{(n\pi a^4)} \quad (5.15)$$

Where η is the dynamic viscosity of the fluid, h the thickness of the porous membrane, U the mean velocity in the pore of radius a and n the surface pore density. Each F_i equation is implemented in equation 5.7 in which the unknown factors are k_b , D_e , $\Delta\pi$. The differences of the pressure for different flow rates of the fluid in the porous membrane is calculated by Poiseuille equation adapted for the porous media, with the conditions that the fluid is laminar and incompressible [279, 280]. It is notable that in this case study the solutes are very small compared to the pores. We introduce L_p as:

$$L_p = \frac{U}{\Delta P} = \frac{n\pi a^4}{8\eta h} = \frac{K'}{h} \quad (5.16)$$

We finally obtain:

$$K' = \frac{n\pi a^4}{8\eta} \quad (5.17)$$

Moreover the reflection coefficient is considered as [280, 281]:

$$\sigma = (1 - (1 - \varnothing)^2)^2 \quad (5.18)$$

where \varnothing is the ratio of the radius of the solute particles to the radius of the pores. This parameter can be calculated by the analysis of SEM images (σ is equal to one for an ideal semi-permeable porous membrane). Using the values of these parameters (σ , K' , h , S , M_∞ respectively: in the range of $0.78 - 0.89$, $1.1 \times 10^{-8} - 7.76 \times 10^{-7} m^2/Pa.s$, it is notable that these two values are the average calculated after SEM figures after finishing the tests for each groups, $0.002 m$, $5554 g/m^3$, M_∞ is related to the drug entrapped in each sample), the model was applied in Matlab in order to compute the unknown values (μ_i , k_b , D_e and $\Delta\pi$) with the Sequential Quadratic Programming algorithm. With these calculated parameters, it is possible to compare the correlations with the results of the experiments. In order to assess the performance of the model, the RMSE and R-squared indicators were calculated [282]. Then equation 5.7 is used for different drug dosages and flow rates. Figure 5.19 shows the comparison between the experimental and calculated results. Table 5.1 gives the contribution of each mechanism in percentages and the values of the related parameters.

$$RMSE = \sqrt{\frac{1}{n} \sum (y_{prediction,i} - y_{experimental})^2} \quad (5.19)$$

$$R^2 = 1 - \frac{\sum (y_{experimental} - y_{prediction})^2}{\sum (y_{experimental} - y_{average})^2} \quad (5.20)$$

Effect of drug dosage

Figure 5.20 and table 5.1 represent the contribution in percentage for each mechanism involved in the drug liberation at the flow rate of $7.5 ml/s$ at the concentrations of 10%, 20% and 30%. One can note that increasing the initial drug percentage results in higher burst release. This phenomenon could be explained by the high drug particles delivery, at the initial time of the liberation. This is due to the higher quantity of drug present on the surface of the samples or in the pores connected to the surface, especially when the drug is hydrophilic and has the potential to stay at the surface of the samples. Moreover, the increase in k_b with the drug concentration shows that the burst phenomenon is enhanced (the kinetics of this phenomenon is faster) with the drug concentration. This fact may be related to an increase in the pore interconnections containing the drug particles and increasing the feasibility of

5.2. MECHANISM-BASED MODEL

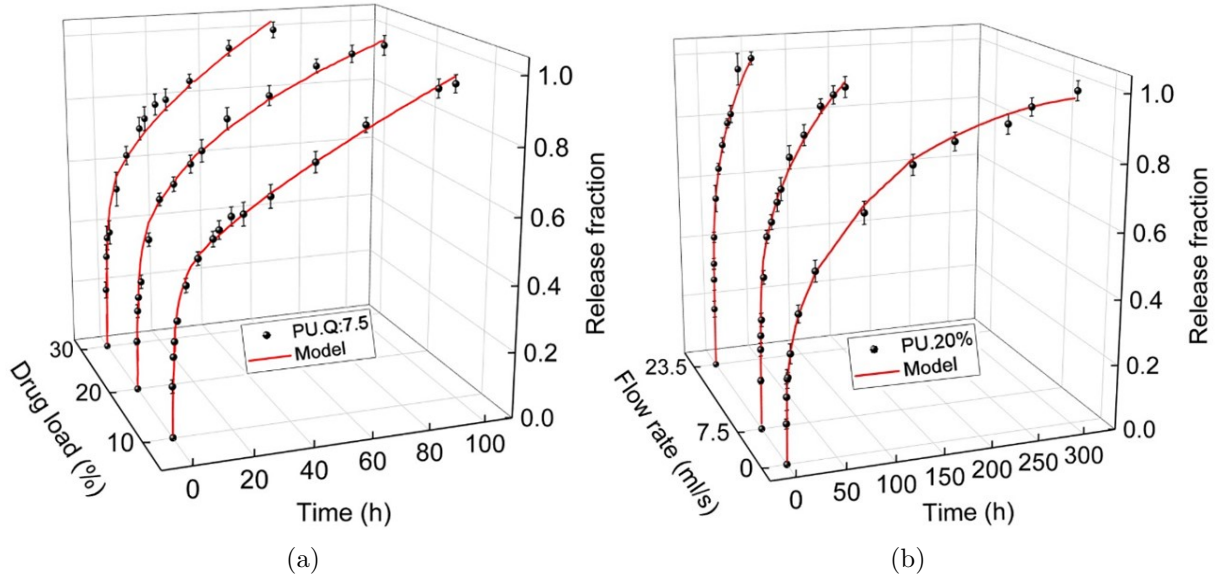


FIGURE 5.19 – Comparing the calculated values with the equation 16 and the experimental data of diclofenac release from the PU matrix, (a) for three different drug concentrations; 10, 20, and 30% at the flow rate of 7.5 ml/s (b) and for the PU with 20% of drug at the flow rates of 0, 7.5, and 23.5 ml/s

TABLE 5.1 – Values related to the percentage of the contribution of the mechanisms associated in the drug release and affecting release kinetic (t_c = characteristic time).

Mechanism	PU-10%DE-Q7.5	PU-20%DE-Q7.5	PU-30%DE-Q7.5	PU-20%DE-Q0	PU-20%DE-Q23.5
Burst (%)	23.2	31.3	36	29	31.9
Osmosis (%)	11.1	12.8	14.7	9	14.6
Diffusion (%)	65.7	55.9	49.3	62	53.5
k_b (h^{-1})	1.5	2.5	3.4	1.7	3.9
$\Delta\pi$ (atm)	0.005	0.009	0.014	0.007	0.012
D_e (m^2/h)	1.1×10^{-8}	1.62×10^{-8}	1.96×10^{-8}	8.7×10^{-9}	2.77×10^{-8}
t_c (h) of burst	0.66	0.40	0.29	0.58	0.25
t_c (h) of osmosis	250.07	203.79	126.34	524.20	106.76
t_c (h) of diffusion	363.63	246.91	204.08	440.33	144.40
RMSE	0.02	0.02	0.03	0.02	0.02
R^2	0.99	0.98	0.97	0.98	0.99

the release in a way similar to the percolation phenomenon. Similarly but less significantly, release by the osmosis mechanism increases with the quantity of the initially loaded drug. Indeed, because of the elevated amount of hydrophilic drug and due to the high number of pores created at the surface of the samples, the permeability of the membrane increases. The osmosis mechanism in the polymeric films is due to the high quantity of the water absorbed by the highly hydrophilic drug particles. Moreover, the osmotic pressure is generated from the unwetted core of the sample to the wetted side of the sample. In this case, it is obvious that the higher percentage of the drug, the higher the exerted osmotic pressure.

On the contrary, the results show that an increase in the drug percentage reduces the contribution of the diffusion mechanism. It is evidently due to the increase of the burst and osmosis phenomena discussed above. However, the kinetic of the release by this mechanism is faster when the initially loaded drug increases (increase in the value of the diffusion coefficients in table 5.1) due the increase in the drug concentration gradients with the initial drug quantity. In addition, it seems that diffusion is present in every period of the release but essentially, it will be the controlling mechanism after the burst and the osmosis, when the whole samples get wet and diffusion can happen in every direction of the sample.

Figure 5.21 shows the variation of the burst constant k_b , of the osmotic pressure $\Delta\pi$, and of the diffusion coefficient D_e versus the initial drug loaded on the samples. It is notable that the kinetics of each release mechanism is enhanced by increasing the drug percentage. However, the influence of the initial drug concentration is more significant first for burst release, then for osmosis and finally for diffusion.

One can note that generally by increasing the drug dosage at a constant flow rate, the characteristic release time for each mechanism decreases. For example in table 5.1, one can see for burst release that $t_c(10\%DE - Q7.5) > t_c(20\%DE - Q7.5) > t_c(30\%DE - Q7.5)$ and so on for osmosis and diffusion. At a given flow rate for each initial drug concentration, one also sees that the characteristic time of diffusion is larger than that of osmosis which itself is much larger than that of burst $t_c(diffusion) > t_c(osmosis) \gg t_c(burst)$. This proves that diffusion controls the kinetics of this drug release. Loading different percentages of drug affects also the physical properties of the polymer matrix. It is noteworthy that increasing the drug content microscopically and macroscopically creates free volume and empty spaces in the polymeric samples, which affect the release behavior. Therefore, the importance of the free volume fraction has to be taken into consideration. The value of free volume fraction coefficient

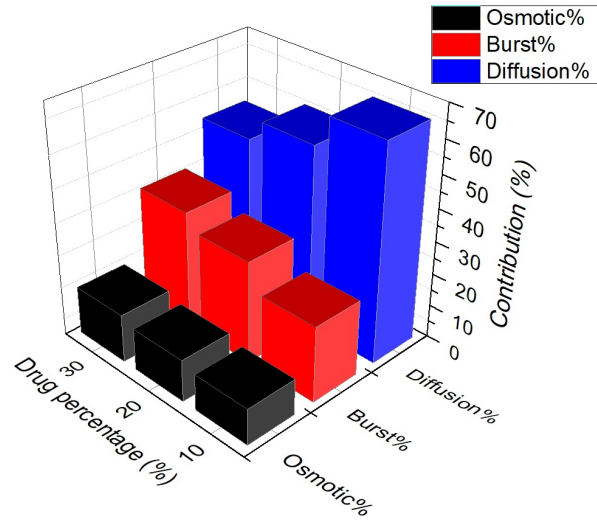


FIGURE 5.20 – Contribution of each mechanism during the drug release from PU films with the three different percentages of the drug at the flow rate of 7.5 ml/s

f_g (see 4.2.3) for PU-10%DE, PU-20%DE and PU-30%DE is calculated to be respectively about 4.18×10^{-3} , 5.03×10^{-3} , 5.94×10^{-3} . Figure 5.22 shows the comparison of the free volume fraction for different percentages of drug and its effect on the osmotic pressure. We note that an increase in the free volume fraction is related to an increase in the osmotic pressure and to the initial drug content.

Effect of flow rate

Figure 5.23 represents the contribution (in %) of each mechanism during the drug release from PU films at the initial drug concentration of 20% at the flow rates of 0, 7.5 and 23.5 ml/s . One can note that by increasing the flow rate, the contribution of the burst release and of osmosis slightly increase while the contribution of diffusion slightly decreases but the distribution of three phenomena is little sensitive to the variation of the flow rate (contrary to the variation of the initial drug concentration): the contribution of diffusion always prevails over that of burst and osmosis. However, the influence of the flow rate is clearly visible on the characteristic times of each phenomena: when the flow rate increases, these characteristic times decrease leading to a faster kinetics of each mechanism ($t_c(20\%DE - Q0) > t_c(20\%DE - Q7.5) > t_c(20\%DE - Q23.5)$) as shown in figure 5.24. Concerning the burst release, it is likely that the acceleration of its kinetics is related to the increase in the wall shear stress with the flow rate, leading to an increased amount of drug particles carried away at the initial moments of the release. Concerning diffusion, it is obvious that an increase of the flow rate results in a thinner mass

5.2. MECHANISM-BASED MODEL

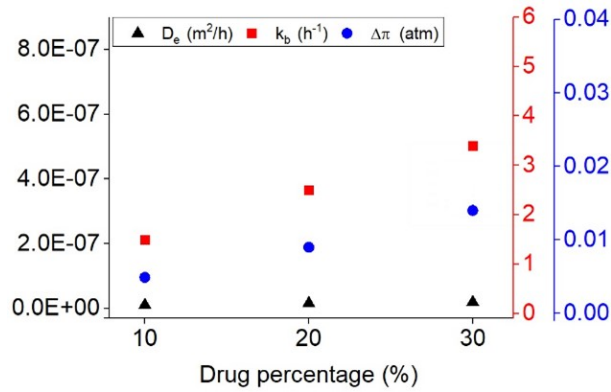


FIGURE 5.21 – The variation of the release parameters (\blacktriangle diffusion coefficient, \blacksquare kinetic of burst, \bullet osmotic pressure) for the drug release from PU films with the three different percentages of the drug (10, 20, and 30%) at the flow rate of 7.5 ml/s

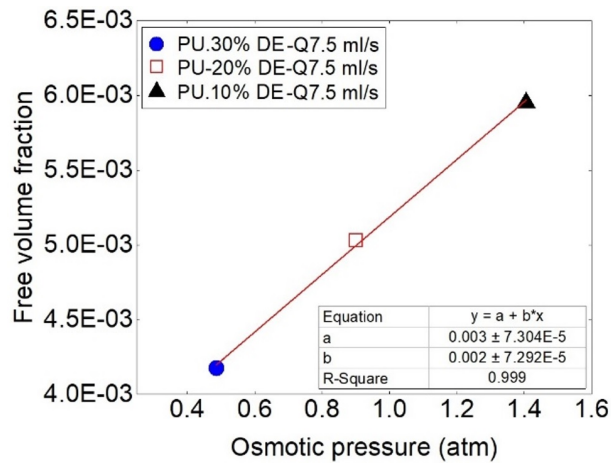


FIGURE 5.22 – Comparison of the values of free volume fraction and osmotic pressure at the flow rate of 7.5 ml/s for the samples with three different drug concentrations (\bullet PU-30%DE, \square PU-20%DE, \blacktriangle PU-10%DE)

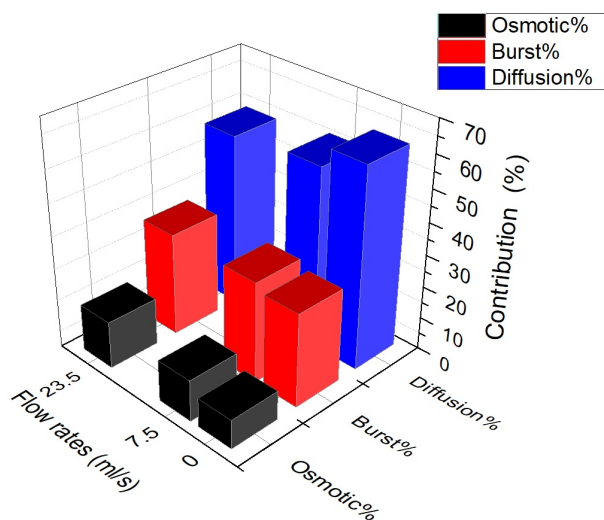


FIGURE 5.23 – Contribution of each mechanism during the drug release from PU-20%DE of the drug at the different flow rates of 0, 7.5 and 23.5 ml/s

boundary layer thus an improved kinetics by diffusion. Finally, for osmosis, an increase in the flow rate also leads to an increase in the osmotic pressure jump as shown in figure 5.25. In the same figure, we also note the increase in the permeability of the porous matrix related to the increase in the pore radius and in the pore density observed experimentally when the flow rate is higher. According to equation 5.14, the characteristic time of osmosis increases with the flow rate in accordance with the previous explanation.

Validation of the model

To analyze the phenomenon of release of diclofenac from PU samples at different drug percentages and flow rates, equation 5.21, considering three mechanisms of burst, diffusion and osmosis, was fitted using some experimental results. It is shown in figure 5.26 that the curves of our 3-mechanism model fit the experimental results with a good agreement. The parameters (k_b , D_e and $\Delta\pi$) issued from the fittings are summarized in table 5.1. Using the values of these parameters, it is possible to obtain correlations between each of these parameters, concentration and flow rate. Concerning the influence of the drug concentration, an exponential law was chosen. For the diffusion coefficient for instance, we have:

$$\ln D_e = A + \frac{B}{C\%} \quad (5.21)$$

with A and B some numerical constants. As for the dependence with the flow rate, a simple linear law

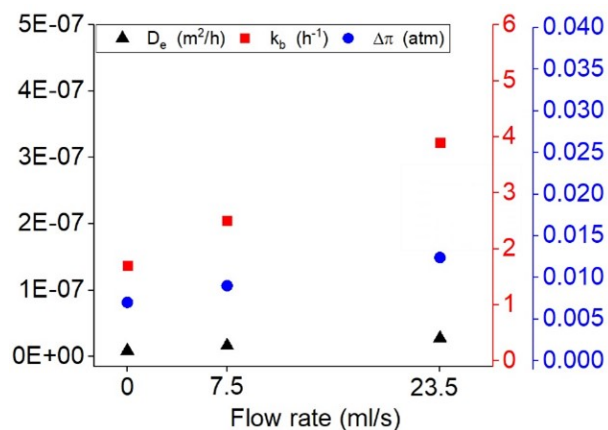


FIGURE 5.24 – The variation of the release variables (\blacktriangle diffusion coefficient, \blacksquare kinetic of burst, \bullet osmotic pressure) for the drug release from PU films with the 20 percentage of the drug at the different flow rates of 0, 7.5 and 23.5 ml/s

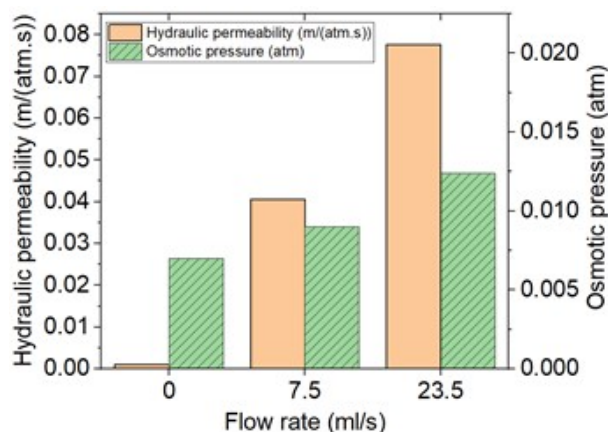


FIGURE 5.25 – Comparison of the values of permeability and osmotic pressure for samples of PU-20%DE at three different flow rates of 0, 7.5 and 23.5 ml/s

5.2. MECHANISM-BASED MODEL

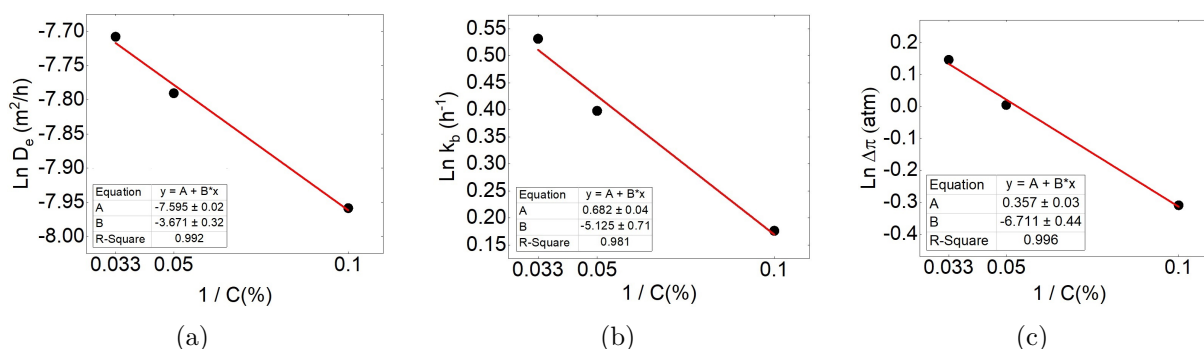


FIGURE 5.26 – Correlation between (a) diffusion coefficient, (b) burst constant, (c) osmotic pressure versus the concentration

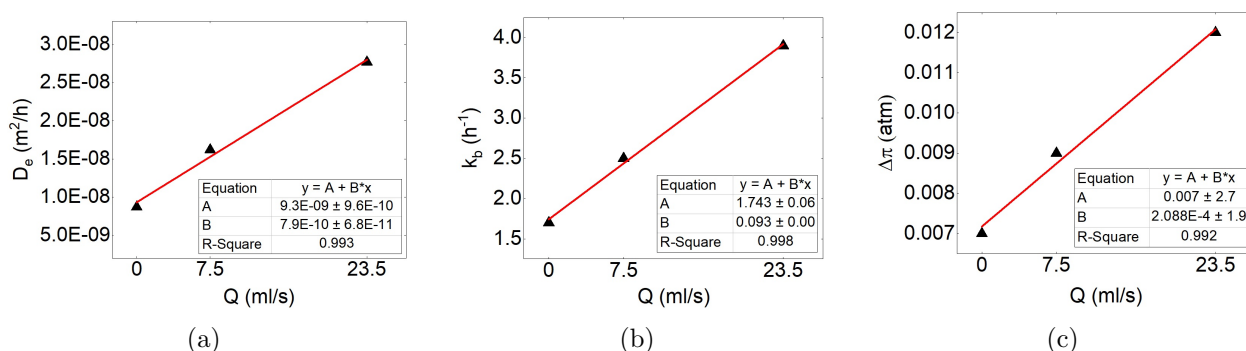


FIGURE 5.27 – Correlation between (a) diffusion coefficient, (b) burst constant, (c) osmotic pressure versus to the flow rate

was considered. For example for the burst constant k_b , we have:

$$k_b = A + B \times Q \quad (5.22)$$

These fits are plotted in figure 5.27. In order to test the accuracy of these correlations, we have compared in figure 5.28 their predictions with some new experimental results for PU films loaded with 15% diclofenac at the flow rate of 7.5 ml/s, and 20% diclofenac at the flow rate of 6.5 ml/s. It can be noted that in both cases a good correlation exists between the model and the experimental results. Thus this kind of approach seems to be very effective to predict the release kinetics of DE from PU, at least within the limits of the flow rate ($Q < 23.5$ ml/s) and the drug concentrations ($C < 30\%$) studied here. However, extrapolating these models far from these limits could be dubious.

5.2. MECHANISM-BASED MODEL

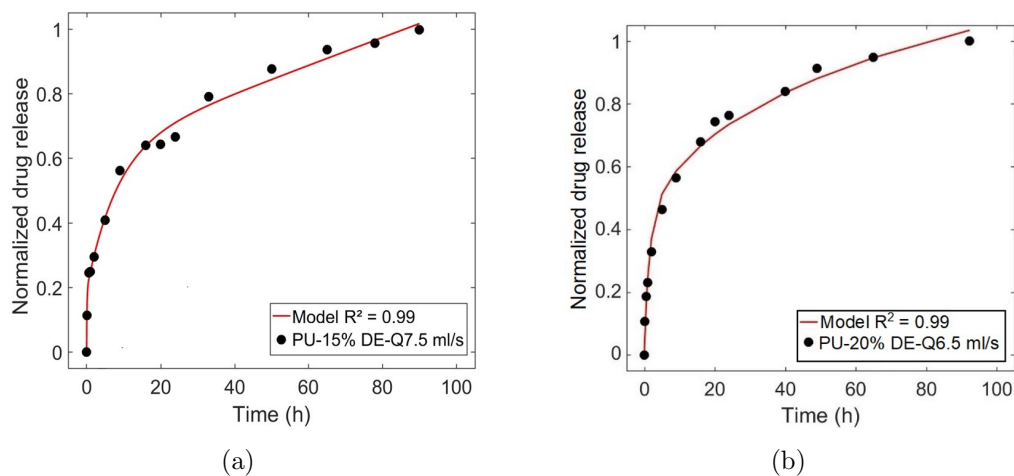


FIGURE 5.28 – Comparison of the predicted release profile obtained by the model and the experimental data for the case (a) PU-15%DE-Q7.5 ml/s , (b) PU-20%DE-Q6.5 ml/s

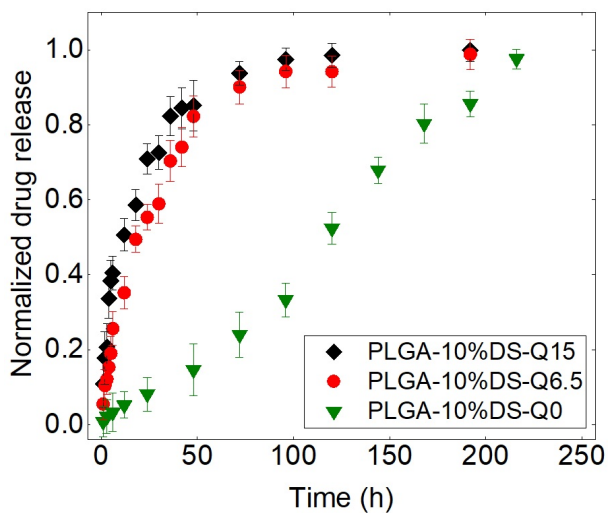


FIGURE 5.29 – Experimental drug release from the PLGA matrix with 10%DS at the flow rates of 0, 6.5 and 15 ml/s

5.2.2 Application of the mechanism-based model for PLGA-DS

In this section, we have applied the model of mechanisms on the release profile of DS from PLGA polymer. The release tests have been performed on the previous test bench at different flow rates of 0, 6.5 and 15 *ml/s* from films of biodegradable PLGA samples loaded with 10% DS. Figure 5.29 shows the results related to the drug release from PLGA-10%DS-Q0, 6.5, 15 *ml/s*. From figure 5.29 one can note that the release profiles can be divided into three regions. The first region is related to the burst release which is occurring at the very beginning of the release with high kinetic. The second stage, which is rather slower, is due to the coupling between the diffusion and swelling mechanisms. The effective parameter affecting the diffusion mechanism is the physical state of the polymer. It is well-known that polymers at the rubbery state have a larger diffusion coefficient than at the glassy state and that the glass transition temperature of the polymers changes when the polymers are exposed to water molecules [283]. In order to release the drug by diffusion, at first drug needs to be dissolved in solution inside the polymer or to be small enough to be transported by the solution before dissolution. That is why diffusion takes place with a relatively small release rate [203]. Meanwhile, swelling mechanism is activated by the rapid water absorption. In fact, the hydrophilic polymer rapidly absorbs water and causes the formation of a porous structure near the surface, which promotes the drug release. Figure 5.30 shows the optical observation of the PLGA-10%DS after (a) 1h and (b) 24h of release at the flow rate of 6.5 *ml/s*. These images show that pores are created and enlarge at the surface of the samples during the release time, accelerating the release rate. Swelling in the polymers can have two different effects. On one side, the solution molecules insert and locate inside or between the polymers chains, resulting in the increase in the free volume between the polymer chains and their flexibility. This causes an increase in the kinetic of the release. On the other hand, swelling of the polymers results in the increase in the dimension of the samples, therefore in the distances required by the drug molecules to release from the samples. This second effect decreases the kinetic of the release. The other most probable mechanism is erosion when the polymer becomes weak from the mechanical point of view. The reasons are related to the polymer degradation resulting in the cleavage of the chains [284], the contact of the surface of the material with the circulating fluid and the friction between them.

As mentioned above and referring to the literature for this type of the drug carrier (PLGA films) and release conditions, the most commonly and frequently mentioned mechanisms for drug release are thus burst-release, diffusion, swelling and erosion [207, 285–288]. The equations related to these four

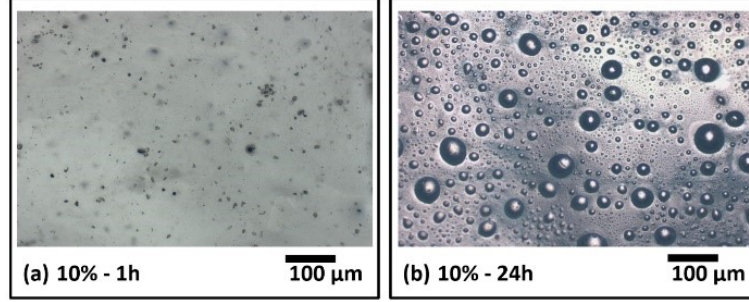


FIGURE 5.30 – Comparing the optical observation of the PLGA-10%DS-Q6.5 after (a) 1h and (b) 24h

release mechanisms are grouped by assigning to each of them a weighting coefficient:

$$\frac{M_t}{M_\infty} = \sum_{i=1}^{i=4} \mu_i \times F_i \quad (5.23)$$

With

$$\sum_{i=1}^{i=4} \mu_i = 1 \quad (5.24)$$

In equation 5.24, F_1 and F_2 , related respectively to burst and diffusion are identical to equation 5.10 and 5.12 of the previous case (PU-DE). The equation for swelling, introducing two new parameters k_s and m , is given by F_3 :

$$F_3 = k_s t^m \quad (5.25)$$

The contribution of erosion, introducing a new parameter k_e , is represented by F_4 :

$$F_4 = 1 + \exp(-2k_e t) - 2 \exp(-k_e t) \quad (5.26)$$

The coefficients $\mu_1, \mu_2, \mu_3, \mu_4$ represent respectively the relative contribution of the mechanisms of burst-release, diffusion, swelling and erosion. The other unknown factors are now k_b, D_e, k_s, k_e and m . Here m is the exponent characteristic of the release mechanism ($m > 0.5$ for swelling) [249], k_b represents the initial burst kinetics constant, D_e is an effective diffusivity of solute, k_s and k_e are respectively the constants related to the swelling and erosion phenomena.

Four-mechanism model

The above definitions can help us to analyze the effect of the flow rate on the kinetics of the different mechanisms. Our model containing the selected above mechanisms (called here BDSE for

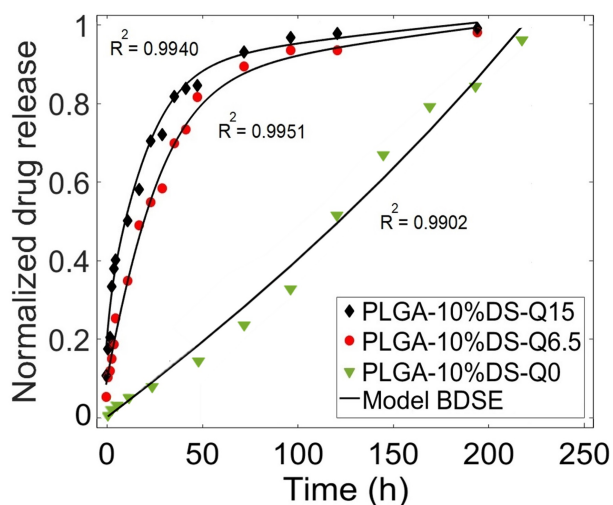


FIGURE 5.31 – Experimental drug release from the PLGA matrix with 10% of drug at the flow rates of 0, 6.5 and 15 ml/s with the adjustment models (considering burst, diffusion, swelling and erosion mechanisms)

Burst-Diffusion-Swelling-Erosion) was applied to the experimental results of PLGA-10%DS with flow rates of 0, 6.5 and 15 ml/s (figure 5.31 shows the adjustments). After applying the BDSE model on the experimental results, the values of every unknown parameters (μ_i , k_b , D_e , k_s , k_e and m) are presented in table 5.2. From the values presented in table 5.2 it is evident that increasing the flow rate increases the burst release from the drug carriers. It is notable that by changing the state of the flow from static to the continuous, the amount of the burst release is increased which clearly shows that the burst phenomenon is related to convection. It is also clear that the phenomenon of diffusion is enhanced when the flow rate increases. This can be due to the high water uptake by the PLGA film when the flow rate increases. Moreover, in the static state the drug is not able to migrate far away from the sample (thick mass boundary layer and low concentration gradients leading to low diffusive flux), whereas in the continuous state the released drug is immediately transported by the flow (thin mass boundary layer and high concentration gradients leading to high diffusive flux). The mechanism of erosion is also accelerated by the flow rate due to the higher friction between the fluid and the sample. Indeed, the higher the flow rate, the higher the shear stress applied to the samples. This results in a more rapid mechanical weakening of the samples. When the flow rate is zero, the results show that the mechanisms of burst release, diffusion and erosion are negligible; this is due to the low shear rate of the flow, low gradient of the concentration and low friction. Therefore swelling

5.2. MECHANISM-BASED MODEL

TABLE 5.2 – Values related to the unknown parameters

Mechanism	PLGA-10%DS -Q0	PLGA-10%DS -Q6.5	PLGA-10%DS -Q15
Burst (%)	0.05	18.99	21.16
Diffusion (%)	0.06	8.25	9.81
Swelling (%)	99.84	21.18	20.16
Erosion (%)	0.05	51.58	48.87
k_b (h^{-1})	0.033	0.169	0.301
D_e (m^2/h) ($\times 10^{-10}$)	18.00	18.00	18.00
k_s (h^{-1})	0.004	0.249	0.310
k_e (h^{-1})	0.002	0.061	0.063
m	1.00	0.72	0.70
R^2	0.9902	0.9951	0.9940

is the prevailing mechanism in the static state for this type of sample leading to a slow kinetics and a slow drug release rate.

Sensitivity of the model to the choice of mechanisms

The choice of the mechanisms contributing to the release profile should be carefully chosen. If a particular mechanism is not considered in the model, it will not consistently fit the experimental results. In this regard, three examples are given. In the first case (BDE model), burst release, diffusion and erosion are considered for PLGA-10%DS-Q0 (swelling is neglected). In the second case (BDS model), burst release, diffusion and swelling mechanisms are considered for PLGA-10%DS-Q6.5 (erosion is neglected). Finally for the last case (DSE model), diffusion, swelling and erosion are considered for PLGA-10%DS-Q15 (burst release is neglected). The results are respectively shown in figure 5.32 (a), (b), (c). They show that neglecting one mechanism will change the accuracy of the adjustment. Especially when the dominant mechanism of the release is not considered. The values related to the adjustment are shown in table 5.3. For example neglecting swelling leads to a non-physically result because the prevailing mechanism at zero flow rate would be erosion.

BDSE-Model and its validation

To find a correlation between the values of the parameters shown in table 5.2, figures 5.33 and ?? were established. In this regard, the equations used to fit the parameters μ_i , k_b , D_e , k_s , k_e and m are of the type:

$$a_i - b_i \times c_i^Q \quad (5.27)$$

5.2. MECHANISM-BASED MODEL

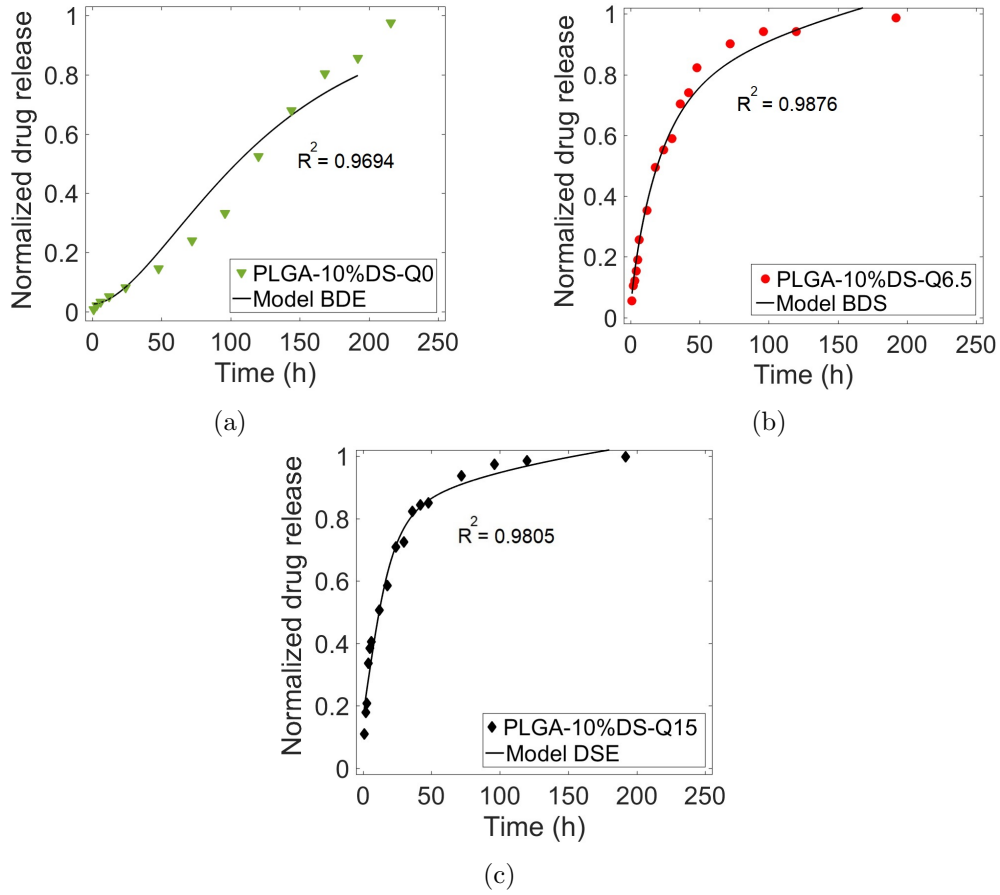


FIGURE 5.32 – Experimental drug release from the PLGA-10%DS-Q0, Q6.5, Q15 with the model adjusted with different mechanisms

TABLE 5.3 – Values related to the unknown parameters with neglecting one mechanism for each case

Mechanism	PLGA-10%DS -Q0	PLGA-10%DS -Q6.5	PLGA-10%DS -Q15
Burst (%)	0.01	49.99	-
Diffusion (%)	2.66	0.01	5.30
Swelling (%)	-	50.00	45.45
Erosion (%)	97.33	-	49.23
$k_b (h^{-1})$	0.005	0.014	-
$D_e(m^2/h) (\times 10^{-10})$	1.296	4.752	18
$k_s (h^{-1})$	-	11.232	115.704
$k_e (h^{-1})$	0.011	-	0.089
m	-	0.43	0.26
R^2	0.9694	0.9876	0.9805

5.2. MECHANISM-BASED MODEL

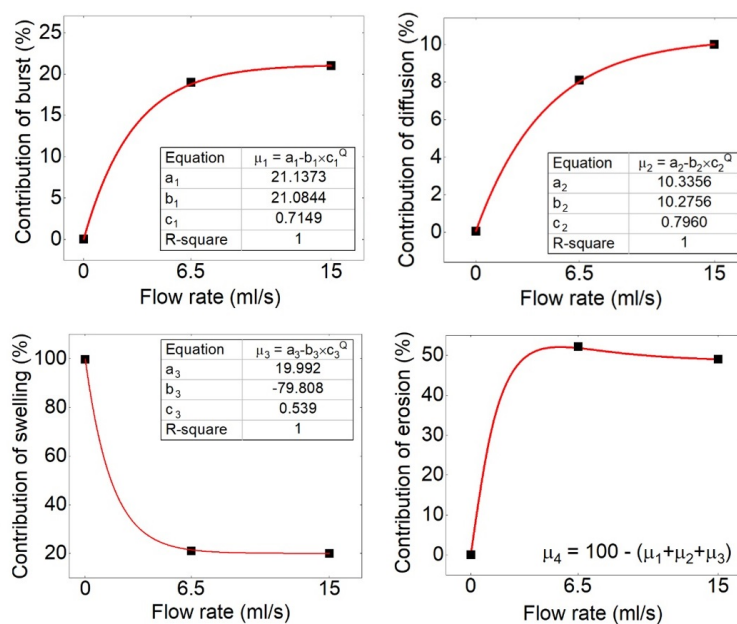


FIGURE 5.33 – Exponential fit of the contribution of each mechanisms in drug release vs flow rate

The correlations between these values give the ability to predict the release for other flow rates. Figure 5.34 shows the prediction of the drug release profile for the PLGA-10%DS-Q7.5 by the modeling approach described above and the experimental results obtained at the flow rate of 7.5 *ml/s*. It is notable that the experimental results show a good agreement with the BSDE model obtained by the correlation of the values of the parameters. Moreover, the direct application of the BDSE model for this new value of the flow rate gives a curve that also matches satisfactorily the experimental results and the results obtained by the method using the correlations described above.

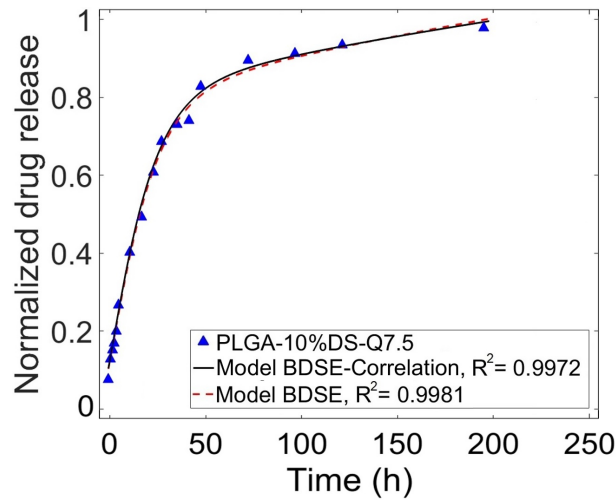


FIGURE 5.34 – Comparison between the results of the BSDE model obtained by the correlation of the values of the parameters and direct application of the BDSE model for PLGA-10%DS-Q7.5 with the experimental results

Table 5.4 shows the values of the constants obtained from both these approaches which are in very good accordance. To conclude, the predictive model and the experimental results show a good agreement provided that the contributing mechanisms in the drug release are rigorously chosen.

TABLE 5.4 – Values related to the unknown parameters for PLGA-10%DS-Q7.5 from the BSDE model obtained by the correlation of the values of the parameters and direct application of the BDSE model

Mechanism	PLGA-10%DS-Q7.5	
	Model BDSE-Direct	Model BDSE-Correlation
Burst (%)	19.00	20.00
Diffusion (%)	8.00	8.00
Swelling (%)	21.00	22.00
Erosion (%)	52.00	50.00
k_b (h^{-1})	0.186	0.114
$D_e(m^2/h)$ ($\times 10^{-10}$)	18.00	18.00
k_s (h^{-1})	0.260	0.198
k_e (h^{-1})	0.061	0.065
m	0.73	0.73

5.3 Numerical simulation

In this section, we present a comparison between numerical results, kinetic model results and experimental data for Diclofnac Epolamine (DE) released from non-degradable polyurethane (PU) samples (dimensions of $30 \times 5 \times 2 \text{ mm}^3$). Several values of the flow rate (0, 6.5, 7.5 and 23.5 ml/s) and of the drug concentrations (mass ratio of drug/(polymer): 10%, 15%, 20% and 30%) are considered. The experimental data are obtained on the test bench described in chapter 3. The fluid circulating in the test bench is water at 37°C with the density and dynamic viscosity of respectively 1000 kg/m^3 and $6.9 \times 10^{-4} \text{ Pa.s}$. polyurethane (PU) has been used as the carrier of drug. Referring to the proposed kinetic model presented in section 5.1, we have:

$$\frac{M_t}{M_{95\%}} = \left(\frac{t}{t_{95\%}}\right)^n \quad (5.28)$$

where M_t is the drug mass released from polymer. In our simulation method it is measured by the difference between initial drug dosage and remained drug dosage in polymer at different times. $M_{95\%}$ corresponds to 95% of the initial drug mass released. n is defined from figure 5.8:

$$n = 0.0502 \overline{Re} + 0.26 \quad (5.29)$$

In order to generalize the value of $t_{95\%}$ for every initial drug concentration, we have chosen to refer this particular time to this particular time at the initial drug concentration of 10%. Using figure 5.9, we obtain the following expression:

$$t_{95\%} = t_{95\%}(C = 10\%) \times (-0.43 \ln C(\%) + 2) \quad (5.30)$$

where $C(\%)$ is the initial drug dosage in polymer. Finally, we derive $t_{(95\%)}$ by fitting its value versus the initial drug concentration. Based on the 10% concentration, this equation gives:

$$t_{95\%}(C = 10\%) = -42.46 \ln(\overline{Re}) + 17.375 \quad (5.31)$$

More details about this kinetic model can be found in the previous section 5.1. The numerical simulations require the value of the drug diffusivity D_p inside the polymer film. To our knowledge, this parameter is unknown in the literature for this kind of drug and this kind of polymer. In order to obtain an estimation of mass D_p , we know, from dimensional analysis, that it is the ratio of the

5.3. NUMERICAL SIMULATION

TABLE 5.5 – Predicted diffusion coefficient (m^2/s) at different conditions

Flow rate (ml/s)	Initial drug dosage			
	10%	15%	20%	30%
0	1.92×10^{-12}	-	2.75×10^{-12}	3.67×10^{-12}
6.5	6.15×10^{-12}	-	8.79×10^{-12}	-
7.5	6.73×10^{-12}	8.15×10^{-12}	9.61×10^{-12}	1.28×10^{-11}
23.5	1.39×10^{-11}	-	1.98×10^{-11}	-

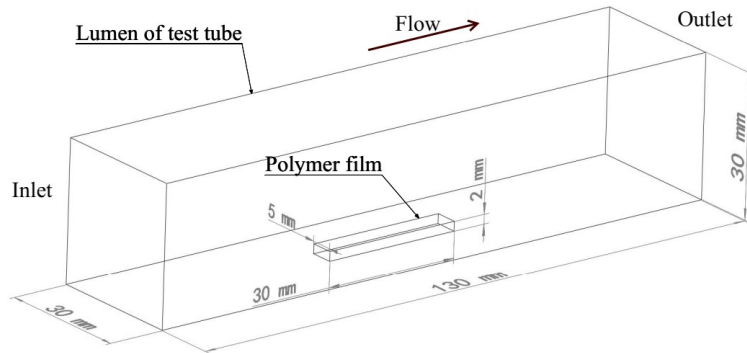


FIGURE 5.35 – Geometrical model of the numerical domain with polymer film

square of a characteristic length L and a characteristic time. In this work, this time is chosen to be $t_{(95\%)}$ and L is chosen as the ratio of the polymer film volume to its surface. Finally, the definition of the diffusion coefficient is (the factor 5 accounts for the 5 out of 6 surfaces of the polymer film in contact with the fluid):

$$D_p = \frac{5L^2}{t_{95\%}} \quad (5.32)$$

The predicted diffusion coefficients at different flow rates and initial drug dosages are shown in table 5.5. These values are of the order of magnitude of the diffusion coefficients found in the literature.

Numerical modeling and methodology

To be consistent with the test facility, the 3D geometrical model of channel with drug-loaded polymer inside has been established as shown in figure 5.35. Two domains are included: flow and polymer domains. The dimensions of the numerical domain are similar to those of the test bench. In order to achieve mesh independence, mesh refinement has been adopted with different mesh size of 3 million, 5.5 million, 8.6 million and 12 million. The grid used in this study consists in tetrahedral elements with local refinement close to the edges of the domain.

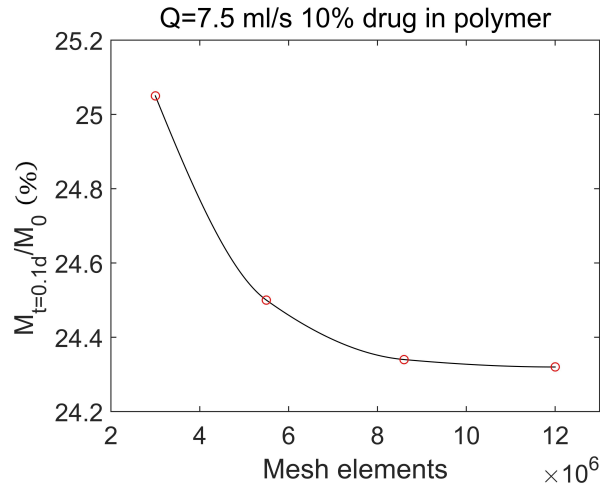
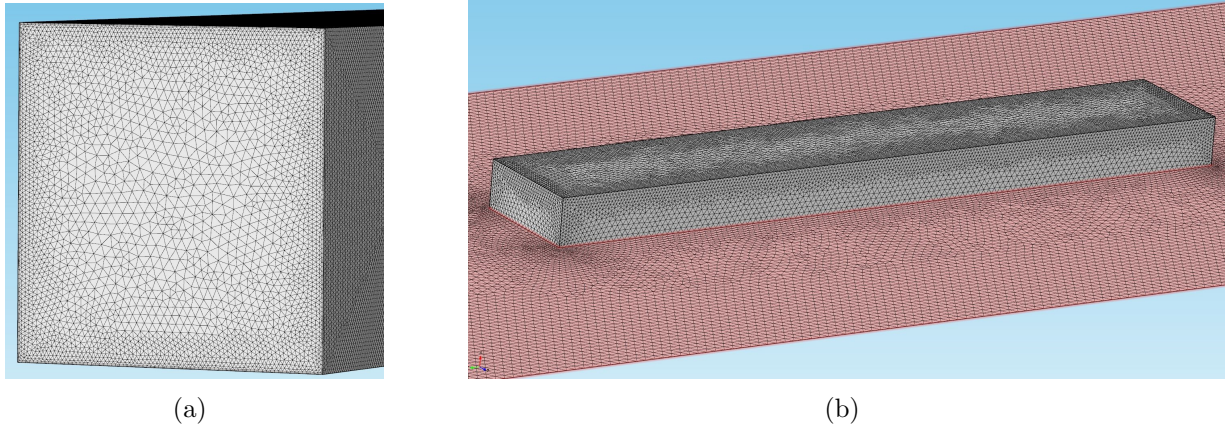
FIGURE 5.36 – Mesh independence study with different mesh sizes at $t = 0.1 d$ 

FIGURE 5.37 – Mesh distribution at (a) inlet of flow channel and (b) around polymer film

In figure 5.36, the drug mass percentage released from polymer at $t = 0.1$ day has been investigated with these different mesh elements when the flow rate is 7.5 ml/s and initial drug dosage is 10% in polymer. As observed, when the mesh size is over 8.6 million elements, the sensibility of the results to the mesh number is below 1%. Thus, the final mesh size of 8.6 million is chosen with the mesh distribution shown in figure 5.37.

To be consistent with the experiments, water (considered to be an incompressible and Newtonian fluid) with density of 1000 kg/m^3 and dynamic viscosity of $6.9 \times 10^{-4} \text{ Pa}\cdot\text{s}$ has been set in the flow domain during the simulations. The governing equations that are solved are: the Navier-Stokes, continuity and advection/diffusion mass transport equations in the fluid domain (equations 5.33, 5.34 and

5.35) and the diffusion mass transport equation in the polymer domain (equation 5.36) [289].

$$\vec{\nabla} \cdot \vec{V} = 0 \quad (5.33)$$

$$\rho \left(\frac{\partial \vec{V}}{\partial t} + \vec{V} \cdot \vec{\nabla} \vec{V} \right) = -\vec{\nabla} p + \vec{\nabla} \cdot (\mu \vec{\nabla} \vec{V}) \quad (5.34)$$

where \vec{V} is the flow velocity, p is the pressure, ρ is the flow density and μ is the dynamic viscosity.

$$\frac{\partial c_f}{\partial t} + \vec{\nabla} \cdot (-D_f \vec{\nabla} c_f) + \vec{V} \cdot \vec{\nabla} c_f = 0 \quad (5.35)$$

where c_f is the drug concentration in flow domain, D_f is the drug diffusion coefficient in flow. Based on the literature [80], $D_f = 3.875 \times 10^{-10} \text{ m}^2/\text{s}$.

$$\frac{\partial c_p}{\partial t} + \vec{\nabla} \cdot (-D_p \vec{\nabla} c_p) = 0 \quad (5.36)$$

where c_p is the drug concentration in polymer, D_p is the diffusion coefficient in polymer. As the flow rates of 0 ml/s, 6.5 ml/s, 7.5 ml/s and 23.5 ml/s have been tested in the experiments, the sectional mean velocity at inlet is fixed to be 0 m/s, 0.0072 m/s, 0.0083 m/s and 0.026 m/s respectively. The corresponding Re number is below 1200 belonging to the laminar regime. A uniform velocity profile is set at the inlet and the polymer is located in a region where the flow is already fully developed. As for the boundary conditions, a constant pressure is fixed at the outlet, the artery wall is considered to be rigid with no-slip, a zero-drug concentration is fixed at the inlet, while a zero-drug flux (adiabatic) is imposed at the outlet. At the interfaces between the flow and polymer domains, the drug flux is considered to be continuous. Initial drug concentrations in polymer are 202 mol/m³, 279 mol/m³, 356 mol/m³ and 591 mol/m³ corresponding to 10%, 15%, 20% and 30%. In the channel, the initial drug concentration is 0. Modeling, meshing and computing have been done with Comsol 5.1 which is based on the finite element method. The solver used in this software applies an iterative method called Generalized Minimal Residual Method (GMRES). The streamline upwinding Petrov-Galerkin (SUPG) scheme and the backward differential formula (BDF) scheme with variable order are adopted for achieving the spatial and temporal discretization of the governing equations. Concerning the stopping criteria, the residual values of 10⁻⁵ for continuity and momentum equation and 10⁻⁴ for diffusion have

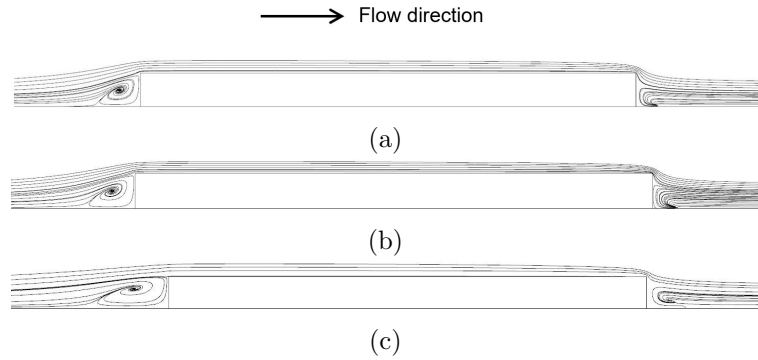


FIGURE 5.38 – Flow topology around polymer film at different flow rate (a) 6.5 ml/s , (b) 7.5 ml/s and (c) 23.5 ml/s

been chosen. The initial time step of 0.001 s is set firstly which can be adaptively adjusted by Comsol during computing process depending on the physics and scheme used. An insight of flow topology around the polymer film is presented in figure 5.38 at different flow rates. A cross section following the flow direction and located in the middle of flow channel has been extracted. As observed in figure 5.38, the vortices are formed both upstream and downstream the polymer as the flow is strongly disturbed by this obstacle. The increased flow rate tends to enlarge the recirculation regions. In order to better understand the effects of flow on drug release, figure 5.39 shows the drug distribution in a cross section located in the middle of the polymer film parallel to the flow direction at different flow rates with initial drug dosage of 10% and $t = 1 \text{ d}$. Smaller drug concentration are observed with increased flow rate. Moreover, the drug concentration gradients decrease faster with the flow rate in the proximal and distal regions of the polymer (black circles in figure 5.39). The reason is the stronger influence of flow convection with increased flow rate.

Figure 5.40 shows the drug distribution at the two symmetrical lateral surfaces of polymer along the flow direction at different time instants with flow rate of 7.5 ml/s and initial drug dosage of 10% . Symmetrical drug concentration can be observed between these two lateral surfaces at different time instants. Furthermore, the drug release tends to be faster at upstream side compared to the downstream side as flow convection is stronger with the incoming flow upstream the polymer.

Figure 5.41 shows the drug distribution at the two symmetrical lateral surfaces of the polymer film along the flow direction at different times at the flow rate of 7.5 ml/s and initial drug dosage of 10% . Symmetrical drug concentration can be observed between these two lateral surfaces at different

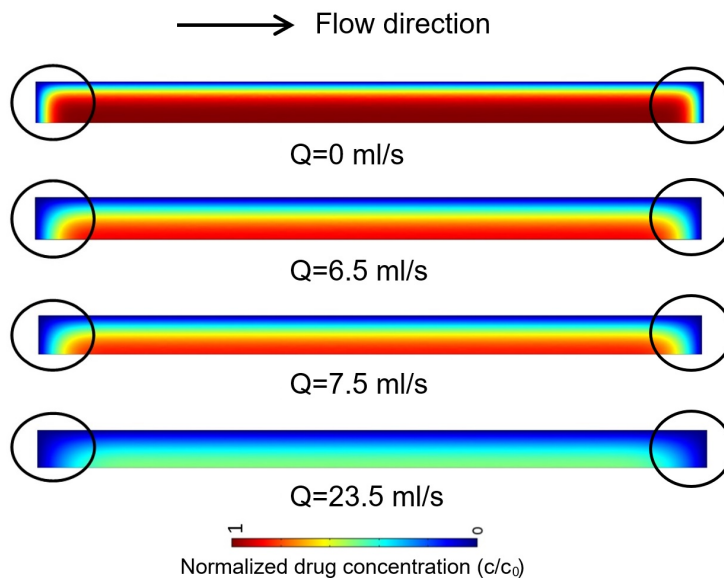


FIGURE 5.39 – Drug distribution in the mid-plane of the polymer film parallelly to the flow direction at different flow rates (initial drug dosage of 10% and $t = 1 d$)

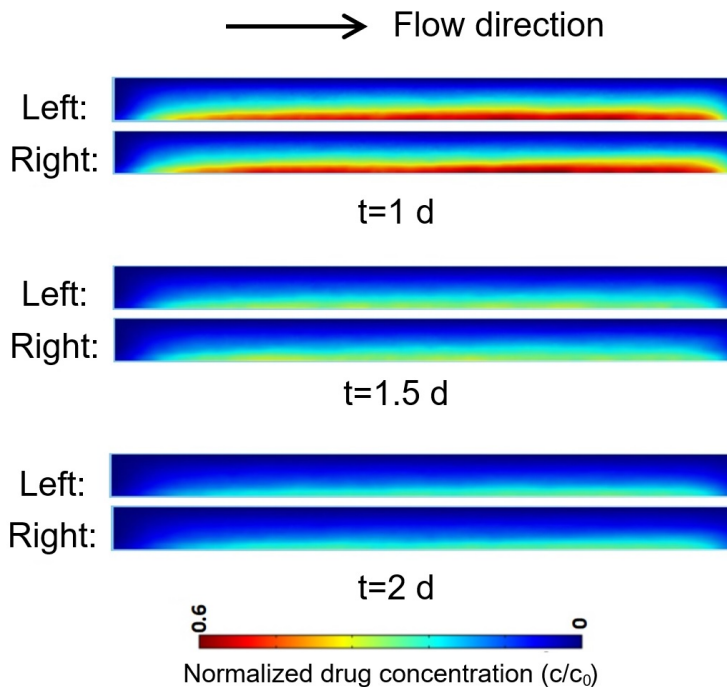


FIGURE 5.40 – Drug distribution on the lateral sides of the polymer film at different time for the flow rate of 7.5 ml/s and initial drug dosage of 10%

5.3. NUMERICAL SIMULATION

times. In comparison to the previous cross-section located in the mid-plane of the polymer film, we observe an asymmetrical drug concentration distribution on the lateral sides in contact with the fluid: the proximal region is more sensitive to convection than the distal region. Figure 5.41 presents the comparison of the drug release profiles obtained experimentally, numerically and by the kinetic model at different flow rates and 10% of initial drug dosage in polymer. Numerically, M_t/M_0 represents the ratio of the volume-averaged drug concentration released from the polymer at time t and the initial drug concentration. The drug distribution in the polymer cross section is displayed at specific times. As observed, a good agreement is found between the numerical results and the in vitro data. Similarly, the comparison of the drug release profiles obtained experimentally, numerically and by the kinetic model at different flow rates and at 15%, 20% and 30% of initial drug dosage in polymer are displayed in figures 5.41, 5.42, 5.43 and 5.44 with a good agreement between the three methods. Increasing the flow rate and the initial drug concentration promote the drug release process with a reduced drug release time due to the increasing effect of the flow convection and of the initial concentration gradient. This is particularly obvious in Figure 5.45, in which we have plotted the characteristic time to achieve a drug release of 80% according to the initial drug content at the flow rates of 0, 6.5, 7.5 and 23.5 ml/s . We observe that $t_{80\%}$ decreases when the flow rate and the drug concentration increase.

5.3. NUMERICAL SIMULATION

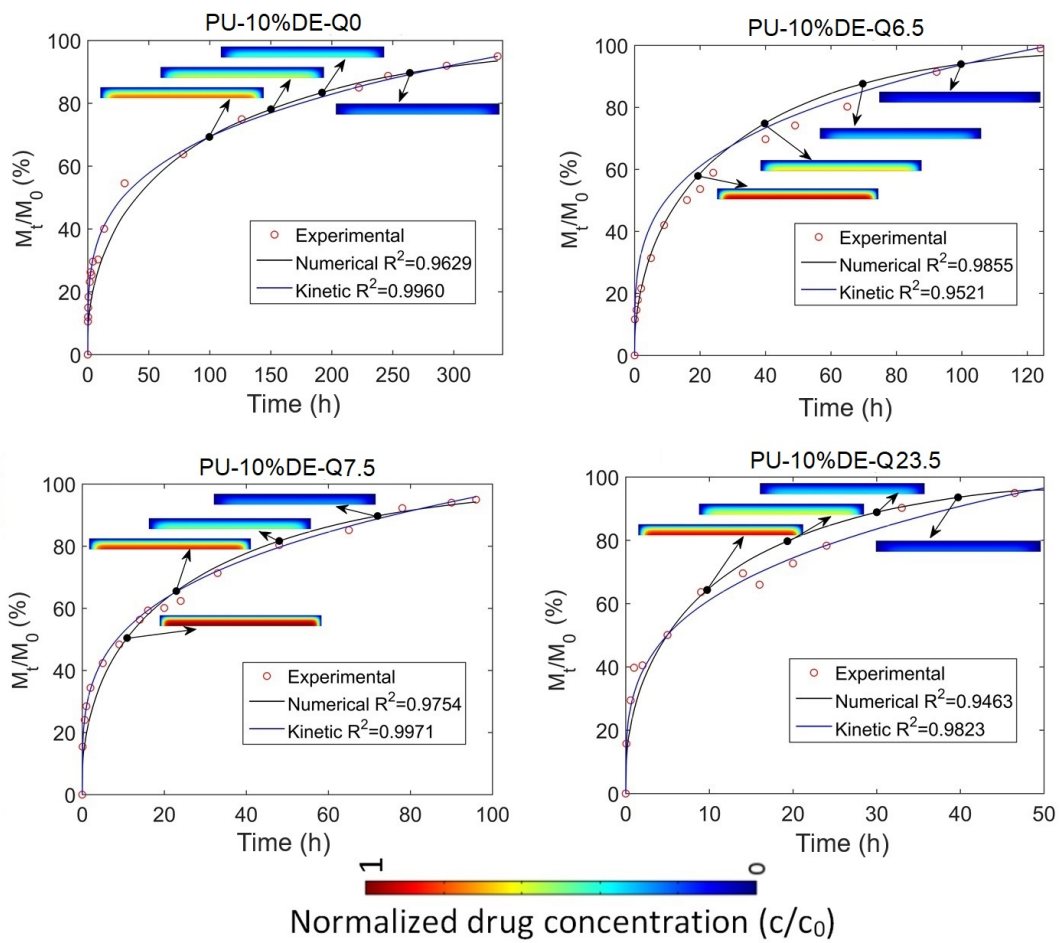


FIGURE 5.41 – Drug release from polymer at different flow rate with drug dosage of 10%

5.3. NUMERICAL SIMULATION

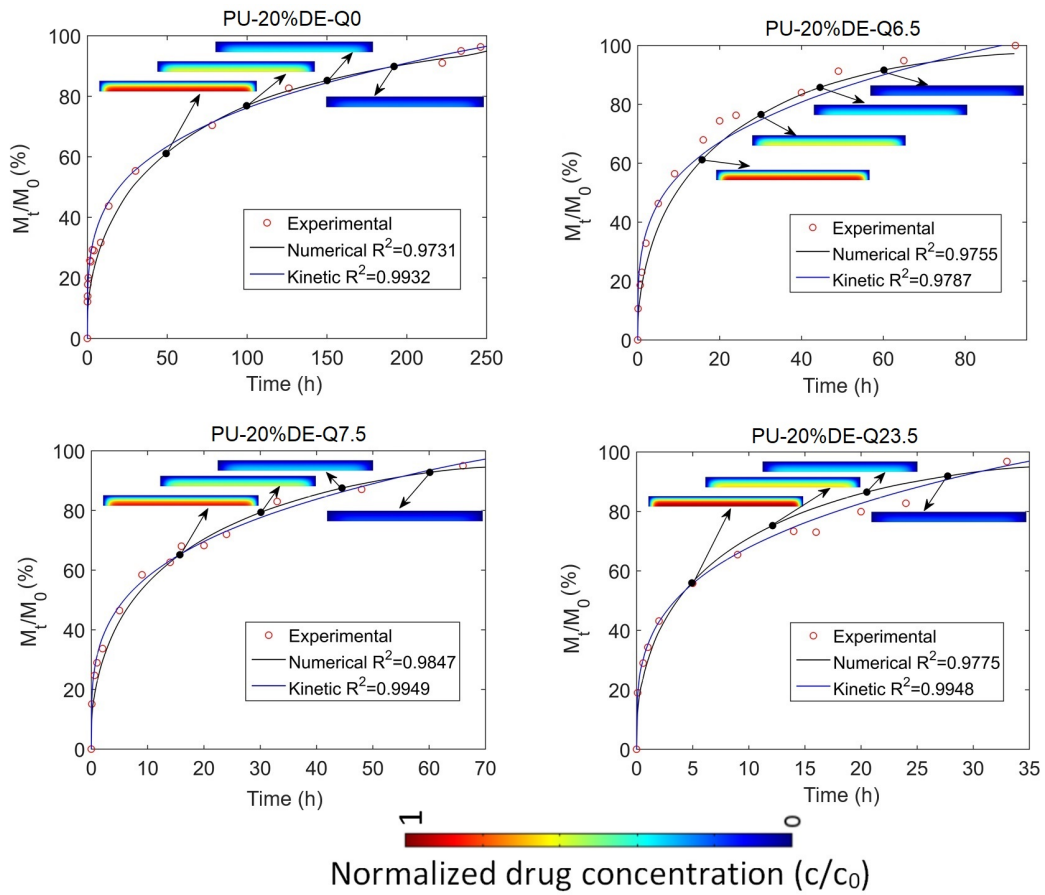


FIGURE 5.42 – Drug release from polymer at different flow rate with drug dosage of 20%

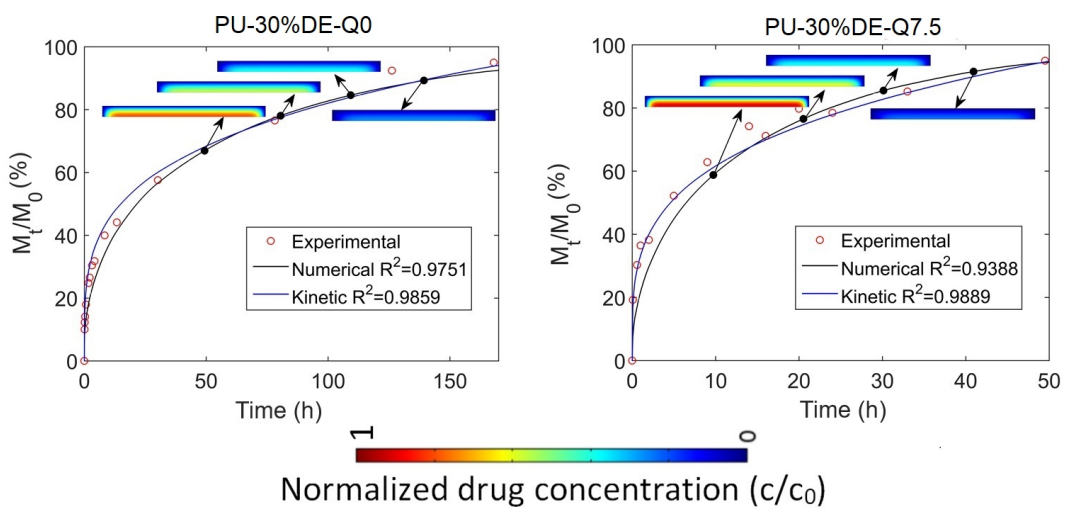


FIGURE 5.43 – Drug release from polymer at different flow rate with drug dosage of 30%

5.3. NUMERICAL SIMULATION

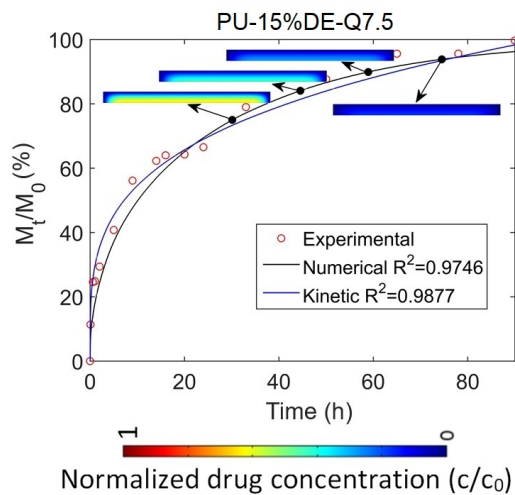


FIGURE 5.44 – Drug release from polymer at different flow rate with drug dosage of 15%

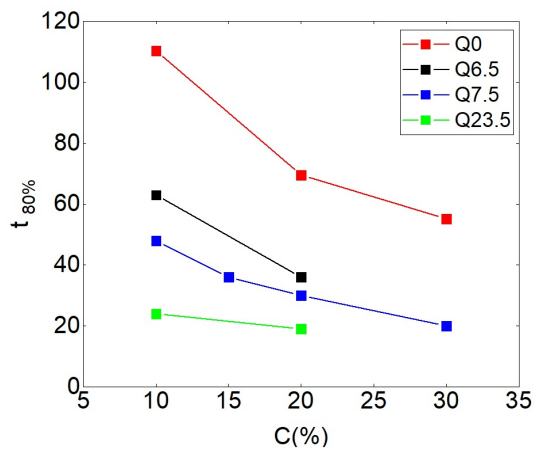


FIGURE 5.45 – Characteristic time versus initial drug concentration at different flow rates

Chapitre 6

Conclusions and perspectives

6.1 Conclusions

This thesis falls within the general framework of thrombosis generated by the employ of drug-eluting stents. Three main scientific and technical locks must be distinguished:

- The absence of the bio-relevant apparatus that can simulate the required conditions. This device can be helpful to analyze the behavior of the DESs.
- The need to understand the mechanisms guiding the kinetics of drug release, by considering the physical, chemical and mechanical properties of the compounds of drug carriers during the drug liberation rather than directly examine drug release profile from a final commodity.
- The lack of modeling allowing a reliable simulation of drug release profiles from DES. Indeed, many models and simulations are available in the literature, but validations based on bio-relevant in vitro tests are missing.

An apparatus capable of simulating both lumen and artery tissue has been developed. The blood flow, continuous or pulsed, is reproduced via a pumping system designed for the occasion. The arterial medium is mimicked by the use of a specific compartment of agarose.

The circulating system comprises two centrifugal pumps. The one ensuring the systolic and diastolic flow is a centrifugal pump developed in the laboratory. It comprises an impeller and a volute. The control of the speed of rotation of the impeller, via an input signal, makes it possible to ensure the desired pulsatility. A circulation vein made up of many and separate channels is designed and produced in Plexiglas. This allows visualization of the flow, and the simultaneous development of multiple assays. The dimensions of the channels and of the polymer films are chosen in such a way as to respect the laws of similarity of the flows. The hydraulic diameter of the chambers is 30 times larger than the normal diameter of the carotid artery. On the bottom wall of each channel, we placed a hydrogel compartment simulating the tissue artery.

Using the developed apparatus, we studied the effects of some factors influencing the drug liberation. These are, but not limited to initial drug loading, type of drug and polymer, flow rate value and flow pattern, evaporation of the solvent when making samples, polymer thickness, etc. The above parameters have shown certain influences on the release profiles:

- Increasing the drug dosage has increased the kinetic of the release and reduced the time of the

6.1. CONCLUSIONS

drug depletion from the carriers. This parameter has more affected the PU samples, due to the increase in the number of the pores, than PLGA samples.

- Increasing the flow rate has also increased the kinetics of the flow, where it was observed that the type of the flow was more influencing factor than the value of flow rate; for example, the kinetic of the release were more influenced by passing from static to steady continuous and to non-steady pulsed flow. PLGA samples were more prone to this influence.

Studying the physical, chemical and mechanical studies of these two types of polymers showed that PU samples are less sensible to the increase of the flow rate. The intrinsic properties of PU, like as the glass-temperature and its mechanical properties, did not change significantly. However, the effect of the drug percentage changes significantly the mechanical properties of this polymer and increases the free volume fraction in the samples. While, the results on the PLGA films presented that by increasing the drug percentage the polymer films become more brittle, importantly by the time of the release. This behavior is much more significant when the flow rate is rising.

We have developed a new model for predicting the release of multi-stage drugs from drug delivery systems. The shape of the release profile can result in one or more kinetic occurring. By summing a series of power functions, the proposed model adjusts this profile. Each function represents a stage and is defined by three factors (M_i , t_i and n_i), which may depend on design data for the drug support or on the conditions of its operation. They grant each stage its kinetic properties. We illustrate the concrete of this approach by presenting several cases of drug carriers. This approach stays easily applicable to other series of administration systems. It is enough to possess a set of representative experimental data. This model can be helpful to predict the release profile for a family of the drug delivery systems with considering the variation of different parameters. However, one should pay attention to the differences in the parameters, which may vary from an experiment to another. Indeed, the parameters such as drug type, flow type, method of fabrication of the samples, drug load can play a role in the disagreement of the results with the predictive model if they are not considered beforehand in the model.

The second model developed in this study is a mathematical model based on the physical mechanisms that can contribute to shaping the drug release profile from carrier-system. We considered here the most likely drug release mechanisms for PU: burst release, osmotic, diffusion and for PLGA: burst release, diffusion, swelling and erosion. The influence of the flow rate and or initial drug load on the drug-released ratios based on these mechanisms has been highlighted. In this regard, the predictive

model and the experimental results showed a good correlation. It is notable that the choice of the contributed mechanisms in the drug release should be chosen rigorously. One can note that generally by increasing the drug dosage at a constant flow rate, the characteristic release time for each mechanism decreases. It is notable that the portion of the contribution of the mechanisms varies by these two parameters which are also sensitive to the time of intervention.

Numerical simulation has been performed to predict drug release profile and visual drug distribution in the polymer during the release. The comparisons of drug release profile between numerical calculations, model of kinetic and experiments have been established, wherein the validations of numerical results have been well achieved. It has also showed that the increased flow rate and initial drug dosage contribute to the reduced drug release period. The vortices have been formed both upstream and downstream from the DES as the flow is strongly disturbed by this obstacle. The increased flow rate brings larger recirculation region and the drug distribution in polymer shows the drug release process from outer to inner of polymer gradually.

6.2 Perspectives

Many perspectives of this work can be stated. We have divided them into three parts:

1. Development of the bio-relevant test apparatus

- Assemble all the operations to provide the kinetic profile of drug carriers in an automated procedure.

- Improve the bio-relevancy of the developed apparatus, without however increasing the complexity of the two media unnecessarily. Indeed, one can consider more bio-discriminating factors such as binding-unbinding phenomena by implanting specific receptors in the hydrogel regarding the drug used. We can also work on the second medium, the circulating fluid, to better mimic the properties of blood. Finally, the device can also be sophisticated to study the other pathology such as hemolysis.

- Improve the design of the apparatus to allow the characterization of all types of stents in vitro and ex vivo trials from the harvested arteries. The results of these actions will make it possible to increase the reliability of the correlations between in vitro and ex vivo tests and thus tend towards better development of vascular implants for personalized therapy.

2. Study the feasibility of drug-eluting stent models obtained by additive manufacturing

6.2. PERSPECTIVES

- The aim here is to study and better understand the behavior of drug carriers produced by the additive manufacturing process. The motivation here is to develop materials whose biocompatibility and release kinetics properties are increased.

3. Increase in the reliability of the modeling and integration of the associated simulation tool

- Take advantage of the resulting experimental database to improve the theoretical models developed. Secondly, valorize the associated simulation software in the design of personalized drug supports.

6.2. PERSPECTIVES

Bibliographie

- [1] T. Hu, J. Yang, K. Cui, Q. Rao, T. Yin, L. Tan, Y. Zhang, Z. Li, and G. Wang, “Controlled Slow-Release Drug-Eluting Stents for the Prevention of Coronary Restenosis : Recent Progress and Future Prospects,” 2015.
- [2] G. Singh, N. A. S. Bs, and S. W. Schreiter, “Widowmaker Right Coronary Artery Treated With Drug-Eluting Stent Implantation,” *JACC Case Reports*, pp. 21–23, 2019.
- [3] W. J. Jang, J. H. Yang, Y. B. Song, J. Y. Hahn, W. J. Chun, J. H. Oh, W. S. Kim, Y. T. Lee, C. W. Yu, H. J. Lee, H. C. Gwon, and S. H. Choi, “Second-generation drug-eluting stenting versus coronary artery bypass grafting for treatment of coronary chronic total occlusion,” *Journal of Cardiology*, vol. 73, no. 5, pp. 432–437, 2019.
- [4] A. Farghadan and A. Arzani, “The combined effect of wall shear stress topology and magnitude on cardiovascular mass transport,” *International Journal of Heat and Mass Transfer*, vol. 131, pp. 252–260, 2019.
- [5] A. I. Barakat, “Blood flow and arterial endothelial dysfunction: Mechanisms and implications,” *Comptes Rendus Physique*, vol. 14, no. 6, pp. 479–496, 2013.
- [6] A. Lafont and Y. Yang, “Magnesium stent scaffolds: DREAMS become reality,” *The Lancet*, vol. 387, no. 10013, pp. 3–4, 2016.
- [7] J. Brown, C. C. O’Brien, A. C. Lopes, K. Kolandaivelu, and E. R. Edelman, “Quantification of thrombus formation in malapposed coronary stents deployed in vitro through imaging analysis,” *Journal of Biomechanics*, vol. 71, pp. 296–301, 2018.
- [8] S. J. Baron, Y. Lei, K. Chinnakondepalli, K. Vilain, E. A. Magnuson, D. J. Kereiakes, S. G. Ellis, G. W. Stone, and D. J. Cohen, “Economic Outcomes of Bioresorbable Vascular Scaffolds Versus

- Everolimus-Eluting Stents in Patients Undergoing Percutaneous Coronary Intervention: 1-Year Results From the ABSORB III Trial,” *JACC: Cardiovascular Interventions*, vol. 10, no. 8, pp. 774–782, 2017.
- [9] Y. Li, L. Wang, S. Chen, D. Yu, W. Sun, and S. Xin, “Biodegradable magnesium alloy stents as a treatment for vein graft restenosis,” *Yonsei Medical Journal*, vol. 60, no. 5, pp. 429–439, 2019.
- [10] S. McGinty, T. T. Vo, M. Meere, S. McKee, and C. McCormick, “Some design considerations for polymer-free drug-eluting stents: A mathematical approach,” *Acta Biomaterialia*, vol. 18, pp. 213–225, 2015.
- [11] K. E. Robertson, “Alternative approaches to the prevention of coronary in-stent restenosis,” Ph.D. dissertation, University of Glasgow, 2014.
- [12] W. Zhang, D. Liu, X. Han, J. Ren, P. Zhou, and P. Ding, “MicroRNA-451 inhibits vascular smooth muscle cell migration and intimal hyperplasia after vascular injury via Ywhaz/p38 MAPK pathway,” *Experimental Cell Research*, vol. 379, no. 2, pp. 214–224, 2019.
- [13] J. Torrado, L. Buckley, A. Durán, P. Trujillo, S. Toldo, J. Valle Raleigh, A. Abbate, G. Biondi-Zoccai, and L. A. Guzmán, “Restenosis, Stent Thrombosis, and Bleeding Complications: Navigating Between Scylla and Charybdis,” *Journal of the American College of Cardiology*, vol. 71, no. 15, pp. 1676–1695, 2018.
- [14] N. Ghousifam, H. Mortazavian, R. Bhowmick, Y. Vasquez, F. D. Blum, and H. Gappa-Fahlenkamp, “A three-dimensional in vitro model to demonstrate the haptotactic effect of monocyte chemoattractant protein-1 on atherosclerosis-associated monocyte migration,” *International Journal of Biological Macromolecules*, vol. 97, pp. 141–147, 2017.
- [15] H. Sun, J. Jiang, L. Gong, X. Li, Y. Yang, and Y. Luo, “Biomedicine & Pharmacotherapy Voltage-gated sodium channel inhibitor reduces atherosclerosis by modulating monocyte / macrophage subsets and suppressing macrophage proliferation,” *Biomedicine & Pharmacotherapy*, vol. 120, no. August, p. 109352, 2019.
- [16] M. C. Kim, I. S. Kim, M. H. Jeong, D. S. Sim, Y. J. Hong, J. H. Kim, Y. Ahn, J. G. Cho, and J. C. Park, “Incidence of cardiac death and recurrent stent thrombosis after treatment for

- angiographically confirmed stent thrombosis,” *Journal of Cardiology*, vol. 74, no. 3, pp. 267–272, 2019.
- [17] S. M. Kim, K. S. Park, E. Lih, Y. J. Hong, J. H. Kang, I. H. Kim, M. H. Jeong, Y. K. Joung, and D. K. Han, “Fabrication and characteristics of dual functionalized vascular stent by spatio-temporal coating,” *Journal of Acta Biomaterialia*, vol. 38, pp. 143–152, 2016.
- [18] F. Bozsak and J.-m. C. Abdul, “Modeling the transport of drugs eluted from stents : physical phenomena driving drug distribution in the arterial wall,” pp. 327–347, 2014.
- [19] S. Garg and P. W. Serruys, “Coronary stents: current status,” *Journal of the American College of Cardiology*, vol. 56, no. 10S, pp. S1–S42, 2010.
- [20] C. Premer, A. J. Kanelidis, J. M. Hare, and I. H. Schulman, “Rethinking Endothelial Dysfunction as a Crucial Target in Fighting Heart Failure,” *Mayo Clinic Proceedings: Innovations, Quality & Outcomes*, vol. 3, no. 1, pp. 1–13, 2019.
- [21] F. Rikhtegar, E. R. Edelman, U. Olgac, D. Poulikakos, and V. Kurtcuoglu, “Drug deposition in coronary arteries with overlapping drug-eluting stents,” *Journal of Controlled Release*, vol. 238, pp. 1–9, 2016.
- [22] P. D. Williams and M. Awan, “Stent selection for percutaneous coronary intervention,” *Journal of Continuing Cardiology Education*, vol. 3, no. 2, pp. 64–69, 2017.
- [23] S. Ganly, “Development of a Gene-eluting stent for the treatment of In-stent restenosis,” Ph.D. dissertation, NUI Galway, 2016.
- [24] R. X. Yin, D. Z. Yang, and J. Z. Wu, “Nanoparticle drug- and gene-eluting stents for the prevention and treatment of coronary restenosis,” *Theranostics*, vol. 4, no. 2, pp. 175–200, 2014.
- [25] W. Kempin, S. Kaule, T. Reske, N. Grabow, S. Petersen, S. Nagel, K. P. Schmitz, W. Weitschies, and A. Seidlitz, “In vitro evaluation of paclitaxel coatings for delivery via drug-coated balloons,” *European Journal of Pharmaceutics and Biopharmaceutics*, vol. 96, pp. 322–328, 2015.
- [26] J. Iqbal, J. Gunn, P. W. Serruys *et al.*, “Coronary stents: historical development, current status and future directions,” *Br Med Bull*, vol. 106, no. 1, pp. 193–211, 2013.

- [27] P. Satuluri, K. Makam, S. Vijaykumar, N. Wasty, and K. Kaid, “Delayed Stent Deformity Secondary To Unrecognized Ballon Angioplasty Behind the Stent Struts,” *Journal of the American College of Cardiology*, vol. 73, no. 9, p. 2848, 2019.
- [28] K. Liou, N. Jepson, C. Cao, R. Luo, S. Pala, and S. Y. Ooi, “Drug-eluting Balloon Versus Second Generation Drug Eluting Stents in the Treatment of In-stent Restenosis: A Systematic Review and Meta-analysis,” *Heart Lung and Circulation*, vol. 25, no. 12, pp. 1184–1194, 2016.
- [29] D. Sun, Y. Zheng, T. Yin, C. Tang, Q. Yu, and G. Wang, “Coronary drug-eluting stents: From design optimization to newer strategies,” *Journal of Biomedical Materials Research Part A*, vol. 102, no. 5, pp. 1625–1640, 2014.
- [30] P. J. Wang, N. Ferralis, C. Conway, J. C. Grossman, and E. R. Edelman, “Strain-induced accelerated asymmetric spatial degradation of polymeric vascular scaffolds,” *Proceedings of the National Academy of Sciences of the United States of America*, vol. 115, no. 11, pp. 2640–2645, 2018.
- [31] M. Kamberi and R. Rapoza, “Stability testing of drug eluting stents,” *Journal of Drug Delivery Science and Technology*, vol. 35, pp. 58–68, 2016.
- [32] F. Bozsak, D. Gonzalez-Rodriguez, Z. Sternberger, P. Belitz, T. Bewley, J. M. Chomaz, and A. I. Barakat, “Optimization of drug delivery by drug-eluting stents,” *PLoS ONE*, vol. 10, no. 6, pp. 1–29, 2015.
- [33] M. Livingston and A. Tan, “Coating techniques and release kinetics of drug-eluting stents,” *Journal of medical devices*, vol. 10, no. 1, 2016.
- [34] K. Zheng, Z. Lin, M. Capece, K. Kunnath, L. Chen, and R. N. Davé, “Effect of Particle Size and Polymer Loading on Dissolution Behavior of Amorphous Griseofulvin Powder,” *Journal of Pharmaceutical Sciences*, vol. 108, no. 1, pp. 234–242, 2019.
- [35] K. Pruessmann, M. Wentzlaff, R. Schilling, and A. Seidlitz, “Influence of Dissolution Vessel Geometry and Dissolution Medium on In Vitro Dissolution Behaviour of Triamterene-Coated Model Stents in Different Test Setups,” *AAPS PharmSciTech*, vol. 20, no. 1, pp. 1–13, 2019.

- [36] F. Farahmandghavi, M. Imani, and F. Hajiesmaelian, "Silicone matrices loaded with levonorgestrel particles: Impact of the particle size on drug release," *Journal of Drug Delivery Science and Technology*, vol. 49, pp. 132–142, 2019.
- [37] T. I. Spiridonova, S. I. Tverdokhlebov, and Y. G. Anissimov, "Investigation of the size distribution for diffusion-controlled drug release from drug delivery systems of various geometries," *Journal of Pharmaceutical Sciences*, vol. 108, no. 8, pp. 2690 – 2697, 2019.
- [38] L. Zhang, J. Alfano, D. Race, and R. N. Davé, "Zero-order release of poorly water-soluble drug from polymeric films made via aqueous slurry casting," *European Journal of Pharmaceutical Sciences*, vol. 117, no. January, pp. 245–254, 2018.
- [39] A. K. S. Chandel, "Devices for controlled release advancements and effectiveness," pp. 103–134, 2018.
- [40] M. Galizia, C. Daniel, G. Guerra, and G. Mensitieri, "Solubility and diffusivity of low molecular weight compounds in semi-crystalline poly-(2, 6-dimethyl-1, 4-phenylene) oxide: The role of the crystalline phase," *Journal of membrane science*, vol. 443, pp. 100–106, 2013.
- [41] A. Raval, J. Parikh, and C. Engineer, "Mechanism of controlled release kinetics from medical devices," *Brazilian Journal of Chemical Engineering*, vol. 27, no. 2, pp. 211–225, 2010.
- [42] J. M. Bermúdez, A. G. Cid, A. I. Romero, M. Villegas, N. A. Villegas, and S. D. Palma, *New trends in the antimicrobial agents delivery using nanoparticles*. Elsevier, 2017.
- [43] S. Fredenberg, M. Wahlgren, M. Reslow, and A. Axelsson, "The mechanisms of drug release in poly(lactic-co-glycolic acid)-based drug delivery systems - A review," *International Journal of Pharmaceutics*, vol. 415, no. 1-2, pp. 34–52, 2011.
- [44] F. Yang, X. Zhang, L. Song, H. Cui, J. N. Myers, T. Bai, Y. Zhou, Z. Chen, and N. Gu, "Controlled Drug Release and Hydrolysis Mechanism of Polymer–Magnetic Nanoparticle Composite," *ACS Applied Materials & Interfaces*, vol. 7, no. 18, pp. 9410–9419, may 2015.
- [45] E. Mayr, *Animal species and evolution*. Harvard University Press, 2013.
- [46] C. F. Jasso-Gastinel, J. F. Soltero-Martínez, and E. Mendizábal, "Introduction: Modifiable Characteristics and Applications," *Modification of Polymer Properties*, pp. 1–21, 2016.

- [47] N. L. Davison, F. Barrère-de Groot, and D. W. Grijpma, *Degradation of biomaterials*. Elsevier, 2014.
- [48] N. Khatri, “Oral osmotic drug delivery system: A Review,” *International Journal of Pharmaceutical sciences and research*, vol. 7, no. 6, pp. 2302–2312, 2016.
- [49] F. Horkay, I. Horkayne-Szakaly, and P. J. Basser, “Measurement of the osmotic properties of thin polymer films and biological tissue samples,” *Biomacromolecules*, vol. 6, no. 2, pp. 988–993, 2005.
- [50] L. Brannon-Peppas *et al.*, “Polymers in controlled drug delivery,” *Medical Plastic and Biomaterials*, vol. 4, pp. 34–45, 1997.
- [51] H. Gasmi, “Controlled release microparticles: impact of swelling on the drug release kinetics,” Ph.D. dissertation, Université du Droit et de la Santé-Lille II, 2015.
- [52] J. Hjærtstam, *Ethyl cellulose membranes used in modified release formulations*. Chalmers University of Technology, 1998.
- [53] E. L. Cussler and E. L. Cussler, *Diffusion: mass transfer in fluid systems*. Cambridge university press, 2009.
- [54] S. Fredenberg, M. Wahlgren, M. Reslow, and A. Axelsson, “The mechanisms of drug release in poly (lactic-co-glycolic acid)-based drug delivery systems—a review,” *International journal of pharmaceutics*, vol. 415, no. 1-2, pp. 34–52, 2011.
- [55] J. Mönkäre, “Novel materials for controlled peptide delivery: mesoporous silicon and photocross-linked poly (ester anhydride) s,” Ph.D. dissertation, Itä-Suomen yliopisto, 2012.
- [56] J. Y. Cherng, T. Y. Hou, M. F. Shih, H. Talsma, and W. E. Hennink, “Polyurethane-based drug delivery systems,” *International Journal of Pharmaceutics*, vol. 450, no. 1-2, pp. 145–162, 2013.
- [57] Q. Guo, P. T. Knight, and P. T. Mather, “Tailored drug release from biodegradable stent coatings based on hybrid polyurethanes,” *Journal of Controlled Release*, vol. 137, no. 3, pp. 224–233, 2009.
- [58] J. Ritums, “Diffusion, swelling and mechanical properties of polymers,” Ph.D. dissertation, Fiber- och polymerteknologi, 2004.

- [59] J. Li, W. C. Huang, L. Gao, J. Sun, Z. Liu, and X. Mao, "Efficient enzymatic hydrolysis of ionic liquid pretreated chitin and its dissolution mechanism," *Carbohydrate Polymers*, vol. 211, no. 5, pp. 329–335, 2019.
- [60] S. McMahon, N. Bertollo, E. D. O’Cearbhaill, J. Salber, L. Pierucci, P. Duffy, T. Dürig, V. Bi, and W. Wang, "Bio-resorbable polymer stents: a review of material progress and prospects," *Progress in Polymer Science*, vol. 83, pp. 79–96, 2018.
- [61] H. Wang, P. Apostolidis, J. Zhu, X. Liu, A. Skarpas, and S. Erkens, "The role of thermodynamics and kinetics in rubber–bitumen systems: a theoretical overview," *International Journal of Pavement Engineering*, pp. 1–16, 2020.
- [62] S. Racovita, M. A. Lungan, I. Bunia, M. Popa, and S. Vasiliu, "Adsorption and release studies of cefuroxime sodium from acrylic ion exchange resin microparticles coated with gellan," *Reactive and Functional Polymers*, vol. 105, pp. 103–113, 2016.
- [63] Y. Gao, J. Yuan, H. Liu, Y. Yang, Y. Hou, and S. Li, "Tramadol loading, release and iontophoretic characteristics of ion-exchange fiber," *International Journal of Pharmaceutics*, vol. 465, no. 1-2, pp. 102–111, 2014.
- [64] R. Shang, C. Liu, P. Quan, H. Zhao, and L. Fang, "Effect of drug-ion exchange resin complex in betahistine hydrochloride orodispersible film on sustained release, taste masking and hygroscopicity reduction," *International Journal of Pharmaceutics*, vol. 545, no. 1-2, pp. 163–169, 2018.
- [65] A. K. SenGupta, *Ion Exchange and Solvent Extraction: A Series of Advances*, 2007, vol. 18.
- [66] T. K. Dash and V. B. Konkimalla, "Poly- ϵ -caprolactone based formulations for drug delivery and tissue engineering: A review," *Journal of Controlled Release*, vol. 158, no. 1, pp. 15–33, 2012.
- [67] K. Mulas, Z. Stefanowicz, E. Oledzka, and M. Sobczak, "Current state of the polymeric delivery systems of fluoroquinolones – A review," *Journal of Controlled Release*, vol. 294, no. December 2018, pp. 195–215, 2019.
- [68] N. C. Billingham, "Degradation and stabilization of polymers," *Materials Science and Technology*, pp. 469–507, 2006.

BIBLIOGRAPHIE

- [69] K. Chakravarty and D. C. Dalal, “A Nonlinear Mathematical Model of Drug Delivery from Polymeric Matrix,” *Bulletin of Mathematical Biology*, vol. 81, no. 1, pp. 105–130, 2019.
- [70] S. McGinty and G. Pontrelli, “A general model of coupled drug release and tissue absorption for drug delivery devices,” *Journal of Controlled Release*, vol. 217, pp. 327–336, 2015.
- [71] A. P. Ijzerman and D. Guo, “Drug – Target Association Kinetics in Drug Discovery,” *Trends in Biochemical Sciences*, pp. 1–11, 2019.
- [72] A. D. Levin, N. Vukmirovic, C. W. Hwang, and E. R. Edelman, “Specific binding to intracellular proteins determines arterial transport properties for rapamycin and paclitaxel,” *Proceedings of the National Academy of Sciences of the United States of America*, vol. 101, no. 25, pp. 9463–9467, 2004.
- [73] C.-W. Hwang, A. D. Levin, M. Jonas, P. H. Li, and E. R. Edelman, “Thrombosis modulates arterial drug distribution for drug-eluting stents,” *Circulation*, vol. 111, no. 13, pp. 1619–1626, 2005.
- [74] A. M. Master, M. E. Rodriguez, M. E. Kenney, N. L. Oleinick, and A. Sen Gupta, “Delivery of the photosensitizer Pc 4 in PEG–PCL micelles for in vitro PDT studies,” *Journal of pharmaceutical sciences*, vol. 99, no. 5, pp. 2386–2398, 2010.
- [75] J. Pang, Y. Luan, F. Li, X. Cai, J. Du, and Z. Li, “Ibuprofen-loaded poly(lactic-co-glycolic acid) films for controlled drug release.” *International journal of nanomedicine*, vol. 6, pp. 659–665, 2011.
- [76] T. W. J. Steele, C. L. Huang, E. Widjaja, F. Y. C. Boey, J. S. C. Loo, and S. S. Venkatraman, “The effect of polyethylene glycol structure on paclitaxel drug release and mechanical properties of PLGA thin films,” *Acta Biomaterialia*, vol. 7, no. 5, pp. 1973–1983, 2011.
- [77] Q. Zheng, Z. Chu, X. Li, H. Kang, X. Yang, and Y. Fan, “The effect of fluid shear stress on the in vitro release kinetics of sirolimus from PLGA films,” *Polymers*, vol. 9, no. 11, pp. 1–12, 2017.
- [78] E. Vey, C. Rodger, J. Booth, M. Claybourn, A. F. Miller, and A. Saiani, “Degradation kinetics of poly(lactic-co-glycolic) acid block copolymer cast films in phosphate buffer solution as revealed

- by infrared and Raman spectroscopies,” *Polymer Degradation and Stability*, vol. 96, no. 10, pp. 1882–1889, 2011.
- [79] Jessica E. Montanez, “Impact of flow pulsatility on arterial drug distribution in stent-based therapy,” *Bone*, vol. 23, no. 1, pp. 1–7, 2012.
- [80] P. R. Vijayaratnam, J. A. Reizes, and T. J. Barber, “Flow-mediated drug transport from drug-eluting stents is negligible: numerical and in-vitro investigations,” *Annals of biomedical engineering*, vol. 47, no. 3, pp. 878–890, 2019.
- [81] F. Chabi, “Etude numérique et expérimentale du transfert de masse, par advection et diffusion en écoulement pulsé, sur des stents actifs.” Ph.D. dissertation, Paris, ENSAM, 2016.
- [82] J. Song, S. Kouidri, and F. Bakir, “Numerical study on flow topology and hemodynamics in tortuous coronary artery with symmetrical and asymmetrical stenosis,” *Biocybernetics and Biomedical Engineering*, vol. 41, no. 1, pp. 142–155, 2021.
- [83] M. G. Mennuni, P. A. Pagnotta, and G. G. Stefanini, “Coronary Stents: The Impact of Technological Advances on Clinical Outcomes,” *Annals of Biomedical Engineering*, vol. 44, no. 2, pp. 488–496, 2016.
- [84] D. Surgery and S. D. College, “Drug delivery through drug eluting stents-A Review,” *International Journal of Scientific Research*, vol. 6, no. 9, pp. 20–22, 2017.
- [85] P. Gasior, Y. Cheng, A. F. Valencia, J. McGregor, G. B. Conditt, G. L. Kaluza, and J. F. Granada, “Impact of Fluoropolymer-Based Paclitaxel Delivery on Neointimal Proliferation and Vascular Healing: A Comparative Peripheral Drug-Eluting Stent Study in the Familial Hypercholesterolemic Swine Model of Femoral Restenosis,” *Circulation: Cardiovascular Interventions*, vol. 10, no. 5, pp. 1–11, 2017.
- [86] A. Ernst and J. Bulum, “New generations of drug-eluting stents-a brief review,” *EMJ Int Cardiol*, vol. 1, pp. 100–6, 2014.
- [87] P. K. Bundhun, M. Pursun, and F. Huang, “Biodegradable polymer drug-eluting stents versus first-generation durable polymer drug-eluting stents,” *Medicine*, vol. 96, no. 47, p. e8878, 2017.

- [88] J. Jang, “3D Bioprinting and In Vitro Cardiovascular Tissue Modeling,” *Bioengineering*, vol. 4, no. 3, p. 71, 2017.
- [89] Z. Othman, B. Cillero Pastor, S. van Rijt, and P. Habibovic, “Understanding interactions between biomaterials and biological systems using proteomics,” *Biomaterials*, vol. 167, pp. 191–204, 2018.
- [90] Y. Guan, L. Wang, J. Lin, and M. W. King, “Compliance study of endovascular stent grafts incorporated with polyester and polyurethane graft materials in both stented and unstented zones,” *Materials*, vol. 9, no. 8, 2016.
- [91] E. H. Seo and K. Na, “Polyurethane membrane with porous surface for controlled drug release in drug eluting stent,” *Biomaterials Research*, vol. 18, no. 1, 2014.
- [92] W. Chen, C. di Carlo, D. Devery, D. J. McGrath, P. E. McHugh, K. Kleinsteinberg, S. Jockenhoevel, W. E. Hennink, and R. J. Kok, “Fabrication and characterization of gefitinib-releasing polyurethane foam as a coating for drug-eluting stent in the treatment of bronchotracheal cancer,” *International Journal of Pharmaceutics*, vol. 548, no. 2, pp. 803–811, 2018.
- [93] R. B. Seymour and C. E. Carraher, *Polymer chemistry*. Marcel Dekker New York, 1981, vol. 181.
- [94] K. Troev, V. Atanasov, R. Tsevi, G. Grancharov, and A. Tsekova, “Chemical degradation of polyurethanes. degradation of microporous polyurethane elastomer by dimethyl phosphonate,” *Polymer Degradation and Stability*, vol. 67, no. 1, pp. 159–165, 2000.
- [95] T. Wang, P. Xue, A. Wang, M. Yin, J. Han, S. Tang, and R. Liang, “Pore change during degradation of octreotide acetate-loaded PLGA microspheres: The effect of polymer blends,” *European Journal of Pharmaceutical Sciences*, vol. 138, no. 30, p. 104990, 2019.
- [96] F. Li, Y. Gu, R. Hua, Z. Ni, and G. Zhao, “In vitro release study of sirolimus from a pdlla matrix on a bioresorbable drug-eluting stent,” *Journal of Drug Delivery Science and Technology*, vol. 48, pp. 88–95, 2018.
- [97] B. M. O’Connell, T. M. McGloughlin, and M. T. Walsh, “Factors that affect mass transport from drug eluting stents into the artery wall,” *Biomedical engineering online*, vol. 9, no. 1, pp. 1–16, 2010.

- [98] A. Gossart, K. G. Battiston, A. Gand, E. Pauthe, and J. P. Santerre, "Mono vs multilayer fibronectin coatings on polar/hydrophobic/ionic polyurethanes: Altering surface interactions with human monocytes," *Acta Biomaterialia*, vol. 66, pp. 129–140, 2018.
- [99] S. Babaei, N. Fekete, C. A. Hoesli, and P. L. Girard-Lauriault, "Adhesion of human monocytes to oxygen- and nitrogen- containing plasma polymers: Effect of surface chemistry and protein adsorption," *Colloids and Surfaces B: Biointerfaces*, vol. 162, pp. 362–369, 2018.
- [100] R. Das, B. Dash, H. Deka, P. S. Das, and P. Saha, "A review on drug eluting stents ," *Current Research Journal of Pharmaceutical and Allied Sciences*, vol. 2, pp. 1–9, 2018.
- [101] C. Zlomke, M. Barth, and K. Mäder, "Polymer degradation induced drug precipitation in plga implants—why less is sometimes more," *European Journal of Pharmaceutics and Biopharmaceutics*, vol. 139, pp. 142–152, 2019.
- [102] C. Thedrattanawong, C. Manaspon, and N. Nasongkla, "Controlling the burst release of doxorubicin from polymeric depots via adjusting hydrophobic/hydrophilic properties," *Journal of Drug Delivery Science and Technology*, vol. 46, pp. 446–451, 2018.
- [103] R. Langer and N. A. Peppas, "Advances in biomaterials, drug delivery, and bionanotechnology," *AIChE Journal*, vol. 49, no. 12, pp. 2990–3006, 2003.
- [104] B. O'Brien, H. Zafar, A. Ibrahim, J. Zafar, and F. Sharif, "Coronary Stent Materials and Coatings: A Technology and Performance Update," *Annals of Biomedical Engineering*, vol. 44, no. 2, pp. 523–535, 2016.
- [105] W. Yao, Y. Bao, and Y. Chen, "Formation of microcapsules by ultrasound stimulation for use in remote-controlled drug-eluting stents," *Medical Engineering and Physics*, vol. 56, pp. 42–47, 2018.
- [106] A. H. Chow, H. H. Tong, P. Chattopadhyay, and B. Y. Shekunov, "Particle engineering for pulmonary drug delivery," *Pharmaceutical Research*, vol. 24, no. 3, pp. 411–437, 2007.
- [107] S. A. Park, S. J. Lee, K. S. Lim, I. H. Bae, J. H. Lee, W. D. Kim, M. H. Jeong, and J. K. Park, "In vivo evaluation and characterization of a bio-absorbable drug-coated stent fabricated using a 3D-printing system," *Materials Letters*, vol. 141, pp. 355–358, 2015.

- [108] S. J. Lee, H. H. Jo, K. S. Lim, D. Lim, S. Lee, J. H. Lee, W. D. Kim, M. H. Jeong, J. Y. Lim, I. K. Kwon *et al.*, “Heparin coating on 3d printed poly (l-lactic acid) biodegradable cardiovascular stent via mild surface modification approach for coronary artery implantation,” *Chemical Engineering Journal*, vol. 378, p. 122116, 2019.
- [109] S. Borhani, S. Hassanajili, S. H. A. Tafti, and S. Rabbani, *Cardiovascular stents: overview, evolution, and next generation*. Springer, 2018, vol. 7, no. 3.
- [110] W. Kempin, C. Franz, L. C. Koster, F. Schneider, M. Bogdahn, W. Weitschies, and A. Seidlitz, “Assessment of different polymers and drug loads for fused deposition modeling of drug loaded implants,” *European Journal of Pharmaceutics and Biopharmaceutics*, vol. 115, pp. 84–93, 2017.
- [111] F. Pilate, A. Toncheva, P. Dubois, and J. M. Raquez, “Shape-memory polymers for multiple applications in the materials world,” *European Polymer Journal*, vol. 80, pp. 268–294, 2016.
- [112] M. Ansari, M. Golzar, M. Baghani, and M. Soleimani, “Shape memory characterization of poly (ϵ -caprolactone)(pcl)/polyurethane (pu) in combined torsion-tension loading with potential applications in cardiovascular stent,” *Polymer Testing*, vol. 68, pp. 424–432, 2018.
- [113] A. C. Bobel, S. Lohfeld, R. N. Shirazi, and P. E. McHugh, “Experimental mechanical testing of Poly (L-Lactide) (PLLA) to facilitate pre-degradation characteristics for application in cardiovascular stenting,” *Polymer Testing*, vol. 54, pp. 150–158, 2016.
- [114] A. Lauto, M. Ohebshalom, M. Esposito, J. Mingin, P. Li, D. Felsen, M. Goldstein, and D. Poppas, “Self-expandable chitosan stent: design and preparation,” *Biomaterials*, vol. 22, no. 13, pp. 1869–1874, 2001.
- [115] W. Shi, C. Gu, H. Jiang, M. Zhang, and M. Lang, “Effects of amphiphilic chitosan-g-poly(ϵ -caprolactone) polymer additives on paclitaxel release from drug eluting implants,” *Journal of Materials Science and Engineering C*, vol. 45, pp. 502–509, 2014.
- [116] W. H. Kaesemeyer, K. G. Sprankle, J. N. Kremsky, W. Lau, M. N. Helmus, and G. S. Ghatnekar, “Bioresorbable polystatin fourth-generation stents,” *Coronary artery disease*, vol. 24, no. 6, pp. 516–521, 2013.

BIBLIOGRAPHIE

- [117] P. Saha and P. S. Das, “Advances in controlled release technology in pharmaceuticals: A review,” *World Journal of Pharmacy and Pharmaceutical Sciences*, vol. 6, no. 9, pp. 2070–2084, 2017.
- [118] C.-W. Hwang, D. Wu, and E. R. Edelman, “Physiological transport forces govern drug distribution for stent-based delivery,” *Circulation*, vol. 104, no. 5, pp. 600–605, 2001.
- [119] Jiang Xu, “Contribution à la fabrication de nanoparticules en utilisant des techniques microfluidiques applications à la libération de médicaments,” Ph.D. dissertation, 2016.
- [120] S. Chakraborty, M. Khandai, A. Sharma, C. N. Patra, V. J. Patro, and K. K. Sen, “Effects of drug solubility on the release kinetics of water soluble and insoluble drugs from HPMC based matrix formulations,” *Acta Pharmaceutica*, vol. 59, no. 3, pp. 313–323, 2009.
- [121] X. Wang, S. S. Venkatraman, F. Y. Boey, J. S. Loo, and L. P. Tan, “Controlled release of sirolimus from a multilayered PLGA stent matrix,” *Biomaterials*, vol. 27, no. 32, pp. 5588–5595, 2006.
- [122] F. C. Nelson, S. J. Stachel, C. Eng, and S. N. Sehgal, “Manipulation of the C(22)–C(27) region of rapamycin: stability issues and biological implications,” *Bioorganic & medicinal chemistry letters*, vol. 9, no. 2, pp. 295–300, 1999.
- [123] C. Naseerali, P. Hari, and K. Sreenivasan, “The release kinetics of drug eluting stents containing sirolimus as coated drug: role of release media,” *Journal of Chromatography B*, vol. 878, no. 7-8, pp. 709–712, 2010.
- [124] K. Pruessmann, M. Wentzlaff, R. Schilling, and A. Seidlitz, “Influence of dissolution vessel geometry and dissolution medium on in vitro dissolution behaviour of triamterene-coated model stents in different test setups,” *AAPS PharmSciTech*, vol. 20, no. 1, pp. 1–13, 2019.
- [125] A. Raval, A. Parmar, A. Raval, and P. Bahadur, “Preparation and optimization of media using pluronic® micelles for solubilization of sirolimus and release from the drug eluting stents,” *Colloids and Surfaces B: Biointerfaces*, vol. 93, pp. 180–187, 2012.
- [126] K. Jelonek, P. Karpeta, J. Jaworska, M. Pastusiak, J. Włodarczyk, J. Kasperczyk, and P. Dobrzyński, “Comparison of extraction methods of sirolimus from polymeric coatings of bioresorbable vascular scaffolds,” *Materials Letters*, vol. 214, pp. 220–223, 2018.

- [127] M. Merciadetz, L. Alquier, R. Mehta, A. Patel, and A. Wang, “A novel method for the elution of sirolimus (Rapamycin) in drug-eluting stents,” *Dissolution Technologies*, vol. 18, no. 4, pp. 37–42, 2011.
- [128] S. McGinty, “A decade of modelling drug release from arterial stents,” *Mathematical biosciences*, vol. 257, pp. 80–90, 2014.
- [129] A. Neubert, K. Sternberg, S. Nagel, C. Harder, K.-p. Schmitz, H. K. Kroemer, and W. Weitschies, “Development of a vessel-simulating flow-through cell method for the in vitro evaluation of release and distribution from drug-eluting stents,” *Journal of Controlled Release*, vol. 130, pp. 2–8, 2008.
- [130] B. Semmling, S. Nagel, K. Sternberg, W. Weitschies, and A. Seidlitz, “Long-term stable hydrogels for biorelevant dissolution testing of drug-eluting stents,” *J Pharm Technol Drug Res*, vol. 2, p. 19, 2013.
- [131] B. Semmling, S. Nagel, K. Sternberg, W. Weitschies, and A. Seidlitz, “Impact of different tissue-simulating hydrogel compartments on in vitro release and distribution from drug-eluting stents,” *European Journal of Pharmaceutics and Biopharmaceutics*, vol. 87, no. 3, pp. 570–578, 2014.
- [132] A. R. Tzafiriri, A. Groothuis, G. S. Price, and E. R. Edelman, “Stent elution rate determines drug deposition and receptor-mediated effects,” *Journal of Controlled Release*, vol. 161, no. 3, pp. 918–926, 2012.
- [133] J. Bandomir, S. Kaule, K.-P. Schmitz, K. Sternberg, S. Petersen, and U. Kragl, “Usage of different vessel models in a flow-through cell: in vitro study of a novel coated balloon catheter,” *RSC Advances*, vol. 5, no. 15, pp. 11 604–11 610, 2015.
- [134] D. M. Martin and F. J. Boyle, “Drug-eluting stents for coronary artery disease: a review,” *Medical engineering & physics*, vol. 33, no. 2, pp. 148–163, 2011.
- [135] M. Joner, G. Nakazawa, A. V. Finn, S. C. Quee, L. Coleman, E. Acampado, P. S. Wilson, K. Skorija, Q. Cheng, X. Xu *et al.*, “Endothelial cell recovery between comparator polymer-based drug-eluting stents,” *Journal of the American College of Cardiology*, vol. 52, no. 5, pp. 333–342, 2008.

- [136] B. Balakrishnan, A. R. Tzafiriri, P. Seifert, A. Groothuis, C. Rogers, and E. R. Edelman, "Strut position, blood flow, and drug deposition: implications for single and overlapping drug-eluting stents," *Circulation*, vol. 111, no. 22, pp. 2958–2965, 2005.
- [137] G. Song, H. Wu, K. Yoshino, and W. C. Zamboni, "Factors affecting the pharmacokinetics and pharmacodynamics of liposomal drugs," *Journal of liposome research*, vol. 22, no. 3, pp. 177–192, 2012.
- [138] S. Bak, S. Tischer, A. Dragon, S. Ravens, L. Pape, C. Koenecke, M. Oelke, R. Blasczyk, B. Maecker-Kolhoff, and B. Eiz-Vesper, "Selective effects of mtor inhibitor sirolimus on naïve and cmv-specific t cells extending its applicable range beyond immunosuppression," *Frontiers in immunology*, vol. 9, p. 2953, 2018.
- [139] M. A. Lovich, C. Creel, K. Hong, C.-W. Hwang, and E. R. Edelman, "Carrier proteins determine local pharmacokinetics and arterial distribution of paclitaxel," *Journal of pharmaceutical sciences*, vol. 90, no. 9, pp. 1324–1335, 2001.
- [140] B. Semmling, S. Nagel, K. Sternberg, W. Weitschies, and A. Seidlitz, "Development of Hydrophobized Alginate Hydrogels for the Vessel-Simulating Flow-Through Cell and Their Usage for Biorelevant Drug-Eluting Stent Testing," vol. 14, no. 3, 2013.
- [141] S. Beier, J. Ormiston, M. Webster, J. Cater, S. Norris, P. Medrano-Gracia, A. Young, and B. Cowan, "Hemodynamics in Idealized Stented Coronary Arteries: Important Stent Design Considerations," *Annals of Biomedical Engineering*, vol. 44, no. 2, pp. 315–329, 2016.
- [142] Y. Huang, S. S. Venkatraman, F. Y. Boey, E. M. Lahti, P. Umashankar, M. Mohanty, S. Arumugam, L. Khanolkar, and S. Vaishnav, "In vitro and in vivo performance of a dual drug-eluting stent (ddes)," *Biomaterials*, vol. 31, no. 15, pp. 4382–4391, 2010.
- [143] W. Khan, S. Farah, A. Nyska, and A. J. Domb, "Carrier free rapamycin loaded drug eluting stent: in vitro and in vivo evaluation," *Journal of Controlled Release*, vol. 168, no. 1, pp. 70–76, 2013.
- [144] N. Abbasnezhad, M. Shirinbayan, A. Tcharkhtchi, and F. Bakir, "In vitro study of drug release from various loaded polyurethane samples and subjected to different non-pulsed flow rates," *Journal of Drug Delivery Science and Technology*, vol. 55, p. 101500, 2020.

- [145] U. Gbureck, E. Vorndran, and J. E. Barralet, "Modeling vancomycin release kinetics from microporous calcium phosphate ceramics comparing static and dynamic immersion conditions," *Acta biomaterialia*, vol. 4, no. 5, pp. 1480–1486, 2008.
- [146] G. Acharya and K. Park, "Mechanisms of controlled drug release from drug-eluting stents," *Advanced drug delivery reviews*, vol. 58, no. 3, pp. 387–401, 2006.
- [147] P. Minghetti, F. Cilurzo, F. Selmin, A. Casiraghi, A. Grignani, and L. Montanari, "Sculptured drug-eluting stent for the on-site delivery of tacrolimus," *European journal of pharmaceuticals and biopharmaceutics*, vol. 73, no. 3, pp. 331–336, 2009.
- [148] M. Arafat, P. Fouladian, A. Wignall, Y. Song, A. Parikh, H. Albrecht, C. A. Prestidge, S. Garg, and A. Blencowe, "Development and in vitro evaluation of 5-fluorouracil-eluting stents for the treatment of colorectal cancer and cancer-related obstruction," *Pharmaceutics*, vol. 13, no. 1, p. 17, 2021.
- [149] M. J. Garcia-Fernandez, M. Maton, Y. Benzine, N. Tabary, E. J. Baptiste, M. Gargouri, M. Bria, N. Blanchemain, and Y. Karrouit, "Ciprofloxacin loaded vascular prostheses functionalized with poly-methylbeta-cyclodextrin: The importance of in vitro release conditions," *Journal of Drug Delivery Science and Technology*, vol. 53, p. 101166, 2019.
- [150] X. Ma, Y. Xiao, H. Xu, K. Lei, and M. Lang, "Preparation, degradation and in vitro release of ciprofloxacin-eluting ureteral stents for potential antibacterial application," *Materials Science and Engineering: C*, vol. 66, pp. 92–99, 2016.
- [151] M.-C. Chen, H.-F. Liang, Y.-L. Chiu, Y. Chang, H.-J. Wei, and H.-W. Sung, "A novel drug-eluting stent spray-coated with multi-layers of collagen and sirolimus," *Journal of controlled release*, vol. 108, no. 1, pp. 178–189, 2005.
- [152] A. Prostyakova, D. Zybin, and D. Kapustin, "In vitro evaluation of drug content in and drug release kinetics from stents with different types of polymer coating," *Pharmaceutical Chemistry Journal*, vol. 52, no. 12, pp. 1011–1015, 2019.
- [153] C. Sarısözen, B. Arıca, A. A. Hıncal, and S. Çalış, "Development of biodegradable drug releasing polymeric cardiovascular stents and in vitro evaluation," *Journal of microencapsulation*, vol. 26, no. 6, pp. 501–512, 2009.

- [154] X. Ma, S. Oyamada, F. Gao, T. Wu, M. P. Robich, H. Wu, X. Wang, B. Buchholz, S. McCarthy, Z. Gu *et al.*, “Paclitaxel/sirolimus combination coated drug-eluting stent: in vitro and in vivo drug release studies,” *Journal of pharmaceutical and biomedical analysis*, vol. 54, no. 4, pp. 807–811, 2011.
- [155] A. Kraitzer, L. Ofek, R. Schreiber, and M. Zilberman, “Long-term in vitro study of paclitaxel-eluting bioresorbable core/shell fiber structures,” *Journal of controlled release*, vol. 126, no. 2, pp. 139–148, 2008.
- [156] A. Seidlitz, W. Schick, T. Reske, V. Senz, N. Grabow, S. Petersen, S. Nagel, and W. Weitschies, “In vitro study of sirolimus release from a drug-eluting stent: comparison of the release profiles obtained using different test setups,” *European Journal of Pharmaceutics and Biopharmaceutics*, vol. 93, pp. 328–338, 2015.
- [157] J. Bandomir, S. Kaule, K. P. Schmitz, K. Sternberg, S. Petersen, and U. Kragl, “Usage of different vessel models in a flow-through cell: In vitro study of a novel coated balloon catheter,” *RSC Advances*, vol. 5, no. 15, pp. 11 604–11 610, 2015.
- [158] N. Benard, D. Coisne, E. Donal, and R. Perrault, “Experimental study of laminar blood flow through an artery treated by a stent implantation: Characterisation of intra-stent wall shear stress,” *Journal of Biomechanics*, vol. 36, no. 7, pp. 991–998, 2003.
- [159] A. Seidlitz, S. Nagel, B. Semmling, N. Grabow, K. Sternberg, and W. Weitschies, “Biorelevant dissolution testing of drug-eluting stents: Experiences with a modified flow-through cell setup,” *Dissolution Technologies*, vol. 18, no. 4, pp. 26–35, 2011.
- [160] N. Benard, R. Perrault, and D. Coisne, “Computational approach to estimating the effects of blood properties on changes in intra-stent flow,” *Annals of Biomedical Engineering*, vol. 34, no. 8, pp. 1259–1271, 2006.
- [161] D. N. Ku and D. P. Giddens, “Pulsatile flow in a model carotid bifurcation,” *Arteriosclerosis*, vol. 3, no. 1, pp. 31–39, 1983.
- [162] X. Zhu and R. D. Braatz, “A mechanistic model for drug release in PLGA biodegradable stent coatings coupled with polymer degradation and erosion,” no. March, pp. 2269–2279, 2014.

BIBLIOGRAPHIE

- [163] N. Fotaki and S. Klein, *In Vitro Drug Release Testing of Special Dosage Forms*. John Wiley & Sons, 2019.
- [164] A. Hermans, P. Dorozynski, F. J. Muzzio, H. Li, S. Nielsen, S. Chen, C. Reppas, S. Klein, S. Patel, M. Wacker *et al.*, “Workshop report: Usp workshop on advancements in in vitro performance testing of drug products,” *Dissolution Technologies*, vol. 27, no. 2, pp. 52–70, 2020.
- [165] N. Abbasnezhad, F. Bakir, M. Shirinbayan, and B. Maurel, “New mathematical model based on the kinetic profile for the prediction of multistage drug release from delivery systems,” *International Journal of Pharmacy*, vol. 10, no. 2, pp. 1–8, 2020.
- [166] J. Siepmann and F. Siepmann, “Mathematical modeling of drug delivery,” *International journal of pharmaceutics*, vol. 364, no. 2, pp. 328–343, 2008.
- [167] J. R. Medina, M. Cortes, and E. Romo, “Comparison of the usp apparatus 2 and 4 for testing the in vitro release performance of ibuprofen generic suspensions,” *Int J Appl Pharm*, vol. 9, no. 4, pp. 90–5, 2017.
- [168] S. Thomas, P. Balakrishnan, and M. S. Sreekala, *Fundamental biomaterials: ceramics*. Woodhead Publishing, 2018.
- [169] P. Bourget, A. Amin, F. Vidal, C. Merlette, P. Troude, and O. Corriol, “Raman spectroscopy applied to analytical quality control of injectable drugs: analytical evaluation and comparative economic versus hplc and uv/visible-ftir,” *Journal de pharmacie de Belgique*, no. 3, pp. 32–45, 2013.
- [170] P. Bourget, A. Amin, F. Vidal, C. Merlette, and F. Lagarce, “Comparison of Raman spectroscopy vs. high performance liquid chromatography for quality control of complex therapeutic objects: Model of elastomeric portable pumps filled with a fluorouracil solution,” *Journal of Pharmaceutical and Biomedical Analysis*, vol. 91, pp. 176–184, 2014.
- [171] X. Huang and C. S. Brazel, “On the importance and mechanisms of burst release in matrix-controlled drug delivery systems,” *Journal of controlled release*, vol. 73, no. 2-3, pp. 121–136, 2001.

- [172] T. Mona, I. Lagzi, and Á. Havasi, "Solving reaction-diffusion and advection problems with richardson extrapolation," *Journal of Chemistry*, vol. 2015, p. 350362, 2015.
- [173] W. S. Lim, K. Chen, T. W. Chong, G. M. Xiong, W. R. Birch, J. Pan, B. H. Lee, P. S. Er, A. V. Salvekar, S. S. Venkatraman, and Y. Huang, "A bilayer swellable drug-eluting ureteric stent: Localized drug delivery to treat urothelial diseases," *Journal of Biomaterials*, vol. 165, pp. 25–38, 2018.
- [174] C. Mircioiu, V. Voicu, V. Anuta, A. Tudose, C. Celia, D. Paolino, M. Fresta, R. Sandulovici, and I. Mircioiu, "Mathematical modeling of release kinetics from supramolecular drug delivery systems," *Pharmaceutics*, vol. 11, no. 3, p. 140, 2019.
- [175] E. Gudiño and A. Sequeira, "3D mathematical model for blood flow and non-Fickian mass transport by a coronary drug-eluting stent," *Applied Mathematical Modelling*, vol. 46, pp. 161–180, 2017.
- [176] T. Higuchi, "Mechanism of sustained-action medication. theoretical analysis of rate of release of solid drugs dispersed in solid matrices," *Journal of pharmaceutical sciences*, vol. 52, no. 12, pp. 1145–1149, 1963.
- [177] H. Baishya, "Application of Mathematical Models in Drug Release Kinetics of Carbidopa and Levodopa ER Tablets," *Journal of Developing Drugs*, vol. 06, no. 02, 2017.
- [178] P. Costa, "An alternative method to the evaluation of similarity factor in dissolution testing," *International journal of pharmaceutics*, vol. 220, no. 1-2, pp. 77–83, 2001.
- [179] G. Singhvi and M. Singh, "In-vitro drug release characterization models," *Int J Pharm Stud Res*, vol. 2, no. 1, pp. 77–84, 2011.
- [180] M. C. Patel and C. C. Patil, "Formulation and Evaluation of Mucoadhesive Buccal Tablets of Repaglinide," *Rajiv Gandhi University of Health Sciences Journal of Pharmaceutical Sciences*, vol. 4, no. 4, pp. 156–165, 2015.
- [181] A. Ranjan and P. K. Jha, "Experiments and modeling of controlled release behavior of commercial and model polymer-drug formulations using dialysis membrane method," *Drug Delivery and Translational Research*, vol. 10, no. 2, pp. 515–528, 2020.

- [182] H. Raslan and H. Maswadeh, "In vitro dissolution kinetic study of theophylline from mixed controlled release matrix tablets containing hydroxypropylmethyl cellulose and glycerylbehenate," *Indian journal of pharmaceutical sciences*, vol. 68, no. 3, 2006.
- [183] M. Ignacio, M. V. Chubynsky, and G. W. Slater, "Interpreting the Weibull fitting parameters for diffusion-controlled release data," *Physica A: Statistical Mechanics and its Applications*, vol. 486, pp. 486–496, 2017.
- [184] K. Galipeau, M. Socki, A. Socia, and P. A. Harmon, "Incomplete Loading of Sodium Lauryl Sulfate and Fasted State Simulated Intestinal Fluid Micelles Within the Diffusion Layers of Dispersed Drug Particles During Dissolution," *Journal of Pharmaceutical Sciences*, vol. 107, no. 1, pp. 156–169, 2018.
- [185] J. Li, J. D. Gu, and L. Pan, "Transformation of dimethyl phthalate, dimethyl isophthalate and dimethyl terephthalate by *Rhodococcus ruber* Sa and modeling the processes using the modified Gompertz model," *International Biodeterioration and Biodegradation*, vol. 55, no. 3, pp. 223–232, 2005.
- [186] I. R. Horvath and S. G. Chatterjee, "A surface renewal model for unsteady-state mass transfer using the generalized danckwerts age distribution function," *Royal Society open science*, vol. 5, no. 5, p. 172423, 2018.
- [187] S. D. Bruck, "Extension of the flory-rehner theory of swelling to an anisotropic polymer system," *Journal of research of the National Bureau of Standards. Section A, Physics and chemistry*, vol. 65, no. 6, p. 485, 1961.
- [188] D. Caccavo, S. Cascone, G. Lamberti, A. A. Barba, and A. Larsson, *Swellable Hydrogel-based Systems for Controlled Drug Delivery*, 2016.
- [189] C. S. Brazel and N. A. Peppas, "Modeling of drug release from swellable polymers," *European journal of pharmaceutics and biopharmaceutics*, vol. 49, no. 1, pp. 47–58, 2000.
- [190] P. Upadhyay, K. Nayak, K. Patel, J. Patel, S. Shah, and J. Deshpande, "Formulation development, optimization, and evaluation of sustained release tablet of valacyclovir hydrochloride by combined approach of floating and swelling for better gastric retention," *Drug Delivery and Translational Research*, vol. 4, no. 5-6, pp. 452–464, 2014.

BIBLIOGRAPHIE

- [191] M. Mudgil and P. K. Pawar, "Preparation and in vitro/ex vivo evaluation of moxifloxacin-loaded plga nanosuspensions for ophthalmic application," *Scientia pharmaceutica*, vol. 81, no. 2, pp. 591–606, 2013.
- [192] H. Kim and R. Fassihi, "Application of binary polymer system in drug release rate modulation. 2. influence of formulation variables and hydrodynamic conditions on release kinetics," *Journal of pharmaceutical sciences*, vol. 86, no. 3, pp. 323–328, 1997.
- [193] J. L. Ford, M. H. Rubinstein, F. McCaul, J. E. Hogan, and P. J. Edgar, "Importance of drug type, tablet shape and added diluents on drug release kinetics from hydroxypropylmethylcellulose matrix tablets," *International journal of pharmaceutics*, vol. 40, no. 3, pp. 223–234, 1987.
- [194] S. Argin, P. Kofinas, and Y. M. Lo, "The cell release kinetics and the swelling behavior of physically crosslinked xanthan-chitosan hydrogels in simulated gastrointestinal conditions," *Food Hydrocolloids*, vol. 40, pp. 138–144, 2014.
- [195] N. A. Peppas and J. J. Sahlin, "A simple equation for the description of solute release. iii. coupling of diffusion and relaxation," *International journal of pharmaceutics*, vol. 57, no. 2, pp. 169–172, 1989.
- [196] P. Costa and J. M. S. Lobo, "Modeling and comparison of dissolution profiles," *European journal of pharmaceutical sciences*, vol. 13, no. 2, pp. 123–133, 2001.
- [197] I. Katzhendler, A. Hoffman, G. Assaf, and F. Michel, "Modeling of Drug Release from Erodible Tablets," *Journal of Pharmaceutical Sciences*, vol. 86, no. 1, pp. 6–11, 1997.
- [198] S. Jonnalagadda and D. H. Robinson, "A bioresorbable, polylactide reservoir for diffusional and osmotically controlled drug delivery," *Aaps Pharmscitech*, vol. 1, no. 4, pp. 26–34, 2000.
- [199] C. M. McKittrick, S. McKee, S. Kennedy, K. Oldroyd, M. Wheel, G. Pontrelli, S. Dixon, S. McGinty, and C. McCormick, "Combining mathematical modelling with in vitro experiments to predict in vivo drug-eluting stent performance," *Journal of Controlled Release*, vol. 303, pp. 151–161, 2019.
- [200] A. N. F. Versypt, D. W. Pack, and R. D. Braatz, "Mathematical modeling of drug delivery from

BIBLIOGRAPHIE

- autocatalytically degradable plga microspheres—a review,” *Journal of Controlled Release*, vol. 165, no. 1, pp. 29–37, 2013.
- [201] M. Grassi and G. Grassi, “Mathematical modelling and controlled drug delivery: matrix systems,” *Current drug delivery*, vol. 2, no. 1, pp. 97–116, 2005.
- [202] L. E. Achenie, N. Pavurala *et al.*, “Modelling of drug release from a polymer matrix system,” *Novel Approaches in Drug Designing & Development*, vol. 2, no. 3, pp. 54–63, 2017.
- [203] C. Algieri, A. Epifanio, A. Garofalo, S. Aljlil, and L. Donato, “Poly (vinyl alcohol)-based membranes for metoprolol transdermal delivery,” *Materials Technology*, pp. 1–10, 2020.
- [204] T. Lu and T. L. Ten Hagen, “A novel kinetic model to describe the ultra-fast triggered release of thermosensitive liposomal drug delivery systems,” *Journal of Controlled Release*, vol. 324, pp. 669–678, 2020.
- [205] R. Hammad, I. U. Khan, S. Asghar, S. H. Khalid, M. Irfan, I. Khalid, S. U. Shah, N. Sabir, A. Ali, A. M. Yousaf *et al.*, “Multistage release matrices for potential antiplatelet therapy: Assessing the impact of polymers and sorb-cel m on floating, swelling, and release behavior,” *Journal of Drug Delivery Science and Technology*, vol. 55, p. 101387, 2020.
- [206] H. Gasmi, “Controlled release microparticles: impact of swelling on the drug release kinetics,” Ph.D. dissertation, Université du Droit et de la Santé-Lille II, 2015.
- [207] Y. Fu and W. J. Kao, “Drug release kinetics and transport mechanisms of non-degradable and degradable polymeric delivery systems,” *Expert opinion on drug delivery*, vol. 7, no. 4, pp. 429–444, 2010.
- [208] A. Lucero-Acuña, C. A. Gutiérrez-Valenzuela, R. Esquivel, and R. Guzmán-Zamudio, “Mathematical modeling and parametrical analysis of the temperature dependency of control drug release from biodegradable nanoparticles,” *RSC Advances*, vol. 9, no. 16, pp. 8728–8739, 2019.
- [209] S. Hossainy and S. Prabhu, “A mathematical model for predicting drug release from a biodurable drug-eluting stent coating,” *Journal of Biomedical Materials Research - Part A*, vol. 87, no. 2, pp. 487–493, 2008.

- [210] B. Balakrishnan, J. F. Dooley, G. Kopia, and E. R. Edelman, “Intravascular drug release kinetics dictate arterial drug deposition, retention, and distribution.” *Journal of controlled release : official journal of the Controlled Release Society*, vol. 123, no. 2, pp. 100–108, nov 2007.
- [211] P. R. Vijayaratnam, T. J. Barber, and J. A. Reizes, “The localized hemodynamics of drug-eluting stents are not improved by the presence of magnetic struts,” *Journal of Biomechanical Engineering*, vol. 139, no. 1, pp. 1–6, 2017.
- [212] S. Morlacchi, C. Chiastra, E. Cutrì, P. Zunino, F. Burzotta, L. Formaggia, G. Dubini, and F. Migliavacca, “Stent deformation, physical stress, and drug elution obtained with provisional stenting, conventional culotte and Tryton-based culotte to treat bifurcations: a virtual simulation study.” *EuroIntervention : journal of EuroPCR in collaboration with the Working Group on Interventional Cardiology of the European Society of Cardiology*, vol. 9, no. 12, pp. 1441–1453, 2014.
- [213] R. Mongrain, I. Faik, R. L. Leask, J. Rodés-Cabau, E. Larose, and O. F. Bertrand, “Effects of diffusion coefficients and struts apposition using numerical simulations for drug eluting coronary stents.” *Journal of biomechanical engineering*, vol. 129, no. 5, pp. 733–742, oct 2007.
- [214] A. P. Mandal, Sarifuddin, and P. K. Mandal, “An unsteady analysis of arterial drug transport from half-embedded drug-eluting stent,” *Applied Mathematics and Computation*, vol. 266, pp. 968–981, 2015.
- [215] V. B. Kolachalama, A. R. Tzafiriri, D. Y. Arifin, and E. R. Edelman, “Luminal flow patterns dictate arterial drug deposition in stent-based delivery,” *Journal of Controlled Release*, vol. 133, no. 1, pp. 24–30, 2009.
- [216] Y. Chen, Y. Xiong, W. Jiang, F. Yan, M. Guo, Q. Wang, and Y. Fan, “Numerical simulation on the effects of drug eluting stents at different reynolds numbers on hemodynamic and drug concentration distribution,” *Biomedical engineering online*, vol. 14, no. 1, pp. 1–12, 2015.
- [217] Y. Chen, Y. Xiong, W. Jiang, M. S. Wong, F. Yan, Q. Wang, and Y. Fan, “Numerical simulation on the effects of drug-eluting stents with different bending angles on hemodynamics and drug distribution.” *Medical & biological engineering & computing*, vol. 54, no. 12, pp. 1859–1870, dec 2016.

BIBLIOGRAPHIE

- [218] J. F. LaDisa, L. E. Olson, I. Guler, D. A. Hettrick, S. H. Audi, J. R. Kersten, D. C. Warltier, and P. S. Pagel, “Stent design properties and deployment ratio influence indexes of wall shear stress: A three-dimensional computational fluid dynamics investigation within a normal artery,” *Journal of Applied Physiology*, vol. 97, no. 1, pp. 424–430, 2004.
- [219] T. Seo, L. G. Schachter, and A. I. Barakat, “Computational study of fluid mechanical disturbance induced by endovascular stents.” *Annals of biomedical engineering*, vol. 33, no. 4, pp. 444–456, apr 2005.
- [220] B. Balakrishnan, A. R. Tzafiriri, P. Seifert, A. Groothuis, C. Rogers, and E. R. Edelman, “Strut position, blood flow, and drug deposition: implications for single and overlapping drug-eluting stents.” *Circulation*, vol. 111, no. 22, pp. 2958–2965, jun 2005.
- [221] J. A. Ferreira, L. Gonçalves, J. Naghipoor, P. de Oliveira, and T. Rabczuk, “The effect of plaque eccentricity on blood hemodynamics and drug release in a stented artery,” *Medical Engineering and Physics*, vol. 60, pp. 47–60, 2018.
- [222] H. Malinowski, P. Marroum, V. R. Uppoor, W. Gillespie, H.-Y. Ahn, P. Lockwood, J. Henderson, R. Baweja, M. Hossain, N. Fleischer *et al.*, “Draft guidance for industry extended-release solid oral dosage forms,” in *In Vitro-in Vivo Correlations*. Springer, 1997, pp. 269–288.
- [223] S. D’Souza, “A review of in vitro drug release test methods for nano-sized dosage forms,” *Advances in Pharmaceutics*, vol. 2014, 2014.
- [224] Y. Qiu and J. Duan, “In vitro/in vivo correlations: Fundamentals, development considerations, and applications,” in *Developing Solid Oral Dosage Forms*. Elsevier, 2017, pp. 415–452.
- [225] P. K. Tuszyński, J. Szlęk, S. Polak, R. Jachowicz, and A. Mendyk, “In vitro-in vivo correlation (ivive): From current achievements towards the future,” *Dissolution Technologies*, vol. 25, no. 3, 2018.
- [226] J. Emami *et al.*, “In vitro-in vivo correlation: from theory to applications,” *J Pharm Pharm Sci*, vol. 9, no. 2, pp. 169–189, 2006.
- [227] T. Jacobs, S. Rossenu, A. Dunne, G. Molenberghs, R. Straetemans, and L. Bijmens, “Combined

- models for data from in vitro-in vivo correlation experiments,” *Journal of Biopharmaceutical Statistics*, vol. 18, no. 6, pp. 1197–1211, 2008.
- [228] K. Sako, T. Sawada, H. Nakashima, S. Yokohama, and T. Sonobe, “Influence of water soluble fillers in hydroxypropylmethylcellulose matrices on in vitro and in vivo drug release,” *Journal of controlled release*, vol. 81, no. 1-2, pp. 165–172, 2002.
- [229] C. Tannergren, A. Bergendal, H. Lennernas, and B. Abrahamsson, “Toward an increased understanding of the barriers to colonic drug absorption in humans: implications for early controlled release candidate assessment,” *Molecular pharmaceuticals*, vol. 6, no. 1, pp. 60–73, 2009.
- [230] H. Lennernäs, “Regional intestinal drug permeation: biopharmaceutics and drug development,” *European Journal of Pharmaceutical Sciences*, vol. 57, pp. 333–341, 2014.
- [231] A. Rawat, U. Bhardwaj, and D. J. Burgess, “Comparison of in vitro–in vivo release of risperdal® consta® microspheres,” *International journal of pharmaceutics*, vol. 434, no. 1-2, pp. 115–121, 2012.
- [232] F. G. Ahsaie, G. Pazuki, T. E. Sintra, P. Carvalho, and S. P. Ventura, “Study of the partition of sodium diclofenac and norfloxacin in aqueous two-phase systems based on copolymers and dextran,” *Fluid Phase Equilibria*, vol. 530, p. 112868, 2021.
- [233] T. Sood, S. Roy, and M. Pathak, “Effect of pulse rate variation on blood flow through axisymmetric and asymmetric stenotic artery models,” *Mathematical biosciences*, vol. 298, pp. 1–18, 2018.
- [234] M. Asuaje, F. Bakir, S. Kouidri, F. Kenyery, and R. Rey, “Numerical modelization of the flow in centrifugal pump: volute influence in velocity and pressure fields,” *International journal of rotating machinery*, vol. 2005, no. 3, pp. 244–255, 2005.
- [235] A. Adánez Ceballo and E. Cano Pleite, “Développement d’un banc biomédical d’étude de la resténose et la mise au point des stents actifs pro-cicatrisants (2),” Master’s thesis, 2011.
- [236] Y. Yao, L. Hao, N. Geng, Y. Jin, S. Du, and L. Xu, “Estimation of carotid artery pressure waveform by transfer function and radial pressure waveform,” in *Proceeding of the 11th World Congress on Intelligent Control and Automation*. IEEE, 2014, pp. 6090–6093.

- [237] W. L. Webber, F. Lago, C. Thanos, and E. Mathiowitz, "Characterization of soluble, salt-loaded, degradable plga films and their release of tetracycline," *Journal of Biomedical Materials Research*, vol. 41, no. 1, pp. 18–29, 1998.
- [238] E. Vey, C. Rodger, J. Booth, M. Claybourn, A. F. Miller, and A. Saiani, "Degradation kinetics of poly (lactic-co-glycolic) acid block copolymer cast films in phosphate buffer solution as revealed by infrared and raman spectroscopies," *Polymer degradation and stability*, vol. 96, no. 10, pp. 1882–1889, 2011.
- [239] J. Floury, S. Jeanson, S. Aly, and S. Lortal, "Determination of the diffusion coefficients of small solutes in cheese: a review," *Dairy Science & Technology*, vol. 90, no. 5, pp. 477–508, 2010.
- [240] H. Sjöberg, S. Persson, and N. Caram-Lelham, "How interactions between drugs and agarose-carrageenan hydrogels influence the simultaneous transport of drugs," *Journal of controlled release*, vol. 59, no. 3, pp. 391–400, 1999.
- [241] J. A. Ferreira, L. Gonçalves, J. Naghipoor, P. de Oliveira, and T. Rabczuk, "The effect of plaque eccentricity on blood hemodynamics and drug release in a stented artery," *Medical engineering & physics*, vol. 60, pp. 47–60, 2018.
- [242] S. P. Velaga, D. Nikjoo, and P. R. Vuddanda, "Experimental studies and modeling of the drying kinetics of multicomponent polymer films," *AAPS PharmSciTech*, vol. 19, no. 1, pp. 425–435, 2018.
- [243] K. Pramod and R. Gangineni, "Influence of solvent evaporation rate on crystallization of poly (vinylidene fluoride) thin films," *Bulletin of Materials Science*, vol. 38, no. 4, pp. 1093–1098, 2015.
- [244] M. Udayakumar, M. Kollár, F. Kristály, M. Leskó, T. Szabó, K. Marossy, I. Tasnádi, and Z. Németh, "Temperature and time dependence of the solvent-induced crystallization of poly (l-lactide)," *Polymers*, vol. 12, no. 5, p. 1065, 2020.
- [245] J. Ritums, "Diffusion, swelling and mechanical properties of polymers," Ph.D. dissertation, Fiber-och polymerteknologi, 2004.

BIBLIOGRAPHIE

- [246] S. Scheler, "The polymer free volume as a controlling factor for drug release from poly (lactide-co-glycolide) microspheres," *Journal of Applied Polymer Science*, vol. 131, no. 1, 2014.
- [247] R. D. Pavaloiu, A. Stoica-Guzun, M. Stroescu, S. I. Jinga, and T. Dobre, "Composite films of poly (vinyl alcohol)-chitosan-bacterial cellulose for drug controlled release," *International journal of biological macromolecules*, vol. 68, pp. 117–124, 2014.
- [248] N. N. Li, C. P. Fu, and L. M. Zhang, "Using casein and oxidized hyaluronic acid to form biocompatible composite hydrogels for controlled drug release," *Materials Science and Engineering: C*, vol. 36, pp. 287–293, 2014.
- [249] P. L. Ritger and N. A. Peppas, "A simple equation for description of solute release i. fickian and non-fickian release from non-swellable devices in the form of slabs, spheres, cylinders or discs," *Journal of controlled release*, vol. 5, no. 1, pp. 23–36, 1987.
- [250] J. M. Unagolla and A. C. Jayasuriya, "Drug transport mechanisms and in vitro release kinetics of vancomycin encapsulated chitosan-alginate polyelectrolyte microparticles as a controlled drug delivery system," *European Journal of Pharmaceutical Sciences*, vol. 114, pp. 199–209, 2018.
- [251] A. M. Master, M. E. Rodriguez, M. E. Kenney, N. L. Oleinick, and A. S. Gupta, "Delivery of the photosensitizer pc 4 in peg-pcl micelles for in vitro pdt studies," *Journal of pharmaceutical sciences*, vol. 99, no. 5, pp. 2386–2398, 2010.
- [252] Q. Wang, J. Wang, Q. Lu, M. S. Detamore, and C. Berkland, "Injectable plga based colloidal gels for zero-order dexamethasone release in cranial defects," *Biomaterials*, vol. 31, no. 18, pp. 4980–4986, 2010.
- [253] B. Gulen and P. Demircivi, "Synthesis and characterization of montmorillonite/ciprofloxacin/tio2 porous structure for controlled drug release of ciprofloxacin tablet with oral administration," *Applied Clay Science*, vol. 197, p. 105768, 2020.
- [254] F. Bueche, "Derivation of the wlf equation for the mobility of molecules in molten glasses," *The Journal of Chemical Physics*, vol. 24, no. 2, pp. 418–419, 1956.
- [255] P. Blasi, S. S. D'Souza, F. Selmin, and P. P. DeLuca, "Plasticizing effect of water on poly (lactide-co-glycolide)," *Journal of Controlled Release*, vol. 108, no. 1, pp. 1–9, 2005.

BIBLIOGRAPHIE

- [256] N. Bink, V. B. Mohan, and S. Fakirov, “Recent advances in plastic stents: A comprehensive review,” *International Journal of Polymeric Materials and Polymeric Biomaterials*, vol. 70, no. 1, pp. 54–74, 2021.
- [257] Z. Yang, H. Peng, W. Wang, and T. Liu, “Crystallization behavior of poly (ϵ -caprolactone)/layered double hydroxide nanocomposites,” *Journal of applied polymer science*, vol. 116, no. 5, pp. 2658–2667, 2010.
- [258] A. Shrivastava, *Introduction to plastics engineering*. William Andrew, 2018.
- [259] C. Pan, Z. Zhou, and X. Yu, “Coatings as the useful drug delivery system for the prevention of implant-related infections,” *Journal of orthopaedic surgery and research*, vol. 13, no. 1, pp. 1–11, 2018.
- [260] Q. Long, X. Xu, K. Ramnarine, and P. Hoskins, “Numerical investigation of physiologically realistic pulsatile flow through arterial stenosis,” *Journal of Biomechanics*, vol. 34, no. 10, pp. 1229–1242, 2001.
- [261] L. Martin, L. Higgins, M. Westwood, and P. Brownbill, “Pulsatility effects of flow on vascular tone in the fetoplacental circulation,” *Placenta*, vol. 101, pp. 163–168, 2020.
- [262] R. Lutz, L. Hsu, A. Menawat, J. Zrubek, and K. Edwards, “Comparison of steady and pulsatile flow in a double branching arterial model,” *Journal of biomechanics*, vol. 16, no. 9, pp. 753–766, 1983.
- [263] M. A. Azrin, J. F. Mitchel, D. B. Fram, C. A. Pedersen, R. W. Cartun, J. J. Barry, L. M. Bow, D. D. Waters, and R. G. McKay, “Decreased platelet deposition and smooth muscle cell proliferation after intramural heparin delivery with hydrogel-coated balloons.” *Circulation*, vol. 90, no. 1, pp. 433–441, 1994.
- [264] D. Caccavo, “An overview on the mathematical modeling of hydrogels’ behavior for drug delivery systems,” *International journal of pharmaceutics*, vol. 560, pp. 175–190, 2019.
- [265] M. Visvalingam and J. D. Whyatt, “The douglas-peucker algorithm for line simplification: re-evaluation through visualization,” in *Computer Graphics Forum*, vol. 9, no. 3. Wiley Online Library, 1990, pp. 213–225.

BIBLIOGRAPHIE

- [266] C. Bode, H. Kranz, A. Fizez, F. Siepmann, and J. Siepmann, “Often neglected: Plga/pla swelling orchestrates drug release: Hme implants,” *Journal of Controlled Release*, vol. 306, pp. 97–107, 2019.
- [267] U. Westedt, M. Wittmar, M. Hellwig, P. Hanefeld, A. Greiner, A. K. Schaper, and T. Kissel, “Paclitaxel releasing films consisting of poly (vinyl alcohol)-graft-poly (lactide-co-glycolide) and their potential as biodegradable stent coatings,” *Journal of controlled release*, vol. 111, no. 1-2, pp. 235–246, 2006.
- [268] T. F. Edgar, D. M. Himmelblau, L. S. Lasdon *et al.*, *Optimization of chemical processes*, 2001.
- [269] S. Muschert, F. Siepmann, B. Leclercq, B. Carlin, and J. Siepmann, “Prediction of drug release from ethylcellulose coated pellets,” *Journal of controlled release*, vol. 135, no. 1, pp. 71–79, 2009.
- [270] A. Mane, N. Maheshwari, P. Ghode, M. C. Sharma, and R. K. Tekade, “Approaches to the development of implantable therapeutic systems,” in *Biomaterials and Bionanotechnology*. Elsevier, 2019, pp. 191–224.
- [271] Y. Fu and W. J. Kao, “Drug release kinetics and transport mechanisms of non-degradable and degradable polymeric delivery systems,” *Expert Opinion on Drug Delivery*, vol. 7, no. 4, pp. 429–444, 2010.
- [272] Y. Zhu, K. A. Mehta, and J. W. McGinity, “Influence of plasticizer level on the drug release from sustained release film coated and hot-melt extruded dosage forms,” *Pharmaceutical development and technology*, vol. 11, no. 3, pp. 285–294, 2006.
- [273] S. S. Cardoso and J. H. Cartwright, “Dynamics of osmosis in a porous medium,” *Royal Society open science*, vol. 1, no. 3, p. 140352, 2014.
- [274] F. Horkay, I. Horkayne-Szakaly, and P. J. Basser, “Measurement of the osmotic properties of thin polymer films and biological tissue samples,” *Biomacromolecules*, vol. 6, no. 2, pp. 988–993, 2005.
- [275] S. Jonnalagadda and D. H. Robinson, “A bioresorbable, polylactide reservoir for diffusional and osmotically controlled drug delivery,” *AAPS PharmSciTech*, vol. 1, no. 4, 2000.

BIBLIOGRAPHIE

- [276] R. A. Keraliya, C. Patel, P. Patel, V. Keraliya, T. G. Soni, R. C. Patel, and M. Patel, “Osmotic drug delivery system as a part of modified release dosage form,” *International Scholarly Research Notices*, vol. 2012, 2012.
- [277] G. M. Zentner, G. S. Rork, and K. J. Himmelstein, “Osmotic flow through controlled porosity films: an approach to delivery of water soluble compounds,” *Journal of Controlled Release*, vol. 2, pp. 217–229, 1985.
- [278] F. Theeuwes, “Elementary osmotic pump,” *Journal of pharmaceutical sciences*, vol. 64, no. 12, pp. 1987–1991, 1975.
- [279] M. Jarzyńska and M. Pietruszka, “The application of the Kedem–Katchalsky equations to membrane transport of ethyl alcohol and glucose,” *Desalination*, vol. 280, no. 1-3, pp. 14–19, 2011.
- [280] H. C. Eyster, “Osmosis and osmotic pressure,” *Botanical Review*, vol. 9, no. 5, pp. 311–324, 1943.
- [281] Z. Liao, E. Klein, C. K. Poh, Z. Huang, J. Lu, P. A. Hardy, and D. Gao, “Measurement of hollow fiber membrane transport properties in hemodialyzers,” *Journal of membrane science*, vol. 256, no. 1-2, pp. 176–183, 2005.
- [282] L. T. Biegler, *Nonlinear programming: concepts, algorithms, and applications to chemical processes*. SIAM, 2010.
- [283] F. Alfonso and C. Fernandez, “Second-generation drug-eluting stents: moving the field forward,” 2011.
- [284] D. J. Hines and D. L. Kaplan, “Poly (lactic-co-glycolic) acid- controlled-release systems: experimental and modeling insights,” *Critical Reviews™ in Therapeutic Drug Carrier Systems*, vol. 30, no. 3, 2013.
- [285] A. Ranjan and P. K. Jha, “Experiments and modeling of controlled release behavior of commercial and model polymer-drug formulations using dialysis membrane method,” *Drug delivery and translational research*, vol. 10, no. 2, pp. 515–528, 2020.
- [286] P. Labroo, S. Ho, H. Sant, J. E. Shea, J. Agarwal, and B. Gale, “Modeling diffusion-based drug release inside a nerve conduit in vitro and in vivo validation study,” *Drug Delivery and Translational Research*, vol. 11, no. 1, pp. 154–168, 2021.

- [287] A. Lucero-Acuña, C. A. Gutiérrez-Valenzuela, R. Esquivel, and R. Guzmán-Zamudio, “Mathematical modeling and parametrical analysis of the temperature dependency of control drug release from biodegradable nanoparticles,” *RSC advances*, vol. 9, no. 16, pp. 8728–8739, 2019.
- [288] A. Fernández-Colino, J. M. Bermudez, F. Arias, D. Quinteros, and E. Gonzo, “Development of a mechanism and an accurate and simple mathematical model for the description of drug release: application to a relevant example of acetazolamide-controlled release from a bio-inspired elastin-based hydrogel,” *Materials Science and Engineering: C*, vol. 61, pp. 286–292, 2016.
- [289] G. Vairo, M. Cioffi, R. Cottone, G. Dubini, and F. Migliavacca, “Drug release from coronary eluting stents: a multidomain approach,” *Journal of biomechanics*, vol. 43, no. 8, pp. 1580–1589, 2010.

BIBLIOGRAPHIE

Annexe A

List of the publications

Related to thesis

• **Abbasnezhad N**, Kebdani M, Shirinbayan M, Champmartin S, Kouidri S, Tcharkhtchi A, Bakir F, “Development of a Model Based on Physical Mechanisms for the Explanation of Drug Release: Application to Diclofenac Release from Polyurethane Films,” *Polymers*, 10 April 2021.

• **Abbasnezhad N**, Zirak N, Shirinbayan M, Tcharkhtchi A, Bakir F, “On the importance of physical and mechanical properties of PLGA films during drug release,” *Journal of drug delivery science and technology*, 25 February 2021.

• **Abbasnezhad N**, Zirak N, Shirinbayan M, Salahinejad E, Tcharkhtchi A, Bakir F, “Controlled release from polyurethane films: Drug release mechanisms,” *Journal of Applied Polymer Science*. 17 October 2020.

• **Abbasnezhad N**, Maurel B, Shirinbayan M, Bakir F, “New mathematical model based on the kinetic profile for the prediction of multistage drug release from delivery systems,” *International Journal of Pharmacy*, 4 July 2020.

• **Abbasnezhad N**, Shirinbayan M, Tcharkhtchi A, and Bakir F, “In vitro study of drug release from various loaded polyurethane samples and subjected to different non-pulsed flow rates,” *Journal of drug delivery science and technology*, 2 January 2020.

• **Abbasnezhad N**, Shirinbayan M, Champmartin S, and Bakir F, “Visco-elastic behavior of drug loaded Polyurethane,” *Journal of Polymers*, submitted.

Other articles

- A. Tcharkhtchi, **N. Abbasnezhad**, M. Zarbini Seydani, N. Zirak, M. Shirinbayan, “An overview of filtration efficiency through the masks: mechanisms of the aerosols penetration,” *Bioactive Materials*, 2 August 2020.
- Shirinbayan M, Montazeri A, Nouri Sedeh M, **Abbasnezhad N**, Fitoussi J, Tcharkhtchi A, “Rotational molding of polyamide-12 nanocomposites: Modeling of the viscoelastic behavior,” *International Journal of Material Forming*, 06 May 2020.
- Shirinbayan M, Fitoussi J, **Abbasnezhad N**, Lucas A, Tcharkhtchi A, “Multi-Scale Damage and Mechanical Behavior of Sheet Molding Compound Composites Subjected to Fatigue, Dynamic, and Post-Fatigue Dynamic Loadings,” *International Journal of Materials and Metallurgical Engineering*, 20 September 2018.
- Shirinbayan M, Fitoussi J, **Abbasnezhad N**, Meraghni F, Surowiec B, Tcharkhtchi A, “Mechanical characterization of a Low Density Sheet Molding Compound (LD-SMC): Multi-scale damage analysis and strain rate effect,” *Composites Part B: Engineering*, 15 December 2017.
- **Abbasnezhad N**, Fitoussi J, Shirinbayan M, Khavandi A, Arabi H, Tcharkhtchi A, “Influence of loading conditions on the overall mechanical behavior of polyether-ether-ketone (PEEK),” *International Journal of Fatigue*, 15 December 2017.
- Shirinbayan M, Beigi Rizi H, **Abbasnezhad N**, Tcharkhtchi A, Fitoussi J, “Tension, compression, and shear behavior of Advanced Sheet Molding Compound (A-SMC): Multi-scale damage analysis and strain rate effect,” *Composites Part B: Engineering*, 15 November 2021.
- Zirak N, Maadani AM, Salahinejad E, **Abbasnezhad N**, Shirinbayan M, “Fabrication, drug delivery kinetics and cell viability assay of PLGA-coated vancomycin-loaded silicate porous microspheres,” *Ceramics International*, 25 August 2021.

Congress

N. Abbasnezhad, et al., “Assessment of a mathematical model considering the effect of flow rate on in-vitro drug-release from PLGA films”, ICCHMT, May 18-21, Paris, France.

J. Song, **N. Abbasnezhad**, et al., “Comparison between Calculation Results and Experimental-Data of a Model of Drug Released from Polyurethane Samples”, ICCHMT, May 18-21, Paris, France.

N. Abbasnezhad, et al., “Investigation of the drug release from the PU films: with and without considering flow rate and tissue-simulating layer”, Innovative development of science, December 10, 2020 Dushanbe, Tadjikestan.

N. Abbasnezhad, et al., “Evaluation of drug release from polymer carriers: mechanical and physical properties”, WBC2020, December 11-15, 2020, Glasgow, Scotland.

N. Abbasnezhad, et al., “Mechanism of foaming during rotational molding”, 4th RTS International Congress, July 10-12, 2019, Paris, France.



Annexe B

Résumé de thèse

Expérimentation et modélisation in vitro de la libération de médicaments à partir de supports polymères pour le développement de stents à élution médicamenteuse

B.1 Introduction

Le système cardiovasculaire est composé du cœur, d'un réseau de vaisseaux sanguins (artères, veines et capillaires) et du sang. Dans ce système complexe, le cœur joue le rôle d'une pompe volumétrique qui pulse et met le sang en mouvement dans les différents vaisseaux avec un débit moyen au repos d'environ 5,4 l/min. Le système cardiovasculaire est sujet à des maladies graves telles que l'athérosclérose (durcissement de l'artère par la formation de plaque lipidique à l'intérieur d'un vaisseau sanguin), ce qui peut conduire à l'obstruction complète (appelée ischémie) du flux sanguin dans le système circulatoire. En se référant à la littérature, les maladies coronariennes sont parmi les causes les plus importantes de décès dans ces dernières décennies. Ils affecteront environ 23,4 millions de personnes d'ici 2030 [1]. Pour surpasser ce problème, des avancées scientifiques sont en cours. Elles ont

commencé il y a environ 40 ans et les techniques continuent de s'améliorer aujourd'hui : angioplastie par ballonnet, stent nu, stent à élution médicamenteuse, stent biorésorbable.

Comme nous le savons, un stent agit comme un objet étranger pour notre système immunitaire et celui-ci peut réagir à cet objet intrusif de diverses manières : les macrophages (globules blancs) s'accumulent autour du stent, et les cellules musculaires lisses voisines (SMC) prolifèrent, perturbant le processus d'endothélialisation ; migration et prolifération des SMC vasculaires de la média vers l'intima, générant une couche matricielle extracellulaire dans l'intima (hyperplasie intimale), suivie d'un rétrécissement de la zone luminale [11, 12]. Il est probable que le phénomène d'épaississement de l'intima est dû aux leucocytes qui adhèrent aux cellules d'endothélium activées et perturbent sa récupération [1, 13–15]. Dans certains cas, les vaisseaux peuvent perdre leur fonctionnalité en raison de la formation d'un caillot sanguin appelé thrombose, réponse de l'endothélium aux forces mécaniques et aux contraintes de cisaillement causées par la procédure d'apposition du stent qui peuvent dénuder la couche intima et provoquer des saignements [13, 16]. Alors que la couche intima est dénudée, elle est rapidement ciblée par une réponse inflammatoire, augmentant l'apoptose [11]. La dénudation d'endothélium pendant l'angioplastie est inévitable, c'est la raison pour laquelle l'hyperplasie néointimale est toujours produite. Cependant, un endothélium sain est nécessaire pour contrôler la prolifération des CML vasculaires et empêcher la formation de thrombus [17, 18]. Le thrombus de stent (ST) est l'une des complications majeures de l'angioplastie. Il est rapporté en 2010 que chaque année, environ 0,3 à 0,6 % des DES sont suivis d'une thrombose de stent suivie d'une augmentation de la mortalité humaine, de 10 à 30 % [19]. La malapposition du stent, la réendothélialisation tardive ou incomplète et l'in-



FIGURE B.1 – Coronary restenosis after coronary angioplasty with the balloon [24]

flammation induite par les polymères sont les principales raisons de l'inflammation et de la thrombose tardive [7, 11, 20]. Le moyen possible de diminuer le ST est de prévenir le risque de saignement après la pose d'un stent en utilisant des anticoagulants et des agents antiplaquettaires (l'endothélium sain fournit également le support anti-inflammatoire grâce à la protéine C anticoagulante naturelle [13]). Le maintien de la dose de médicament pendant le traitement peut minimiser le risque de thrombose [21]. Pour surmonter ces problèmes, la quantité de médicament, son type et sa stratégie de libération, doivent être optimisées. Les toutes premières angioplasties, basées sur l'expansion par ballonnet dans l'artère, se sont heurtées aux problèmes de recul d'élasticité et hyperplasie néointimale était à l'origine de 40 à 60% des resténoses dans les années 1977-90 [22, 23]. La figure B.1 montre le phénomène de resténose après angioplastie avec ballonnet seul.

Il est à noter qu'il existe une deuxième génération de ballons enduits de médicaments, généralement du paclitaxel, pour surmonter la resténose intra-stent. Dans ce cas, le médicament doit être transféré rapidement pendant la contact du ballon avec la paroi du vaisseau, qui dure environ une minute. Certains chercheurs s'intéressent à cette technique car cette méthode diminue le risque d'hémorragie, évite la présence à risque d'un corps étranger dans le corps et limite les effets secondaires [25]. Cependant, cette méthode n'a pas été complètement développée pour diverses raisons, principalement en raison

B.1. INTRODUCTION

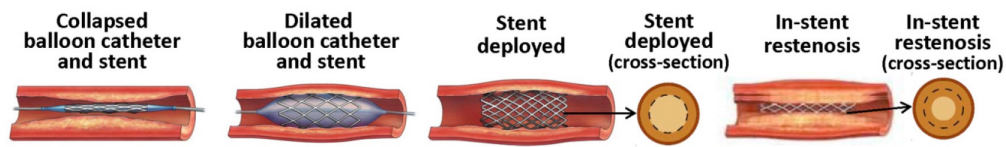


FIGURE B.2 – Resténose coronaire intra-stents après angioplastie coronaire avec les stents métalliques nus [24]

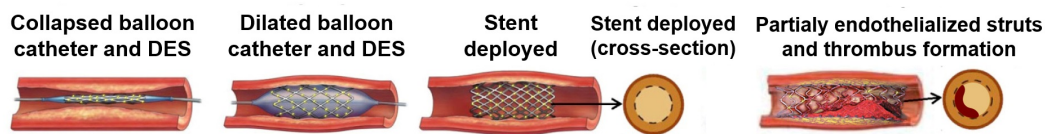


FIGURE B.3 – Thrombose tardive après stents à élution médicamenteuse, adoptée et modifiée à partir de [24]

des résultats prometteurs des stents. La première génération d'endoprothèses était des endoprothèses en métal nu dans la quelle l'incidence de la resténose diminuait à 20-30% en raison de l'élimination du recul élastique entre 1991-2003 (figure B.2) [26–28].

Afin de diminuer encore les cas de resténose et d'hyperplasie néointimale, la deuxième génération de stents est apparue en 2003 [29] : les stents à élution médicamenteuse. Ces stents étaient recouverts d'une couche de polymère contenant une substance active utilisée pour réduire l'hyperplasie néointimale. L'incidence de la resténose diminue à environ 3-20 % (illustré à la figure B.3).

Le scénario ne s'arrête pas là et le DES n'a pas encore répondu à toutes les demandes en angioplastie. Bien que l'utilisation du DES ait plutôt résolu le problème de la resténose, les problèmes d'intima dénudé, l'inflammation et la thrombose associées, persistent et ouvrent un large éventail de recherches à ce sujet [13, 18, 30]. Ces problèmes ont pu être résolus grâce à une optimisation de la cinétique de libération du médicament (qui affecte fermement le maintien du médicament dans la paroi tissulaire et

influence la guérison vasculaire et le processus thérapeutique) et l'apposition du stent dans le vaisseau [31]. La distribution du médicament dans la paroi artérielle dépend de nombreux paramètres tels que le type de médicament et sa concentration initiale, le taux de libération du médicament dans le paroi artérielle, la solubilité du médicament, la taille des particules, les liants, le mouillage, les propriétés de la matrice polymère, les méthodes de revêtement, la direction d'élution, l'épaisseur de revêtement, les tailles de pores dans le revêtement, les conditions de libération du milieu, la température et le pH, le nombre de Reynolds et la cinétique du flux sanguin, . . . [1, 32–34]. L'optimisation de ces paramètres et l'étude de leurs effets peuvent améliorer la cinétique de libération du médicament pendant la thérapie. Les recherches actuelles, à cet égard, basées sur des modèles humains et animales, rencontrent plusieurs limites. L'incapacité d'effectuer régulièrement des prélèvements *in vivo* de tissus et de sang diminue la possibilité pour étudier la libération du médicament et caractériser le porteur du médicament pendant le temps de libération. De plus, les expériences *in vivo* se concentrent généralement sur les niveaux de médicaments dans le sang plutôt que sur les concentrations de médicaments dans la paroi du vaisseau sanguin, bien que ce soit le but de la thérapie [35]. Cependant, la concentration de médicament dans le tissu ne peut être déterminée qu'après le retrait du stent chez les modèles animales. De nombreuses études ont montré que réduire le besoin de sacrifier le corps vivant ainsi que réduire les coûts des essais *in vivo* n'a pas été possible sans augmenter la précision des essais *in vitro*. De plus, l'utilisation de l'environnement *ex vivo* a été l'un des moyens les plus efficaces pour analyser les propriétés physiques, chimiques, mécaniques et autres du tissu en interaction avec l'implant biomatériau. Bien que ces méthodes ne puissent pas reproduire exactement les conditions qui se produisent à l'intérieur d'un

organisme, ils peuvent cependant imiter les conditions *in vivo* et conduire à des résultats de test fiables en fournissant des environnements contrôlés. Par conséquent, reproduire des conditions similaires reste un énorme défi pour les chercheurs. De plus, la cinétique de la libération du médicament peut être modélisée et estimée par des modèles mathématiques et/ou physiques qui peuvent aider à prédire le profil de libération sous différentes conditions.

B.2 Etat de l'art

B.2.1 Mécanismes de libération de médicament

Il existe différents mécanismes qui peuvent contrôler la libération de médicament dans un système d'administration de médicament : la dissolution, la diffusion, l'osmose, la dégradation, le gonflement et l'érosion font partie de ces mécanismes. Leur présence dépend de l'ensemble du système de libération et peut agir simultanément ou à différentes étapes d'un processus de libération. Il est courant qu'un système ou un dispositif en présente plusieurs, mais la classification des mécanismes de libération est généralement basée sur le mécanisme principal. Outre les propriétés du revêtement polymère, l'administration de la substance active, la cinétique et les mécanismes associés dépendent du type de substance active et des conditions environnementales. Certains paramètres clés sont par exemple les propriétés physiques et chimiques de la substance active, telles que le poids moléculaire, la solubilité dans l'eau, la taille des particules, la viscosité du solvant, . . . [18, 36–38]. Certains de ces paramètres sont utilisés dans des modèles mathématiques afin de nous aider à prédire le comportement de libération à partir des supports des médicaments. Les modèles mathématiques ont toujours été l'un des moyens les plus efficaces pour améliorer la conception et le développement de différents supports pour le système

d'administration de médicaments (coûts inférieurs et tests de laboratoire moins nombreux). De plus, ils ont toujours été importants pour déterminer les mécanismes de libération du médicament et la cinétique de libération des divers systèmes, tels que les systèmes osmotiques, les systèmes dégradables ou non dégradables.

B.2.2 Conception de stents à élution médicamenteuse

B.2.2.1 Différents modèles géométriques de stents à élution médicamenteuse

Un stent ressemble à un petit tube cylindrique extensible en treillis métallique qui agit comme un échafaudage permanent pour maintenir les vaisseaux sanguins ouverts lorsqu'ils sont sujets à l'athérosclérose. Ils sont utilisés à différents endroits du corps mais nous nous concentrons ici uniquement sur ceux utilisés pour soigner les maladies cardiovasculaires. Selon les fabricants, différentes géométries existent [26]. Comme le révèle cette étude, il existe divers paramètres géométriques dans les stents et il est très difficile d'évaluer comment un paramètre particulier influence le comportement de libération. Pour obtenir une conclusion claire et cohérente, il serait préférable de limiter la variation de ces paramètres. C'est la stratégie utilisée dans de nombreuses études (d'ailleurs lorsque les autres paramètres externes sont les mêmes, les résultats peuvent être bénéfiques pour les autres types de systèmes d'administration de médicaments (DDS) tels que les patches, les implants, les microparticules, etc). Par exemple Joachim Loo et al. [74] ont étudié expérimentalement la libération de deux types de médicaments hydrophobes et hydrophiles à partir de deux types de revêtements polymères (films PLGA et PLLA). Dans cette étude, la surface active est un carré $2 \times 2 \text{ cm}^2$ parallèle à l'écoulement avec une épaisseur de $55 \mu\text{m}$ fabriqué par une approche multicouche irradiée. Dans un autre article,

Pang et al. [75] étudient la libération d'ibuprofène à partir de films PLGA d'une dimension d'environ 33 cm^2 et d'une épaisseur comprise entre 2 et $5 \mu\text{m}$. Dans d'autres études [79–82], l'ensemble du stent est modélisé sous la forme d'une seule entretoise rectangulaire pour étudier la distribution du médicament.

B.2.2.2 Polymères dans le cas des stents à élution médicamenteuse

Les polymères utilisés pour revêtir les stents sont nombreux : revêtement poly(éthylène-co-acétate de vinyle) (PEVA) pour une meilleure biocompatibilité [83], poly(méthacrylate de butyle) (PBMA) pour une libération lente et prolongée du médicament [84], fluoropolymère durable [85, 86], silicone et polyuréthane. Ces polymères peuvent être responsables d'inflammations vasculaires, de retards d'endothélialisation/cicatrisation et de réactions d'hypersensibilité, ils sont donc associés à un risque accru de thrombose de stent [87].

Certains autres stents sont recouverts de divers revêtements biocompatibles et biodégradables. En référence aux différents chercheurs, les principaux polymères utilisés sont le poly(L)-acide lactique (P(L)LA) [88], le PDLA [89], le poly(lactide-co-caprolactone) (PCL) [88], le poly (lactide-co-glycolide) (PLGA) [88] le polyéthylène glycol (PEG), le polyglycolide (PGA) [60], PLGA-PEG, PU [90–92], etc. Les polymères mentionnés peuvent entraîner une dégradation chimique entraînant la scission des chaînes polymères telles que leurs liaisons ester [93], des groupes phosphonate [94] ou par élimination des atomes de chlore et libération simultanée des composés médicamenteux qu'elles portent [95]. Ces polymères doivent avoir des propriétés telles que la biocompatibilité, l'élasticité (nécessaire pour l'expansion du stent) et des propriétés de libération de médicament adéquates. Les chercheurs,

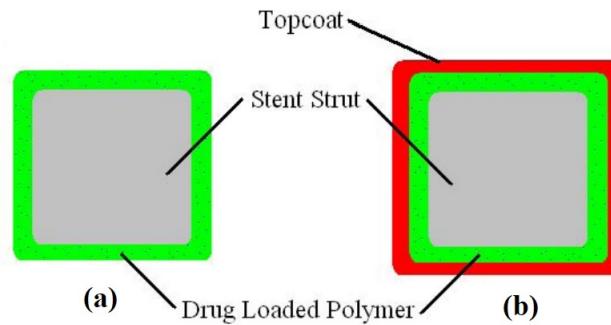


FIGURE B.4 – Les sections transversales de l’entretoise de stent à élution médicamenteuse, (a) est une entretoise DES avec une matrice polymère chargée de médicament et l’entretoise de stent (b) a un moyen de transport couche de finition régulatrice [97]

afin de contrôler la libération régulière du médicament et de réduire la première libération soudaine pendant la cicatrisation vasculaire, ont exploré de nombreuses stratégies. Le phénomène de libération en rafale est très fréquent pour les stents recouverts d’une couche de polymère et de médicament. De nombreux chercheurs [1, 96] ont proposé une couche de polymère avec un médicament et un ou plusieurs revêtements de médicament libres comme couches supérieures. La figure B.4 montre le schéma de cette conception. Dans leur étude, Li et al. [96] ont étudié les performances de libération du médicament avec différentes épaisseurs de la couche supérieure (couche polymère sans médicament). Ils ont conclu que la couche supérieure d’épaisseur moyenne ou élevée empêche la libération brutale du médicament, la couche supérieure jouant le rôle de barrière de diffusion et entravant le contact du médicament avec le flux sanguin.

De plus, certains DES sont complètement biorésorbables, ce qui signifie qu’ils contiennent une structure non métallique et que seul l’échafaudage polymère supporte les propriétés mécaniques du stent. De toute évidence, les produits de dégradation doivent être non toxiques, facilement absorbés [1, 26]. Les stents vasculaires biorésorbables idéaux supporteraient la structure vasculaire de 3 à 6

mois puis disparaissent complètement de 3 à 18 mois après la cicatrisation vasculaire. Les polymères utilisés dans ce type de stents sont par exemple : le poly caprolatone (PCL) [88, 107], le poly(L-lactide) (PLA) [108–111] (le poly acide lactique est également fabriqué dans notre propre sang et le corps le reconnaît et le décompose en composants sûrs tels que l'eau et l'oxygène); le polyuréthane (PU) [112] est également un candidat intéressant pour la fabrication d'échafaudages avec une biocompatibilité modérée et d'excellentes propriétés mécaniques [1], le poly(ester d'anhydride) [60], le poly(D,L-lactide) (PDLLA) [113], le polymère de polycarbonate (PC) [60], le chitosan (CS) [114] sont parmi les polymères naturels les plus populaires et les plus appliqués pour les systèmes d'administration de médicaments [115]. La principale faiblesse de ces échafaudages polymères, par rapport aux structures métalliques, est qu'ils sont moins capables mécaniquement de maintenir la lumière vasculaire ouverte [13]. De plus, certaines études ont révélé qu'une dégradation précoce ou non uniforme de ces polymères pouvait provoquer une thrombose tardive du stent et même une crise cardiaque chez les patients [18, 30].

B.2.2.3 Médicaments dans le cas des stents à élution médicamenteuse

La cinétique d'administration du médicament et les mécanismes associés dépendent fortement du type de substance active (propriétés physiques et chimiques de la substance active, telles que le poids moléculaire, la solubilité dans l'eau, la taille des particules ... [18, 36–38]). L'hydrophilie ou l'hydrophobie est également déterminante pour la libération du médicament pendant la thérapie. Les substances actives hydrophobes sont plus favorables, car les substances actives hydrophiles sont rapidement éliminées par le fluide, suivies de la libération brutale du médicament [117] et les substances actives hydrophobes sont plus susceptibles de se lier aux récepteurs. Cette question est très importante

dans les cas cardiovasculaires. Comme le montre [118], les médicaments hydrophobes ont une variabilité moyenne plus importante que les médicaments hydrophiles et les premiers restent relativement plus proches de l'intima que les médicaments hydrophiles à tous les nombres de Peclet de médicaments [118]. Un autre paramètre clé lié à la substance active est sa solubilité dans l'eau et son état physique dans la matrice polymère. Bien entendu, la cinétique de libération n'est pas la même lorsque la substance active est dissoute par absorption d'eau dans la matrice polymère et lorsqu'elle n'est pas hydrosoluble et reste dispersée dans la matrice polymère. Par exemple, dans une étude de Chakraborty et al. [120], les cinétiques de libération de médicaments hydrosolubles et insolubles à partir d'une matrice à base de HPMC (hydroxypropylméthylcellulose) ont été étudiées. L'étude révèle que la cinétique de libération du médicament soluble est un transport de diffusion non-fickien anormal alors que le médicament insoluble suit une cinétique de libération d'ordre zéro.

B.2.3 Caractéristiques de la condition d'essai

B.2.3.1 Lumière artificielle

L'un des paramètres les plus importants pour obtenir une libération précise de médicament à partir du DES dans des conditions in vitro est le milieu fluide : une large gamme de solutions et de fluides a été utilisée à cette fin, en essayant de s'approcher le plus possible de l'environnement corporel. L'eau, la solution saline tamponnée au phosphate (PBS), le composant organique/PBS et le composant inorganique/PBS sont de telles solutions couramment utilisées. En particulier, le pH et la viscosité du milieu sont des paramètres importants, qui affectent la cinétique de libération du médicament. En général, le PBS avec un pH de 7,4 est considéré dans de nombreuses études comme

un bon milieu pour analyser la libération du médicament [121] en raison de sa capacité à maintenir le pH constant et de la proximité de ses ions avec les ions du corps. Cependant, l'utilisation de ce milieu pour étudier la libération de certains médicaments tels que le Sirolimus semble être un défi. En effet, certaines études montrent que le sirolimus a une très faible stabilité dans cette solution tampon à pH 7,4 [122].

B.2.3.2 Tissu artificiel

L'influence du milieu fluide sur la libération du médicament par le DES n'est qu'une partie du sujet. L'autre partie est : quelle quantité de médicament est diffusée dans l'artère ? C'est certainement l'objectif clinique principal et le domaine le plus difficile à étudier. Les cliniciens conseillent d'atteindre une concentration de médicament uniforme à travers la paroi artérielle et de maintenir la concentration dans une certaine fenêtre thérapeutique [128]. À cet égard, des études tentent de mesurer la quantité de médicament qui a pénétré dans le vaisseau à l'aide de différents gels pouvant simuler l'artère du vaisseau. Neubert et al. [129] ont considéré l'hydrogel d'alginate de calcium pour la simulation de l'artère vasculaire. La teneur en eau du gel était d'environ 96 %. Les principales raisons du choix de la matrice hydrogel d'alginate de calcium sont : sa stabilité à 37 °C, la possibilité d'adapter la résistance et l'élasticité du gel, et les conditions de gélification douces qui permettent l'incorporation de diverses substances telles que des protéines ou des cellules vivantes. Le mode opératoire expérimental utilisé pour fabriquer le gel (concentration, température, additifs...) affecte également le temps de gélification et la diffusion du médicament dans le gel. Selon les conditions environnementales de configuration pour l'analyse du médicament libéré par les stents, certaines propriétés des hydrogels telles que les propriétés

mécaniques, la dégradation et le gonflement font partie des facteurs qui conditionnent leur sélection. Dans une étude de Semmling et al. [130] les hydrogels de 2 % en poids d'agar, 2 % en poids d'agarose, 10 % en poids de PAA et 15 % en poids de PVA ont été sélectionnés. Afin de trouver une mesure de la stabilité à long terme des gels, les propriétés mécaniques des gels préparés ont été déterminées par analyse de texture. À cet égard, les courbes de contrainte des gels natifs, ainsi que des gels qui avaient été perfusés avec une solution saline tamponnée au phosphate (PBS) à $\text{pH} = 7,4$ dans leur configuration pendant 28 jours, ont été étudiés. Leurs résultats ont montré que le gel d'agarose semble être le candidat le plus approprié pour les tests de dissolution à long terme puisque les paramètres du gel cible sont pertinents pour leur utilisation en tant que compartiment de simulation tissulaire.

B.2.4 Méthodes d'essai de relargage

B.2.4.1 État statique

La méthode statique a été utilisée comme méthode courante pour mesurer la libération de médicament à partir de stents imprégnés de médicament et d'autres systèmes d'administration de médicament. En général, dans cette méthode, le stent est immergé dans une certaine quantité de milieu, puis le prélèvement du milieu se fait à certaines périodes. La température est maintenue constante pendant le test de libération du médicament. L'un des points importants pour tester la libération du médicament à l'état statique est l'échantillonnage du milieu. Certains supports sont retirés du système à différents intervalles de temps et doivent être remplacés par des supports frais [142]. Par exemple, dans l'étude de Khan et al. [143], la rapamycine libérée par les stents à élution médicamenteuse a été évaluée dans des conditions statiques. Une question importante se pose : quelle est la précision de ces tests dans

des conditions statiques ? Abbasnezhad et al. [144] ont montré la différence significative entre la libération du médicament dans des conditions statiques et dynamiques. De même, comme la libération du médicament à l'état statique a une cinétique plus lente qu'à l'état dynamique [145], plus de temps est nécessaire pour effectuer les tests. Cependant, en raison de la disponibilité de cette méthode, il semble que des informations de base utiles puissent être obtenues à partir de cette approche statique.

B.2.4.2 État dynamique

La libération de médicament à partir des stents à élution de médicament a plusieurs mécanismes de libération de médicament. Les mécanismes les plus importants consistent en la libération de médicament contrôlée par la diffusion, la libération de médicament contrôlée par dissolution/dégradation, la libération de médicament par échange d'ions et la libération contrôlée par osmose [146]. Des études ont montré l'effet de la présence du débit sur ces mécanismes. Il convient de noter que chaque mécanisme fournit une libération cinétique différente du stent. Par exemple, dans certains cas, la présence d'un mécanisme de dégradation peut augmenter la vitesse de libération du médicament par le stent. L'utilisation d'agitateurs fait partie des méthodes courantes de mesure de la quantité de médicament libéré dans des conditions dynamiques. A cet effet, un certain nombre de stents sont placés dans un récipient rempli de milieu (flacons en verre vissé [147], tubes [148] ou flacons [149]), puis le test est réalisé à une certaine agitation du shaker. Dans la plupart des études, la température prévue pour l'expérience était maintenue constante à 37 °C par un incubateur [150] ou un bain-marie [147, 151]. La vitesse d'agitation de l'agitateur dans les études est généralement de 50 [152, 153], 75 [57, 154], 80 [149], 100 [147, 150], 120 [151], 130 [155], 175 [148], 250 and 300 [156] tr/min. Un des inconvénients de

ces études est qu'elles ne justifient pas spécifiquement le choix de la vitesse d'agitation pour évaluer la libération du médicament. Par conséquent, les conditions expérimentales créées par les agitateurs ne sont pas facilement comparables à celles rencontrées dans les tests *in vivo*. En dehors des agitateurs, il existe une autre méthode pour les conditions dynamiques qui est la circulation du flux à débit constant. Cette condition peut avoir plus de similitudes avec le cas réel par rapport aux shakers. Par exemple, dans une étude de Bandomir et al. [157], le débit de 35 ml/min a été choisi pour étudier l'administration de médicament à partir du ballon enduit de médicament, alors que dans une étude de Zheng et al. [77] les débits de 3, 10, 30 ml/s ont été choisis pour la libération du sirolimus à partir du DES. Dans une enquête de Seidlitz et al. [159] le débit de 35 ml/min est utilisé en référence au débit dans les vaisseaux coronaires, ainsi que le débit de 4 ml/s pour deux types de médicaments différents. Leur analyse a indiqué que la variation du débit n'a pas d'effet distinct sur la libération et la distribution du médicament, mais ils ont conclu que l'effet du débit devrait être analysé au cas par cas par des évaluations individuelles.

B.2.5 Appareils pour les essais de libération de médicament

Comme vu ci-dessus, la libération de médicaments *in vitro* à partir du DES est un grand défi et implique de nombreux chercheurs. A cet égard, la conception d'un appareil pouvant imiter les conditions *in vivo* est très difficile. En effet, un tel montage doit être capable de fournir un schéma de flux systolo-diastolique, mimer les différents milieux (flux sanguin, revêtement polymère et paroi artérielle) et doit pouvoir mesurer les transferts médicamenteux dans ces milieux en fonction du temps et de l'espace. Nous décrivons ci-dessous les appareils les plus couramment utilisés pour atteindre certains

de ces objectifs. A l'état statique, des flacons de laboratoire sont généralement utilisés. Cependant à l'état dynamique, de nombreuses études utilisent des appareils de test de dissolution comme ceux couramment utilisés dans l'industrie pharmaceutique pour évaluer les performances d'un médicament. Aux États-Unis, ces appareils sont appelés appareils USP (United States Pharmacopeia). Les appareils USP 1 (panier) et 2 (pagaie) ont été introduits dans les années 1970 dans le but de fournir une plateforme pour évaluer les performances in vitro des formes posologiques dans des conditions standardisées. On peut également citer l'appareil à cylindres alternatifs USP 3 qui a été développé pour imiter le test gastro-intestinal, l'appareil à cellules à flux continu (USP 4) qui a une circulation à flux continu et a été conçu pour les médicaments peu solubles, les implants et les suppositoires. Appareil 5 (pagaie sur disque) est similaire au système de pagaie (USP 2) mais avec un disque supplémentaire monté dessus. Le type à cylindre ou USP 6 ressemble au type à panier mais le panier et l'arbre sont remplacés par un élément d'agitation cylindrique. USP 5 et USP 6 sont normalement destinés à la libération du médicament à partir des timbres transdermiques. Enfin, l'appareil à support alternatif avec agitation (USP 7) est l'appareil le plus récent destiné à différents types de supports de médicaments tels que comprimés, capsules, transdermiques, pompes osmotiques et stents artériels, avec différentes vitesses d'agitation. Généralement, dans le cas des études de DES, ces appareils ne sont pas assez sophistiqués car ils ne sont pas capables de reproduire le débit systolo-diastolique et la variation de pression inhérente qui sont des paramètres importants à prendre en compte comme le prouvent diverses études numériques [144, 162, 163]. La présence d'un tissu artériel artificiel est un autre élément important affectant la libération. À cet égard, le développement de la méthode vFTC (vessel-simulating flow-through cell)

[164] a été entrepris (montré sur la figure B.5). Cependant, jusqu'à présent, le tissu simulé ne reproduit pas fidèlement les caractéristiques du réelles [165, 166]. Parmi tous ces dispositifs, les appareils USP 2, USP 4, USP 7 et vFTC sont principalement utilisés dans l'étude de l'administration de médicaments à partir du DES. Pour évaluer l'effet de certaines de ces configurations sur le profil de libération, Medina et al. [167] ont comparé le profil de libération de l'ibuprofène à l'aide des appareils USP 2 et USP 4 avec le profil de libération d'une référence. Leurs résultats ont indiqué que le profil de libération obtenu par l'appareil USP 4 était similaire au profil de la référence. Dans un autre article Pruessmann et al. [35] ont étudié la libération de triamterène d'un DES à l'aide de trois configurations de test différentes : appareil USP 7, appareil USP 4 (FTC) et cellule d'écoulement simulant un vaisseau (vFTC). Leurs résultats ont indiqué que la géométrie de la cuve de dissolution (appareil USP) et le volume moyen n'avaient aucune influence sur le comportement de libération, tandis que la méthode de la cellule à écoulement avait un taux de libération inférieur à celui de l'appareil USP 7. La méthode vFTC a également été utilisée par Seidlitz et al. [159] pour étudier la dissolution et la libération de fluorescéine sodique et de triamterène des revêtements de stent. Ils ont comparé leurs résultats avec ceux obtenus par l'appareil standard à palettes (USP 2) et à cellule à écoulement continu (USP 4). Les résultats ont montré que la libération du revêtement était ralentie dans l'appareil USP 2 par rapport à l'USP 4 (figure B.6 (a)). Cependant, dans une autre étude de Pruessmann et al. [35] à propos de la libération de triamterène avec les méthodes de FTC et vFTC, il est montré que la libération du médicament était plus élevée au premier stade avec vFTC avant d'être dépassée par la libération de médicament obtenue par méthode FTC (figure B.6 (b)). En résumé, les études dans ce domaine montrent que de nombreuses

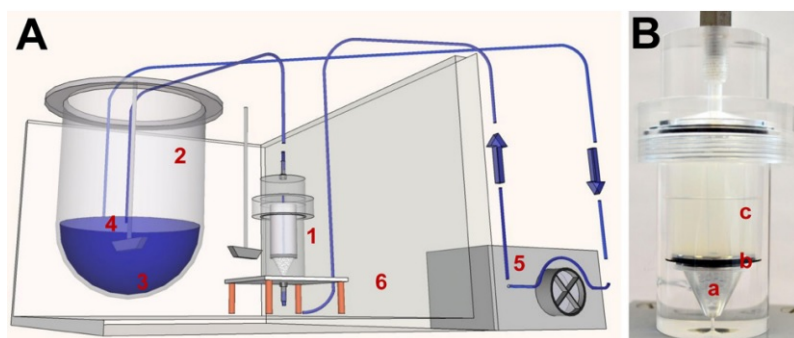


FIGURE B.5 – Aperçu schématique de la configuration de test in vitro (A) et photographie du vFTC équipé d'un gel d'agarose à 2 (B); 1) vFTC, 2) conteneur de média, 3) PBS de pH 7,4, 4) palette agité à 50 tr/min, 5) pompe péristaltique, 6) bain-marie chauffé, a) billes de verre, b) disque en acier inoxydable, c) hydrogel [140]

tentatives ont déjà été faites pour étudier expérimentalement la libération de médicament à partir de stents à élution médicamenteuse, mais ces solutions ne sont pas totalement satisfaisantes. De plus, les corrélations in vitro/in vivo, prenant en compte les différents paramètres, afin de personnaliser la thérapie et ainsi augmenter son efficacité, restent un sujet difficile.

B.2.6 Modélisation et simulation

B.2.6.1 Modèles semi-empiriques

Les modèles mathématiques ont toujours été l'un des moyens les plus efficaces d'améliorer la conception de différents supports pour le système d'administration de médicaments. De plus, il a toujours été important de déterminer le mécanisme de libération du médicament (qui a été discuté dans la section des mécanismes physiques) et de plus d'identifier la cinétique de la libération de divers systèmes, tels que les systèmes osmotiques, les systèmes dégradables ou non dégradables. Cela se traduit par des coûts inférieurs ainsi que des tests de laboratoire inférieurs. Les modèles mathématiques couramment utilisés pour déterminer le profil de libération/dissolution du médicament sont la cinétique d'ordre

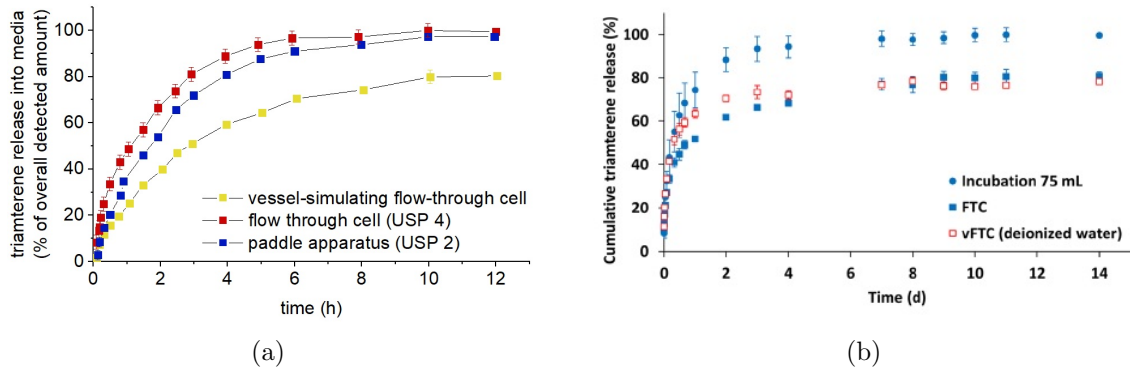


FIGURE B.6 – (a) Installation d’incubation réalisée dans des flacons en verre de 100 *ml*. Les cellules à flux continu ont été équipées d’un hydrogel d’agarose à base d’eau déminéralisée (vFTC (eau désionisée)) ou ont fonctionné sans deuxième compartiment (FTC). (b) triamterène des revêtements de stents dans les médias au fil du temps avec un écoulement simulant le vaisseau cellule, cellule à écoulement continu (USP 4) ou appareil à palettes (USP 2); débit 35 *ml/min*, vitesse de pagaie 50 *tr/min* [35, 159]

zéro, la cinétique de premier ordre, Hixon-Crowell, le modèle Higuchi, le modèle Weibull, le modèle Baker-Lonsdale, le modèle Korsmayer-Peppas et le modèle Hopfenberg. En dehors des mécanismes physiques, la libération depuis la surface de la particule entraîne un effet de libération par rafale. Cette partie de la libération a lieu à la première étape du profil de libération, qui n’est pas totalement acceptée pour être catégorisée comme un mécanisme physique.

B.2.6.2 Simulation du profil de libération du médicament

Outre la modélisation mathématique, les simulations numériques sont des outils très utiles dans la prédiction du profil de libération du médicament. Dans ce cas, certaines études ont effectué le calcul en une dimension [209], certains en deux dimensions [210, 211] et aussi en trois dimensions [199, 212]. À cet égard, il est possible de calculer la concentration de médicament dans les trois régions en contact avec le stent. Certaines études ont prédit la libération du médicament dans la lumière et le domaine sanguin. D’un autre côté, certaines études se sont concentrées sur la teneur en médicament dans le

tissu artériel (à des fins thérapeutiques). Enfin, certaines études se sont concentrées sur la libération du médicament à partir du film polymère recouvrant les stents [81, 213, 214]. Dans certaines études, la concentration initiale du médicament est considérée comme constante pendant la libération, ce qui ne correspond pas à la réalité [214–217]. Comme pour la modélisation mathématique, on retrouve aussi couramment dans les simulations numériques quelques hypothèses et simplifications. Par exemple, dans certaines études, le débit constant est considéré au lieu du débit pulsé, car ils ont déclaré que l'effet de la pulsatilité sur la libération du médicament du DES est négligeable [79, 80]. Cependant, certaines autres études parlent de l'importance du débit pulsé. Dans le but d'optimiser les stents, plusieurs études numériques ont porté sur l'influence de certains paramètres géométriques et sur les propriétés du polymère et du médicament (coefficient de diffusion, espacement des entretoises, effet de la plaque dans l'artère sténosée) [218–220]. Par exemple, Barakat et al. [18, 32] ont étudié la concentration de médicament dans le tissu pour deux types différents de médicament et ils ont analysé la cinétique de l'absorption du médicament. L'un des avantages de la simulation numérique est sa capacité à fournir quantitativement et qualitativement la distribution du médicament dans les différentes régions (lumière, tissu et polymère). Dans une étude de Vijayaratnam et al. [211] ils ont étudié qualitativement la distribution du médicament autour du stent et dans les tissus. Dans ce premier travail en 2D, ils considèrent le flux comme constant et également la teneur en médicament dans le polymère comme constante au cours du temps. Ils ont obtenu la distribution qualitative du médicament dans le tissu qui a été fortement affectée par le débit. Cependant, dans une autre étude [80], la réduction variant dans le temps du médicament du stent revêtu a été modélisées à un flux constant et pulsé. Les résultats de

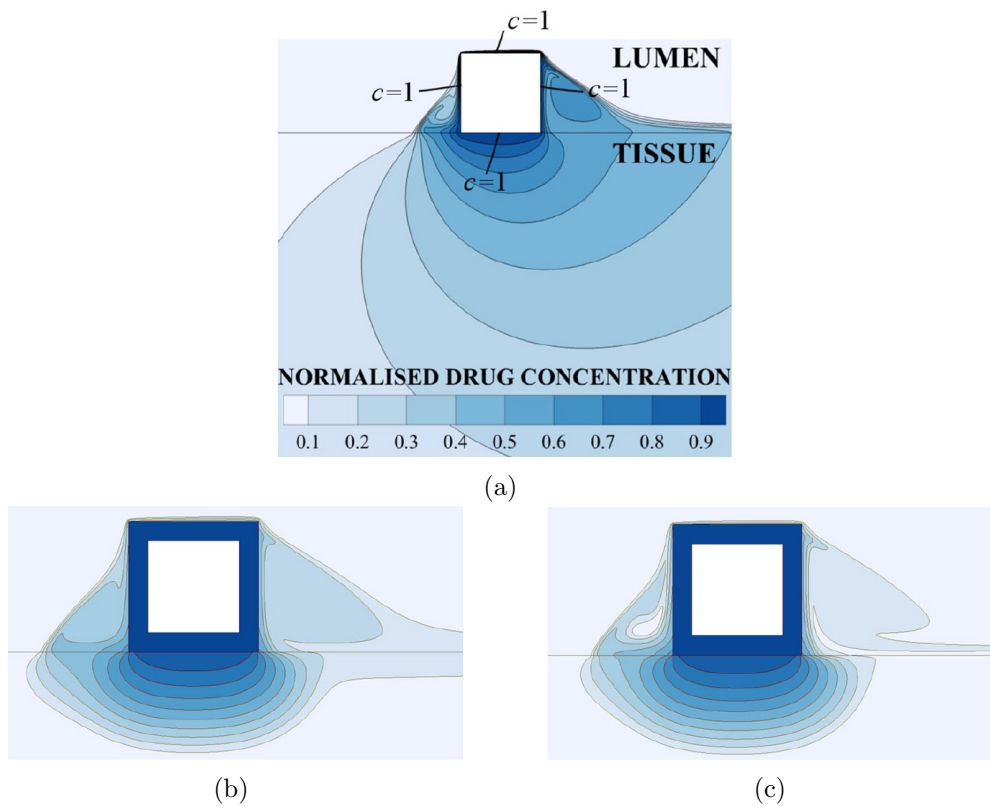


FIGURE B.7 – Distribution de concentration de médicament normalisée (a) dans la première étude en considérant une concentration de médicament constante, dans la deuxième étude avec une concentration variable (b) à un débit à l'état d'équilibre et (c) un schéma de flux pulsé [80]

la simulation ont montré que la modification du schéma de flux sanguin luminal, les propriétés non newtoniennes du sang et son comportement complexe près de la paroi ont un effet négligeable sur l'absorption du médicament. La figure B.7 montre ces résultats.

B.3 Résultats expérimentaux

B.3.1 Libération de médicaments dans la lumière artificielle

B.3.1.1 Effet du pourcentage initial du médicament chargé

Dans le système d'administration de médicaments, lorsque nous parlons du support polymère, il est à noter que la libération se produit en raison d'une force motrice, dans cette étude, cette force

B.3. RÉSULTATS EXPÉRIMENTAUX

motrice peut être liée à l'absorption d'eau, il est donc nécessaire d'étudier l'effet du pourcentage de drogue sur ce phénomène. La figure B.8 (a) montre les taux d'absorption d'eau pour quatre cas différents, PU pur et PU avec une charge médicamenteuse de 10, 20 et 30% en masse de DE. Il est à noter que l'eau pénètre même dans le PU pur, mais avec une valeur plus faible, proche de 5%. En revanche, pour les échantillons de PU chargés de médicament, ce taux augmente avec le pourcentage initial, alors que pour les échantillons de 30%DE, il atteint environ 70%. La présence du médicament joue donc un rôle prépondérant dans l'absorption de l'eau. Cela est dû à la propriété hydrophile du médicament choisi. On peut noter que cette valeur est affectée par la différence de densité du médicament ($450,7 \text{ mg/l}$) et de l'eau (997 mg/l) où ils sont substitués dans la même zone. Dans cette partie, la méthode de mesure était la méthode de gravimétrie, par conséquent, dans le calcul de la libération du médicament, tous les composants du médicament (épolamine, excipients) sont pris en considération. Pour la libération du médicament à partir d'échantillons de PU non dégradables, trois pourcentages différents du médicament (10, 20, 30 %) ont été chargés dans le polymère. La figure B.8 (b) montre le pourcentage de libération de médicament pour trois échantillons de PU chargés en DE différents. Il est à noter que l'augmentation du médicament initial n'a pas entraîné la libération prolongée. En revanche, en comparant les trois courbes du PU avec 10, 20 et 30% de médicament, il apparaît qu'en augmentant la teneur en médicament, il y a une diminution du temps maximum de libération. De plus, la cinétique et la quantité de libération sont augmentées. Nous pouvons obtenir de la figure B.8 (b) que la libération est commencée par une libération de rafale initiale. En outre, la libération est suivie d'une cinétique de libération plus élevée avec l'augmentation du pourcentage

B.3. RÉSULTATS EXPÉRIMENTAUX

de médicament. Dans ce but, connaître les mécanismes de la libération est important pour analyser l'origine des phénomènes. Comme il est obtenu à partir de la figure B.8 (a) Il est à noter que dans le cas d'un médicament hydrophile, l'augmentation de la teneur en médicament a augmenté la teneur en eau absorbée. Le polyuréthane est presque connu pour être un polymère hydrophobe. Par conséquent, la diffusion de l'eau vers le polymère se fait très probablement à travers les pores. Dans ce cas, le contact avec le médicament hydrophile entraîne la dissolution rapide du médicament et sa libération à travers les pores remplis d'eau. Dès lors, on peut noter l'importance du mécanisme de la diffusion dans ce système. D'autre part, l'absorption d'une grande quantité d'eau due à la présence du médicament hydrophile dans une structure poreuse d'une matrice entraîne la pression osmotique. La pression créée entraîne l'expulsion du médicament dissous avec la solution aqueuse à travers les pores, où elle montre une augmentation de la cinétique de libération. Il est à noter que le médicament libéré, puis l'espace libre laissé dans les échantillons contribuent à une plus grande absorption d'eau et à un espace libre pour libérer le médicament restant. Sachant que le mécanisme de gonflement peut entraîner la variation dimensionnelle des échantillons, nous avons donc mesuré la géométrie des échantillons avant et après essais. Les résultats ont montré que les échantillons polymères n'avaient aucun changement de dimension.

De plus, l'effet du pourcentage de médicament a été étudié dans le cas d'un débit constant au débit de $7,5 \text{ ml/s}$. Les résultats de l'absorption d'eau et de la libération du médicament en condition continue, $Q = 7,5 \text{ ml/s}$ sont présentés dans la figure B.9. Sur cette figure, on peut noter l'effet de la charge médicamenteuse initiale sur les résultats de libération. En comparant les résultats de l'ab-

B.3. RÉSULTATS EXPÉRIMENTAUX

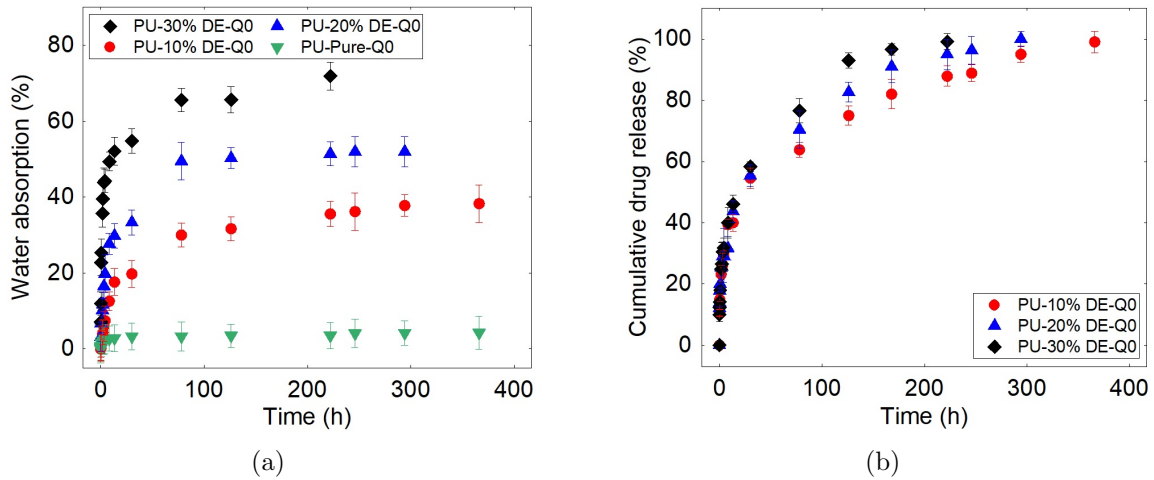


FIGURE B.8 – (a) Absorption d'eau et (b) pourcentage de libération de médicament pour le PU avec un pourcentage différent de DE à l'état sans écoulement

sorption d'eau pour les tests avec le débit de 7.5 ml/s et avec différents pourcentages de médicament, on peut noter que l'eau peut pénétrer dans le polymère d'environ 32% dans le cas du PU avec 10 % de médicament, et il augmente lentement avec le pourcentage de médicament à 56% PU avec 30% de médicament. La figure B.9 (b) montre qu'à partir de la pente de la deuxième partie de la courbe, on peut noter le même mécanisme de libération de médicament dans cette condition à différents pourcentages de médicament. Globalement, le même comportement d'absorption d'eau et de libération de médicament peut être observé dans un cas continu et un état sans flux avec différents pourcentages de médicament.

La figure 4.18 montre les micrographies de DE, les tailles de pores dans les échantillons chargés de PU-10%DE et de polyuréthane après 1h de test de libération au débit de $7,5 \text{ ml/s}$. La figure B.10 (a) montre que la taille moyenne des particules DE est d'environ $40 \mu\text{m}$. La comparaison des figures B.10 (a) et (b) indique que la taille des pores est plutôt égale ou plus grande que les particules DE. En analysant les micro-graphes montrés dans la figure B.10 (b), (c), (d) et (e), les observations suivantes

B.3. RÉSULTATS EXPÉRIMENTAUX

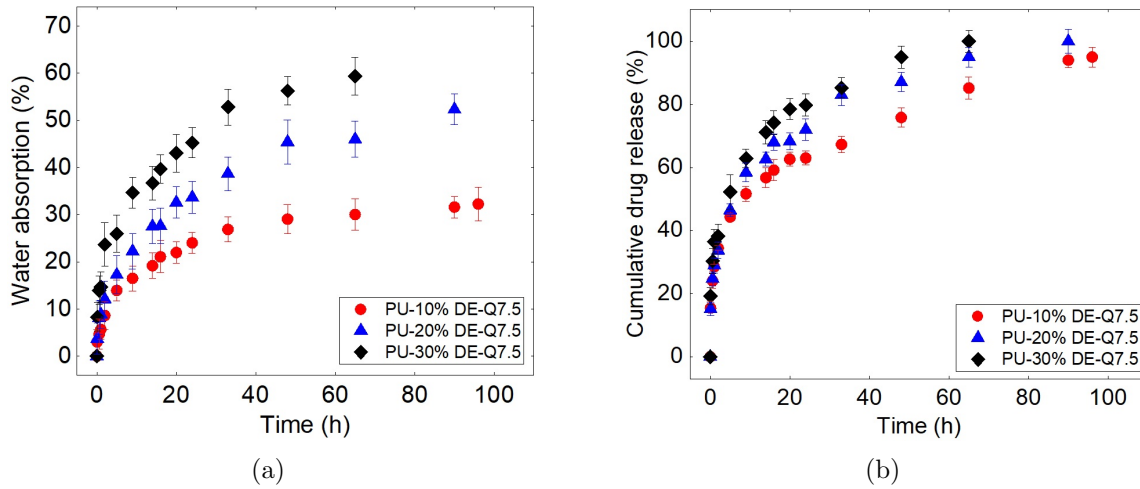


FIGURE B.9 – (a) Absorption d'eau et (b) Libération de médicament pour différents pourcentages de médicament à débit constant avec un débit de $Q=7.5 \text{ ml/s}$

peuvent être obtenues :

- Pour de très faibles concentrations de médicament, certaines particules peuvent être isolées dans la matrice et ainsi ne jamais entrer en contact avec l'eau ;
 - En augmentant le pourcentage de médicament, la connexion entre les pores est augmentée ;
 - Pour le pourcentage plus élevé de médicament, une plus grande quantité de pores est observée ;
 - Un risque de percolation existe pour les échantillons à plus forte teneur en médicament. De plus, les vides sont plus proches, et la possibilité d'un lien entre eux peut établir le lien pour la circulation du liquide, ce qui provoque la libération rapide du médicament. En conclusion, la taille, la concentration et la distribution des particules de médicament dans la matrice représentent des facteurs qui peuvent affecter la libération de médicament.
- Cependant, la matrice poreuse aide à libérer le médicament de la matrice [145] mais son contenu optimisé dépend de l'objectif de la thérapie.

B.3. RÉSULTATS EXPÉRIMENTAUX

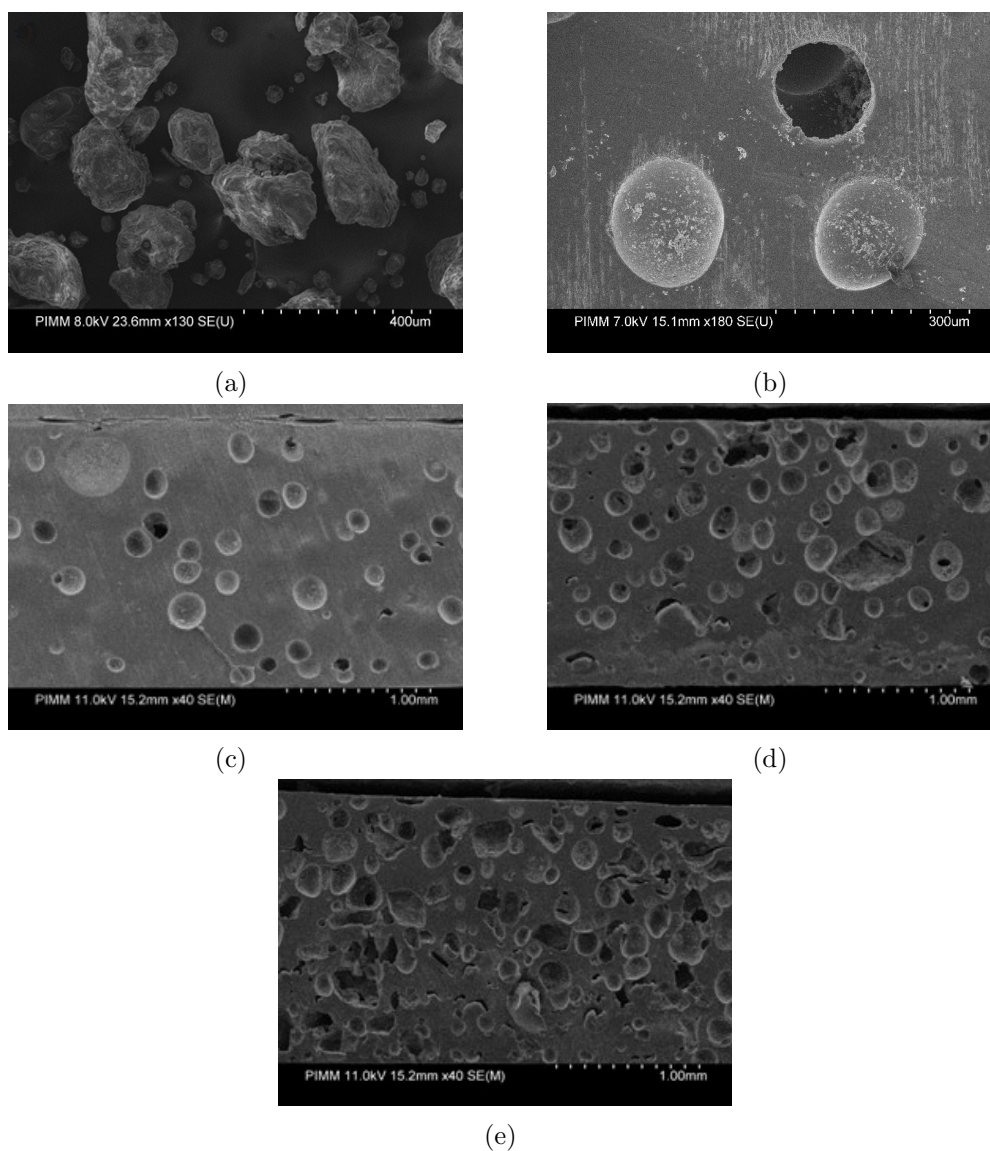


FIGURE B.10 – Micrographies SEM : (a) DE (b) PU-10%DE ($300\ \mu\text{m}$) (c) PU-10%DE ($1\ \text{mm}$) (d) PU-20%DE ($1\ \text{mm}$) et (e) PU-30%DE ($1\ \text{mm}$) du côté épaisseur des échantillons après une heure de test au débit de $7,5\ \text{ml/s}$

B.3.1.2 Effet du débit

En raison de la présence de flux dans l'étude de l'administration de médicaments dans le cas des stents, il est important d'étudier l'effet de ce paramètre.

Dans cette section, la libération de médicament (DS) à partir d'échantillons PLGA chargés de 10% de DS à différents débits de 0, 6,5, 7,5 et 23,5 *ml/s* dans du PBS à la température de 37°C a été étudiée.

La figure B.11 montre les profils de libération de médicaments des films PLGA-10%DS à différents débits de 0, 6,5, 7,5 et 15 *ml/s*. Les résultats montrent qu'en augmentant le débit, la cinétique de libération est augmentée (comme discuté pour les échantillons PU-DE). Cependant, on obtient de la figure B.11 qu'à partir du débit de 0 à 6,5 *ml/s* cette différence est significative. Alors que, de 6,5 à 15, il n'y a pas une grande différence dans la cinétique de la libération. Ceci souligne que l'effet du type d'écoulement est plus important dans ce type de support polymère. La première peut être due à l'apport des mécanismes de libération.

Il est à noter que les échantillons à différents types de flux et débits sont réduits du médicament presque en même temps. De plus, les résultats montrent que presque la même cinétique et les mêmes mécanismes de libération des échantillons à différents débits dans l'état continu se produisent.

L'analyse des mécanismes qui se produisent lors de la libération dans ces systèmes est importante pour des investigations ultérieures. Les résultats montrés dans la figure B.11 indiquent la présence de la libération en rafale de manière significative pour les échantillons exposés en régime continu d'écoulement avec des débits différents. A cet égard, initialement le film est sec puis il est exposé à

B.3. RÉSULTATS EXPÉRIMENTAUX

l'environnement aquatique, après la libération de la salve initiale due au gradient de la concentration entre les films et l'environnement aquatique le mécanisme de diffusion se produit. Deux autres mécanismes qui ont été observés lors du test sont, le gonflement et l'érosion des échantillons. Un gonflement des échantillons a été fortement observé après une heure de test pour les échantillons exposés en flux continu. De plus, l'observation des petites particules dans la chambre de relargage lors du largage indique la présence de l'érosion (dégradation physique) entraînant la perte de masse du polymère.

En considérant la figure B.11, environ 78,8% du médicament a été libéré de PLGA-10%DS au débit de 7,5 *ml/s* au cours des 48 premières heures, tandis que l'échantillon PLGA avec 10% de le médicament à 48 heures ne libère que 17,8% de médicament à l'état statique. Il convient de noter que le temps nécessaire à la libération des 80% du médicament à l'état statique est environ quatre fois supérieur à celui de l'état continu. On peut mentionner que selon des études, la présence de débit a augmenté la pénétration du fluide dans le support ce qui va augmenter la quantité d'eau absorbée. L'eau pénétrée dans les films polymères entraîne la dissolution des particules de médicament et également le gonflement de la couche polymère, après quoi la substance active quitte la couche polymère par le mécanisme probable de diffusion. La dégradation est un autre mécanisme important pour ce type de polymère mais selon les études de la littérature, l'incidence de la dégradation chimique dans la courte durée du test est loin de l'attendu. Cependant la dégradation physique telle que l'érosion ou les contraintes environnementales aboutissant à la fissuration peut être une autre cause de libération, notamment avec la présence de l'écoulement. Une explication plus détaillée des mécanismes sera discutée dans le chapitre 4.

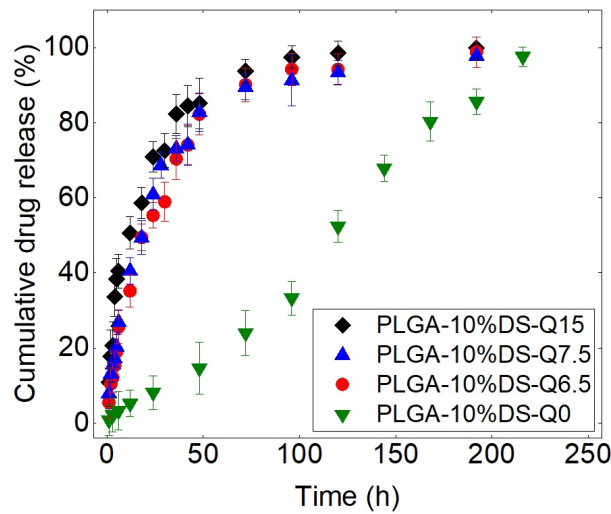


FIGURE B.11 – Libération cumulative de médicament à partir de films PLGA avec 10% DS aux débits de 0, 6,5, 7,5 et 15 ml/s

La figure B.12 montre les micrographies SEM du PLGA-10%DS après 48 heures de test de libération à deux débits différents de 0 et 7,5 ml/s . L'effet du débit sur la structure des films PLGA est évident à partir de ces figures. On observe que dans la condition de libération sans écoulement (représentée sur la figure B.12 (a) et (c)) les bulles sont créées par absorption d'eau, cependant dans le cas avec écoulement (représenté sur la figure B.12 (b) et (d)), les bulles semblent avoir déjà explosées et la structure poreuse est visible, ce qui entraîne une plus grande libération du médicament et, bien sûr, une diminution des propriétés mécaniques des échantillons. De plus, la figure B.12 (b) montre clairement la présence du gonflement du polymère à l'état continu. Les résultats montrent que le débit modifie significativement la morphologie du polymère, où il augmente la rugosité des échantillons à l'échelle méso. Il ressort de la figure B.12 (d), qui est la plus grande échelle de la figure B.12 (b), montre que le gonflement entraîne l'augmentation du détachement des chaînes polymères et augmente l'espacement moléculaire. Ce dernier entraîne la libération du médicament des chaînes polymères et provoque également une

B.3. RÉSULTATS EXPÉRIMENTAUX

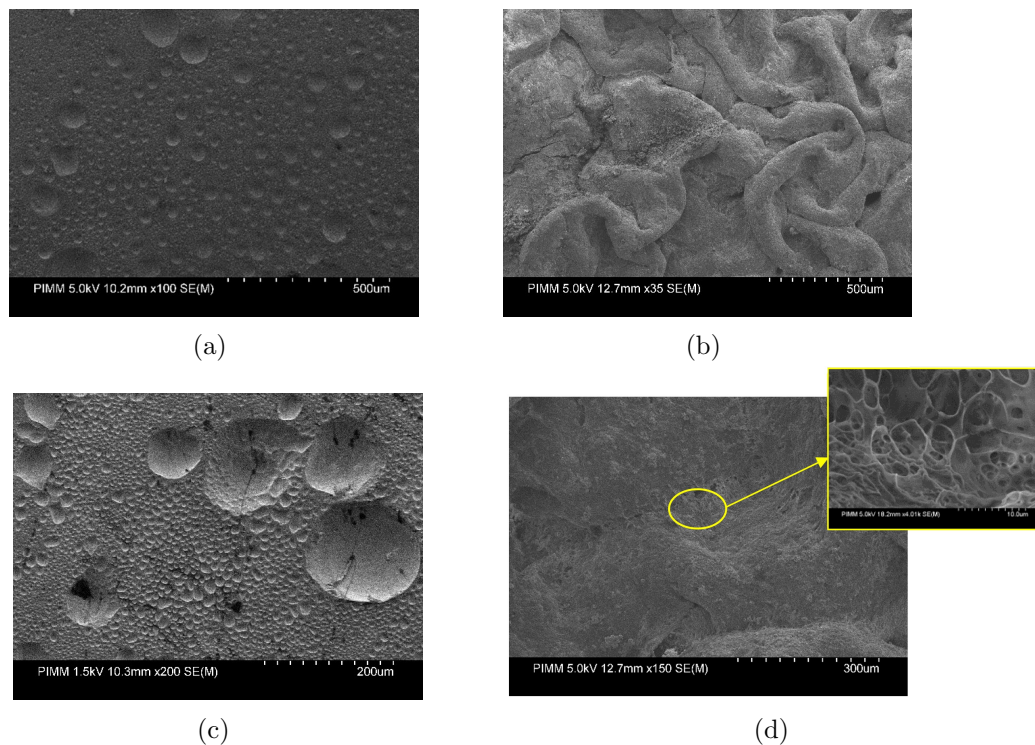


FIGURE B.12 – Micrographies SEM de PLGA-10%DS après 48 heures de libération du médicament en (a) et (c) le débit de 0, (b) et (d) un débit de 7,5 ml/s, mais à différents grossissements

structure fragile du polymère.

B.3.2 Évaluation des propriétés mécaniques, physiques et chimiques des supports polymères de médicaments pendant la libération

B.3.2.1 PU chargé de diclofénac épolamine

Propriétés mécaniques du PU

La figure B.13 (a), (b) montre les courbes de traction des échantillons de PU avec 0 et 10% de médicament à différents temps d'incubation dans l'état statique. Les résultats montrent que l'effet du médicament sur les propriétés mécaniques des échantillons polymères est significatif. La figure B.13 (a) montre que le temps d'immersion pour les échantillons de PU pur ne modifie pas significativement les propriétés de traction. Cependant, la figure B.13 (b) indique qu'une augmentation de 10% du

B.3. RÉSULTATS EXPÉRIMENTAUX

médicament a réduit les propriétés mécaniques d'environ la moitié. De plus, la présence du médicament provoque la variation des propriétés mécaniques pendant le temps de libération par rapport au polymère pur.

La figure B.13 (c), (d) et (e) montre le comportement en traction des échantillons de PU avec 0, 10 et 20% du médicament au débit de 7,5 *ml/s*. Les résultats de ces chiffres montrent que l'ajout de 10% de médicament diminue les propriétés mécaniques d'environ la moitié et l'ajout de 20% de médicament les diminue d'environ un quart par rapport au PU pur. Alors que l'on peut noter sur les figures B.13 (a) avec B.13 (c) et B.13 (b) avec B.13 (d) que la comparaison des débits de 0 et 7,5 *ml/s* pour PU-Pure, les contraintes et déformations passent de 3,95 à 3,36 *MPa* et de 330 à 269 ce qui montre que l'effet du débit sur le comportement mécanique n'est pas très sensible pour ce type de polymère. De plus, les propriétés mécaniques des échantillons de PU avec 0, 10 et 20% de la substance active avant le positionnement dans le fluide, ont montré l'effet élevé de la charge médicamenteuse sur les propriétés des supports (montré sur la figure B.13 (c), (d) et (e)). Cela indique que l'ajout de la substance active entraîne une faible élasticité du support polymère. Où après le contact initial des échantillons chargés de médicament avec le milieu aquatique (1h) et l'absorption d'eau de la substance active et du polymère, le support devient plus déformable (illustré aux figures B.13 (d), et (e)). Les figures B.14 (a)-(f) montrent la comparaison du module, de la résistance ultime et des valeurs de déformation à la rupture pour les différents pourcentages du médicament (0, 10% et 20%) à différents intervalles de temps des tests de libération statique et continue. Les résultats des figures B.14 (a), (b) montrent que l'effet du pourcentage de médicament sur le comportement mécanique des échantillons

B.3. RÉSULTATS EXPÉRIMENTAUX

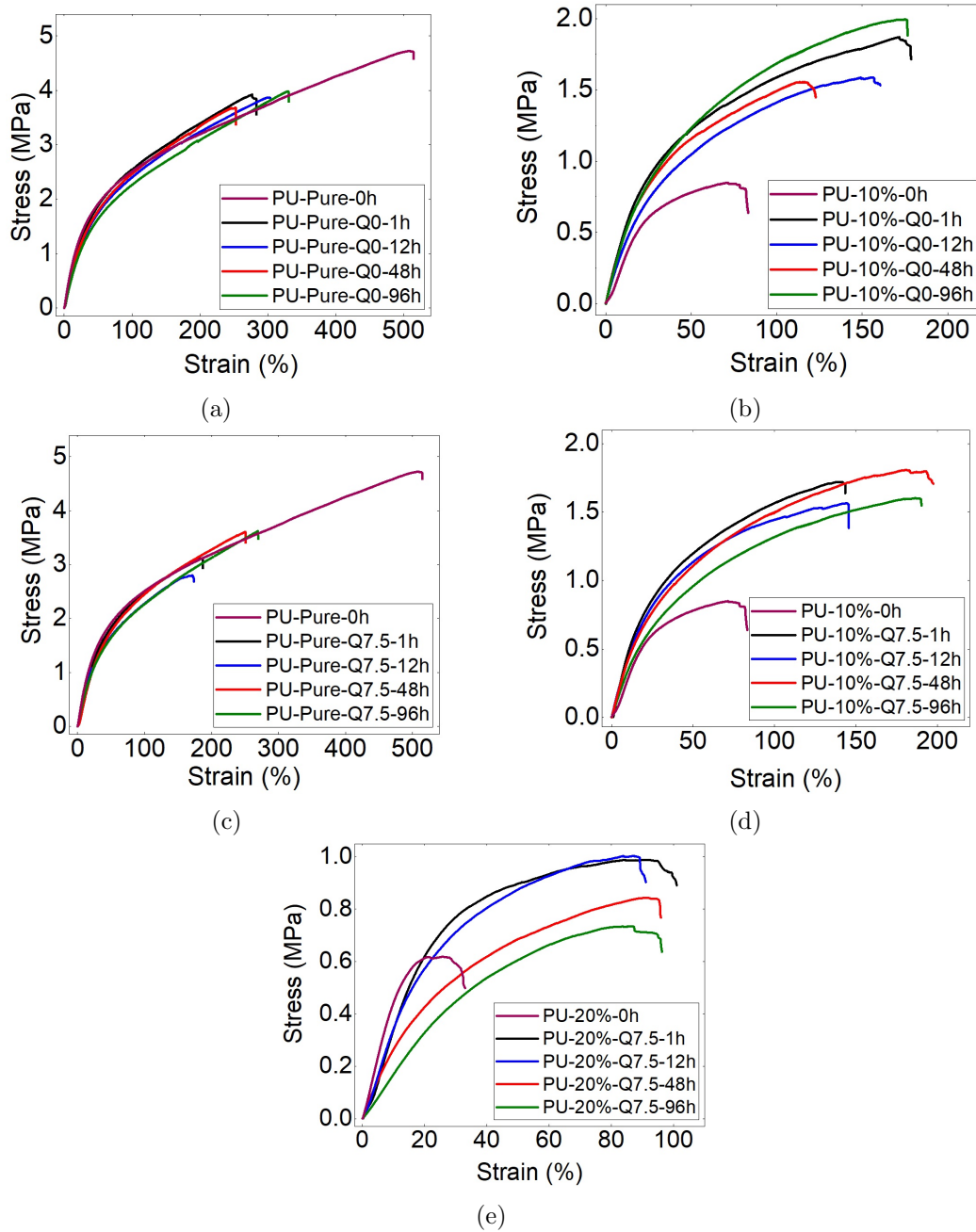


FIGURE B.13 – Courbes contrainte-déformation des échantillons PU avec (a) 0 et (b) 10%DE, au débit de zéro et (c) 0, (d) 10%DE et (e) 20%DE au débit de 7,5 ml/s , à différents intervalles de temps

B.3. RÉSULTATS EXPÉRIMENTAUX

est plus significatif par rapport au débit, où l'augmentation du pourcentage de médicament diminue la valeur du module d'Young. Les résultats montrent que le temps d'incubation diminue légèrement la valeur du module, où cet effet est plus visible pour les polymères chargés que pour les polymères purs. Les figures B.14 (c), (d) montrent la résistance ultime du PU avec différents pourcentages de médicament aux débits de 0 et 7,5 *ml/s*. En comparant ces valeurs, l'impact du débit et du temps d'incubation n'est pas significatif, mais l'augmentation de la charge initiale du médicament diminue fortement la résistance ultime des échantillons de PU. La variation de la force pendant le temps d'incubation initial peut être due à l'effet plastifiant des molécules d'eau sur les composants du DDS. Les figures B.14 (e) et (f) montrent la contrainte à la rupture pour le PU avec un pourcentage différent de médicament aux débits de 0 et 7,5, respectivement. La comparaison des résultats de la déformation à la rupture pour le PU montre que l'augmentation du pourcentage de médicament diminue l'élongation des échantillons polymères. Cependant, l'élongation des échantillons avec le temps d'incubation ne diffère pas de manière significative mais en raison de la plastification après 96 heures, il a une légère augmentation.

A partir des résultats mécaniques, on peut observer que le module, la contrainte et l'élongation à la rupture les plus élevés parmi tous les résultats avec/sans médicament, avant ou après test se réfèrent au PU pur vierge. Alors que PU-20%DE avant le test d'incubation a la valeur la plus faible du stress et de la contrainte. Cela peut s'expliquer lorsque les pourcentages du médicament augmentent, le nombre de pores dans les échantillons augmente, ce qui entraîne une diminution des propriétés mécaniques. En revanche, le débit n'affecte pas de manière notable les propriétés mécaniques des échantillons.

B.3. RÉSULTATS EXPÉRIMENTAUX

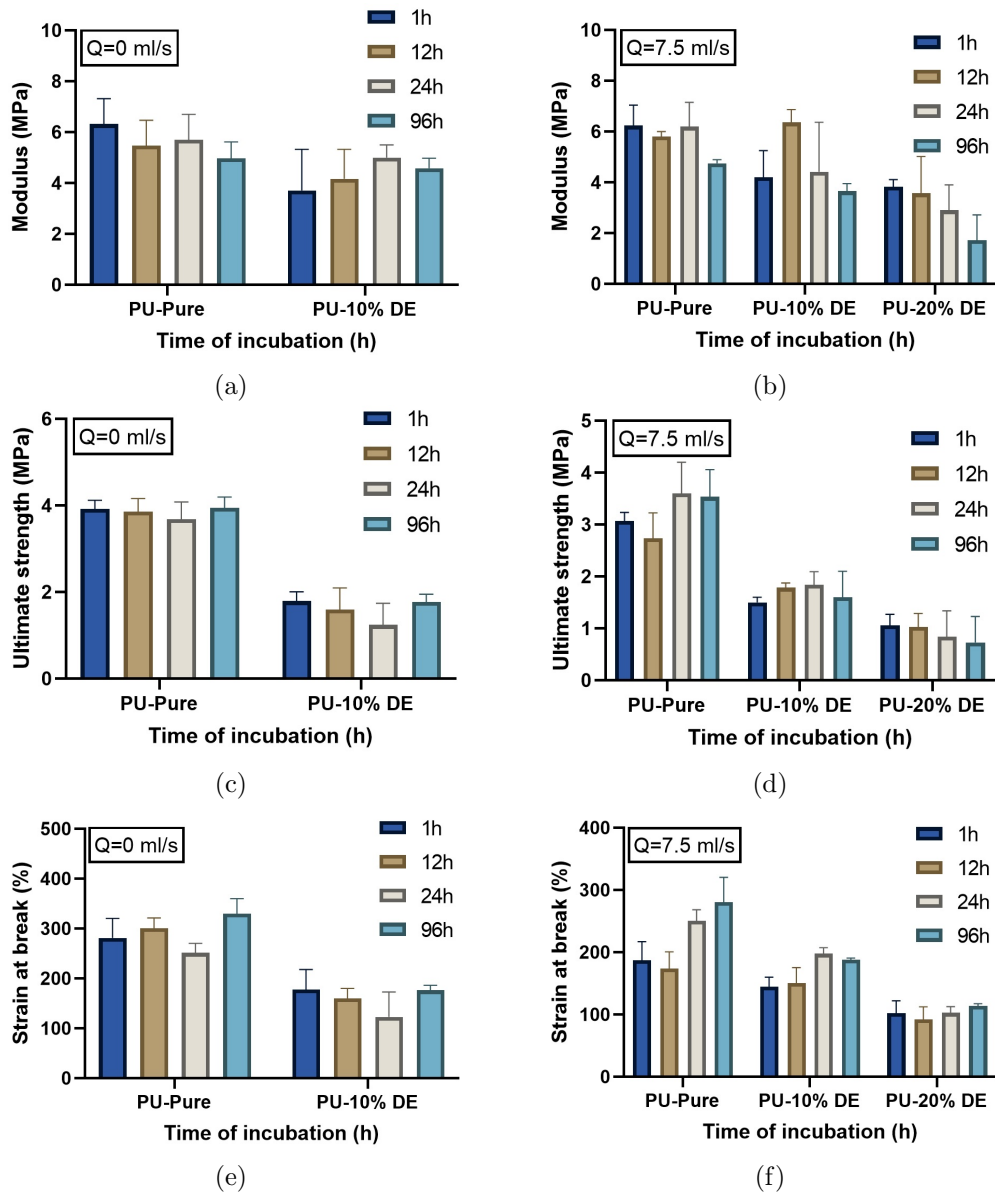


FIGURE B.14 – Caractéristiques matérielles des échantillons PU avec différents pourcentages de DE après test de libération à l'état statique et continu

B.3. RÉSULTATS EXPÉRIMENTAUX

Les résultats ont montré qu'en augmentant le débit, la cinétique de libération du médicament est augmentée, mais ce paramètre n'a pas modifié de manière significative les propriétés intrinsèques du matériau comme le T_g et le module. Où, les pourcentages de médicament modifient les propriétés mécaniques du polymère et augmentent la fraction de volume libre dans les échantillons, mais la transition vitreuse du polymère reste plutôt constante (en comparant les chiffres ?? et ??) .

B.3.2.2 PLGA chargé de diclofénac sodique

Dégradation du polymère PLGA

Afin d'analyser la dégradation chimique et physique des supports polymères, des spectres FTIR et des observations SEM ont été respectivement utilisés. Pour les échantillons PLGA-Pure aux débits de 0 et 7,5 ml/s à différents intervalles de temps, les résultats FTIR sont présentés dans la figure B.16. Des diminutions relativement identiques de la taille des pics lors de la libération sont montrées sur la figure B.16, elles sont liées à la diminution de l'épaisseur des échantillons à cause de la dilatation observée dans la largeur et la longueur des échantillons lors de la temps d'immersion. Les résultats ont montré qu'il n'y a pas de dégradation chimique après 48 heures du temps d'immersion, à l'état statique. Cependant, il est nécessaire d'effectuer le test après plusieurs temps d'immersion pour confirmer s'il y a un phénomène de dégradation chimique.

Des microscopies de la morphologie de surface des films PLGA-Pure avant et après 1, 12, 24, 48 heures d'incubation en PBS au débit de zéro sont présentées sur la figure B.15. La surface des échantillons avant incubation est lisse. En rentrant dans le temps de libération, les échantillons acquièrent une surface opaque blanche et rugueuse constituée de bulles microscopiques à cause de l'absorption

d'eau et déclenche le phénomène de dégradation physique qui est évident sur la figure B.15 (c). Comme le montre cette figure suivant le temps, les bulles seront transformées en pores. Enfin, les pores sont connectés les uns aux autres et entraînent la faiblesse des propriétés mécaniques des échantillons et entraîne leur rupture.

Propriétés mécaniques de PLGA

En utilisant les films PLGA comme exemple, la courbe contrainte-déformation peut être divisée en une région élastique et d'écrouissage. La figure B.17 montre que dans tous les échantillons, la plasticité du polymère après 1 heure d'immersion dans le PBS augmente là où ils ont une déformation élevée par rapport aux échantillons vierges, c'est pour l'effet plastifiant de l'eau sur les échantillons de PLGA. Cependant, après une heure l'effet de la température d'essai, 37°C qui est proche de la température de transition du polymère utilisé et aussi l'effet anti-plastifiant de la substance médicamenteuse dans le polymère [255], l'effet du gonflement et l'érosion, de plus la création de pores diminue l'élongation des échantillons. On obtient à partir de la figure B.17 qu'en augmentant le temps d'immersion des échantillons, le polymère devient cassant, là où le module d'Young et la contrainte maximale des échantillons augmentent.

Cette différence est plus remarquable lorsque certains pourcentages du médicament ont été ajoutés aux films polymères. Cependant, en augmentant le pourcentage du médicament de 5% à 10%, on observe une augmentation de l'élongation, une diminution du module de Young et une contrainte maximale. On peut noter que le plus grand élongation pour les échantillons de PLGA-10%DS par rapport au PLGA-5%DS peut être dû aux pores de petite taille qui ont été observés dans les observations

B.3. RÉSULTATS EXPÉRIMENTAUX

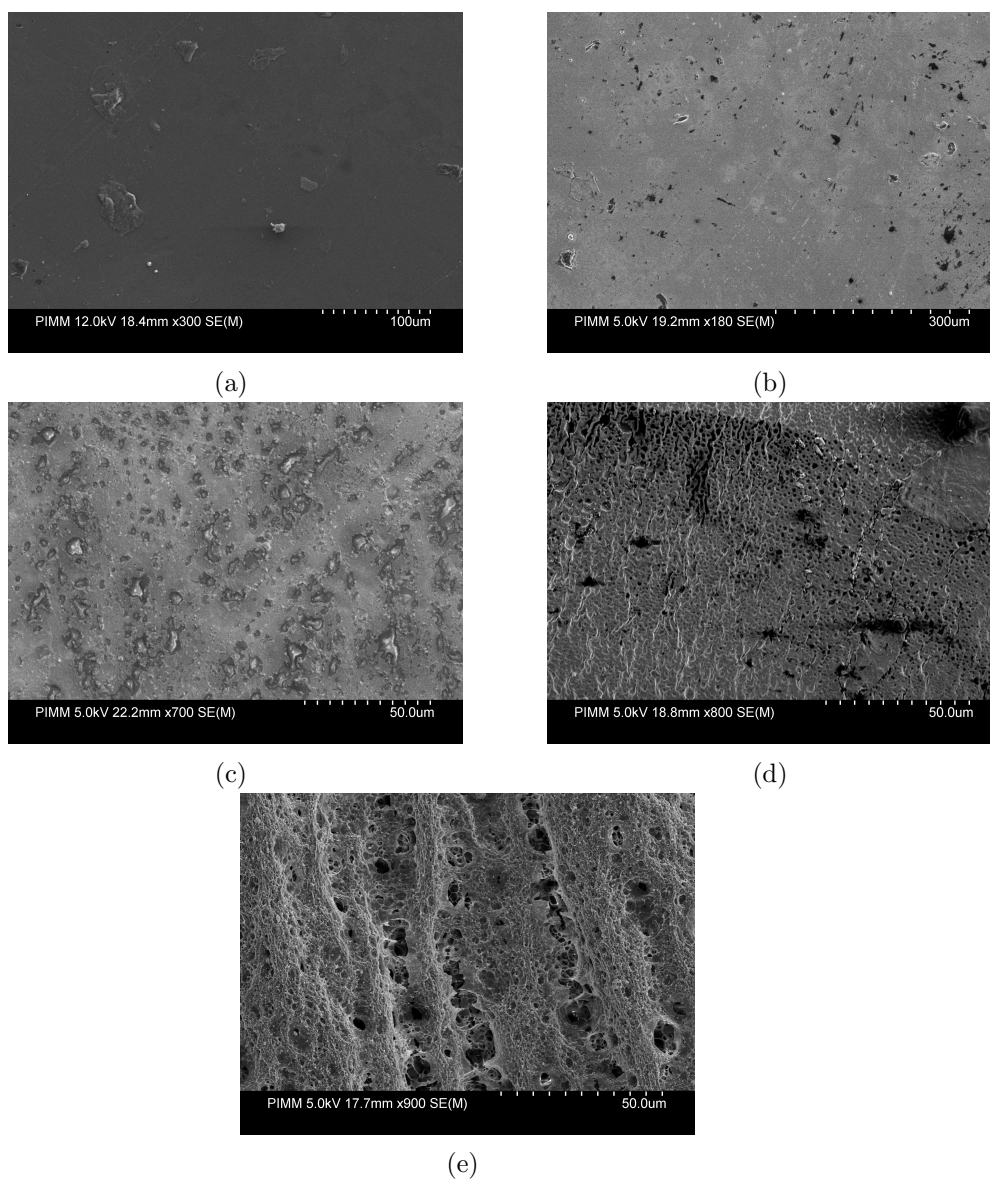


FIGURE B.15 – Micrographies des échantillons PLGA en PBS à débit nul après (a) 0, (b) 1, (c) 12, (d) 24, (e) 48 heures

B.3. RÉSULTATS EXPÉRIMENTAUX

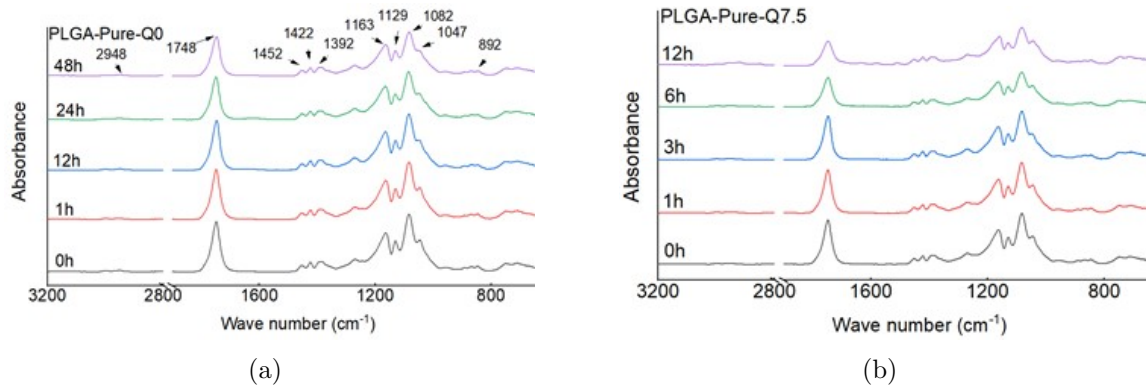


FIGURE B.16 – Spectroscopie FTIR après (a) libération statique et (b) continue du médicament pour le PLGA pur après un certain temps d'incubation

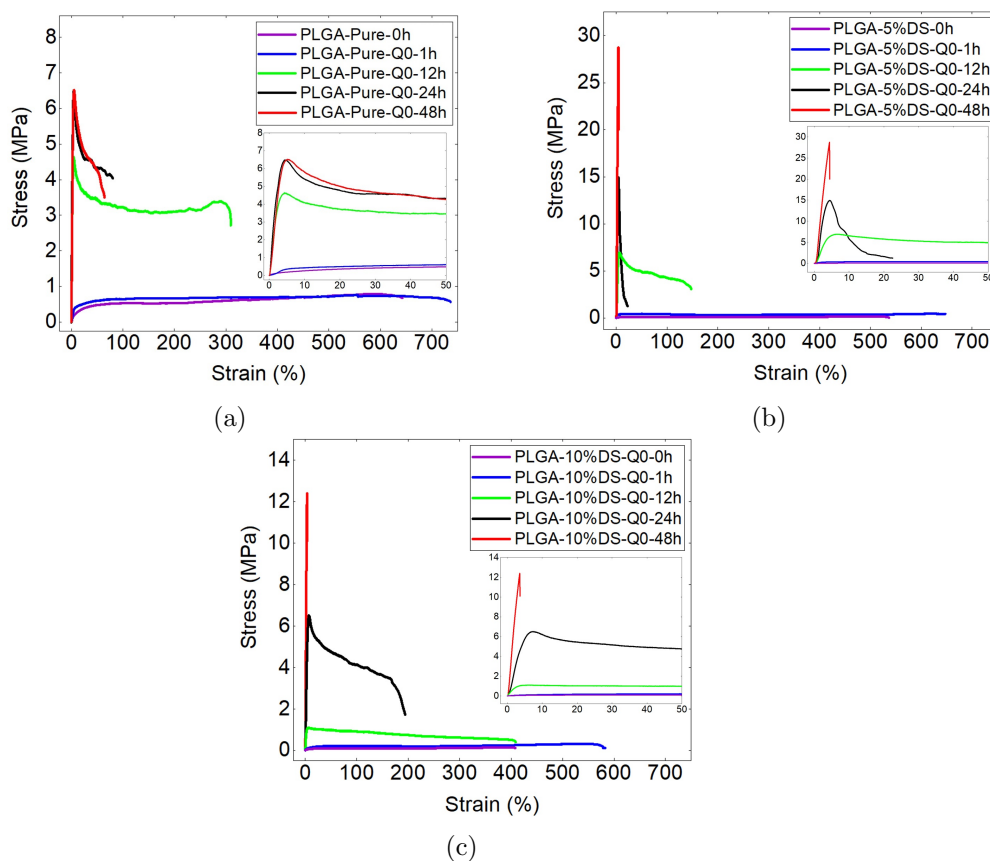


FIGURE B.17 – Courbes contrainte-déformation de l'essai de traction pour les échantillons de PLGA (a) pur, (b) 5%, et (c) 10%DS après incubation à l'état statique

B.3. RÉSULTATS EXPÉRIMENTAUX

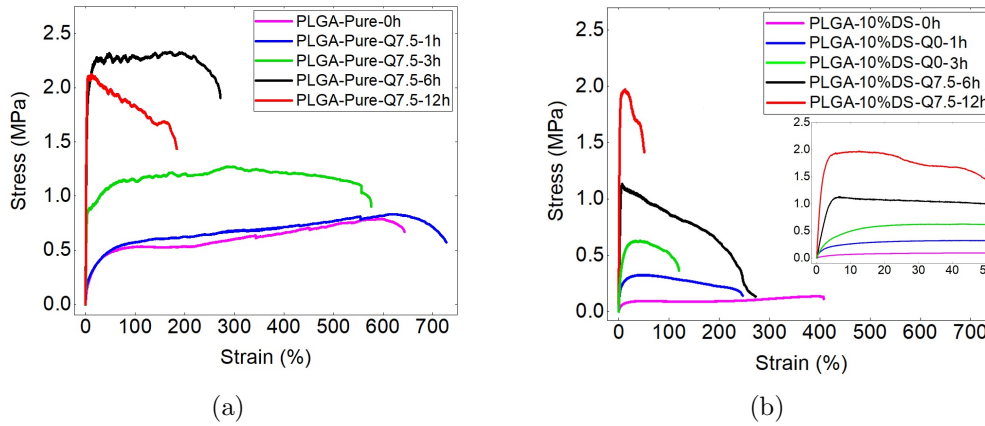


FIGURE B.18 – Courbes contrainte-déformation du PLGA (a) pur et (b) 10% DS après test de libération au débit de $7,5 \text{ ml/s}$

microscopiques optiques. Dans le cas de l'état continu avec un débit de $7,5 \text{ ml/s}$, l'effet des pourcentages de médicament n'était pas hautement détectable sur la contrainte maximale du polymère. Cependant, l'élongation à la rupture a diminué d'environ la moitié (montré sur la figure B.18).

Les figures B.19 (a)-(f) montrent la comparaison du module de Young, de la contrainte ultime et des valeurs de déformation à la rupture pour les différents pourcentages du médicament (0, 5% et 10%) à différents moments intervalles des tests de libération statique et continue. Les résultats des figures B.19 (a) et (b) montrent qu'en augmentant le débit de 0 à $7,5 \text{ ml/s}$ le module de Young des échantillons a diminué jusqu'à moins de la moitié. Cette diminution était beaucoup plus significative pour les échantillons contenant 10% de médicament. Une autre remarque est qu'en comparant ces deux graphiques on peut constater que la variation du pourcentage de médicament fait plus de variance dans les propriétés mécaniques que la variation du débit. La présence du médicament a augmenté le module de Young des échantillons polymères, en revanche, l'augmentation du débit les a diminués.

Les figures B.19 (c) et (d) montrent la contrainte maximale du PLGA avec différents pourcentages

B.3. RÉSULTATS EXPÉRIMENTAUX

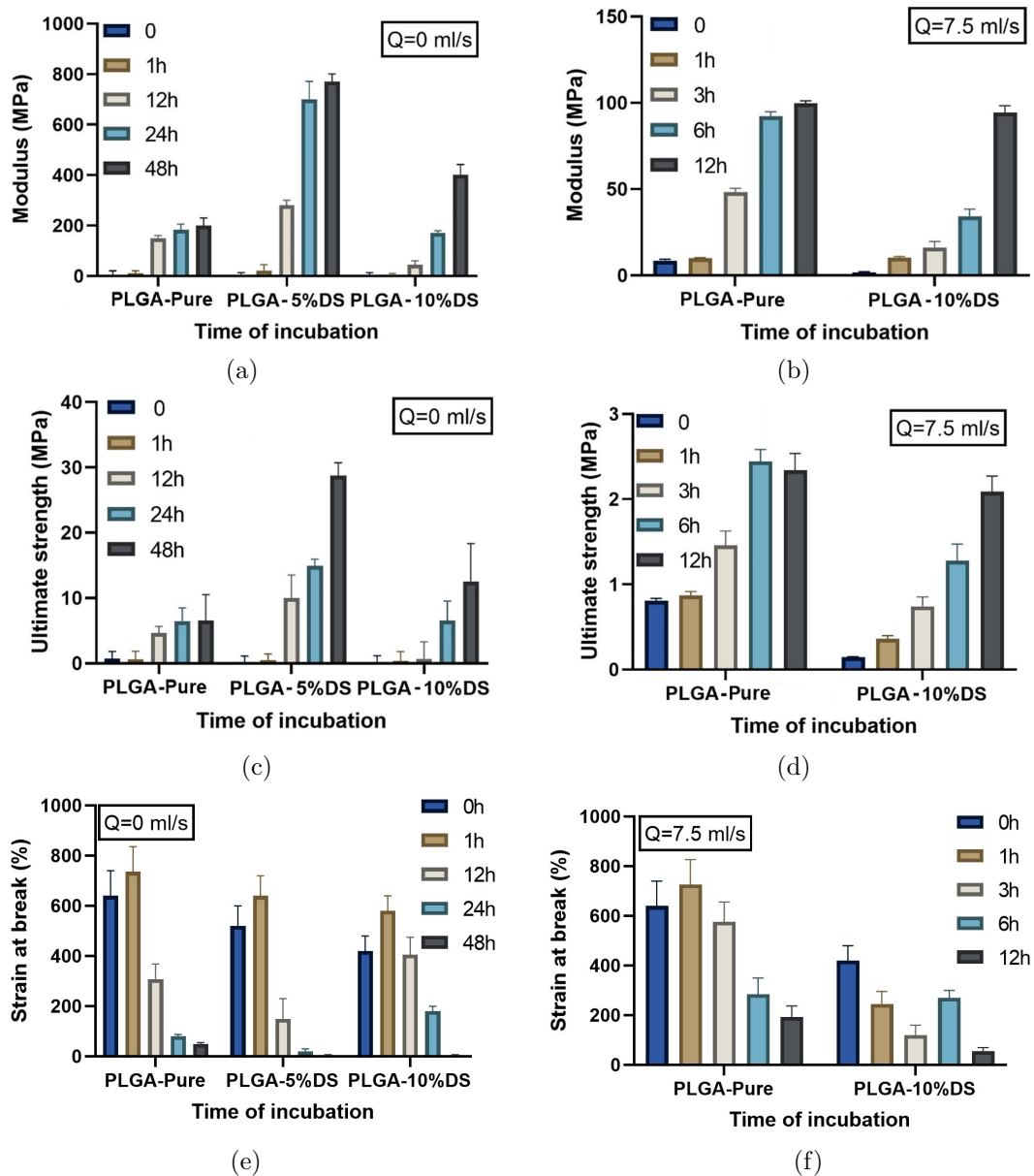


FIGURE B.19 – Caractéristiques matérielles des échantillons PLGA avec différents pourcentages de DS après test de libération du médicament à l'état statique et continu

B.3. RÉSULTATS EXPÉRIMENTAUX

de médicament aux débits de 0 et 7,5 ml/s , respectivement. D'après la figure B.19 (c), il est évident que l'augmentation du pourcentage de médicament à 5% de diclofénac sodique augmente le stress maximal, cependant dans le cas de 10% cette valeur est diminuée. Ce dernier peut s'expliquer par le gonflement plus élevé des échantillons de PLGA-10%DS par rapport à PLGA-5%DS. En comparant les figures B.19 (c) et (d), l'effet du débit sur la contrainte maximale est évident. Où en changeant le débit de 0 à 7,5 ml/s , la contrainte maximale a diminué d'environ 5 MPa à 2,5 MPa pour les échantillons de PLGA-Pure après 12 heures de test de libération. Alors que cette différence est plus notable pour les échantillons de PLGA-10%DS. Les figures B.19 (e) et (f) montrent la déformation à la rupture pour le PLGA avec différents pourcentages de médicament aux débits de 0 et 7,5, respectivement. La comparaison des résultats de la déformation à la rupture montre que l'augmentation de la charge initiale de médicament et du débit a diminué l'élongation à la rupture. Où l'effet du débit est très notable lorsque les échantillons sont chargés de médicament. De plus, l'effet du débit et du pourcentage de médicament est plus important en augmentant le temps de libération.

A partir des résultats mécaniques, on peut observer que le module le plus élevé et la contrainte maximale sont pour les échantillons de PLGA-5%DS. Ceci peut s'expliquer par une plus grande homogénéité des échantillons dans ce cas. Cela signifie que le médicament peut jouer un rôle de renforcement pour la PLGA, mais pas pour tous les pourcentages. Cependant, lorsque le pourcentage du médicament est augmenté, la perte de propriétés peut être due à une homogénéité moindre.

La figure B.20 (a) montre la fissure propagée après le test de traction pour les échantillons de PLGA-10%DS après 48h de libération du médicament. Comme il est mis en évidence avec les cercles sur la

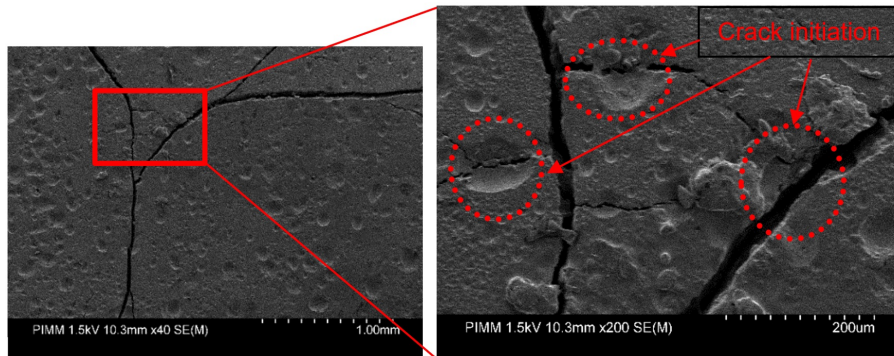


FIGURE B.20 – Micrographies SEM du PLGA-10%DS après libération du médicament de 48h à l'état statique après essai de traction avec un grossissement de (gauche) 1 *mm* et (droite) 200 μm

figure B.20 (b) il a été constaté que les pores de grande taille peuvent être à l'origine de l'amorçage de la fissure et de la fracture des échantillons. En analysant la fractographie des échantillons, on peut constater que ces microfissures, qui sont à l'origine du phénomène d'endommagement local, en outre, leur coalescence peut entraîner la rupture définitive de l'échantillon. Ainsi, selon les résultats de traction, les échantillons du PLGA-5%DS avaient une déformation à la rupture inférieure par rapport au PLGA-10%DS.

B.3.3 Libération de médicaments dans la lumière et le tissu artificiel

Dans cette partie, l'effet de certains paramètres sur la libération de médicament à partir d'échantillons polymères dans la partie de la lumière artificielle et dans la partie du tissu artificiel (afin de simuler l'artère) est étudié.

B.3.3.1 Débits constants et non constants (pulsatile)

À titre d'exemple important au cours des dernières décennies, l'hémodynamique des artères malades a été largement étudiée et l'effet du flux continu sur la libération du médicament n'est plus

B.3. RÉSULTATS EXPÉRIMENTAUX

inconnue [81]. Cependant, plusieurs facteurs n'ont pas encore été complètement explorés relativement au comportement pulsatoire du flux sanguin et à son effet sur la libération artérielle du médicament. Pour caractériser l'influence du flux luminal sur la diffusion du médicament dans la paroi artérielle, il est important de considérer de nombreux aspects associés au flux sanguin. En fait, les schémas de flux sanguin systolique-diastolique induits par le pouls cardiaque produisent une nature de flux complexe qui peut affecter le profil global de libération du médicament [260]. Les mécanismes directeurs du flux pulsé qui régulent la libération du médicament restent encore partiellement élucidés.

Dans cette section, nous étudions comment la pulsativité du flux affecte la libération de médicament par les stents à élution de médicament dans la zone de la lumière et également dans le composant tissulaire et nous comparons ces effets au cas où le débit est constant. Cet effet a été analysé par la comparaison des résultats de libération de deux débits en régime permanent à 7,5 et 15 ml/s (correspondant respectivement aux pressions de 75 et 112 $mmHg$), et du débit pulsé qui varie entre ces valeurs (montré dans la figure B.21) à 70 battements cardiaques par minute. Les expériences ont été menées en considérant une entretoise d'un stent, modélisée par un film polymère de PLGA (50:50) chargé de 10% de médicament et de gel d'agarose (1%) comme couche de tissu artificiel. Pour mimer le sang, le milieu circulant choisi est le PBS à 37°C. La figure ?? montre la forme d'onde transmise au moteur et reçue par le débitmètre, la forme d'onde de pression mesurée, la température et le nombre d'impulsions par minute pour ce type de test de déclenchement.

La figure B.23 (a), (b) montre les résultats de la libération de DS des échantillons de PLGA dans le milieu PBS et dans le compartiment de gel. La figure B.23 (a) montre qu'en augmentant le débit de 7,5

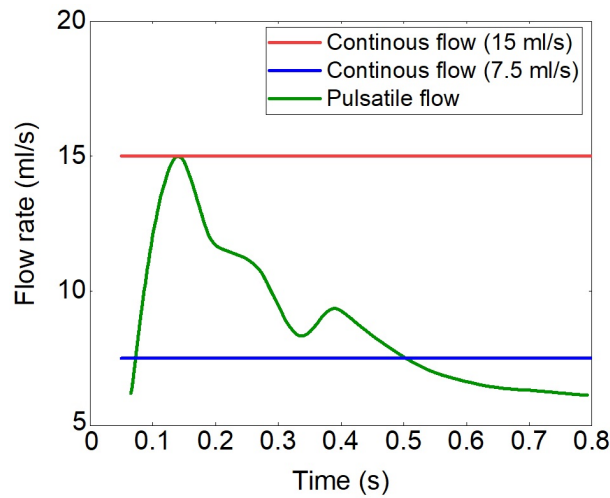


FIGURE B.21 – Débits liés aux trois modèles de flux réalisés dans cette étude (correspondant au flux dans l'artère carotide)

à 15 ml/s , le taux de libération du médicament dans le PBS est augmenté, mais cette différence n'est pas très notable. Outre la comparaison des résultats de libération du médicament, à l'état d'équilibre (débits : $7,5$ et 15 ml/s) avec le débit pulsé, nous notons une différence significative dans le taux de libération. Dans le cas du débit pulsé, le taux de libération est beaucoup plus élevé qu'en régime permanent surtout à la deuxième période de la libération après le phénomène d'éclatement. Il est également remarquable qu'en changeant l'état de l'écoulement de stationnaire à pulsé, le phénomène d'éclatement augmente. Le deuxième mécanisme connexe est la diffusion qui, outre la solubilité du médicament, dépend également du débit et de la propriété stationnaire/instationnaire de l'écoulement : on peut noter que pour les cas à l'état stationnaire, l'augmentation du débit du fluide augmente la diffusion du médicament du polymère. De plus, la diffusion est améliorée dans le flux pulsé par rapport aux flux stationnaires. Les résultats montrent que pour tous les débits, environ 90% du médicament sont libérés dans le PBS au temps de 192h. Pour analyser plus en profondeur ces résultats, la

B.3. RÉSULTATS EXPÉRIMENTAUX

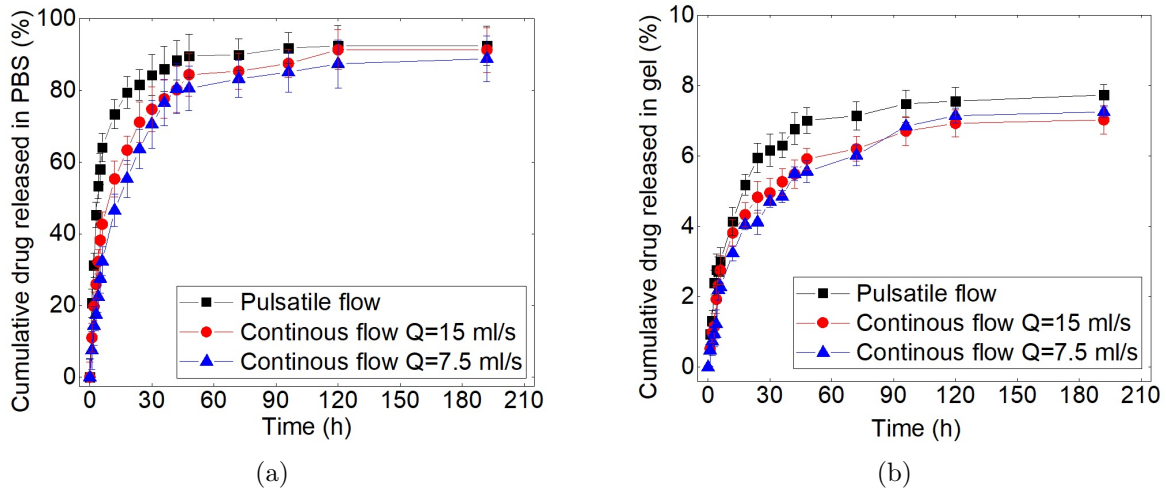


FIGURE B.23 – Libération de médicaments à partir des films PLGA avec 10% DS à différents débits dans (a) PBS, (b) gel

microstructure des échantillons a été observée en microscopie SEM.

La figure B.24 montre les micrographies SEM des échantillons PLGA avec 10% de DS (a) au débit constant de $7,5 \text{ ml/s}$ et (b) au débit instable après 48 heures. A partir de cette figure, on peut noter dans les deux situations (stationnaire et instable) la création de pores et le plissement du polymère lors de la libération. Ainsi, il dénote la présence des mécanismes de gonflement et de diffusion dans les deux cas. Il est évident que la diffusion est affectée par le phénomène de gonflement (changement de la microstructure de la matrice polymère, modifications de la porosité du matériau et des dimensions des échantillons...). Du point de vue mécanistique, on remarque également qu'en augmentant le débit, l'épaisseur des couches limites hydrodynamiques et massiques diminuent (figure B.25). Ainsi, la partie convective du flux de médicament dans la lumière augmente avec le débit. Cela provoque des gradients de concentration plus élevés du médicament entre l'échantillon de polymère et le fluide conduisant à un flux de diffusion plus élevé. Ainsi, un débit plus élevé entraîne une plus grande quantité de médicament

B.3. RÉSULTATS EXPÉRIMENTAUX

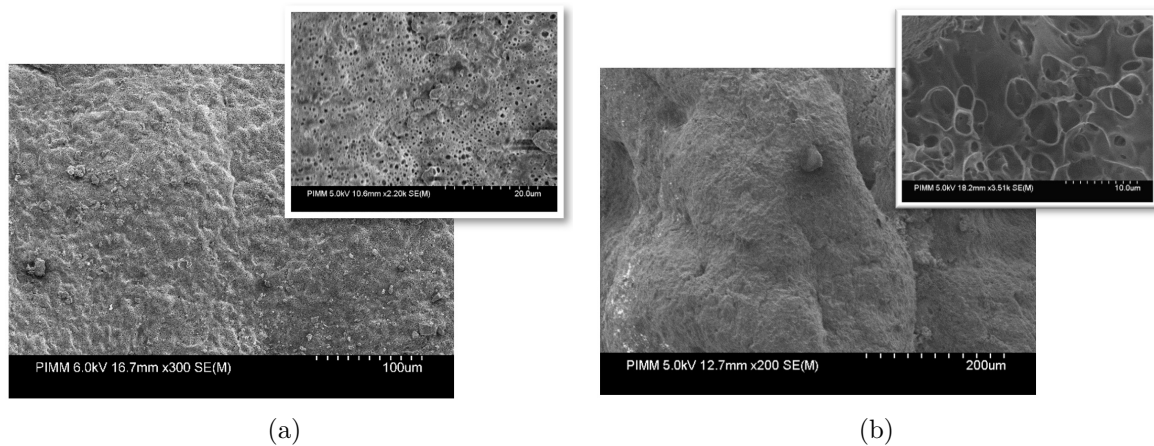


FIGURE B.24 – Micrographies SEM d'échantillons PLGA-10%DS après 48h pour (a) un débit pulsé et (b) un débit constant à $7,5 \text{ ml/s}$

libéré des échantillons polymères. Il est à noter que l'analyse de la couche limite dans le cas d'un écoulement pulsé n'est pas aussi facile. On peut noter que la libération de médicament à partir des films polymères dans le cas d'un flux pulsé instable est toujours plus élevée que dans le cas stable. Il s'agit d'un effet de la pulsativité du flux sur l'amélioration du transfert de médicament comme déjà noté dans le travail de doctorat de Chabi [81]. Un autre mécanisme contribuant à la libération du médicament à partir des films polymères PLGA est le mécanisme de dégradation/érosion qui entraîne le clivage des chaînes polymères et peut aider à la libération du médicament. A cet égard, il semble évident que l'augmentation du débit entraîne des gradients de vitesse plus élevés surtout près de la surface du polymère, donnant ainsi plus de friction entre le fluide et le polymère. C'est une raison de l'affaiblissement mécanique du polymère et de l'augmentation de la vitesse d'érosion. Bien sûr, dans l'écoulement instationnaire, la contrainte de cisaillement de paroi et le frottement de paroi seront plus élevés que dans la situation stationnaire [262].

L'autre mécanisme le plus probable pour la libération du médicament par les porteurs de PLGA

B.3. RÉSULTATS EXPÉRIMENTAUX

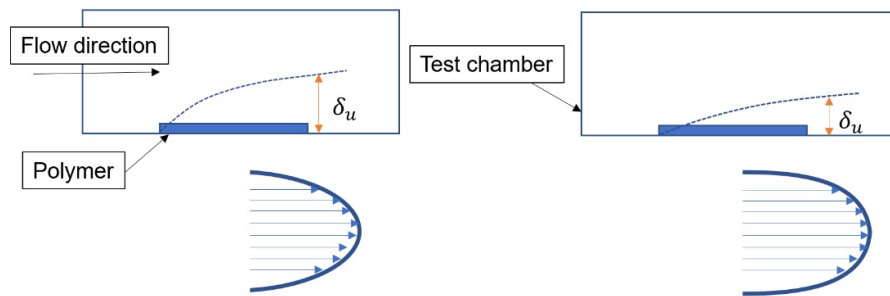


FIGURE B.25 – Schéma représentant l'épaisseur des couches limites créées à deux débits différents (la figure de droite est pour le cas avec un débit plus élevé que la figure de gauche)

est le gonflement, qui est le résultat d'une forte absorption d'eau. Le PLGA 50:50 est un polymère qui absorbe suffisamment d'eau pour gonfler. À cet égard, de petites bulles sont également créées, en fonction des autres conditions environnementales telles que la pression ou la contribution d'autres mécanismes telle que l'érosion. Ces bulles peuvent éclater et rendre la surface du polymère plus poreuse et adaptée à la libération du médicament. La figure B.23 (b) montre la concentration de médicament absorbée par l'hydrogel en fonction du temps de libération. Le mécanisme de contrôle du transport du médicament du polymère dans le gel est la diffusion. Dans un premier temps, l'existence de gradients élevés de concentration médicamenteuse explique la croissance rapide des courbes. A l'état d'équilibre, une augmentation du débit induit une légère augmentation du médicament diffusé dans l'hydrogel. Les valeurs au débit de 15 ml/s ne sont que légèrement supérieures à celles au débit inférieur de $7,5 \text{ ml/s}$. En revanche, les résultats pour le flux pulsé montrent que la quantité de médicament diffusée dans l'hydrogel est plus élevée que dans les cas stables.

Une raison peut être due aux différentes tailles des tourbillons dans les régions proximale et distale à proximité des échantillons polymères à l'état d'écoulement pulsé. Le premier se traduit par une turbulence élevée par rapport à l'écoulement en régime permanent. Cela peut être la raison pour

laquelle, à l'état pulsé, davantage de médicament est libéré dans le flux et diffusé dans l'hydrogel. Généralement, les résultats montrent une réduction plus élevée du médicament à partir des supports polymères dans le cas d'un état instable par rapport à une valeur encore plus élevée du débit à l'état stable.

B.3.3.2 Présence de la couche métallique sur la couche polymère

Dans les sections précédentes, nous avons étudié le transfert de médicament à partir du polymère exclusivement sans la présence d'un échafaudage métallique. Cependant, la plupart des DES contiennent une structure métallique qui peut supporter la couche polymère. Dans cette section, nous étudions l'influence d'une feuille métallique, en acier inoxydable d'une épaisseur de 0,3 *mm*, simulant la présence de l'échafaudage métallique d'un véritable stent, sur la libération de médicament (DS) d'un PLGA 50:50 film. La figure B.26 montre la comparaison de la libération de médicament dans le cas d'un débit pulsé avec et sans prise en compte de la couche métallique sur le support de médicament polymère. La figure B.26 (a) montre la libération du médicament dans le fluide PBS. Les résultats montrent une grande différence dans les profils de libération avec ou sans la couche métallique. Afin de les comparer, le rapport du médicament libéré dans le PBS sans la couche métallique à celui avec la feuille métallique varie dans la gamme $1,1 < R < 2,8$ avec une valeur moyenne autour de 2. L'influence de la couche métallique est donc nettement notable : recouvrant la face supérieure du polymère avec la tôle, on la prive de sa plus grande surface en contact avec le flux de PBS. Cet effet est particulièrement fort au début de la libération (certainement à cause de l'absence de libération rafale), atteint un maximum à $t = 5h$ puis décroît lentement. Ce bouclier sur le polymère peut également diminuer les effets

B.3. RÉSULTATS EXPÉRIMENTAUX

du mécanisme d'érosion. Par conséquent, la libération est principalement contrôlée par les mécanismes de diffusion et de gonflement. La figure B.27 montre approximativement l'hydratation des échantillons polymériques avec et sans la présence de la couche métallique. A partir de cette figure, on peut noter que la présence de la couche métallique diminue le contact du polymère en surface supérieure avec le milieu aqueux et donc diminue le taux d'absorption d'eau de ce côté, par rapport au côté hydrogel. Comme les mécanismes de diffusion et de gonflement dépendent fortement de l'hydratation et de l'absorption d'eau des échantillons polymères, le médicament transporté vers l'hydrogel est augmenté en cas de présence de la couche métallique.

On peut proposer l'explication suivante à ce fait : initialement la couche de polymère est sèche et commence à absorber l'eau. Il est à noter que lorsqu'il y a une couche métallique, la cinétique d'hydratation est plus lente. L'absorption d'eau et le gonflement commencent des côtés du film polymère et évoluent vers l'intérieur. A ce moment, la partie non gonflée du film impose une contrainte de compression sur la partie gonflée qui pousse le médicament vers la partie gonflée de l'échantillon en contact avec l'hydrogel. Dans ce cas, une grande quantité de médicament est dirigée vers l'hydrogel (car c'est la face qui est bien mouillée). De plus, une barrière métallique de l'autre côté empêche la libération du médicament dans le milieu fluide, contribuant à maintenir des gradients de concentration élevés de médicament dans le film polymère et résultant en un transport diffusif élevé. Il est à noter que lorsque l'échantillon est entièrement humide, la contrainte de compression diminue et le médicament peut facilement diffuser dans toutes les directions [245]. Cependant, il est évident que l'échantillon gonflé augmente ses dimensions et que des distances plus grandes réduisent la cinétique de la libéra-

B.3. RÉSULTATS EXPÉRIMENTAUX

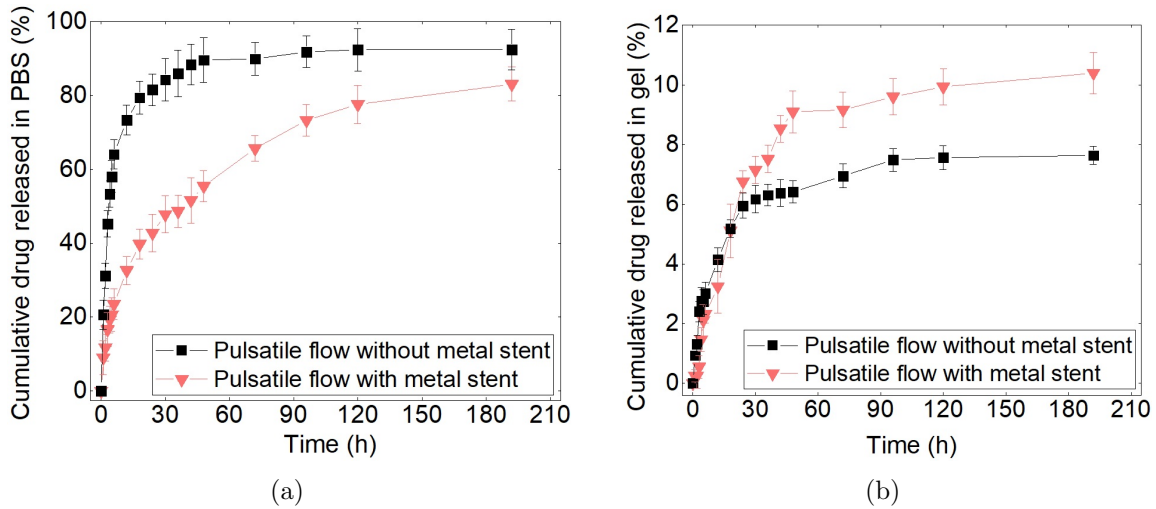


FIGURE B.26 – La libération du médicament résulte du PLGA-10% DS vers (a) le milieu PBS, (b) l’hydrogel, au débit pulsé avec et sans présence de couche métallique

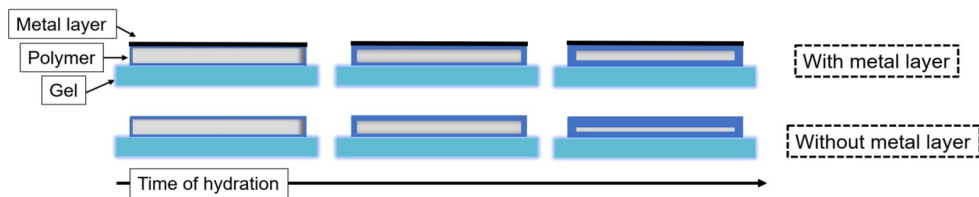


FIGURE B.27 – Hydratation des échantillons polymériques en contact avec fluide et hydrogel avec et sans présence de couche métallique

tion. Cet effet est moins important en présence de la couche métallique car le gonflement est plus lent. La figure B.28 résume schématiquement ces mécanismes lors des premières étapes de gonflement et au moment où l’ensemble de l’échantillon est gonflé. Les résultats obtenus indiquent que la présence d’une barrière métallique est importante dans les stents à élution médicamenteuse. Par conséquent, le remplacement d’un échafaudage métallique par un échafaudage en polymère doit être soigneusement envisagé en fonction de cet « effet barrière » de la couche métallique sur la libération.

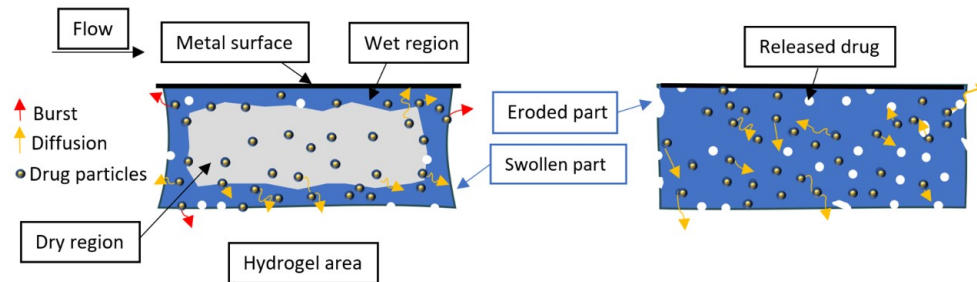


FIGURE B.28 – Représenter les mécanismes qui ont contribué à la libération du médicament au moment (a) initial et (b) tardif de l’hydratation des échantillons polymères

B.3.3.3 Distribution des particules de luminescence dans le gel

Jusqu’à présent, les résultats montraient l’effet des différents paramètres sur la libération dans le milieu fluide et dans l’hydrogel. En plus de la quantité de médicament diffusée dans l’hydrogel comme dans la figure B.26, il est également important d’observer la distribution spatiale des particules de médicament dans l’hydrogel. Cela peut être utile dans la conception des stents, en particulier pour la géométrie des entretoises. Dans cette section, pour observer qualitativement la diffusion de la substance active dans l’hydrogel, les particules de médicament ont été remplacées par des particules phosphorescentes. Les tests ont été effectués en conditions d’écoulement pulsé (comme le montre la figure ??) dans le milieu PBS et compartiment hydrogel en présence d’une feuille métallique (acier inoxydable) au-dessus d’un film polymérique PLGA chargé à 30%(w/ w) de particules luminescentes. La figure B.29 est un schéma qui montre comment les échantillons sont placés sur l’hydrogel et quelles tranches sont choisies pour analyser qualitativement la diffusion de la phosphorescence dans l’hydrogel. La figure B.30 montre la distribution qualitative de la phosphorescence dans l’hydrogel de la tranche 1, qui est la tranche verticale placée sous l’échantillon polymère. Les résultats montrent l’étalement diffusif avec le temps des particules phosphorescentes dans l’hydrogel. Ces images mettent en évidence

B.3. RÉSULTATS EXPÉRIMENTAUX

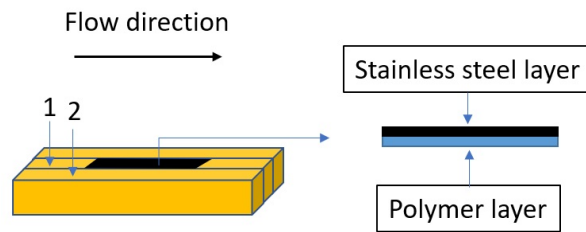


FIGURE B.29 – Schéma de la position de la couche polymère + métal sur l'hydrogel et les deux tranches choisies pour l'analyse

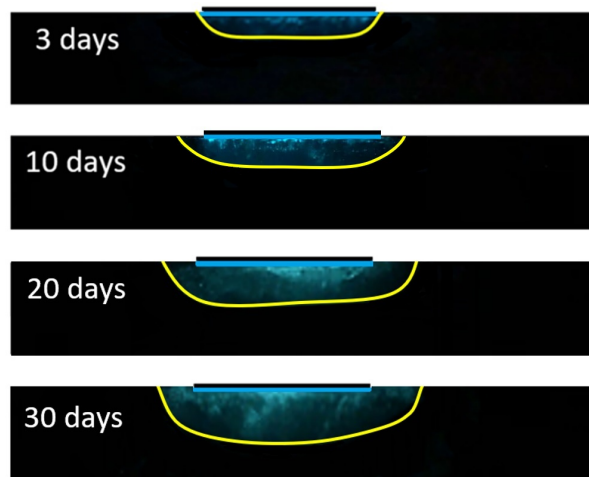


FIGURE B.30 – Distribution qualitative de la phosphorescence dans l'hydrogel (tranche 1 représentée sur la figure B.29)

la diffusion rapide dans le sens vertical (dans la profondeur de l'hydrogel) par rapport à la diffusion lente dans les directions horizontales (dans la longueur de l'hydrogel). On peut noter que la distribution des particules est légèrement asymétrique en position distale en raison des effets convectifs. La figure B.31 montre la distribution de la phosphorescence dans l'hydrogel après des pas de temps définis dans la tranche 2. On peut voir que même à des temps longs, les particules phosphorescentes sont très peu nombreuses dans cette tranche. Ceci met en évidence la faible diffusion dans l'hydrogel dans les régions non directement en contact avec le film polymérique et la faible diffusion dans le sens transversal de la tranche 1 à la tranche 2.

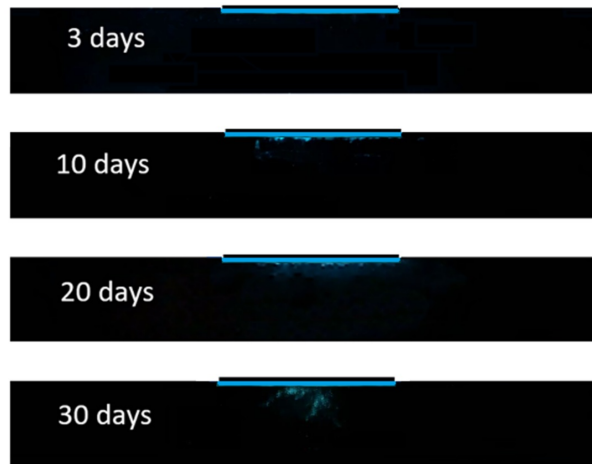


FIGURE B.31 – Répartition qualitative de la phosphorescence dans l'hydrogel (à partir de la tranche 2 représentée sur la figure B.29)

B.4 Modélisation et simulation

B.4.1 Modèle cinétique

De manière générale, les modèles empiriques sont développés pour une famille de porteurs de médicaments sur la base de données expérimentales. Pour conserver tout leur intérêt, ils doivent rester précis dans la prédiction du profil de relargage à partir de l'ensemble de données utilisé pour l'ajustement. De plus, la complexité des systèmes d'administration de médicaments rend difficile la compréhension de leurs mécanismes sous-jacents, en particulier *in vivo*. L'alternative consiste à adopter des approches d'ajustement pour capturer les ensembles de données expérimentales. Ces modèles d'ajustement contiennent généralement moins de facteurs que les modèles purement mécanistiques. L'avantage de ce type de modèles réside dans la simplicité d'utilisation permettant leur diffusion au sein de la communauté scientifique [264]. Cependant, leur validité est limitée au milieu utilisé pour définir ses données de réglage. Pour une famille de porteurs de médicaments, il est nécessaire de bien

ajuster la précision du modèle en identifiant le nombre de facteurs les plus influents.

Dans cette section, un modèle mathématique prédictif innovant basé sur la cinétique est proposé. Ce modèle devrait être applicable à divers modes d'administration tels que les comprimés, les patches, les stents à élution médicamenteuse, etc. L'objectif de ce nouveau modèle est de formuler une fonction pour calculer la libération cumulative de médicament pour un groupe d'agents d'administration de médicament ayant des propriétés similaires . Ce modèle, devrait in fine :

- Tenir compte de l'influence des paramètres de conception et des conditions opératoires sur la quantité de médicament libérée par les vecteurs de médicament. Ces réglages ou conditions sont par exemple : le débit du fluide en circulation, la charge initiale de médicament ; le type de support polymère, etc.
- Permet de prendre en compte l'évolution de la cinétique de libération du médicament en fonction du temps tout au long de la période de libération.

L'équation B.1, basée sur l'équation de Korsmeyer-Peppas, décrit ce modèle :

$$\text{Log}M_t = \text{Log}K + n_i \text{Log}t \tag{B.1}$$

où K est une constante, différente pour chaque étape du profil de libération et dépendant à la fois de la concentration et du temps. Par conséquent, K peut être facilement obtenu par les valeurs maximales de la concentration et du temps dans cette étape particulière. Le modèle sera donc présenté sous la

forme ci-dessous :

$$\text{Log}M_t = \text{Log}\left(\frac{M_i}{t_i^{n_i}}\right) + n_i \text{Log}t \quad (\text{B.2})$$

où M_t est le médicament libéré au temps t , M_i et t_i sont respectivement la quantité maximale de médicament libéré, et le temps maximum de la libération, à l'étape i^{th} . Cette équation est applicable à quelles que soient les dimensions des transporteurs de médicaments et des variables. Les coefficients de puissance n_i correspondent aux pentes des droites identifiées dans le système de coordonnées Log-Log. Leur distinction démontre la présence de différentes cinétiques et les deux autres paramètres t_i et M_i peuvent dépendre de nombreux facteurs tels que la concentration de la substance active dans les supports, l'épaisseur des couches matricielles, les propriétés physicochimiques des médicament et polymère (solubilité, hydrophilie, hydrophobie, taille des particules du médicament, porosité, durabilité du polymère, etc.). Pour reproduire efficacement n'importe quel profil de libération de médicament, il suffit de calculer avec précision les valeurs de l'ensemble n_i , t_i et M_i . L'algorithme Douglas-Peucker [265] est adapté à cette fin.

Evaluation du modèle sur les données expérimentales de PU chargé avec DE

Cette section traite des données expérimentales obtenues dans ce travail de thèse et des données trouvées par les auteurs dans la littérature. Concernant nos données expérimentales, nous étudions l'effet simultané du débit et de la concentration du médicament pour un profil de libération en une seule étape. Concernant les données de la bibliographie, une étude de [266] a été utilisée : où les auteurs ont étudié l'effet de la concentration du médicament pour un profil de libération en deux étapes.

B.4. MODÉLISATION ET SIMULATION

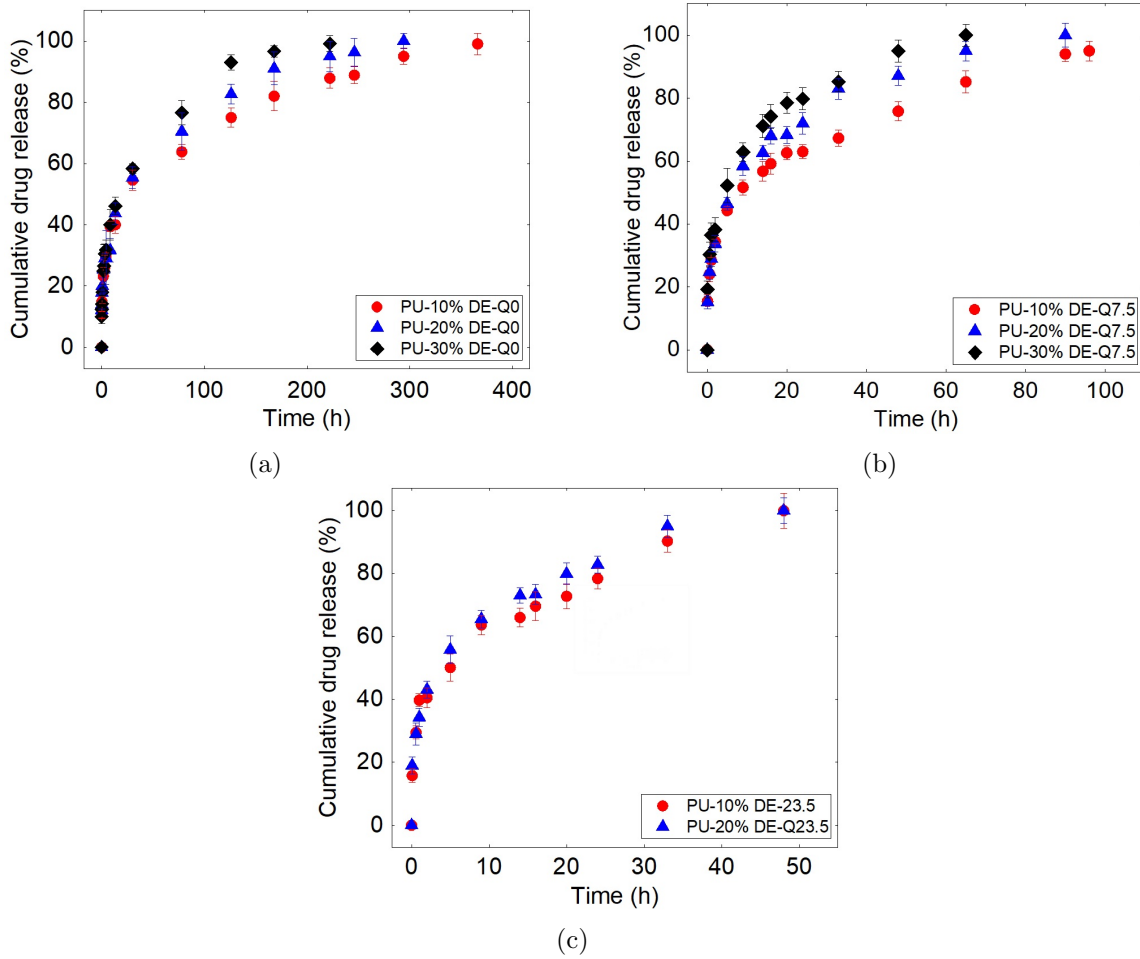


FIGURE B.32 – Cumulative release of DE from PU matrix in (a) $Q = 0 \text{ ml/s}$ (b) $Q = 7.5 \text{ ml/s}$ and (c) $Q = 23.5 \text{ ml/s}$

Dans nos résultats expérimentaux *in vitro*, nous avons observé l'influence du débit et de la concentration du médicament sur la cinétique du diclofénac épolamine libéré des films de polyuréthane. Ensuite, ces paramètres sont employés dans le modèle développé dans la section précédente. Pour rappel, ces données concernent trois débits distincts : 0 ml/s , $7,5 \text{ ml/s}$ et $23,5 \text{ ml/s}$, et trois concentrations de médicament : 10%, 20% et 30%. Figure B.32 illustre l'ensemble de ces résultats.

Sur la figure B.33, dans un système de coordonnées Log-Log, nous avons tracé la masse du médicament M_t normalisée par la masse $M_{95\%}$ (correspondant à une libération de 95% de la masse initiale)

B.4. MODÉLISATION ET SIMULATION

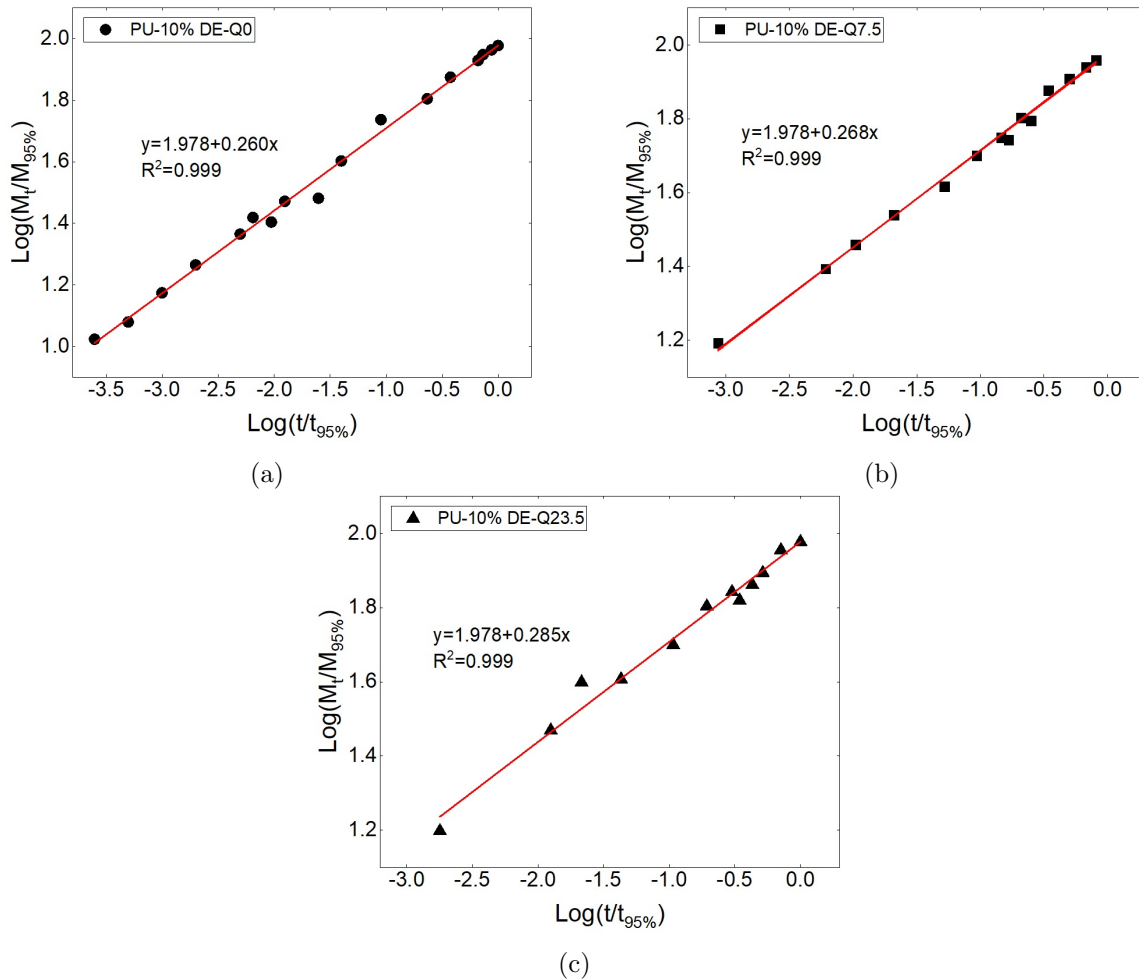


FIGURE B.33 – Résultats expérimentaux obtenus à partir de PU-10%DE en (a) $Q = 0 \text{ ml/s}$, (b) $Q = 7,5 \text{ ml/s}$, (c) $Q = 23,5 \text{ ml/s}$, et tracé sous la forme du journal $(M_t/M_{95\%})$ par rapport au journal $(t/t_{95\%})$

en fonction du temps normalisé par le $t_{95\%}$ (temps auquel 95% de la masse initiale est libérée). Ces données sont correctement ajustées par une seule interpolation linéaire suggérant en conséquence une cinétique de libération en une étape.

La figure B.34 montre l'évolution des pentes de ces régressions linéaires à la concentration DE de 10% (ces pentes donnent accès aux valeurs des coefficients de puissance $n_i = n_1$ en équation 4.2) en

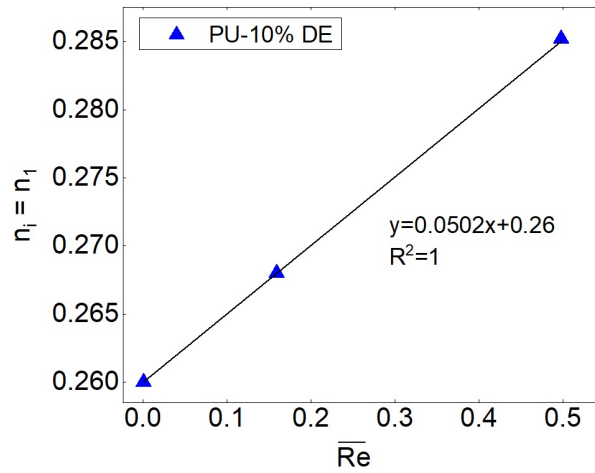


FIGURE B.34 – Corrélation entre les valeurs de $n_i = n_1$ et réduite Le numéro de Reynold

fonction du débit, représenté par un Reynolds réduit :

$$\overline{Re} = \frac{Re}{Re_c} \quad (\text{B.3})$$

avec $Re_c = 2300$ (le nombre de Reynolds accepté pour la transition laminaire-turbulente pour l'écoulement dans un tuyau) et le nombre de Reynolds :

$$Re = \frac{VD_H}{\nu} \quad (\text{B.4})$$

avec $V = Q/S$ la vitesse moyenne. On remarque, dans ce cas, que $n_i = n_1$ augmente légèrement avec le débit. La figure B.35 (a) montre, pour les trois débits, l'évolution du paramètre $t_i = t_{95\%}$ en fonction de la concentration. Sur cette figure nous avons également tracé le point (0;100%), correspondant à l'expérience théorique pour laquelle il n'y aurait aucun support polymère et pour laquelle la libération de la totalité du médicament serait pratiquement instantanée ($t_i = 0$). La figure B.35 (b) donne

les valeurs des coefficients A et B, extraites des régressions proposées dans la figure B.35 (a) en fonction du nombre de Reynolds réduit. Une fois ces paramètres obtenus, il est possible d'évaluer la robustesse de notre modèle pour différents paramètres expérimentaux. Comme premier exemple, nous comparons sur la figure B.36 (a) notre modèle aux données expérimentales pour le débit de 6,5 *ml/s* et les concentrations de 10% et 20% de DE dans PU. De même sur la figure B.36 (b), nous avons tracé la prédiction pour le débit de 7,5 *ml/s* et la concentration de 15% avec les valeurs expérimentales. Dans les deux cas, les comparaisons avec les données expérimentales sont satisfaisantes. Enfin, la figure B.37 montre la prédiction de notre modèle pour un débit de 7,5 *ml/s* et diverses concentrations allant de 5% à 80%. On peut noter que les paramètres variants choisis dans cette étude, débit et concentration médicamenteuse, peuvent être considérés comme un paramètre d'accélération de la cinétique de libération. Par conséquent, le modèle développé ici est un modèle d'accélération où la figure B.37, en considérant le paramètre accéléré de concentration de médicament, a montré les profils de libération prédits.

B.4.2 Modèle basé sur les mécanismes

Dans cette section, nous présentons une méthode pour prédire le profil de libération du médicament sur la base des mécanismes physiques qui peuvent intervenir dans la libération du médicament à partir d'un transporteur de médicament. L'application présentée ici intègre les effets de la concentration du médicament et des débits en fonction du débit circulant dans la chambre d'essai. La méthode développée dans ce travail est illustrée dans l'organigramme donné sur la figure B.38. Ça implique:

- i) Déterminer, à partir d'une base de données d'essais bien documentée, les mécanismes impliqués

B.4. MODÉLISATION ET SIMULATION

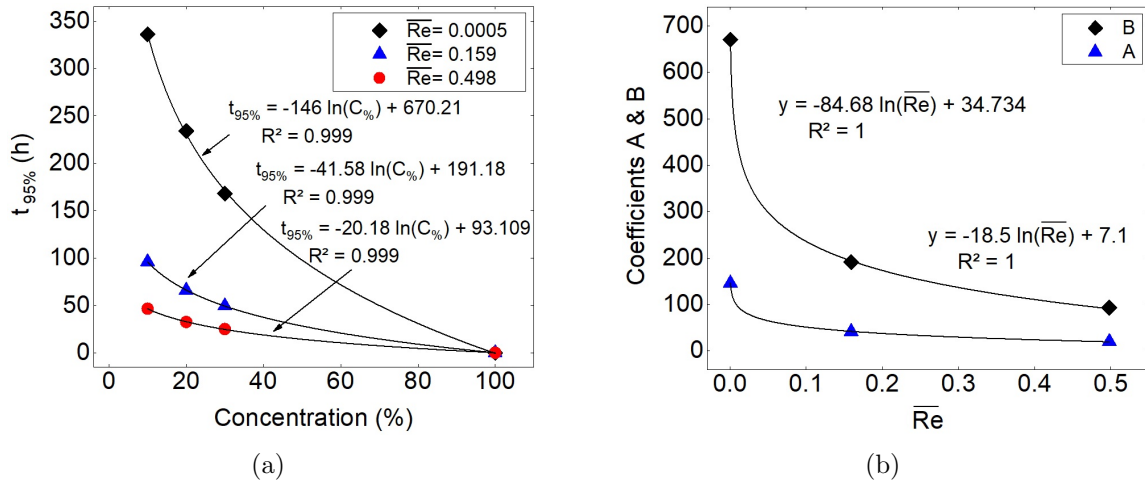


FIGURE B.35 – (a) Corrélation entre les valeurs du temps maximum de libération en fonction de la concentration du médicament (équation d'ajustement : $y = -A \times \ln(C\%) + B$) (b) Valeurs des coefficients obtenues à partir de la figure reff4.9 (a) par rapport au nombre \overline{Re}

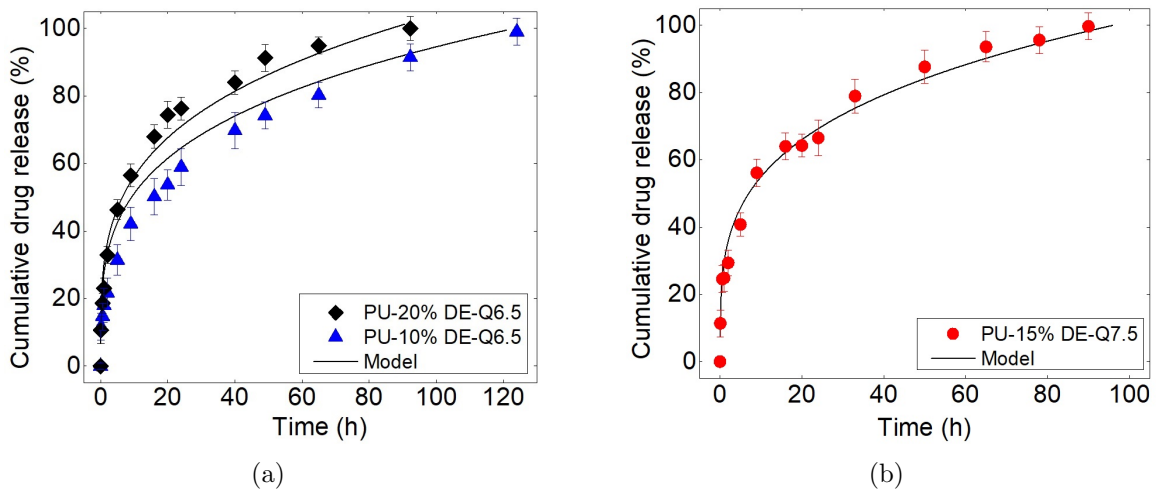


FIGURE B.36 – Les données expérimentales obtenues avec (a) PU-10 et 20% DE au débit de 6.5 ml/s, R^2 sont respectivement de 0.99 et 0.98 (b) PU-15%DE au débit taux de 7,5 ml/s, $R^2 = 0,98$; à $T=37^\circ\text{C}$

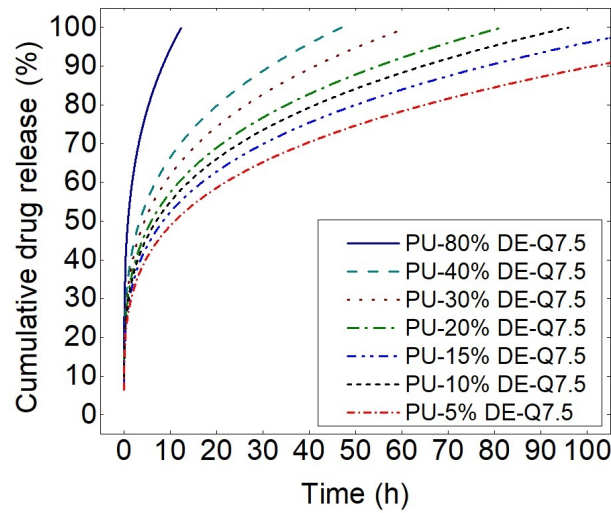


FIGURE B.37 – Résultats pour prédire le comportement de libération de différents pourcentages de DE dans la matrice du PU au débit de 7.5 ml/s

dans la libération. ii) Résoudre un système d'équations non linéaires, modéliser le problème d'optimisation et calculer le inconnues pour cette base de données. iii) Développer à partir de ces résultats un modèle spécifique prédisant le profil de libération. iv) Appliquer le modèle aux données réservées pour valider le modèle construit. En fait, nous essayons d'ajuster les résultats expérimentaux avec un modèle du type :

$$\frac{M_t}{M_\infty} = \sum_{i=1}^{i=N} \mu_i \times F_i \quad (\text{B.5})$$

où F_i est l'équation liée à un mécanisme de libération spécifique (éclatement, diffusion, gonflement, osmose...) et μ_i la contribution relative de chaque mécanisme de libération. Afin d'obtenir le μ_i et les paramètres de chaque équation F_i , nous avons utilisé l'algorithme de programmation quadratique séquentielle. Cet algorithme est connu comme l'une des procédures les plus efficaces pour résoudre les problèmes d'optimisation non linéaire [268].

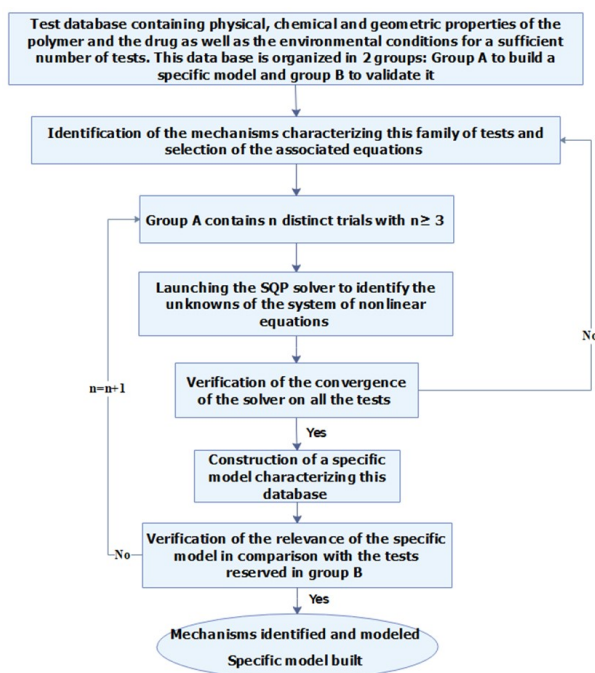


FIGURE B.38 – Organigramme de la méthode proposée

Application du modèle basé sur les mécanismes pour PLGA-DS

Dans cette section, nous avons appliqué le modèle de mécanismes sur le profil de libération de DS du polymère PLGA. Les tests de libération ont été réalisés sur le banc d'essai précédent à différents débits de 0, 6,5 et 15 ml/s à partir de films d'échantillons PLGA biodégradables chargés en 10% DS. La figure ?? montre les résultats liés à la libération du médicament de PLGA-10%DS-Q0, 6.5, 15 ml/s . D'après la figure ??, on peut noter que les profils de libération peuvent être divisés en trois régions. La première région est liée à la libération en rafale qui se produit au tout début de la libération avec une cinétique élevée. La seconde étape, un peu plus lente, est due au couplage entre les mécanismes de diffusion et de gonflement. Le paramètre efficace affectant le mécanisme de diffusion est l'état physique du polymère. Il est bien connu que les polymères à l'état caoutchouteux ont un coefficient de diffusion plus

important qu'à l'état vitreux et que la température de transition vitreuse des polymères change lorsque les polymères sont exposés à des molécules d'eau [283]. Afin de libérer le médicament par diffusion, le médicament doit d'abord être dissous dans une solution à l'intérieur du polymère ou être suffisamment petit pour être transporté par la solution avant dissolution. C'est pourquoi la diffusion a lieu avec un taux de libération relativement faible [203]. Pendant ce temps, le mécanisme de gonflement est activé par l'absorption rapide d'eau. En effet, le polymère hydrophile absorbe rapidement l'eau et provoque la formation d'une structure poreuse près de la surface, ce qui favorise la libération du médicament. Le gonflement des polymères peut avoir deux effets différents. D'un côté, les molécules de la solution s'insèrent et se localisent à l'intérieur ou entre les chaînes polymères, entraînant l'augmentation du volume libre entre les chaînes polymères et leur flexibilité. Ceci provoque une augmentation de la cinétique de libération. D'autre part, le gonflement des polymères se traduit par l'augmentation de la dimension des échantillons, donc des distances nécessaires aux molécules médicamenteuses pour se libérer des échantillons. Ce deuxième effet diminue la cinétique de libération. L'autre mécanisme le plus probable est l'érosion lorsque le polymère s'affaiblit du point de vue mécanique. Les raisons sont liées à la dégradation du polymère entraînant le clivage des chaînes [284], le contact de la surface du matériau avec le fluide circulant et le frottement entre elles.

Comme mentionné ci-dessus et en référence à la littérature pour ce type de support de médicament (films PLGA) et de conditions de libération, les mécanismes de libération de médicament les plus couramment et fréquemment mentionnés sont donc la libération en rafale, la diffusion, le gonflement et l'érosion [207, 285, 287? , 288]. Les équations liées à ces quatre mécanismes de libération sont

regroupées en attribuant à chacun d'eux un coefficient de pondération :

$$\frac{M_t}{M_\infty} = \sum_{i=1}^{i=4} \mu_i \times F_i \quad (\text{B.6})$$

avec

$$\sum_{i=1}^{i=4} \mu_i = 1 \quad (\text{B.7})$$

Dans l'équation B.7, F_1 et F_2 , liés respectivement au libération rafale et à la diffusion sont identiques à l'équation ?? et ?? du précédent cas (PU-DE). L'équation de gonflement, introduisant deux nouveaux paramètres k_s et m , est donnée par F_3 :

$$F_3 = k_s t^m \quad (\text{B.8})$$

La contribution de l'érosion, introduisant un nouveau paramètre k_e , est représentée par F_4 :

$$F_4 = 1 + \exp(-2k_e t) - 2 \exp(-k_e t) \quad (\text{B.9})$$

Les coefficients $\mu_1, \mu_2, \mu_3, \mu_4$ représentent respectivement la contribution relative des mécanismes de "burst-release", diffusion, gonflement et érosion. Les autres facteurs inconnus sont maintenant k_b, D_e, k_s, k_e et m . Ici m est l'exposant caractéristique du mécanisme de libération ($m > 0.5$ pour le gonflement) [249], k_b représente la constante initiale de la cinétique d'éclatement, D_e est une diffusivité effective de soluté, k_s et k_e sont respectivement les constantes liées aux phénomènes de gonflement et d'érosion.

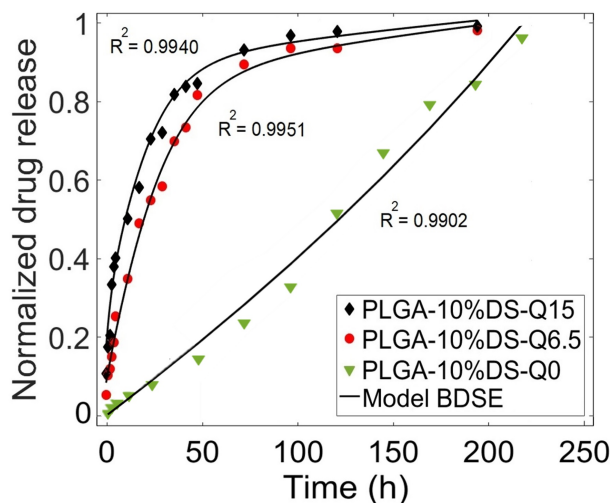


FIGURE B.39 – Libération expérimentale de médicament à partir de la matrice PLGA avec 10% de médicament aux débits de 0, 6,5 et 15 ml/s avec les modèles d'ajustement (compte tenu des mécanismes d'éclatement, de diffusion, de gonflement et d'érosion)

Modèle à quatre mécanismes

Les définitions ci-dessus peuvent nous aider à analyser l'effet du débit sur la cinétique des différents mécanismes. Notre modèle contenant les mécanismes sélectionnés ci-dessus (appelé ici BDSE pour Burst-Diffusion-Swelling-Erosion) a été appliqué aux résultats expérimentaux de PLGA-10%DS avec des débits de 0, 6,5 et 15 ml/s (figure B.39 montre les ajustements).

Après avoir appliqué le modèle BDSE sur les résultats expérimentaux, les valeurs de tous les paramètres inconnus (μ_i , k_b , D_e , k_s , k_e et m) sont présentés dans le tableau B.1. D'après les valeurs présentées dans le tableau B.1, il est évident que l'augmentation du débit augmente la libération en rafale des supports de médicament. Il est à noter qu'en changeant l'état de l'écoulement de statique à continu, la quantité de libération d'éclatement est augmentée, ce qui montre clairement que le phénomène d'éclatement est lié à la convection. Il est également clair que le phénomène de diffusion

TABLE B.1 – Valeurs liées aux paramètres inconnus

Mechanism	PLGA-10%DS -Q0	PLGA-10%DS -Q6.5	PLGA-10%DS -Q15
Burst (%)	0.05	18.99	21.16
Diffusion (%)	0.06	8.25	9.81
Swelling (%)	99.84	21.18	20.16
Erosion (%)	0.05	51.58	48.87
k_b (h^{-1})	0.033	0.169	0.301
D_e (m^2/h) ($\times 10^{-10}$)	18.00	18.00	18.00
k_s (h^{-1})	0.004	0.249	0.310
k_e (h^{-1})	0.002	0.061	0.063
m	1.00	0.72	0.70
R^2	0.9902	0.9951	0.9940

est accentué lorsque le débit augmente. Cela peut être dû à la forte absorption d'eau par le film PLGA lorsque le débit augmente. De plus, à l'état statique, le médicament n'est pas capable de migrer loin de l'échantillon (couche limite de masse épaisse et faibles gradients de concentration conduisant à un faible flux diffusif), alors qu'à l'état continu le médicament libéré est immédiatement transporté par le flux (fine couche limite de masse et gradients de concentration élevés conduisant à un flux diffusif élevé). Le mécanisme d'érosion est également accéléré par le débit en raison de la friction plus élevée entre le fluide et l'échantillon. En effet, plus le débit est élevé, plus la contrainte de cisaillement appliquée aux échantillons est élevée. Il en résulte une fragilisation mécanique plus rapide des échantillons. Lorsque le débit est nul, les résultats montrent que les mécanismes d'éclatement, de diffusion et d'érosion sont négligeables ; ceci est dû au faible taux de cisaillement de l'écoulement, au faible gradient de concentration et au faible frottement. Par conséquent, le gonflement est le mécanisme dominant à l'état statique pour ce type d'échantillon conduisant à une cinétique lente et à une vitesse de libération du médicament lente.

Sensibilité du modèle au choix des mécanismes

B.4. MODÉLISATION ET SIMULATION

TABLE B.2 – Valeurs liées aux paramètres inconnus en négligeant un mécanisme pour chaque cas

Mechanism	PLGA-10%DS -Q0	PLGA-10%DS -Q6.5	PLGA-10%DS -Q15
Burst (%)	0.01	49.99	-
Diffusion (%)	2.66	0.01	5.30
Swelling (%)	-	50.00	45.45
Erosion (%)	97.33	-	49.23
k_b (h^{-1})	0.005	0.014	-
$D_e(m^2/h)$ ($\times 10^{-10}$)	1.296	4.752	18
k_s (h^{-1})	-	11.232	115.704
k_e (h^{-1})	0.011	-	0.089
m	-	0.43	0.26
R^2	0.9694	0.9876	0.9805

Le choix des mécanismes contribuant au profil de libération doit être soigneusement choisi. Si un mécanisme particulier n'est pas pris en compte dans le modèle, il ne correspondra pas systématiquement aux résultats expérimentaux. À cet égard, trois exemples sont donnés. Dans le premier cas (modèle BDE), la libération rafale, la diffusion et l'érosion sont considérés pour PLGA-10%DS-Q0 (le gonflement est négligé). Dans le second cas (modèle BDS), les mécanismes de libération rafale, de diffusion et de gonflement sont considérés pour PLGA-10%DS-Q6.5 (l'érosion est négligée). Enfin pour le dernier cas (modèle DSE), la diffusion, le gonflement et l'érosion sont considérés pour le PLGA-10%DS-Q15 (le "burst" release est négligé). Les résultats sont respectivement montrés dans la figure B.40 (a), (b), (c). Ils montrent que négliger un mécanisme modifiera la précision de l'ajustement. Surtout quand le mécanisme dominant de la libération n'est pas pris en compte. Les valeurs liées à l'ajustement sont indiquées dans le tableau B.2. Par exemple, négliger le gonflement conduit à un résultat non physique car le mécanisme dominant à débit nul serait l'érosion.

Modèle BDSE et sa validation

Pour trouver une corrélation entre les valeurs des paramètres figurant dans le tableau B.1, une

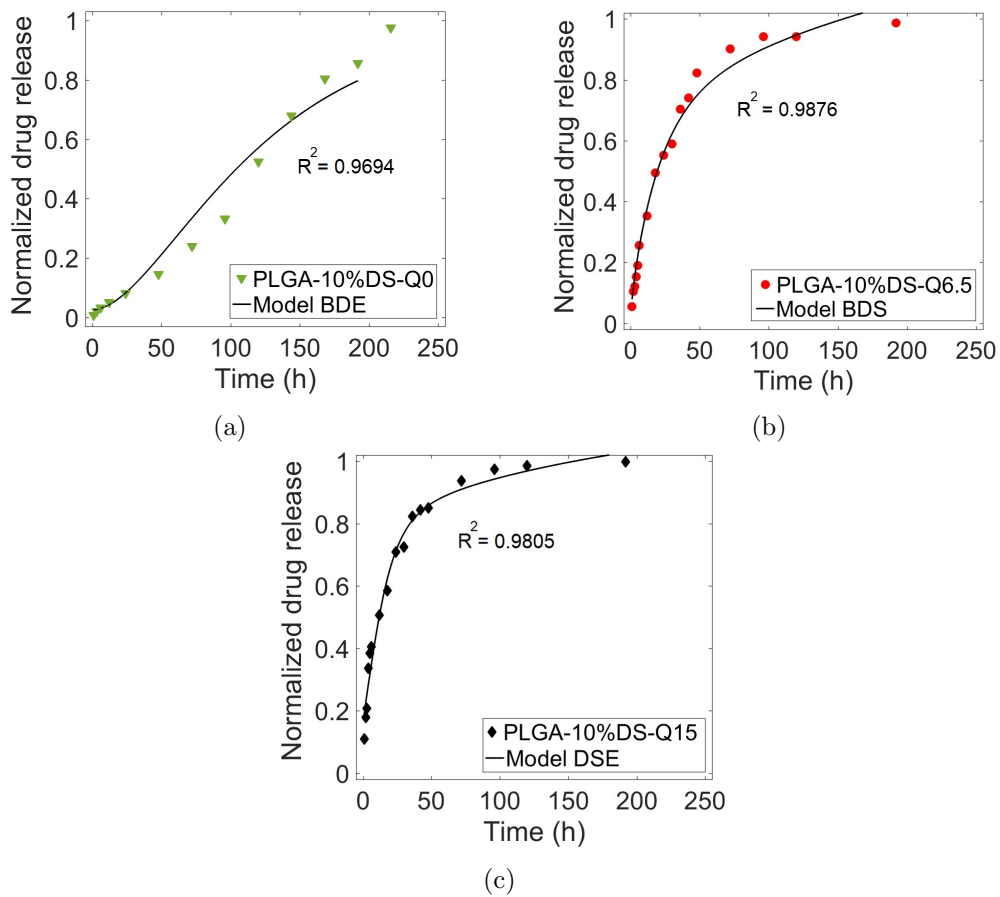


FIGURE B.40 – Libération expérimentale de médicament à partir du PLGA-10%DS-Q0, Q6.5, Q15 avec le modèle ajusté avec différents mécanismes

B.4. MODÉLISATION ET SIMULATION

équation de type exponentielle indiquée ci-dessous a été utilisée pour ajuster les paramètres μ_i , k_b , D_e , k_s , k_e et m :

$$a_i - b_i \times c_i^Q \quad (\text{B.10})$$

Les corrélations entre ces valeurs permettent de prédire le libération pour d'autres débits. La figure B.41 montre la prédiction du profil de libération du médicament pour le PLGA-10%DS-Q7.5 par l'approche de modélisation décrite ci-dessus et les résultats expérimentaux obtenus au débit de 7,5 ml/s . Il est à noter que les résultats expérimentaux montrent un bon accord avec le modèle BSDE obtenu par la corrélation des valeurs des paramètres. De plus, l'application directe du modèle BDSE pour cette nouvelle valeur du débit donne une courbe qui correspond également de manière satisfaisante aux résultats expérimentaux et aux résultats obtenus par la méthode utilisant les corrélations décrites ci-dessus.

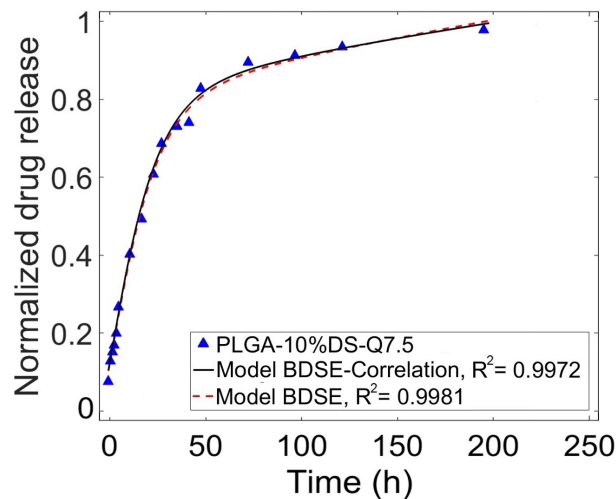


FIGURE B.41 – Comparaison entre les résultats du modèle BSDE obtenus par la corrélation des valeurs des paramètres et application directe du modèle BDSE pour PLGA-10%DS-Q7.5 avec les résultats expérimentaux

B.4.3 Simulation numérique

Dans cette section, nous présentons une comparaison entre les résultats numériques, les résultats du modèle cinétique et les données expérimentales pour le Diclofnac Epolamine (DE) libéré à partir d'échantillons de polyuréthane (PU) non dégradables (dimensions de $30 \times 5 \times 2 \text{ mm}^3$). Plusieurs valeurs du débit (0, 6,5, 7,5 et 23,5 ml/s) et des concentrations médicamenteuses (rapport massique médicament/(polymère) : 10%, 15%, 20% et 30%) sont considérées. Les données expérimentales sont obtenues sur le banc d'essai décrit au chapitre ???. Le fluide circulant dans le banc d'essai est de l'eau à 37°C avec la densité et la viscosité dynamique de respectivement 1000 kg/m^3 et $6,9 \times 10^{-4} \text{ Pa.s}$. le polyuréthane (PU) a été utilisé comme support de médicament. Afin d'obtenir une estimation de la masse D_p , on sait, par analyse dimensionnelle, que c'est le rapport du carré d'une longueur caractéristique L et d'un temps caractéristique. Dans ce travail, ce temps est choisi pour être $t_{(95\%)}$ et L est choisi comme le rapport du volume du film polymère à sa surface. Enfin, la définition du coefficient de diffusion est (le facteur 5 représente les 5 surfaces sur 6 du film polymère en contact avec le fluide) :

$$D_p = \frac{5L^2}{t_{95\%}} \quad (\text{B.11})$$

Les coefficients de diffusion prédits à différents débits et dosages initiaux du médicament sont indiqués dans le tableau B.3. Ces valeurs sont de l'ordre de grandeur des coefficients de diffusion retrouvés dans la littérature.

Modélisation numérique et méthodologie

Pour être cohérent avec l'installation d'essai, le modèle géométrique 3D du canal avec un polymère

B.4. MODÉLISATION ET SIMULATION

TABLE B.3 – Coefficient de diffusion calculé (m^2/s) à différentes conditions

Flow rate (ml/s)	Initial drug dosage			
	10%	15%	20%	30%
0	1.92×10^{-12}	-	2.75×10^{-12}	3.67×10^{-12}
6.5	6.15×10^{-12}	-	8.79×10^{-12}	-
7.5	6.73×10^{-12}	8.15×10^{-12}	9.61×10^{-12}	1.28×10^{-11}
23.5	1.39×10^{-11}	-	1.98×10^{-11}	-

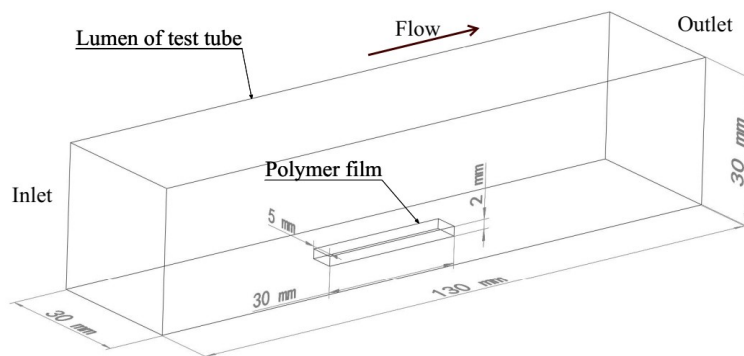


FIGURE B.42 – Modèle géométrique du domaine numérique avec film polymère

chargé de médicament à l'intérieur a été établi comme le montre la figure B.42. Deux domaines sont inclus : les domaines de flux et de polymère. Les dimensions du domaine numérique sont similaires à celles du banc d'essai. Afin d'obtenir l'indépendance du maillage, le raffinement du maillage a été adopté avec différentes tailles de maillage de 3 millions, 5,5 millions, 8,6 millions et 12 millions. Lorsque la taille du maillage est supérieure à 8,6 millions d'éléments, la sensibilité des résultats au nombre de mailles est inférieure à 1%. Ainsi, le maillage final de 8,6 millions est choisi. Le maillage utilisé dans cette étude est constitué d'éléments tétraédriques avec raffinement local proche des bords du domaine, montré dans la figure B.43

Pour être cohérent avec les expériences, de l'eau (considérée comme un fluide incompressible et newtonien) avec une densité de $1000 \text{ kg}/m^3$ et une viscosité dynamique de $6.9 \times 10^{-4} \text{ Pa}\cdot\text{s}$ a été dans

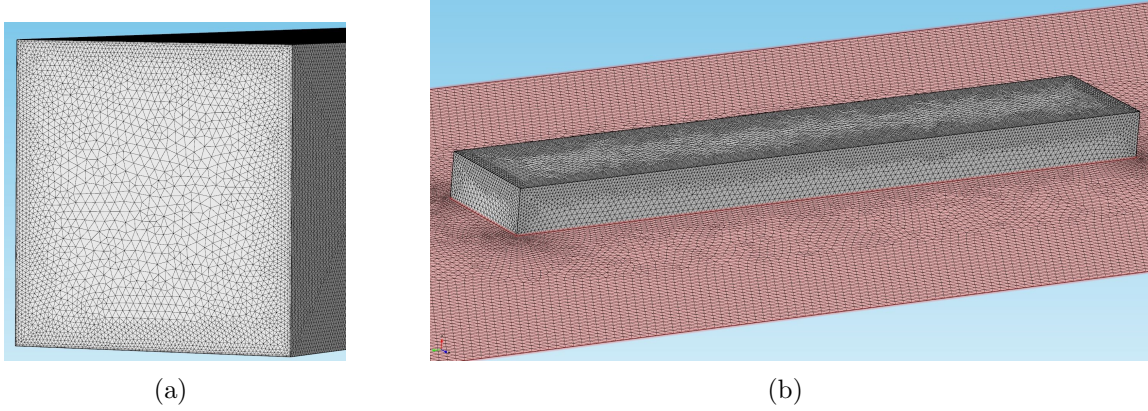


FIGURE B.43 – Répartition des mailles à (a) l’entrée du canal d’écoulement et (b) autour du film polymère

le domaine de l’écoulement lors des simulations. Les équations déterminantes qui sont résolues sont : les équations de Navier-Stokes, de continuité et de transport de masse par advection/diffusion dans le domaine fluide (équations B.12, B.13 et B.14) et l’équation de transport de masse de diffusion dans le domaine polymère (équation B.15) [289].

$$\vec{\nabla} \cdot \vec{V} = 0 \quad (\text{B.12})$$

$$\rho \left(\frac{\partial \vec{V}}{\partial t} + \vec{V} \cdot \vec{\nabla} \vec{V} \right) = -\vec{\nabla} p + \vec{\nabla} \cdot (\mu \vec{\nabla} \text{Vec} V) \quad (\text{B.13})$$

où \vec{V} est la vitesse d’écoulement, p est la pression, ρ est la densité d’écoulement et μ est la viscosité dynamique.

$$\frac{\partial c_f}{\partial t} + \vec{\nabla} \cdot (-D_f \vec{\nabla} c_f) + \vec{V} \cdot \vec{\nabla} c_f = 0 \quad (\text{B.14})$$

où c_f est la concentration du médicament dans le domaine du flux, D_f est le coefficient de diffusion

du médicament dans le flux. Basé sur la littérature [80], $D_f = 3.875 \times 10^{-10} \text{ m}^2/\text{s}$.

$$\frac{\partial c_p}{\partial t} + \vec{\nabla} \cdot (-D_p \vec{\nabla} c_p) = 0 \quad (\text{B.15})$$

où c_p est la concentration du médicament dans le polymère, D_p est le coefficient de diffusion dans le polymère. Comme les débits de 0 ml/s , $6,5 \text{ ml/s}$, $7,5 \text{ ml/s}$ et $23,5 \text{ ml/s}$ ont été testés dans les expériences, la vitesse moyenne de section à l'entrée est fixée à 0 m/s , $0,0072 \text{ m/s}$, $0,0083 \text{ m/s}$ et $0,026 \text{ m/s}$ respectivement. Le nombre Re correspondant est inférieur à 1200 appartenant au régime laminaire. Un profil de vitesse uniforme est défini à l'entrée et le polymère est situé dans une région où l'écoulement est déjà pleinement développé. Quant aux conditions aux limites, une pression constante est fixée en sortie, la paroi de l'artère est considérée comme rigide sans glissement, une concentration de médicament nulle est fixée à l'entrée, tandis qu'un flux de médicament nul (adiabatique) est imposé à la sortie. Aux interfaces entre les domaines d'écoulement et de polymère, le flux de médicament est considéré comme continu. Les concentrations initiales de médicament dans le polymère sont de 202 mol/m^3 , 279 mol/m^3 , 356 mol/m^3 et 591 mol/m^3 correspondant à 10% , 15%, 20% et 30%. Dans le canal, la concentration initiale en médicament est de 0. La modélisation, le maillage et le calcul ont été effectués avec Comsol 5.1 qui est basé sur la méthode des éléments finis. Le solveur utilisé dans ce logiciel applique une méthode itérative appelée méthode résiduelle minimale généralisée (GMRES). Le schéma aérodynamique de Petrov-Galerkin (SUPG) et le schéma de formule différentielle arrière (BDF) avec ordre variable sont adoptés pour réaliser la discrétisation spatiale et temporelle des équations gouvernantes. Concernant les critères d'arrêt, les valeurs résiduelles de 10^{-5} pour l'équation

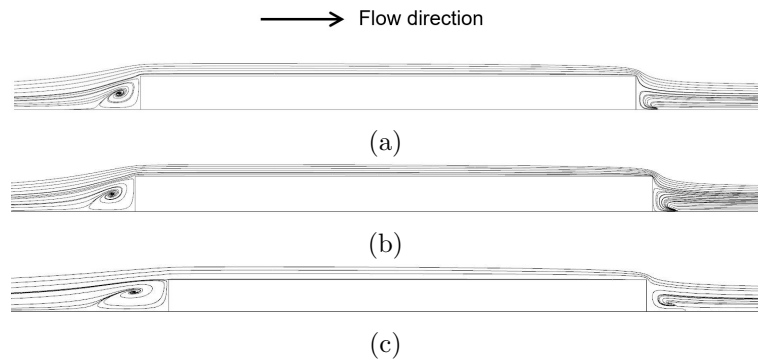


FIGURE B.44 – Topologie d’écoulement autour du film polymère à différents débits (a) $6,5 \text{ ml/s}$, (b) $7,5 \text{ ml/s}$ et (c) $23,5 \text{ ml/s}$

de continuité et de quantité de mouvement et de 10^{-4} pour la diffusion ont été choisies. Le pas de temps initial de $0,001s$ est d’abord défini et peut être ajusté de manière adaptative par Comsol pendant le processus de calcul en fonction de la physique et du schéma utilisés. Un aperçu de la topologie de l’écoulement autour du film polymère est présenté sur la figure B.44 à différents débits. Une section transversale suivant la direction de l’écoulement et située au milieu du canal d’écoulement a été extraite. Comme observés sur la figure B.44, les tourbillons se forment aussi bien en amont qu’en aval du polymère car l’écoulement est fortement perturbé par cet obstacle. L’augmentation du débit a tendance à agrandir les régions de recirculation. Afin de mieux comprendre les effets du flux sur la libération du médicament, la figure B.45 montre la distribution du médicament dans une section transversale située au milieu du film polymère parallèlement à la direction du flux à différents débits avec une dose initiale de médicament de 10% et $t = 1 d$. Une concentration de médicament plus faible est observée avec un débit accru. De plus, les gradients de concentration de médicament diminuent plus rapidement avec le débit dans les régions proximale et distale du polymère (cercles noirs sur la figure B.45). La raison en est l’influence plus forte de la convection d’écoulement avec un débit accru.

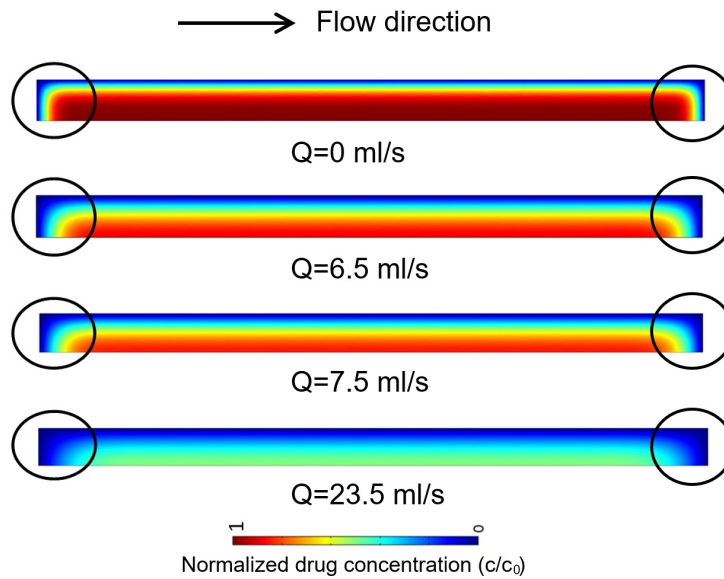


FIGURE B.45 – Répartition du médicament dans le plan médian du film polymère parallèlement à la direction du flux à différents débits (dose initiale de 10% et $t = 1 d$)

La figure B.46 montre la distribution du médicament sur les deux surfaces latérales symétriques du polymère le long de la direction d'écoulement à différents instants avec un débit de $7,5 \text{ ml/s}$ et une dose initiale de 10 %. Une concentration symétrique de médicament peut être observée entre ces deux surfaces latérales à des instants différents. En outre, la libération du médicament a tendance à être plus rapide du côté amont par rapport au côté aval car la convection du flux est plus forte avec le flux entrant en amont du polymère.

La figure B.47 montre la distribution du médicament sur les deux surfaces latérales symétriques du film polymère le long de la direction d'écoulement à différents moments au débit de $7,5 \text{ ml/s}$ et à la dose initiale de médicament de 10%. Une concentration symétrique de médicament peut être observée entre ces deux surfaces latérales à des moments différents. Par rapport à la coupe précédente située dans le plan médian du film polymère, nous observons une distribution asymétrique de la concentration

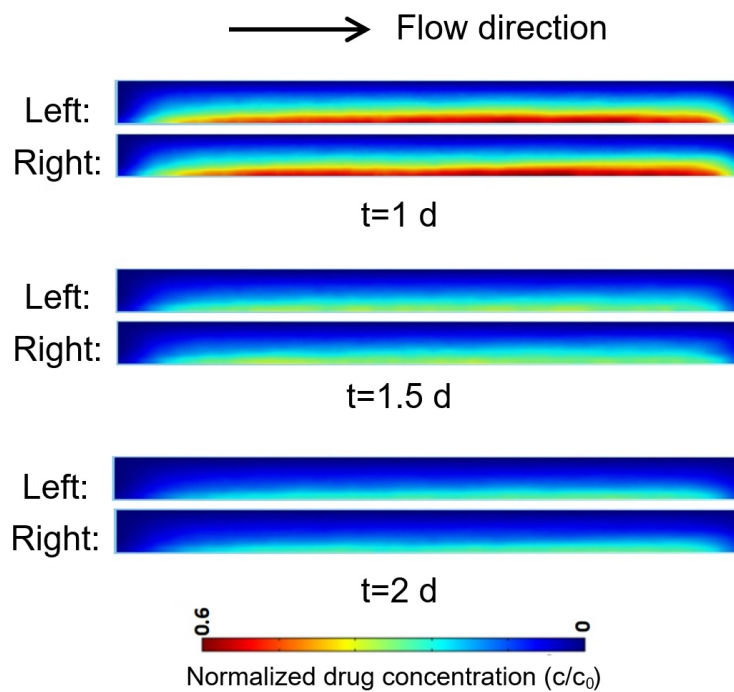


FIGURE B.46 – Répartition du médicament sur les faces latérales du film polymère à différents instants pour un débit de $7,5 \text{ ml/s}$ et un dosage initial du médicament de 10%

médicamenteuse sur les faces latérales en contact avec le fluide : la région proximale est plus sensible à la convection que la région distale. La figure B.47 présente la comparaison des profils de libération de médicament obtenus expérimentalement, numériquement et par le modèle cinétique à différents débits et 10% de la dose initiale de médicament en polymère. Numériquement, M_t/M_0 représente le rapport de la concentration moyenne en volume de médicament libérée par le polymère au temps t et la concentration initiale de médicament. La distribution du médicament dans la section transversale du polymère est affichée à des moments spécifiques. Comme observé, un bon accord est trouvé entre les résultats numériques et les données in vitro. L'augmentation du débit et de la concentration initiale du médicament favorise le processus de libération du médicament avec un temps de libération du médicament réduit en raison de l'effet croissant de la convection du flux et du gradient de concentration initiale.

B.5 Conclusion

Cette thèse s'inscrit dans le cadre général de la thrombose générée par l'emploi de stents à élution médicamenteuse. Il faut distinguer trois verrous scientifiques et techniques principaux :

- L'absence d'appareils bio-pertinents pouvant simuler les conditions requises. Ce dispositif peut être utile pour analyser le comportement des DES.
- La nécessité de comprendre les mécanismes guidant la cinétique de libération du médicament, en considérant les propriétés physiques, chimiques et mécaniques des composés des porteurs de médicament pendant la libération du médicament plutôt que d'examiner directement le profil de libération

B.5. CONCLUSION

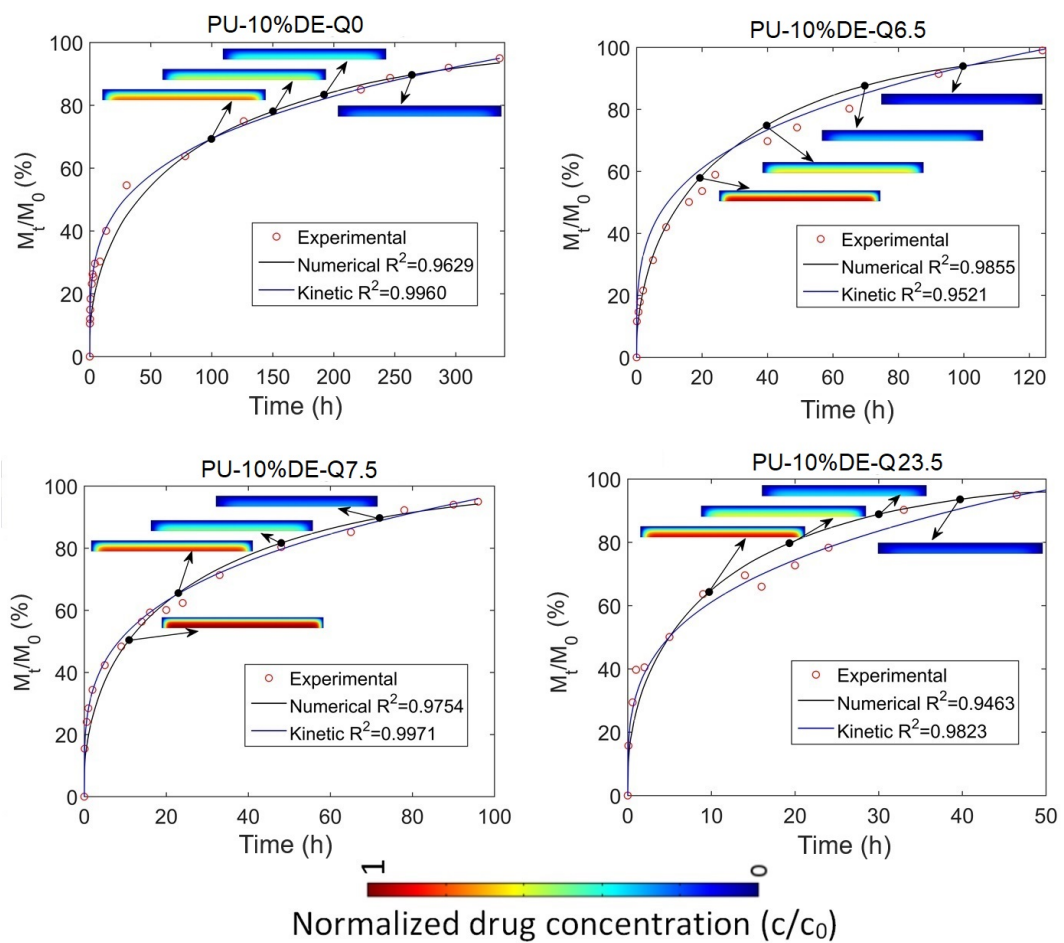


FIGURE B.47 – Libération de médicament à partir d'un polymère à différents débits avec un dosage de 10%

du médicament à partir d'un produit final.

- Le manque de modélisation permettant une simulation fiable des profils de libération de médicaments à partir du DES. En effet, de nombreux modèles et simulations sont disponibles dans la littérature, mais les validations basées sur des tests *in vitro* bio-pertinents font défaut. Un appareil capable de simuler à la fois la lumière et le tissu artériel a été développé. Le sang le débit, continu ou pulsé, est reproduit via un système de pompage conçu pour l'occasion. L'artère milieu est mimé par l'utilisation d'un compartiment spécifique d'agarose. Le système de circulation comprend deux pompes centrifuges. Celle qui assure la systolique et la diastolique flow est une pompe centrifuge développée en laboratoire. Elle comprend une roue et une volute. Le contrôle de la vitesse de rotation de la roue, via un signal d'entrée, permet d'assurer la pulsatilité souhaitée. Une veine de circulation composée de plusieurs canaux séparés est conçue et produite en plexiglas. Cela permet la visualisation du flux et le développement simultané de plusieurs tests. Les dimensions des canaux et des films polymères sont choisies de manière à respecter les lois de similitude des flux. Le diamètre hydraulique des chambres est 30 fois plus grand que le diamètre normal de l'artère carotide. Sur la paroi inférieure de chaque canal, nous avons placé un hydrogel compartiment simulant l'artère tissulaire. À l'aide de l'appareil développé, nous avons étudié les effets de certains facteurs influençant le ratio de libération de drogue. Ceux-ci sont, mais sans s'y limiter, le chargement initial du médicament, le type de médicament et de polymère, la valeur du débit et le modèle d'écoulement, l'évaporation du solvant lors de la fabrication d'échantillons, l'épaisseur du polymère, etc. Les paramètres ci-dessus ont montré certaines influences sur les profils de libération :

B.5. CONCLUSION

- L'augmentation du dosage du médicament a augmenté la cinétique de la libération et réduit le temps d'épuisement du médicament des porteurs. Ce paramètre a plus affecté les échantillons PU que les échantillons PLGA, du fait de l'augmentation du nombre de pores.

- L'augmentation du débit a également augmenté la cinétique de l'écoulement, où il a été observé que le type d'écoulement était plus facteur d'influence que la valeur du débit ; par exemple, la cinétique de la libération était plus influencée par le passage d'un flux statique à un flux continu permanent et à un flux pulsé non stationnaire. Les échantillons PLGA étaient plus sujets à cette influence. L'étude des études physiques, chimiques et mécaniques de ces deux types de polymères a montré que les échantillons de PU sont moins sensibles à l'augmentation du débit. Les propriétés intrinsèques du PU, comme la température transition vitreuse et ses propriétés mécaniques, n'ont pas changé de manière significative. Cependant, l'effet du pourcentage de médicament modifie de manière significative les propriétés mécaniques de ce polymère et augmente la fraction de volume libre dans les échantillons. Alors que les résultats sur les films PLGA ont montré qu'en augmentant le pourcentage de médicament, les films polymères deviennent plus cassants, surtout au moment de la libération. Ce comportement est beaucoup plus important lorsque le débit augmente. Nous avons développé un nouveau modèle pour prédire la libération de médicaments en plusieurs étapes à partir de systèmes d'administration de médicaments. La forme du profil de libération peut entraîner une ou plusieurs cinétiques. En sommant une série de fonctions de puissance, le modèle proposé ajuste ce profil. Chaque fonction représente une étape et est définie par trois facteurs (M_i , t_i et n_i), qui peuvent dépendre des données de conception du support médicamenteux ou des conditions de son fonctionnement. Ils confèrent à chaque étage

B.5. CONCLUSION

ses propriétés cinétiques. Nous illustrons la validité de cette approche en présentant plusieurs cas de porteurs de médicaments. Cette approche reste facilement applicable à d'autres séries de systèmes d'administration. Il suffit de posséder un ensemble de données expérimentales représentatives. Ce modèle peut être utile pour prédire le profil de libération pour une famille de systèmes d'administration de médicaments en tenant compte de la variation de différents paramètres. Cependant, il faut faire attention aux différences des paramètres, qui peuvent varier d'une expérience à l'autre. En effet, les paramètres tels que le type de médicament, le type de flux, la méthode de fabrication des échantillons, la charge médicamenteuse peuvent jouer un rôle dans le désaccord des résultats avec le modèle prédictif s'ils ne sont pas pris en compte au préalable dans le modèle. Le deuxième modèle développé dans cette étude est un modèle mathématique basé sur les mécanismes physiques qui peuvent contribuer à façonner le profil de libération du médicament à partir du système porteur. Nous avons considéré ici les mécanismes de libération de médicaments les plus probables pour le PU : libération en rafale, osmotique, diffusion et pour la PLGA : libération en rafale, diffusion, gonflement et érosion. L'influence du débit et/ou de la charge médicamenteuse initiale sur les rapports de libération de médicament en fonction de ces mécanismes a été mise en évidence. À cet égard, le modèle prédictif et les résultats expérimentaux ont montré une bonne corrélation. Il est à noter que le choix des mécanismes contribuant à la libération du médicament doit être choisi de manière rigoureuse. On peut noter que généralement en augmentant le dosage du médicament à débit constant, le temps de libération caractéristique de chaque mécanisme diminue. Il est à noter que la part de la contribution des mécanismes varie selon ces deux paramètres qui sont également sensibles au temps d'intervention.

B.5. CONCLUSION

Une simulation numérique a été réalisée pour prédire le profil de libération du médicament et la distribution visuelle du médicament dans le polymère pendant la libération. Les comparaisons du profil de libération du médicament entre les calculs numériques, le modèle de cinétique et les expériences ont été établies, dans lesquelles les validations des résultats numériques ont été bien réalisées. Il a également montré que le débit accru et le dosage initial du médicament contribuent à la réduction de la période de libération du médicament. Les tourbillons se sont formés aussi bien en amont qu'en aval du DES car l'écoulement est fortement perturbé par cet obstacle. Le débit élevé apporte une plus grande région de recirculation et la distribution du médicament dans le polymère montre le processus de libération du médicament de l'extérieur vers l'intérieur du polymère progressivement.

Résumé : Le système cardiovasculaire est sujet à des maladies graves telles que l'athérosclérose, principale cause de décès au cours des dernières décennies. Les techniques thérapeutiques continuent de s'améliorer aujourd'hui : angioplastie par ballonnet, stent nu, stent à élution médicamenteuse, stent biorésorbable. La thrombose de stent est l'une des complications graves de l'angioplastie. Le maintien d'une dose adéquate d'anticoagulants et d'agents antiplaquettaires pendant le traitement peut minimiser le risque de thrombose. L'optimisation de certains paramètres peut améliorer la cinétique de libération du médicament au cours de cette thérapie. Dans cette thèse, nous avons développé un appareil bio-pertinent dans lequel nous pouvons considérer l'impact des choix de conception, et celui des propriétés des deux milieux mimés sur la libération du médicament. Ces deux milieux sont la circulation sanguine systolique-diastolique et la paroi artérielle. De plus, nous avons analysé et quantifié l'effet du schéma d'écoulement, du revêtement polymère et du type de médicament sur les tests de libération in vitro. Nous avons également développé des modélisations robustes permettant de caractériser le comportement cinétique des porteurs de médicaments. Ces développements permettent ainsi de définir des choix de conception pour de nouveaux systèmes d'administration de médicaments en réponse à un profil de libération souhaité.

Mots clés : Appareil bio-relevant, Stent à élution de médicament, Mécanismes et cinétique de libération, Écoulement sanguin pulsatile, Modélisation, Simulations numérique.

Abstract : The cardiovascular system is prone to severe diseases such as atherosclerosis, most important cause of death in the recent decades. Therapeutic techniques continue to improve today: balloon angioplasty, bare stent, drug-eluting stent, bioresorbable stent. Stent thrombosis is one of the severe complications of the angioplasty. Maintaining an adequate dose of anticoagulants and antiplatelet agents during the therapy can minimize the risk of thrombosis. Optimizing some parameters can improve the kinetics of the drug release during this therapy. In this thesis, we have developed a bio-relevant apparatus in which we can consider the impact of the design choices, and that of the properties of the two mimicked media on the release of the drug. These two media are the systolic-diastolic blood circulation and the arterial wall. Furthermore, we have analyzed and quantified the effect of the flow pattern, polymer coating and type of drug on the in-vitro release tests. We have also developed some robust modeling allowing the characterization of the kinetic behavior for the drug carriers. These developments make it possible to set design choices for new drug delivery systems in response to a desired release profile.

Keywords : Bio-relevant apparatus, Drug-eluting stents, Drug release mechanisms and kinetic, Pulsatile blood flow, Modeling, Numerical simulations.